



VCU

Virginia Commonwealth University
VCU Scholars Compass

Theses and Dissertations

Graduate School

2022

Therapeutic Injectable Iron-Chelating Hydrogels

Debbie Campbell-Rance
Virginia Commonwealth University

Follow this and additional works at: <https://scholarscompass.vcu.edu/etd>



Part of the [Life Sciences Commons](#), and the [Polymer Science Commons](#)

© The Author

Downloaded from

<https://scholarscompass.vcu.edu/etd/7055>

This Dissertation is brought to you for free and open access by the Graduate School at VCU Scholars Compass. It has been accepted for inclusion in Theses and Dissertations by an authorized administrator of VCU Scholars Compass. For more information, please contact libcompass@vcu.edu.

©Debbie Campbell-Rance 2022

All Rights Reserved

Therapeutic Injectable Iron-Chelating Hydrogels

A dissertation submitted in partial fulfillment of the requirements for the degree of Doctor of
Philosophy at Virginia Commonwealth University

By

Debbie S. Campbell-Rance

Master of Science in Chemistry, Virginia Commonwealth University, 2011

Bachelor of Science in Chemistry, University of the West Indies, Mona Campus, 1999

Advisor: Xuejun Wen, M.D., Ph.D.

Alice T. and William H. Goodwin Jr. Endowed Chair Professor in Regenerative Medicine Institute for
Engineering and Medicine

Department of Chemical and Life Science Engineering

Virginia Commonwealth University

Richmond, Virginia

May 2022

ACKNOWLEDGEMENTS

“Trust in the LORD with all thine heart; and lean not unto thine own understanding. In all thy ways acknowledge him, and he shall direct thy paths.” (Proverbs 3:5-6)

Throughout the course of my graduate studies that lead to the writing of this dissertation, I received tremendous support from many sources. First, I would like to acknowledge my Lord and Savior, Jesus Christ who sustained me and gave me the will to persevere and complete this work. Additionally, I am grateful for the support of my spouse, Marvin, who supported and prayed for me every step of the way. I want to extend my sincerest gratitude to my beautiful daughter, Zhenya, who accompanied me to the lab on numerous occasions at odd hours to care for those “fragile and fickle” neural stem cells. I would also like to thank my friends, Waddell Gordon, Joy Dodd, Sophia Brown and Alicia Aralu for their prayers and support.

My research endeavors would not have been fruitful without the contributions of my mentors and group members. I am very appreciative to my research advisor Professor Xuejun Wen for his support, immense knowledge, guidance and patience throughout the time it took me to complete my studies. His supportive attitude, yet hands-off approach was exactly what worked for me. He understood that I needed to set my own timelines to facilitate the other important factors in my life. Additionally, I would like to thank Dr. Ning Zhang for her encouragement, guidance and feedback, especially during the early stages of my research. This Ph.D. would not have been possible without the insightful discussions, advice from Dr. Bo Xue. Dr. Xue was my sounding board during this process; he listened to my concerns and encouraged me think outside of the box. Furthermore, he has been very instrumental in ensuring that supplies were available for the

experiments and he was always willing to teach me whatever he knows. I would also like to thank all the other members of my lab, especially Chenyang Jiang and Xiaomei Zeng. Chenyang trained me in cell culture techniques and Xiaomei ensured that I has the proprietary coating material I needed for culturing adherent neural stem cells.

My sincerest thanks go to the members of my committee who took the time to read my thesis proposal and now my dissertation. Dr. Gupton, thank you for your encouragement and for having faith in my abilities. Dr. Peters, thank you for caring to ask how things were progressing with my research. Thanks to Dr. Wynne for his valuable discussions regarding polymer properties and characterization. I would like to thank Dr. Sun for providing useful insights, by way of her publications on CNS injuries and to Dr. Collinson; I appreciate the fact that you were willing and ready to join my Ph.D. committee when asked. Additionally, I want to thank you for the useful discussions about analytical techniques and chemistry in general.

Finally, I want to acknowledge Virginia State University (VSU), my place of work. Special thanks to Dr. Keith Williamson (former Dean of the School of Engineering) and Dawit Haile (current Dean of the school of Engineering) who supported me during my studies by way of time release. I also want to thank Mrs. Fran Thomas (Administrative Assistant) and Mr. William Jones (Laboratory Technician) for providing the necessary support services for the classes I teach at VSU.

Table of Contents

ACKNOWLEDGEMENTS	3
LIST OF TABLES	11
ABSTRACT	16
CHAPTER 1	19
1 Introduction	19
1.2 Central Nervous System Injuries.....	19
1.3 Treatment of CNS Injuries.....	21
1.4 Our Approach.....	23
CHAPTER 2	24
2 Specific Aims	24
2.1 Background and Significance.....	24
2.2 Specific Aim 1: To explore the role of iron chelation in protection of human neural stem cells (hNSCs) by hyaluronic acids (HAs) of different molecular weight.	29
2.3 Specific aim 2: To synthesize and characterize families of iron chelator-polymer conjugates (ICCs) based on the combination of four iron chelators and two polymers.....	30
2.4 Specific Aim 3: To engineer injectable iron chelator-bound hydrogel (ICH) scaffolds as permissive niche for neural stem cell growth, viability, and proliferation.....	30
CHAPTER 3	31

3	The Role of iron Chelation in Protection of Human Neural Stem Cells (hNSC) by Hyaluronic Acid (HA)	31
3.1	Introduction	31
3.2	Experimental Section	34
3.2.1	Materials	34
3.2.2	Iron (III) Calibration Curve.....	34
3.2.3	Iron Chelation Efficiency of HA	35
3.2.4	Inhibition of Iron/Ascorbate-induced Lipid Peroxidation of α -Linoleic acid by HA	35
3.2.5	Cell Culture.....	36
3.2.6	Inhibition of Iron/Ascorbic Acid-Induced Lipid Peroxidation in hNSCs by HA	37
3.2.7	Influence of HA on Iron/Ascorbate-induced Oxidative Stress on the Viability of hNSCs. 37	
3.2.8	Histochemical staining with Fluorescent Phallotoxin and DAPI to determine morphology of hNSC via Confocal Microscopy.	38
3.3	Results.....	40
3.3.1	Iron Chelation Efficiency of Hyaluronic Acid.....	40
3.3.2	Inhibition of Iron/Ascorbate-induced Lipid Peroxidation of α -Linoleic acid by HA	43
3.3.3	Inhibition of Iron/Ascorbic Acid-Induced Lipid Peroxidation in hNSCs by HA	46
3.3.4	Influence of HA on Iron/Ascorbate-induced Oxidative Stress on the Viability of hNSC.	48
3.3.5	Inhibition of Iron/Ascorbic Acid-Induced Lipid Peroxidation in hNSCs by HA	52

3.3.6	Influence of HA on Iron/Ascorbate-induced Oxidative Stress on the Viability of hNSCs.	
	Error! Bookmark not defined.	
3.4	Discussion.....	52
3.4.1	Iron Chelation Efficiency of Hyaluronic Acid.....	52
3.4.2	Inhibition of Iron/Ascorbate-induced Lipid Peroxidation of α -Linoleic acid by HA	53
3.4.3	Inhibition of Iron/Ascorbic Acid-Induced Lipid Peroxidation in hNSCs by HA	54
3.4.4	Influence of HA on Iron/Ascorbate-induced Oxidative Stress on the Viability of hNSCs.	56
3.5	Conclusion.....	58
4	Polymer-Modified Small Molecule Iron Chelators for Improved Regeneration.	59
4.1	Introduction	59
4.2	Materials and Methods.....	78
4.2.1	Synthesis of the Oxidizing Agent (Jones Reagent)	79
4.2.2	Synthesis of POE 4600-Dicarboxylic Acid.....	80
4.2.3	Estimation of Carboxylic Groups per PEG Molecule	80
4.2.4	Iron Chelation Efficiency of Small Molecule Iron Chelators.....	81
4.2.5	Synthesis of Iron Chelator Modified POE-4600-Carboxylic Acid.....	82
4.2.6	Synthesis of Hyaluronic Acid Modified HOOC-PEG-Chelator.....	84
4.2.7	Characterization of HOOC-PEG-Chelator and HA-PEG-Chelator Conjugates.....	85
4.2.8	The inhibition of Lipid Peroxidation of Linoleic Acid by HA and HA-PEG-Chelator	85

4.2.9	Cell Culture.....	86
4.2.10	Inhibition of Iron(II)/Ascorbic Acid-Induced Lipid Peroxidation in hNSCs by HA and HA-PEG-Chelator.....	87
4.2.11	Influence of HA and/or HA-PEG-Chelator on Iron (II)/Ascorbate-induced Oxidative Stress on the Viability of hNSCs.....	88
4.2.12	Histochemical staining with Fluorescent Phalloxin and DAPI to determine morphology of hNSC via Confocal Microscopy.	88
4.3	Results.....	91
4.3.1	Oxidation of Terminal Hydroxyl Groups of Polyethylene Glycol (PEG).....	91
4.3.2	Estimation of Carboxylic Groups per PEG Molecule	92
4.3.3	Iron Chelation Efficiency of Small Molecule Iron Chelators.....	93
4.3.4	Synthesis of Iron Chelator Modified POE-4600-Carboxylic Acid.....	94
4.3.5	Synthesis of Hyaluronic Acid Modified HOOC-PEG-Chelator.....	99
4.3.6	102
4.3.7	Inhibition of Iron/Ascorbate-Induced Lipid Peroxidation of α -Linoleic Acid by HA, HA-PEG-5A8HQ, HA-PEG-Cur, and HA-PEG-Quer.	104
4.3.8	Influence of HA, HA-PEG-5A8HQ, HA-PEG-Cur, and HA-PEG-Quer on Iron/Ascorbate-induced Oxidative Stress on the Viability of hNSC.....	108
4.4	Discussion.....	118
4.4.1	Synthesis and Characterization of HOOC-PEG-COOH.....	118

4.4.2	Iron Chelation Efficiency of Small Molecule Iron Chelators.....	119
4.4.3	Synthesis and Characterization of Iron Chelator Modified POE-4600-Carboxylic Acid.....	121
4.4.4	Synthesis of Hyaluronic Acid Modified HOOC-PEG-Chelator.....	123
4.4.5	Inhibition of Iron/Ascorbate-Induced Lipid Peroxidation of α -Linoleic Acid by HA, HA-PEG-5A8HQ, HA-PEG-Cur, and HA-PEG-Quer.	124
4.4.6	Influence of HA, HA-PEG-5A8HQ, HA-PEG-Cur, and HA-PEG-Quer on Iron/Ascorbate-induced Oxidative Stress on the Viability of hNSC.....	127
4.5	Conclusion.....	130
5	Injectable Iron-Chelating Hyaluronic Acid-Based Hydrogel for Improved Central Nervous System Regeneration.	132
5.1	Introduction	132
5.2	Materials and Methods.....	143
5.2.1	Synthesis of thiolated HA and HA-PEG-Chelator	144
5.2.2	Quantitating Sulfhydryl Groups Using a Cysteine Standard	144
5.2.3	The Gelation time of HA-SH or HS-HA-PEG-Chelator hydrogel.....	145
5.2.4	Cell Culture (2D- and 3D-Culture)	146
5.3	Results.....	147
5.3.1	Synthesis of thiolated HA and HA-PEG-Chelator	147
5.3.2	Quantitating Sulfhydryl Groups Using a Cysteine Standard	153

5.3.3	Preparation of PEGTA Cross-linked HA-SH or HS-HA-PEG-Chelator Injectable Hydrogels via Thiol-Acrylate Michael Addition	155
5.3.4	2D- and 3D-cell Culture on HA-S-PEGTA and PEGTA-S-HA-PEG-Cur Hydrogels.....	157
5.4	Discussion.....	160
5.4.1	Thiolated HA-SH/PEGTA and HS-HA-PEG-Cur/PEGTA Hydrogels.	160
5.4.2	Quantitating Sulfhydryl Groups Using a Cysteine Standard	161
5.4.3	HA-S-PEGTA and PEGTA-S-HA-PEG-Cur Injectable Hydrogels	161
5.4.4	2D- and 3D-cell Culture on HA-S-PEGTA and PEGTA-S-HA-PEG-Cur Hydrogels.....	162
5.5	Conclusion.....	165
6	Conclusions and Future Directions	166
6.1.1	Chapter 3.....	167
6.1.2	Chapter 4.....	167
6.1.3	Chapter 5.....	168
6.2	Future Works	169
6.2.1	Hydrogel Optimization Study.....	169
6.2.2	In vivo evaluation of the therapeutic effect of bioengineered injectable hydrogel optimized for pediatric mice brain tissue.	171
	Appendix A	234
	Central Nervous System Injuries and Treatments	234
A.1	Structure, Organization and Function of the Central Nervous System	234

A.2 Central Nervous System Injuries.....	237
A.2.1 Traumatic Brain Injury	238
A.2.2 Traumatic Spinal Cord Injuries.....	247
A.3 Economic Burden of CNS Injuries	256
A.4 Treatment of CNS Injuries.....	259
A.4.1 Medical Intervention	259
A.4.2 Surgical Intervention.....	261
A.4.3 Pharmacological Treatment.....	261
A.4.5 Cell treatment.....	263
A.5 Our Approach.....	265

LIST OF TABLES

Table 3.1: Iron Chelation Efficiency of Hyaluronic Acid	Error! Bookmark not defined.
Table 4.2: Iron Chelation Efficiency of Small Molecule Iron Chelators	94

TABLE OF FIGURE

LIST OF SYMBOLS AND ABBREVIATIONS

TBI	Traumatic Brain Injury
SCI	Spinal Cord Injury
CNS	Central Nervous System
NTE	Neural Tissue Engineering
DNA	Deoxyribonucleic acid
HA	Hyaluronic Acid
hNSC	Human Neural Stem Cells
PEG	Polyethylene Glycol
ICCs	Iron Chelator-Polymer Conjugates
EMC	Extracellular Matrix
ROS	Reactive Oxygen Species
ICP	Intracranial Pressure
ISP	Intraspinal Pressure
CBF	Central Blood Flow
EAA	Excitatory Amino Acids
LPO	Lipid Peroxidation
BBB	Blood-Brain Barrier
SC	Stem Cells
BM-MSCs	Bone Marrow Mesenchymal Stem Cells
U-MSCs	Umbilical Mesenchymal Stem Cells
AD-MSCs	Adipose-Derived Mesenchymal Stem Cells
NSC	Neural Stem Cells

NCPs	Neural Progenitor Cells
ESCs	Embryonic Stem Cells
i-PSCs	Induced Pluripotent Stem Cells
PEGTA	Polyethylene Glycol Tetra Aqulate
NMDA	N-methyl D-aspartate
AChEIs	Acetylcholinesterase Inhibitors
EPO	Erythropoietin
NAC	N-Acetylcysteine
GM-1	Gangliosidosis
Nogo-A	Anti-Nogo
ESCs	Embryonic Stem Cells
iPSCs	Pluripotent Stem Cells
MSCs	Mesenchymal Stem Cells
ICH	Intracerebral Hemorrhage
ER	Endoplasmic Reticulum
PUFA	Polyunsaturated Fatty Acids
·OH	Hydroxyl Radical
LA	Linoleic Acid
PBS	Phosphate Buffered Saline
AA	Ascorbic Acid
BHT	Butylated Hydroxytoluene
EGF	Epidermal Growth Factor

FGF	Fibroblast Growth Factor
RCF	Relative Centrifugal Force
CDs	Cytochrome D
UV-VIS	Ultraviolet–Visible Spectroscopy
DAPI	4',6-Diamidino-2-Phenylindole
PFA	Paraformaldehyde
RHAMM	Receptor for Hyaluronan-Mediated Motility
FDA	Food and Drug Administration
DFO	Deferoxamine
DFP	Deferiprone
DFX	Deferasirox
HBED	Monohydrochloride
DMSO	Dimethyl Sulfoxide
RT-PCR	Reversed Transcription-Polymerase Chain Reaction
GFAP	Glial Fibrillary Acidic Protein
AD	Alzheimer’s Disease
LPI	Labile Plasma Iron
ALT	Alanine Transaminases
ANC	Absolute Neutrophil Count
ALT	Alanine Transaminase
PTSD	Post-Traumatic Stress Disorder
GCS	Glasgow Coma Scale
CDC	Center for Disease Control

DAI	Diffuse Axonal Injuries
AMPA	2-Amino-3-(3-hydroxy-5-methyl-isoxazol-4-yl)propanoic acid
NO	Nitric Oxide
mPTP	Mitochondrial Permeability Transition Pores
ANT	Adenine Nucleotide Translocator
AIF	Apoptosis Inducing Factor
ROO·	Peroxyl
4-HNE	4-Hydroxynonenal
3-NT	3-Nitrotyrosine
PN	Peroxynitrite
NOS	Nitric Oxide Synthase
RIPK	Receptor Interacting Protein Kinase
TGF- β 1	Transforming growth factor beta 1
MCP-1	Monocyte chemoattractant protein-1
TNF- α	Tumor Necrosis Factor alpha
INF- γ	Interferon gamma
C-C motif	Chemokine
CCL5	Ligand
MIP-2	Macrophage Inflammatory Protein-2
NF	Neuro-Filament
β -APP	Beta-Amyloid Precursor Protein
CT	Computer Tomography

ISNCSCI	International Standards for Neurological Classification of Spinal Cords
ASIA	American Spinal Injury Association
GBD	Global Burden of Diseases
NSCISC	National Spinal Cord Injury Statistical Center
TSCI	Traumatic Spinal Cord Injury
MCU	Mitochondrial Calcium Uniporter
NADPH	Nicotinamide Adenine Dinucleotide Phosphate
Nox	Nicotinamide Adenine Dinucleotide Phosphate Oxidase
MRI	Magnetic Resonance Imaging

ABSTRACT

Therapeutic Injectable Iron-Chelating Hydrogels for Improved Central Nervous System
Regeneration

By

Debbie S. Campbell-Rance

A dissertation submitted in partial fulfillment of the requirements of the degree of Doctor of
Philosophy at Virginia Commonwealth University 2021.

Director: Xuejun Wen, M.D., Ph.D., AIMBE Fellow, Alice T. and William H. Goodwin Jr.

Endowed Chair Professor in Regenerative Medicine, Institute for Engineering and Medicine,

Severe traumatic brain and spinal cord injuries are major global public health and socioeconomic problems in terms of mortality and morbidity. Currently there are two main lines of treatment under development for traumatic brain injury (TBI) and spinal cord injury (SCI): the use of pharmacological agents and stem cell therapy. Both therapies exhibit potential but fail to restore function of the damaged brain and spinal cord. Pharmacotherapy failed because it focused mainly on neuroprotection of the remaining nervous tissues while ignoring the regeneration of damaged tissues. On the other hand, the stem cell therapies still have not generated consistent results because these studies failed to address the hostile microenvironment at the lesion site and the lack of combinatorial strategies since multiple pathways are involved in the pathophysiology of the secondary damages in TBI and SCI.

To facilitate CNS injury repair, it is essential to transplant stem cells in a favorable microenvironment that is conducive for their long-term survival and integration within the host tissue. Attributes such as three dimensionality of the graft and adhesive support for transplanted cells facilitates integration. Neural tissue engineering (NTE) is a promising strategy for overcoming the limitations of using pharmacological agents or cell therapy alone for the treatment of CNS injuries. It includes the practice of combining biomaterial scaffolds, stem cells and bioactive molecules to create functional constructs that replace, regrow, restore, maintain or improve damaged or diseased tissues. Researchers have shown that they can manipulate the microenvironment at the site of TBI and SCI to show signs of tissue regeneration, but not enough

to restore full motor and cognitive functions in the impaired. This suggests that an oversight in the treatment strategy might be playing a pivotal role in preventing full functional recovery.

Biochemical inspection at the CNS injury sites indicates that this microenvironment has an unusually high concentration of iron. Iron is an essential nutrient for cellular processes including electron transport and catalysis. Iron's ability to redox cycle is an important aspect of its essential functions in the body and controlling iron levels in the body is critical since both over- and under-load of iron can cause cellular dysfunction. Experimental and clinical evidence indicate that excess iron is lethal to cells due to its ability to promote free radical production and the ensuing oxidative stress which is mainly produced by Fenton or/and Haber-Weiss reactions. The free radicals produced induce cellular damage via their interactions with proteins, lipids, carbohydrate and deoxyribonucleic acid (DNA).

This research developed an NTE strategy that mitigates against build-up of iron at the injury site and alleviates the associated deleterious events, improving the survival and functionality of the transplanted stem cells. The end goal of this work was to develop a therapeutic injectable iron-chelating hydrogel to deliver stem cells to the injury site. The hydrogel fills the lesion site and forms a microenvironment that mimics that of the brain and spinal cord. The hydrogel will enable the stem cells to survive at the injury site and secrete bioactive molecules that will facilitate neuro-regeneration. Selecting a polymeric material for engineering the injectable hydrogel, involved the design of in vitro experiments that investigated the effect of the polymer on the viability and proliferation of human neural stem cells as well as its ability to mitigate against iron (II)/ascorbic acid-induced oxidative stress and lipid peroxidation. Hyaluronic acid (HA) was the chosen polymeric material because of its known neuroprotection in wound healing and rheological

properties tunable to mimics the microenvironment of the CNS. In order to explain the neuroprotective effect of the HA on hNSC when oxidative stress was induced *in vitro*, we performed iron chelation efficiency studies. Further, we reduced the cytotoxicity of three small molecule iron chelators via chemical modification with HA and PEG. This resulted in three families of iron chelator-polymer conjugates (ICCs) for preliminary studies on hNSC and ultimately to be incorporated into the design of the injectable hydrogel. This project will provide a possible solution to overcome the toxicity caused by high iron concentration at the CNS injury sites.

CHAPTER 1

1 Introduction

1.2 Central Nervous System Injuries

Injuries to the central nervous system (CNS) can cause tissue damage in the brain or spinal cord and lead to a disruption of the CNS framework and subsequent loss of neuronal cell bodies, axons, and related glial support. The result of physical injury to the CNS include traumatic brain injury (TBI) and spinal cord injury (SCI). Pathophysiology of central nervous tissue injury is a complex process. These damages fall into two categories: (1) primary injury, the damages arising from the mechanical forces during the physical impact to the brain or spinal cord tissue (2) secondary injury, which pertains to further cellular and tissue damages following the primary injury.[1] The primary injury causes damage to neuronal cell bodies, axons and glial cells and may ultimately lead to

necrosis due to the compromise of the blood supply at the injury site. This also causes the occurrence of hematomas and epidural, subdural and intracerebral hemorrhages.[2]

Secondary injury is transitory, consisting of the acute, sub-acute, and chronic phases. The acute phase starts directly after the physical insult to the CNS tissues and involves vascular damage, increased cell permeability, ionic imbalance, neurotransmitter accumulation, excitotoxicity, free radical formation, lipid peroxidation, inflammation, edema and necrotic cell death.[3-5] The sub-acute injury phase evolves within 48 hours to 14 days following injury. It involves programmed cell death (apoptosis), axon demyelination, degeneration, retraction of axon from the lesion site (axonal) dieback, extracellular matrix (ECM) remodeling and glial scar formation at the injury site. The chronic phase begins three (3) months following injury, with progressive axonal dieback as a cystic cavity forms at the injury site and maturation of the glial scar.[3, 6-9] Following CNS injuries, larger vessels usually remain intact, while the microvasculature (smaller vessels such as capillaries), which are more predisposed to traumatic damage ruptures leading to the extravasation of leucocytes and red blood cells.[10-12] Increased pressure due to tissue edema and hemorrhage-induced vasospasm in the intact vessels promotes further disruption in blood flow to the injury site. The damaged vascular system, along with hemorrhage and ischemia eventually lead to cell death and tissue destruction via multiple mechanisms such as excitotoxicity, free radical formation, hypoxia, ionic imbalance and necrotic cell death.[13] Hemorrhage and cell death creates a milieu in which iron accumulates at the injury site. Eventually, hematoma formation occurs within the CNS parenchyma and this triggers a series of events leading to further secondary damages and neurological deficits[14] As the red blood cells in the hematoma extravasate, hemoglobin and hemoglobin breakdown products are released.[15] Iron, a hemoglobin degradation product, plays a vital role in cell and tissue degeneration in many disease states and an accumulation of iron in

the brain can cause oxidation of lipids and free radical generation.[16, 17] Evidence indicates that iron accumulation, lipid peroxidation (LPO) and subsequent oxidative stress contribute to delayed edema formation after ICH.[18-20] Most of this intracellular iron released from ferritin and transferrin co-localizes with activated microglia/macrophages.[21] The released iron redox cycle between Fe^{2+} and Fe^{3+} while producing more superoxide anion radicals. Subsequently, the Fenton reaction between Fe^{3+} and hydrogen peroxide produces highly reactive hydroxyl radicals.[22] ROS are able to cause oxidative damage to macromolecules such as lipids, proteins, and DNA leading to lipid peroxidation, formation of protein-protein crosslinks, and oxidation of polypeptide backbones resulting in protein fragmentation, DNA damage and DNA strand breakage. High doses of ROS, generated during acute or chronic injuries are cytotoxic.[23]

1.3 Treatment of CNS Injuries

Currently, no clinical treatment exists that will regenerate and restore the damaged CNS. The existing treatment strategy involves medical management of the primary injuries and neuroprotection with pharmacological agents to mitigate the deleterious effects of the secondary damages. Further, rehabilitation plays a role in the treatment of CNS injuries.

Medical intervention typically start at the scene of injury and include injury assessment, airway maintainers, immobilization to prevent further damage, lower intracranial pressure (ICP)/intraspinal pressure (ISP) and maintain cerebral blood flow (CBF), hyperventilation, prophylactic antiepileptic, hypothermia, hyperosmolar therapy, and medically inducing a comatose state.

If epidural hematoma, subdural hematoma or severe internal bleeding occurs, craniotomy surgical intervention is necessary, including decompressive craniectomy at acute phase, evacuation of subdural hematomas to release the blood after acute phase.[24] In some cerebral edemas, where obliteration of the basal cisterns occurs, hemicraniectomy and/or bilateral decompressive craniectomy saves the patient from life threatening danger.[25]

Pharmacological treatments were used to remediate the secondary injury, such as excitatory amino acids (EAA) modulation, calcium channel blocker, reactive oxygen species (ROS) scavenging, inflammation control, caspases inhibitors, calpain inhibitors, endocrinological treatment, etc.[26-37]

Due to the high concentration of oxidizable fatty acids in the brain but low levels of antioxidants, oxidative damage results from lipid peroxidation (LPO).[38] additionally, the pathophysiology of TBI indicate that iron accumulates at the TBI injury site and iron initiates the formation of ROS.[39] The inhibition of ROS and ROS-mediated damage has been the topic of many studies. Medicines in the Tirilazad mesylate family show limited protective capability but has very limited BBB penetration. It mainly lowers ROS level indirectly through maintaining normal blood-brain barrier (BBB) permeability.[40, 41] Metal chelators, such as deferoxamine, mediate ROS by removing the catalyst metal ions in the ROS formation process.[42, 43] Compounds in Choline family protect brain tissue from ROS damage by attenuate the activation of phospholipase A2.[44, 45] Nitron compounds exhibit neuroprotective capability by adducting with ROS.[46, 47] Antioxidant enzyme superoxide dismutase and endothelial Nitric oxide also exhibit neuron protective ability.[48, 49] Compounds targeting brain inflammation, caspases, and neuroendocrine abnormalities are also extensively studied.[50-58]

The most common clinical interventions for SCI is the administration of high doses of methylprednisolone to reduce secondary injury processes. This treatment is controversial due to the adverse side effects, which include gastric bleeding, sepsis, pneumonia, acute corticosteroid myopathy, and wound infection.[59] Baclofen and opioid painkillers are other pharmacological agents used to treat spasticity and severe to moderate pain in SCI, respectively.[60, 61] Morphine is a popular opioid analgesic used in SCI management because morphine has a strong affinity for the mu-receptor located in the CNS.[61]

Stem Cells (SCs) treatment of TBI is promising and several therapies recently entered the clinic trail.[62, 63] In regenerative medicine, SCs differentiate to neural cells, then restore the functionality of the injured area.[64] There are many studies in the preclinical stage on CNS injury animal models where SCs transplantation show the potential to improve neurological activities.[65] In most of the cases, neural stem cells (NSCs) show the capability to regenerate brain tissue in several vivo studies.[64, 65] SC therapy hold much potential for the treatment of SCI because there are multiple features in SCI pathology that stems transplantation can target. Experimental cell culture models , animal and clinical trials tested numerous types are of SCs including bone marrow mesenchymal stem cells (BM-MSCs), umbilical mesenchymal stem cells (U-MSCs), adipose-derived mesenchymal stem cells (AD-MSCs), neural stem cells (NSCs), neural progenitor cells (NPCs), embryonic stem cells (ESCs), and induced pluripotent stem cells (i-PSCs). Searchers and clinicians have come to realize that mono-modal cell therapy offers limited benefits to regeneration in SCI.[66]

1.4 Our Approach

Spontaneous regeneration in the CNS is deficient following injury and one main reason is the hostile microenvironment at the injury site, which is comprised of many inhibitory molecules. Extensive research efforts are in progress to shed light on the mechanisms that drives these inhibitory factors, which is the core strategic principle in promoting regeneration in the CNS. Stem cell are promising for repair in the CNS but low viability of the transplanted cells becomes a major hurdle to neuroregeneration. This work addresses this issue by creating an artificial niche for stem cells via the synthesis of a series of in situ crosslinkable hydrogels based on PEGTA and iron-chelator polymer-conjugates. The iron-chelator polymer-conjugate is comprised of small a molecule chelator (5-amino-8-hydroxyquinoline, curcumin or quercetin), PEG, and/or hyaluronic acid. We will this series of in situ crosslinkable hydrogels in its ability to grow and proliferate hNSCs both in two and three dimensional cell culture. Additionally, this crosslinkable hydrogel may mitigate oxidative stress and lipid peroxidation in *in vitro* experiments.

CHAPTER 2

2 Specific Aims

2.1 Background and Significance

CNS injuries significantly affect both the individual and society and are major causes of disability and mortality worldwide. The neurological damages caused by TBIs or SCIs may occur immediately from the primary injuries, and from the secondary injury sequelae that ensue minutes, hours and days after the primary injury. Thus, prevention, proper management and treatment of the secondary injuries are also critical for improved outcomes from TBIs and SCIs. [67]

Currently there are no curative treatments for severe TBI and SCI but advancement in the treatment modalities for both types of injuries is a source of inspiration towards the continued search for optimal therapies. The clinical management of TBI and SCI are multifaceted as are illustrated by the multiple ways in which they present and the wide array of treatment strategies. Traditional treatment strategies include medical management of injuries, frequent radiographic imaging, neurological examinations, invasive intracranial monitoring and surgical decompression.[68]

Since TBI and SCI, injuries are a combination of structural, functional, cellular, and vascular damages; scientists in basic and applied research have searched for therapeutic strategies that address the first impact damages as well as mitigating against the secondary damage after CNS injuries. This therapeutic intervention seeks to stabilize the injury site, to attenuate the ongoing damages from the secondary sequelae, prevent further neuronal damage, enhance the restoration of neural network and promote functional recovery.[68, 69] Most multi-center clinical trials conducted over the past three decades involved primarily the use of pharmacological agents as an approach to treat TBI and SCI. These pharmacological agents target secondary injury mechanisms such as calcium channel blockers, corticosteroids, excitatory amino acid inhibitors, N-methyl D-aspartate (NMDA) receptor antagonist, free radical scavengers, magnesium sulfate, and growth factors.[70] In the case of TBI, several phase II clinical trials illustrated favorable effects for a number of pharmacological agents but unfortunately, none of these agents showed substantial efficacy in the overall TBI population when tested in the phase III clinical trial.[71] Some of the most promising pharmacological agents studied in pre-clinical and/or phase II clinical trials include acetylcholinesterase inhibitors (AChEIs), erythropoietin (EPO), glyburide, growth hormones, minocycline, N-acetylcysteine (NAC), progesterone and statins.[72]

So far, clinicians have evaluated five (5) pharmacological agents in phase III trials for the treatment of SCI but none of them became the gold standard of care. This include neuroprotective agents such as methylprednisolone, naloxone, tirilazad and nimodipine and a family of neuroregenerative agents collectively known as GM-1 ganglioside (Sygen).[73-79] Additionally, there are a number of neuroprotective and neuroregenerative agents in development for the treatment of SCI. The drugs include neuroprotective agents such as riluzole, minocycline, and basic fibroblast growth factor and neuroregenerative agents such as cethrin and anti-Nogo (Nogo-A).[80-86] Even though these drugs are promising, they are yet to show efficacy beneficial to the SCI population in phase III clinical trials.

Since drug therapy alone failed to achieve the expected success in the treatment of TBI and SCI, scientist had to develop novel therapeutic interventions to delay and limit the extent of damaging pathophysiological effects associated with the secondary injury sequelae. Hypothermia is an excellent therapeutic approach to achieve this goal. Experimental and clinical studies show the neuroprotective effects of hyperthermia in the treatment of traumatic CNS injuries.[87] The studies used a wide range of animal SCI and TBI models and the results demonstrated neurological benefits in dogs, monkeys and pigs. [88-93] The earlier studies used localized hypothermia but studies using systematic hypothermia showed better neuroprotective effects when applied in animal models utilizing rabbits, pigs, dogs, and rats.[94-99] Additionally, studies conducted with mild-to-moderate hypothermia reported lower mortality, less adverse side effects and better neuroprotective effects than those performed with profound hypothermia. Even though a substantial body of work has reported on the use of hypothermia in CNS injuries, the studies have presented mixed reviews regarding its use as a standard of care and despite the fact that it has translated to clinical use; there are still some unanswered questions and procedural optimization

to achieve. Experimenters and clinicians alike are still in the dark about the exact therapeutic window of hypothermia, the optimum duration of the procedure and the most appropriate re-warming rates.[87, 100]

In recent decades, researchers and clinicians focused much research efforts on the use of stem cells as a viable therapeutic option for the treatment of traumatic CNS injuries. The implantation of stem cells at the injury site should provide neuroprotection against systemic inflammatory processes and neuro-regenerative benefits such as improved neurogenesis and angiogenesis.[101, 102] Basic researchers and clinicians tested several types of stem cells for post-traumatic CNS injury therapy, including human neural stem cells (hNSCs), embryonic stem cells (ESCs), induced pluripotent stem cells (iPSCs), and mesenchymal stems cells (MSCs) derived from adipose tissues (AD-MSCs), bone marrow (BM-MSCs) and umbilical cord (UC-MSCs).[65] In experimental TBI and SCI models, all of these stem cells have demonstrated the capacity to improve neurological outcomes.

Even though the use of stem cells in CNS injuries is a potentially useful tool to improve neurological and functional outcome for TBI and SCI patients, there is a failure to translate this success routinely in the clinical setting. The major reasons cited for the failure of stem cell therapy in CNS injuries are the hostile microenvironment at the injury site and the lack of combinatorial strategies since multiple pathways are involved in the pathophysiology of the secondary damages in TBI.[103] Furthermore, there are still some unresolved issues such as the most appropriate route of administration of cell therapy in order to maximize the survival of the transplanted cells, the optimal therapeutic window for cell transplantation after traumatic CNS injuries, and the best regenerative strategy for restoring the microstructure at the injury site.[104] Because CNS injuries

are complex in nature involving many secondary injury mechanisms, the scientific community believe that the best approach to the treatment of CNS injuries is one that uses a combination of therapies.[104]

The objective of this work is to use combination strategies for the future treatment of CNS injuries. This strategy involves optimally designed injectable biomaterial hydrogels with iron chelating effects and cell loading functions.. To facilitate traumatic CNS regeneration, it is essential that neural stem cells are transplanted in a favorable microenvironment that is conducive for their long term survival and integration within the host tissue. Attributes such as three dimensionality of the graft and adhesive support for transplanted cells facilitates regeneration and integration.[105] Neural tissue engineering (NTE) is a promising strategy for overcoming the limitations of using pharmacological agents or cell therapy alone for the treatment of TBI. It includes the practice of combining biomaterial scaffolds, stem cells and bioactive molecules to create functional constructs that replace, regrow, restore, maintain or improve damaged or diseased tissues.[106, 107] It has the ability to bridge the structural gaps resulting from CNS injuries and allows the reconnection of neuronal processes. Researchers have shown that they can manipulate the microenvironment at the site of TBI to show signs of tissue regeneration, but not enough to restore full motor and cognitive functions in the impaired. This suggests that an oversight in the treatment strategy might be playing a pivotal role in preventing full functional recovery. Biochemical inspection at the TBI injury site indicates that this microenvironment has an unusually high concentration of iron.[108, 109]

Experimental and clinical evidence indicate that excess iron is lethal to cells due to its ability to promote free radical production and the ensuing oxidative stress which is mainly produced by

Fenton or/and Haber-Weiss reactions. The free radicals produced induce cellular damage via their interactions with proteins, lipids, carbohydrate and deoxyribonucleic acid (DNA).[109-112]

It is our belief that mitigate against build-up of iron at the injury site will help to alleviate deleterious events and improve the chance for improved functional recovery. To achieve this goal we will develop several families of iron chelator-polymer conjugates (ICCs) for future traumatic CNS injury treatment. The designed ICCs are hydrogels; whose components when mixed and injected will gel at the injury site. Local delivery at the injury site via injection will help to overcome the challenges of systemic delivery of therapeutics across the BBB. These injectable hydrogels used as NTE scaffolds, will mimic the microstructure of brain extracellular matrix (ECM). The overall hypothesis to be tested is that the prepared iron ICC will facilitate efficient iron chelation and support neural stem cell survival and proliferation. To test this hypothesis, we formulated three specific aims:

2.2 Specific Aim 1: To explore the role of iron chelation in protection of human neural stem cells (hNSCs) by hyaluronic acids (HAs) of different molecular weight.

HA renowned for its traditional biomedical applications in ophthalmology, orthopedic surgery, cosmetic products, dermatology and plastic surgery because of its viscoelastic, viscous lubricating, osmotic, wound healing and space filling properties. However, a recent application of HA is its use as biomaterial scaffold to deliver cells and therapeutic agents at the lesion site. We hypothesize that HA will act as an iron chelator, removing the excess iron via complex formation of HA and Fe^{3+} . To test this hypothesis, we will determine the iron chelation efficiency of HA; determine HA inhibitory effect on Fe^{2+} /ascorbate-induced lipid peroxidation (LP) of linoleic acid as well as in

human neural stem cells (hNSCs). Further, we will study the influence of HA on Fe²⁺/ascorbate-induced oxidative stress on the viability and proliferation of hNSCs.

2.3 Specific aim 2: To synthesize and characterize families of iron chelator-polymer conjugates (ICCs) based on the combination of three iron chelators and two polymers.

Each conjugate will contain either the polymer hyaluronic acid (HA) or poly (ethylene) glycol (PEG) and an iron chelator. Four families of ICCs resulted from the synthesis based on the iron chelator conjugated to the polymer, namely quinolones, siderophores, flavonoids or curcuminoids. The sub-hypothesis tested here is that each component of the conjugate will play a specific role in protecting neural stem cells under high iron concentrations. HA and PEG are highly hydrophilic, biocompatible, non-immunogenic and non-antigenic polymers used in an impressive range of biomedical applications. Addition of these polymers to the iron chelators or bioactive molecules will greatly enhance their water solubility, circulation half-life and reduce their cytotoxicity. PEG and HA are ideal polymers for constructing hydrogels for future CNS tissue regeneration, as their mechanical properties are tunable by the degree of crosslinking and molecular weight of polymer to mimic the native microenvironment of the CNS tissues. HA and the iron chelator both have iron chelating abilities and removing the excess iron will help to protect neural cells. The ICCs will be synthesized using facile chemical reactions; mainly EDC/NHS mediated bioconjugation under aqueous conditions. The prepared ICCs were characterized and verified by Fourier transform infrared spectroscopy.

2.4 Specific Aim 3: To engineer injectable iron chelator-bound hydrogel (ICH) scaffolds as permissive niche for neural stem cell growth, viability, and proliferation.

The sub-hypothesis tested here is: if the designed, highly biocompatible ICHs mimic the biochemical and biomechanical properties of the native CNS tissues, then they will improve the viability and proliferation of neural stem cells. If this is a valid assumption, then it is highly probable that they will promote cellular and regenerative processes when administered *in vivo* at the CNS injury site in the future studies.

CHAPTER 3

3 The Role of iron Chelation in Protection of Human Neural Stem Cells (hNSC) by Hyaluronic Acid (HA).

3.1 Introduction

Hyaluronic acid (HA) is a naturally occurring polysaccharide composed of alternating β -1, 4-glucuronic acid, and β -1, 3-N-acetylglucosamine units. [113] It is found throughout the body as a structural component of the extracellular matrix (ECM) with molecular weight as high as 10^7 Dalton.[114] HA mediates many physiological functions including cell proliferation, cell

migration, cell adhesion, morphogenesis, angiogenesis, tumorigenesis, inflammation, differentiation, and wound repair.[115-117] The ability to modulate the aforementioned cellular processes and its significant level in the ECM of the central nervous system (CNS) makes HA an attractive biomaterial for CNS regeneration.[118]

Experimental and clinical studies indicate that free radicals play a key role in secondary CNS injuries and uncontrolled reactive oxygen chain reactions can create an endless pool of free radicals which will ultimately induce oxidative damage and massive neuronal death.[119, 120] Currently, HA is widely applied in the field of CNS tissue engineering for its neuroprotective effects, which stem from its ability to scavenge free radicals *in vitro* and *in vivo*. [121-124] Several researchers investigated the neuroprotective effects of HA oligosaccharides in the CNS. Wakao et al. and Wang et al. applied HA4 (HA with two (2) disaccharide units) to spinal cord injury (SCI) sites in a clinically relevant rat model. They observed that HA4 exhibited neuroprotection because functional recovery in rats treated with this oligosaccharide improved significantly.[125-127] Torigoe et al. and Lin et al investigated the neuroprotective effect of HA4 using a film model method. Torigoe et al hypothesized that HA4 can promote the viability of neurons *in vivo* after injury and promote their regeneration. They found that optimal axonal outgrowth occurred when the films were treated with 100 µg/mL of HA4.[128] Lin et al. created a cortical lesion in the brains of rats, coated it with 3% HA gel, and later retrieved the brains at acute time points (4, 8 and 12 weeks) after treatment. They observed that the thickness of gliosis and the numbers of glial fibrillary acid protein-positive (GFAP+) cells were significantly reduced in groups treated with HA.[129] *In vivo* CNS applications of HA is frequently in the form of chemically or physically modified hydrogel scaffolds because native HA is not mechanically durable and it is rapidly degraded by hyaluronidase, an enzyme that is ubiquitous throughout the body.[130, 131] In recent

times, a number of research groups have used HA hydrogel scaffolds to deliver bioactive agents and neural stems to the CNS. In all investigations the HA scaffold exhibited neuroprotection as cell viability and survival were enhanced.[132-135]

The neuroprotective effect of HA in the CNS is well researched but the exact mechanism(s) through which it exerts its neuroprotection is not clearly elucidated. Most researchers agree that HA facilitates healing by interrupting the molecular processes involved in the secondary damages during traumatic CNS injuries. Demopoulos et al. and Ortega et al. proposed the idea that the CNS is highly prone to tissue damage by reactive oxygen species (ROS) due to several reasons. First, membrane lipids are rich in cholesterol and polyunsaturated fatty acids (PUFA), which are highly susceptible to free radicals. Secondly, the CNS has low levels of catalase and moderate amounts of superoxide dismutase and glutathione peroxidase, which limits the capacity of these endogenous antioxidants to combat free radical damage and maintain the balance of free radicals produced in the CNS.[136-138] The current perspective on the neuroprotective role of HA suggests that it exerts neuroprotection against ROS via the transfer of hydrogen atoms or electrons.[139] However, this perspective does not account for all the mechanisms by which HA could possibly protect CNS tissues from damage by ROS. Another mechanism could involve the ability of HA molecules to chelate iron (II) ions; these ions are essential in the Fenton reaction, which produces the highly reactive hydroxyl radical ($\cdot\text{OH}$). This therapeutic approach reduces the availability of these ions via chelation with HA, thus making iron (II) ions unavailable to participate in the generation of $\cdot\text{OH}$. [140] Close examination of the structure of HA reveals that it is a poly-anionic molecule due to the presence of carboxylic acid groups on the glucuronic acids of the disaccharide repeating units. This poly-anionic character allows for the formation of ligand-metal interaction between HA and iron (II).

In this paper, we hypothesized that HA facilitates healing in CNS injuries in part by acting as an iron chelator via complex formation between HA and iron (II). The HA should reduce the level of iron at the site of injury as well as reduce the catalyst's needed for the generation of •OH. A reduction in the formation of oxygen reactive species will attenuate oxidative stress and minimize tissue damage as a result of the oxidation of lipids, proteins, and DNA.[141] In the present study we evaluated (i) the iron chelation capacity of HA, (ii) the antioxidant capacity of HA for inhibiting the lipid peroxidation (LPO) of linoleic acid (LA) and hNSCs, (iii) the inhibitory effect of HA on iron/ascorbate induced oxidative stress in hNSCs.

3.2 Experimental Section

3.2.1 Materials

All reagents were purchased from Sigma Aldrich Chemical Co. (St. Louis MO) or VWR International unless otherwise noted. The reagents used in this study were iron (III) chloride hexahydrate ($\text{FeCl}_3 \cdot 6\text{H}_2\text{O}$), iron (II) chloride tetrahydrate ($\text{FeCl}_2 \cdot 4\text{H}_2\text{O}$), hydrochloric acid (HCl), hyaluronic acid (HA), sodium citrate, hydroquinone, phenanthroline, α -linolenic acid (α -LA), sodium acetate, acetic acid, sulfuric acid (H_2SO_4), Brij 35, dichloromethane (CH_2Cl_2), phosphate buffer saline (PBS), accutase, butylated hydroxytoluene (BHT), and, ascorbic acid (AA). The CellTiter-Blue assay kit was from Promega (Madison, WI) and multiwell plates (for suspension culture) from Greiner Bio-One (Monroe, NC).

3.2.2 Iron (III) Calibration Curve

Prepare a series of acidified iron (III) standards ranging in concentration from 14.2 μM to 114.0 μM . Use hydroquinone to reduce the iron (III) in solution to iron (II) by adjusting the pH to 3.5 with sodium citrate. Add a solution of 1, 10-phenanthroline to the solution and allow the orange-

red complex to develop. Analyze the solution with UV-visible spectroscopy and prepare the calibration curve for iron (III) from the absorbance maximum of each spectrum.

3.2.3 Iron Chelation Efficiency of HA

The chelation efficiencies of HA with different molecular weights (5 - 2130 kDa) were assessed. First, prepare HA-iron (III) complexes by mixing iron (III) solution (in excess) with HA, and leave the solution under magnetic stirring overnight to facilitate complex formation. The next day, determine the amount of unreacted (iron (III)) in the samples in a similar fashion as described above.

3.2.4 Inhibition of Iron/Ascorbate-induced Lipid Peroxidation of α -Linoleic acid by HA

The micelle model of LPO used in this work was adapted from the procedure of Sy and coworkers.[142] The method in brief, the micelle working solution contained 250 μ L of 56 mM α -LA and 2.0 mL of a 40.0 mM stock solution of 30% (w/w) Brij 35 in CH_2Cl_2 . To test the influence of HA on the LPO of α -LA, add 0.0200 g HA dissolved in 250 μ L of H_2O to the micelle solution. Vortex the samples using a vortex mixer for 30 seconds to disperse the fatty acid. Remove the CH_2Cl_2 under reduced pressure (N_2) and dissolve the dried viscous residue in 20.0 mL of aqueous 0.2 M acetate buffer. Cover the sample vial with foil paper to protect it from light. Prepare three replicate sample for the LPO experiment. First, cover the vials with foil paper, add 250 μ L of micelle solution to each vial and dilute to 5 mL with sodium acetate buffer. A sample blank was prepared using 5 mL of 0.2 M sodium acetate buffer. Initiate oxidation in the samples by adding 400 μ L of 1 mM Fe^{2+} solution acidified with 0.1 M H_2SO_4 and 1 mM AA. Add a magnetic stirrer to each vial, stir the solution at 37°C, and follow the LPO of the samples by monitoring the concentration of the CDs every 0.5 h by UV-VIS spectroscopy at 234 nm.

3.2.5 Cell Culture

This study used human neural stem cells (hNSCs) purchased from Millipore Sigma (Billerica, MA). The stem cell is an immortalized human neural progenitor cell line derived from the ventral mesencephalon region of human fetal brain and immortalized by retroviral transduction with the v-myc oncogene. The hNSCs were cultured in maintained in DMEM/F12 basal medium (Thermo Fisher Scientific, MA, USA) supplemented with 20 ng ml⁻¹ basic fibroblast growth factor (FGF-2, Peprotech, Rocky Hill, NJ) and 20 ng ml⁻¹ epidermal growth factor (EGF, Peprotech). Culture flask and well plates (24 or 48-well plates) pre-treated with PVAVS and proprietary integrin-based peptides were the surfaces used for adherent hNSC culture. First, add PVAVS to the surfaces for 5 minutes, and then rinsed with PBS. The PVAVS formed a thin layer of hydrogel containing disulfide linkages on the cell culture surfaces, which facilitated the adhesion of the integrin-based peptides to the surface. The integrin-based peptides remained on the cell culture surfaces for 90 minutes under incubation conditions. After the incubation period, remove the peptide solution from the cell culture surfaces and rinse with PBS. The surfaces are now ready for the culture of adherent hNSC.

Add the culture medium to the cell culture container: 10-12 mL in the 250 mL flasks, 500 μ L per well in 24 well plates and 250 μ L per well in the 48-well plates. Rapidly thaw cryo-preserved hNSCs in a 37°C water bath, ensuring that the cap of the cryo vial is above the water. Once thawed, spray the vial with 70% alcohol and wipe with Kim wipe, transfer the cells to a 15 mL conical centrifuge flask and add 10 mL of complete media. Centrifuge at 220 RCF (relative centrifugal force) for 5 minutes and remove the supernatant to eliminate the DMSO. Re-suspend the cells in 1-5 mL complete media and gently mix by micro pipetting the solution up and down to break up cell aggregates into small clusters. Transfer the cells to the pre-treated flasks or well plates and

incubate at 37°C and humidified air with 5% CO₂. Feed the cells within 24 hours of passaging and every 48 hours thereafter. The cells used in this study did not exceed the tenth generation of passaging.

3.2.6 Inhibition of Iron/Ascorbic Acid-Induced Lipid Peroxidation in hNSCs by HA

An evaluation of CDs in cell lysate samples facilitated the determination of the extent of LPO in the hNSCs cultures. The cultured hNSCs adhered to the surface of six-well plates pre-coated with an integrin-based sulfur-cross-linked peptides designed to enhance cell adhesion. Add HA solution to the appropriate wells and incubate for 4 h, when the cells attained 80% confluence. The subsequent addition of 40 mM stock iron (II) solution to the appropriate wells induced oxidative stress to obtain a final iron (II) concentration of 1.0 mM, 2.5 mM, and 5.0 mM, respectively. Add 50 mM ascorbic acid to the wells with the exception of the controls to ensure that iron (II) was recycled in solution. Further, incubate the cell samples for another 2.0 h to allow time for free radical production, and then wash twice with 1.0 mL of PBS buffer. Add cold sterile water to each well and sonicate the cells for 1 minute at a power setting of 180 W. Sonicate the cells in short bursts (10 s sonication and 10 s rest for each cycle) and keep the sample on ice during the sonication process. A chloroform/methanol (2:1) mixture facilitated the extraction of lipids from the cell lysate and subsequently dried the samples under an atmosphere of nitrogen. Dissolve the residue in cyclohexane and use a derivative spectrophotometric (UV-VIS) to evaluate the amount of CDs from the cell content.

3.2.7 Influence of HA on Iron/Ascorbate-induced Oxidative Stress on the Viability of hNSCs.

CellTiter Blue assay facilitated the determination of the effect of HA on the viability of hNSCs following iron (II)-induced oxidative stress. Culture adherent hNSCs in 24-well plates at a seeding density of 7,500 cells per well and incubate for 16-24 h. On Day 0, when the cells firmly attach, replace the culture medium with 500 μ L of CellTiter Blue Solution (CellTiter Blue and medium in a ratio of 9:1). Incubate the cells for 2 h, after the incubation period remove the CellTiter Blue solution from the 24-well plate and add at least four 100 μ L amounts of each group to 96-wellplates and obtain fluorescence readings at 560 nm/590 nm (excitation/emission wavelength) using a microplate reader (SpectraMax, Molecular Devices). Prior to CellTiter Blue assay, on days 1, 3, 5 and 7, add fresh medium with and without HA (1.0 mg/mL in each well) to the assigned wells and incubate for 4 h. Subsequently add Fe^{2+} (0.75 mM, 1.0 mM, 1.25 mM, 1.5 mM and 3.0 mM) and 50 mM AA to the assigned wells. Add media only (Do not add iron) to the wells assigned to the three control groups containing media only, HA and AA, respectively. Incubate the well plates for an additional 2 h for free radical production. At the end of the incubation period, aspirate the medium and add fresh media. The next day, evaluate the viability of the cells via CellTiter Blue assay.

3.2.8 Histochemical staining with Fluorescent Phallotoxin and DAPI to determine morphology of hNSC via Confocal Microscopy.

Each day, after the CellTiter Blue viability assay, fix and stain the adherent hNSC grown in monolayer in the well plates with actin and DAPI dyes and later examine their morphology via confocal microscopy.

3.2.8.1 Fix Adherent hNSCs with 4% Paraformaldehyde Solution in PBS

First, make 250 mL of 16% paraformaldehyde (PFA) stock solution using the procedure described herein. Add 160 mL 1x PBS to a 600 mL glass beaker in a water bath, with stirring in a

ventilated hood. Ensure that the temperature of the water bath remain under 70°C to prevent the evaporation of the PFA. Allow the PFA (stored in the refrigerator) to come to room temperature and then add 40 g of the powder to the heated PBS solution. The powder will not immediately dissolve; slowly increase the pH by adding 1 M NaOH dropwise from a pipette until the solution clears. Once the PFA dissolves, cool and filter the solution and adjust the volume to 250 mL with 1x PBS in the fume hood. Re-check the pH and adjust it with small amounts of dilute HCl to pH 7.4 if needed. The solution is aliquoted and frozen (-80°C) and can be stored for at least 5 years.

Fix the hNSCs with a 4% PFA working solution. This solution is prepared using the procedure described herein. Pipette 8 mL of 16% PFA stock solution in a 50 mL tube with 32 mL 1x PBS and mix well. Aspirate cell culture medium from the well plates and wash the well by adding 250 µL (48-well plate) or 500 µL of 4% PFA solution per well. Aspirate the PFA, and add the same volume of PFA solution to each well and incubate at room temperature for 25 minutes. After the time has elapsed, aspirate the PFA solution and wash the cells with PBS at least three times. Wrap the fixed cells in parafilm and store at 2-8°C and use within six (6) months.

3.2.8.2 Staining hNSCs with Actin Dye (Phalloidin-iFluor 555 conjugate) and DAPI Dye.

Permeabilize hNSCs prior to staining with actin dye by adding 0.1 % triton x-100 in PBS to the well plates for 5 minutes. Wash three times with PBS; wait 5 minutes between each wash. Additionally, pre-incubate fixed/permeabilized hNSCs with PBS containing 1% BSA for 25 minutes prior to adding actin dye as this reduces background staining. Warm the vial with phalloidin conjugate to room temperature and centrifuge briefly before use. Prepare a 1x phalloidin conjugate working solution by adding 1 µL of the supplied stock solution (1000x phalloidin conjugate in DMSO) to 1 mL of PBS containing 1% BSA. Add the staining solution to the well

plates containing the fix/permeabilized cells and incubate for 20 minutes at 37°C. To avoid evaporation, keep the well plates covered during the incubation. Rinse gently with PBS twice to remove excess phalloidin conjugates before imaging under the microscope.

Perform 4',6-diamidino-2-phenylindole (DAPI) staining after all other staining. First, prepare the 5mg/mL DAPI stock solution (14.3 mM for the dihydrochloride or 10.9 mM for the dilactate) by dissolving the content of one vial (10 mg) in 2 mL de-ionized water or dimethylformamide (DMF). Equilibrate the sample briefly by adding PBS to the wells for about 3 minutes. Dilute the DAPI stock solution to 300 nM in PBS; remove the PBS from the well plates and DAPI solution ensuring that the cells are completely covered. Incubate for 5 minutes, and then rinse the sample several times in PBS. Add PBS to the wells; view the samples using a fluorescent microscope with appropriate filters. Wrap the sample with parafilm wrap and store the sample at 2-8°C for a short time if additional microscopic analysis is required.

3.2.9 Statistical Analysis

All data in this study are presented as mean \pm SD. Data were analyzed in excel and p-values obtained from the data regression analysis tool

3.3 Results

3.3.1 Iron Chelation Efficiency of Hyaluronic Acid

This paper presents the idea that HA provides neuroprotection and facilitates healing in CNS injuries because HA has the ability to chelate iron. HA-iron (III) complexes were formed by mixing iron (III) with HA of various molecular weights (5 -2000 kDa). Prior to the formation of HA-iron (III) complexes, a calibration curve was prepared from a series of iron (III) standards up to 114.0 μ M. The method used to prepare the calibration curve was adapted from the work of

Atkins.[143] In brief, sodium citrate used to adjust the pH of the iron (III) standards and hydroquinone used to reduce iron (II) ions. A solution of 1, 10-phenanthroline was added and the orange-red complex allowed to develop. Analyze each complex via UV-VIS spectroscopy and the absorbance maximum at ~510 nm used to create the calibration curve shown in **Figure 3.1**. After the formation of HA-iron (III) complexes, the free iron (III) in solution was reduced by hydroquinone and complexed to 1, 10-phenanthroline and analyzed by UV-Vis spectroscopy. The concentration of free iron (III) in solution was calculated from the absorbance maxima and the calibration curve, assuming that all the unreacted iron (III) was converted to iron (II). The concentration of iron (III) complexed to HA was determined by taking the difference between the initial concentration of iron (III) mixed with HA solutions and the free iron (III) concentrations. The UV-VIS spectra of the tris (1, 10-phenanthroline) iron (II) complexes prepared from the free iron (III) present in the HA-iron (III) complexes are shown in **Figure 3.2**.

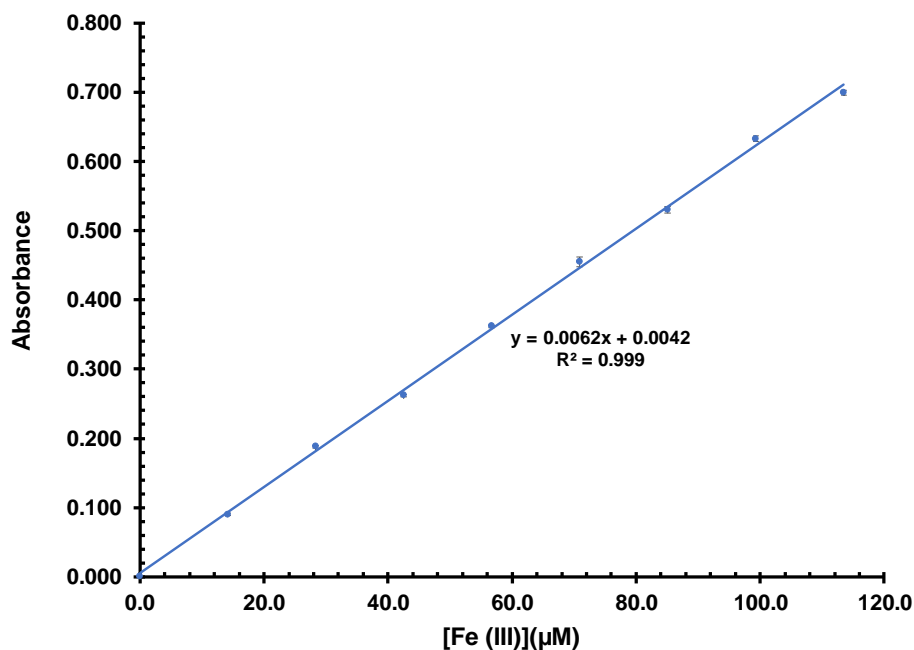


Figure 3.1: Calibration curve for iron (III) standards obtained from the absorption spectrum of the (1, 10-phenanthroline) Fe (II) complex.

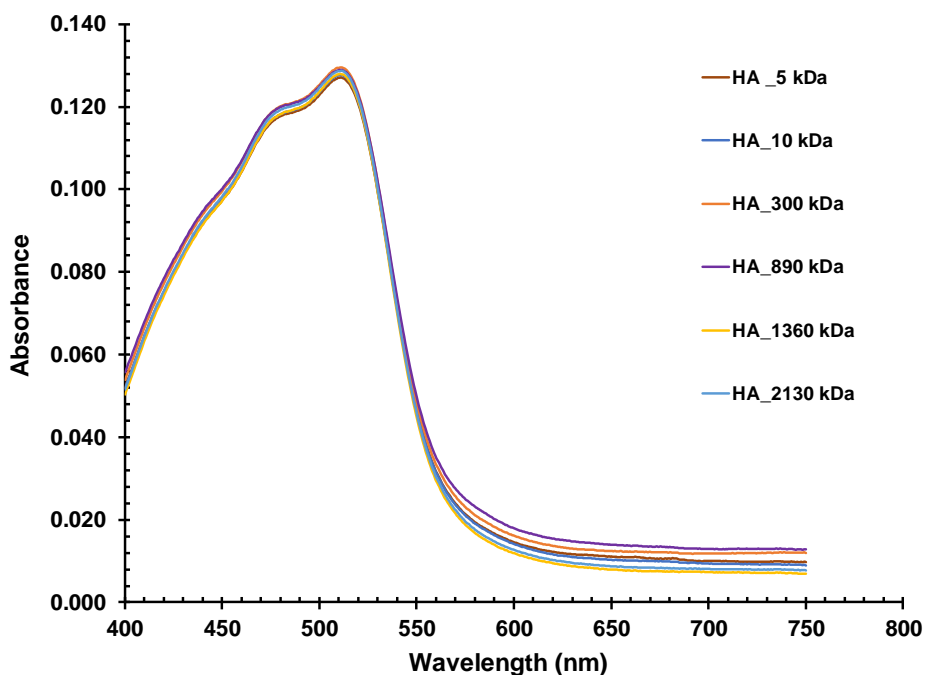


Figure 3.2: UV-VIS Spectra for Tris (1, 10-phenanthroline) iron (II) complexes formed from unreacted iron (III) following HA-iron (III) complexation.

The iron chelation efficiency of HA of different molecular weights were evaluated by a comparison of the iron (III) complexed to HA with the initial amount of iron (III) added to the reaction vessel. The iron chelation efficiencies shown in **Table 3.1** are the results of calculations from **Equation 3.1**.

% Chelation Efficiency

$$= \frac{[\text{Fe (III)}]_{\text{complex formation}}}{[\text{Total Fe (III)}]_{\text{amount prior to complexation}}} \times 100 \quad \text{eqn. 3.1}$$

Table 3.1 provides a summary of the iron chelation efficiency of HA of different molecular weights. The chelation efficiency of HA is independent of its molecular weight; it has a chelation efficiency of ~74.00%.

Table 3.1: The iron chelation efficiency of hyaluronic acid of different molecular weights

Molecular Weight HA (kDa)	Fe (II)-phenanthroline complex		Fe (II)-phenanthroline Complex after complexation with HA		Chelation Efficiency (%)
	[Fe (II)] (μM)	ABS	[Fe (II)] (μM)	ABS	
5	57.34	0.3574	15.08	0.0977	73.70
10	57.34	0.3574	14.98	0.0971	73.89
300	57.34	0.3574	15.27	0.0989	73.37
890	57.34	0.3574	15.12	0.0980	73.63
1360	57.34	0.3574	15.00	0.0972	73.84
2130	57.34	0.3574	15.11	0.0979	73.65

3.3.2 Inhibition of Iron/Ascorbate-induced Lipid Peroxidation of α -Linoleic acid by HA

Iron (II) /ascorbate-induced LPO was carried out LA in the micelle model. Oxidation of LA results in the formation of CDs which serves as an indicator of oxidation and can be estimated with UV-VIS spectroscopy.[144] UV-VIS spectroscopic monitoring of LPO in the absence and presence of HA is shown in **Figures 3.3a** and **3.3b** respectively. The characteristic absorption band was observed at ~ 234 nm, indicative of CDs monitored during spectroscopic analysis.[145] The amount of CD produced during LPO increased over the time span of the experiment. The greatest increase in conjugated diene signal was seen in the first 30 minutes of the experiment because initially all the LA molecules were available to be converted to CD. The amount of LA available for CD formation became less as the experiment progressed and consequently there was a smaller gradual increase in CD signals. Further, the propagation rate for LPO in the presence of HA was lower than in the control (LPO of LA). In fact, HA inhibited LPO for each measurement taken when compared to the control.

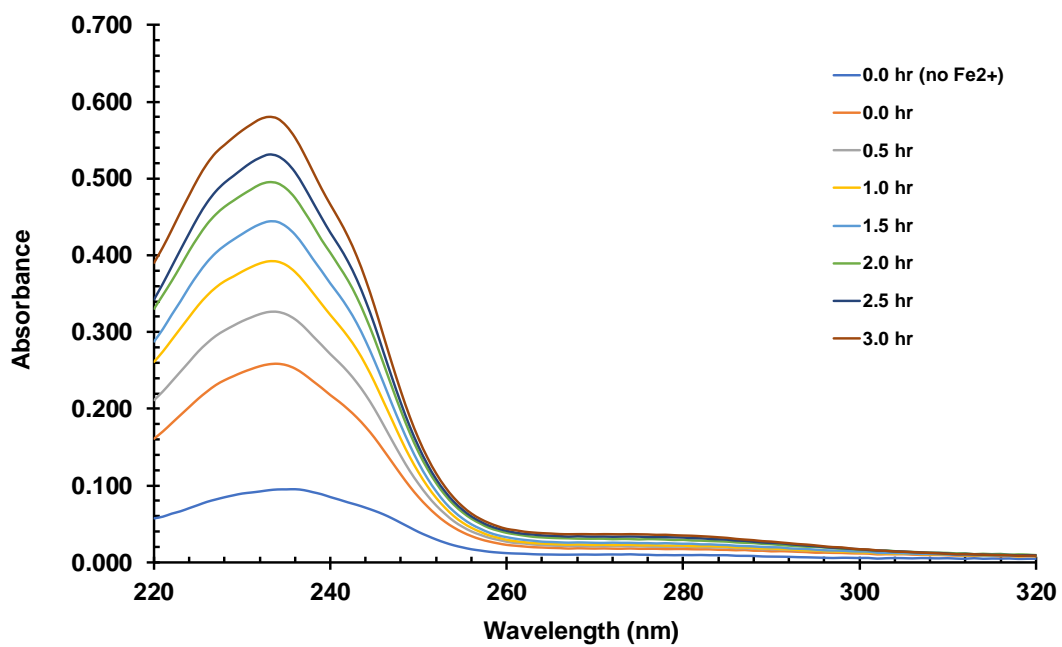


Figure 3.3a: Fe-induced lipid peroxidation of linoleic acid in a pH 4.0 micelle model. The UV-vis spectrum shows the accumulation of CDs measured over three hours.

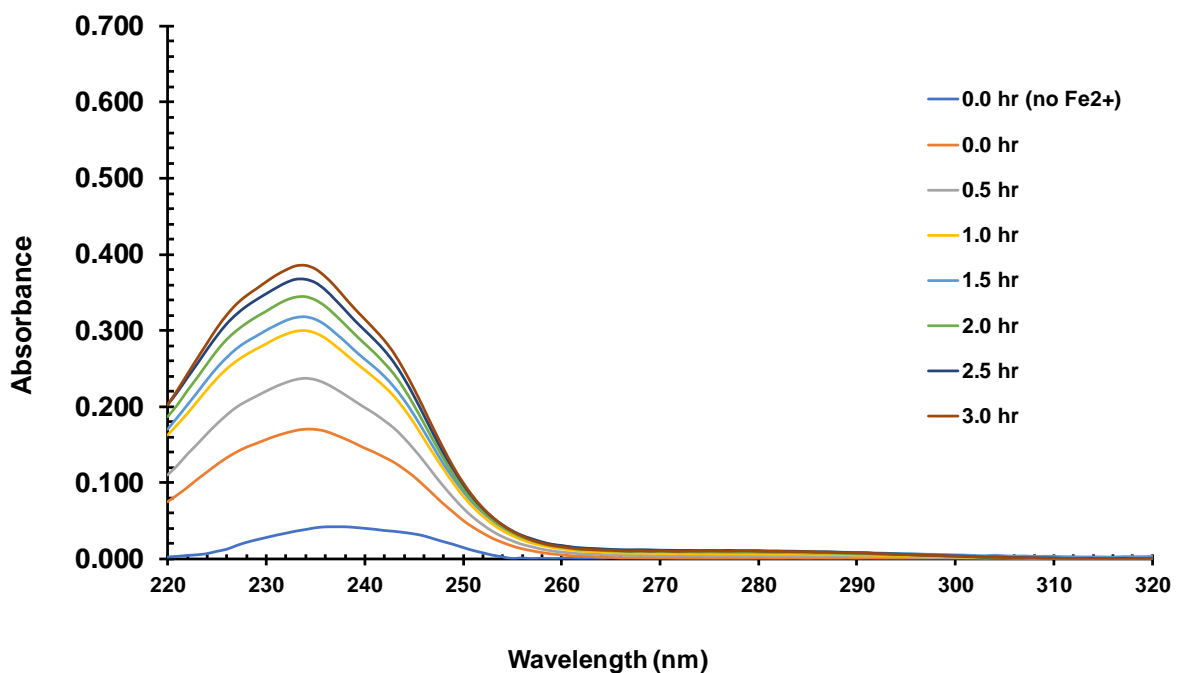


Figure 3.3b: HA inhibition of Iron-induced lipid peroxidation of linoleic acid in a pH 4.0 micelle model. The UV-vis spectrum shows the accumulation of CDs measured over three hours.

Additionally, kinetic curves plotted from the spectroscopic data obtained for LPO in the presence and absence of HA also illustrate the inhibitory effect of HA. **Figure 3.4** compares the rate of formation of CDs in the presence and absence of HA. The kinetic curves show that CDs formed rapidly in the first 30 minutes of the experiment for both HA-treated LA and LA. The rate of CD formation plateaued for HA-treated LA while the rate of CD formation continued unabated for LA in the absence of HA. This proves that HA inhibits LPO of LA possibly by chelating Fe^{2+} making less available for LPO and CD production.

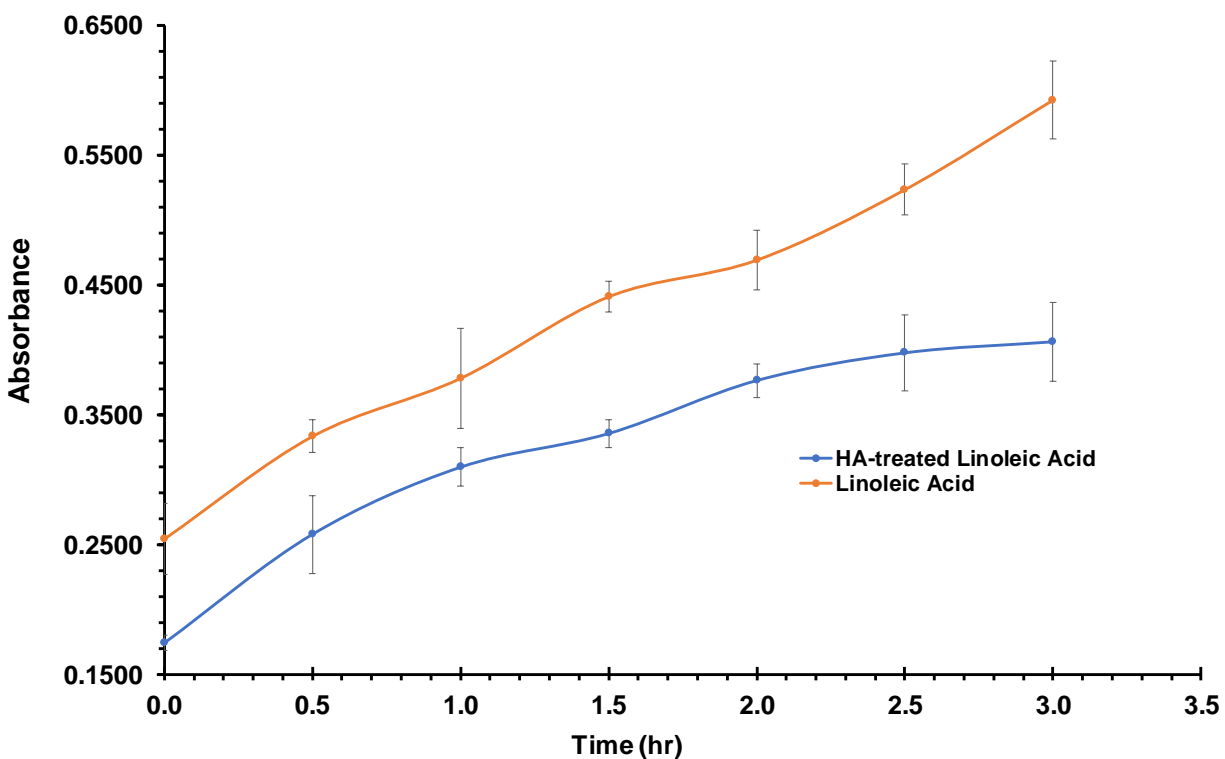


Figure 3.4: Kinetic curves for conjugated diene formation in the presence and absence of HA

3.3.3 Inhibition of Iron/Ascorbic Acid-Induced Lipid Peroxidation in hNSCs by HA

In this work, hNSC lysates were the *in vitro* model for assessing iron (II) / ascorbate-induced LPO in hNSCs. Diene conjugation accumulation estimated the extent of LPO and this was determined through UV-VIS spectroscopy. **Figure 3.5a** shows the UV-VIS spectra for CDs extracted from cell lysates in which LPO was induced by 1.0, 2.5, and 5.0 mM iron II)/ascorbate.

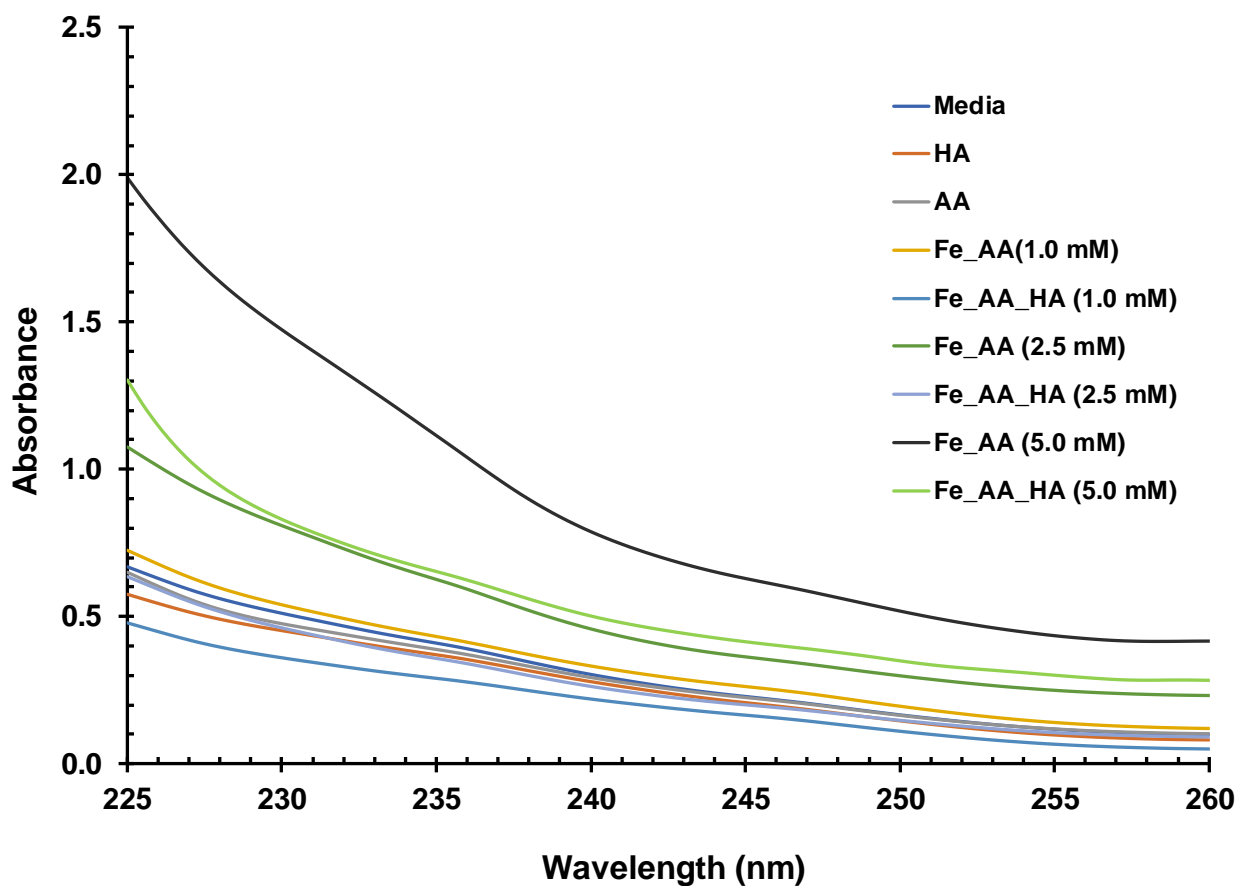


Figure 3.5a: Conjugated dienes extracted from hNSC lysates after iron (II)/ascorbate-induced lipid peroxidation (Normal spectra).

The characteristic CD absorption peak between 233-235 nm was absent from normal UV-VIS spectroscopy. **Figure 3.5b** shows the derivative spectra for the CD extracted from cell lysates and the representative CD peak at ~235 nm. The control groups show low concentrations of CD, values typical under normal physiological conditions. Iron (II) influenced the rate of formation of conjugated dienes in a concentration-dependent manner. As observed from the derivative spectra, the greater the iron (II) concentration, the greater the signal of the conjugated diene. The increased level of iron in the system facilitated sustained LPO and as a consequence, a higher concentration

of CDs. The Addition of HA inhibited LPO, in all instance the signal for CDs in the presence of HA was lower than in its absence.

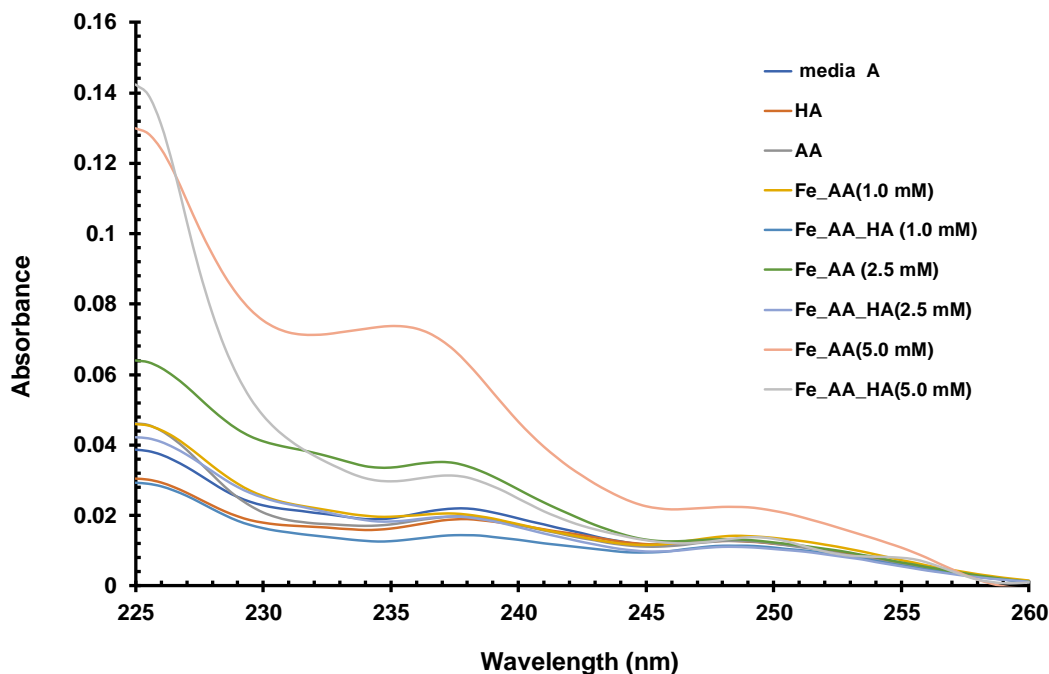


Figure 3.5b: Conjugated dienes extracted from hNSC lysates after iron (II)/ascorbate-induced lipid peroxidation (derivative spectra)

3.3.4 Influence of HA on Iron/Ascorbate-induced Oxidative Stress on the Viability of hNSC.

The effect of HA on iron (II)/ascorbate-induced oxidative stress on cell viability was investigated over a seven-day period. Iron (II) concentrations ranging 0.75 - 3.00 mM induced oxidative stress in hNSCs and 50 mM ascorbic acid served as an reducing agent redox cycling iron (III) to iron (II). Initial exposure of cells to iron (II)/ascorbate did not produce a noticeable difference between the groups, shown in **Figure 3.6a**. However, repeated exposure of hNSCs to iron/ascorbate-induced oxidative stress resulted in higher mortality and growth inhibition in cells not treated with HA. On day 3 (**Figure 3.6b**), the cells treated with 0.75 mM iron (II) proliferated at a rate equivalent to that of cells in the control groups.

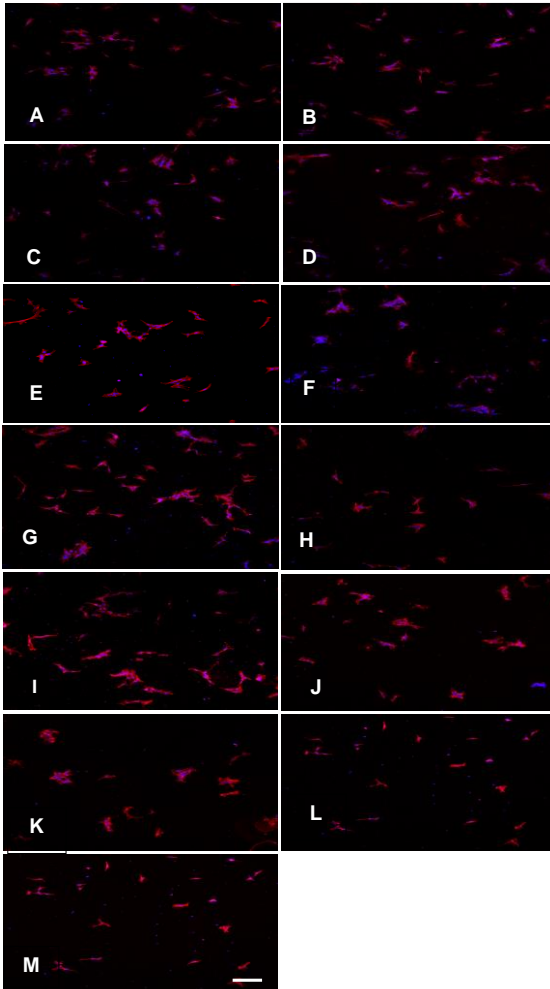


Figure 3.6a: Confocal images on day 1 (A) media, (B) HA, (C) AA, (D) 0.75mM Fe_AA, (E) 0.75 mM Fe_AA_HA, (F) 1.0 mM Fe_AA, (G) 1.0 mM Fe_AA_HA, (H) 1.25 mM Fe_AA, (I) 1.25 mM Fe_AA_HA, (J) 1.5 mM Fe_AA, (K) 1.5 mM Fe_AA_HA, (L) 3.0 mM Fe_AA, (M) 3.0 mM Fe_AA_HA.

Scale bar = 50 μ m

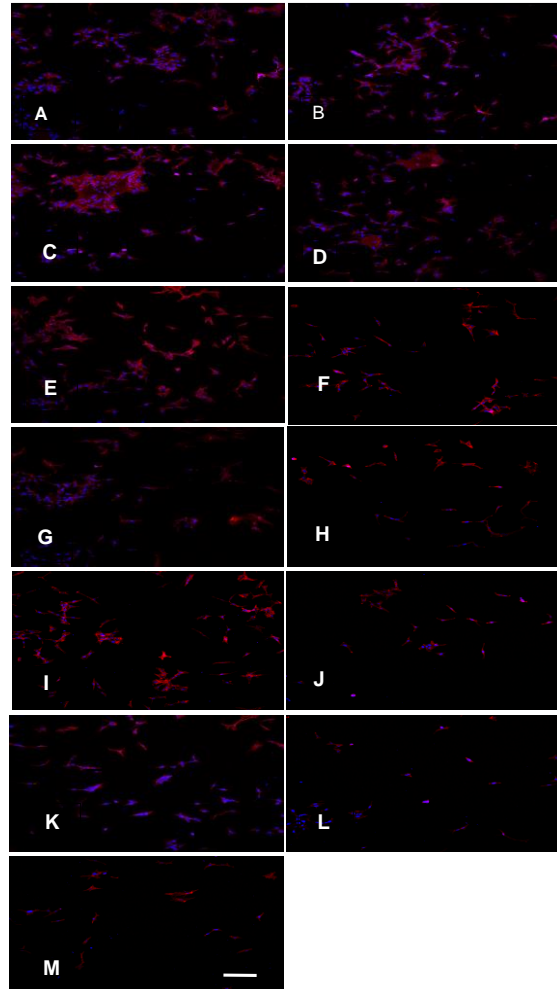


Figure 3.6b: Confocal images on day 3 (A) media, (B) HA, (C) AA, (D) 0.75mM Fe_AA, (E) 0.75 mM Fe_AA_HA, (F) 1.0 mM Fe_AA, (G) 1.0 mM Fe_AA_HA, (H) 1.25 mM Fe_AA, (I) 1.25 mM Fe_AA_HA, (J) 1.5 mM Fe_AA, (K) 1.5 mM Fe_AA_HA, (L) 3.0 mM Fe_AA, (M) 3.0 mM Fe_AA_HA.

Scale bar = 65 μ m

Cells treated with 1.0- and 1.5-mM iron (II) in the presence of HA proliferated more compared to those treated with 1.0- and 1.5-mM iron (II) alone. The cells treated with 1.25-3.0 mM Fe²⁺ only experienced higher mortality and growth inhibition due to more intensive ROS production. Confocal images of cells on days 5 and 7, **Figures 3.6c and 3.6d respectively**, exhibited similar trends to that

observed on day 3. Cells treated with 0.75 mM Fe²⁺ in the absence and presence of HA and cells treated with 1.0 mM Fe²⁺ in the presence of HA grew at a similar rate to that of the control groups. While cells treated with higher concentrations of iron experienced growth inhibition and greater mortality.

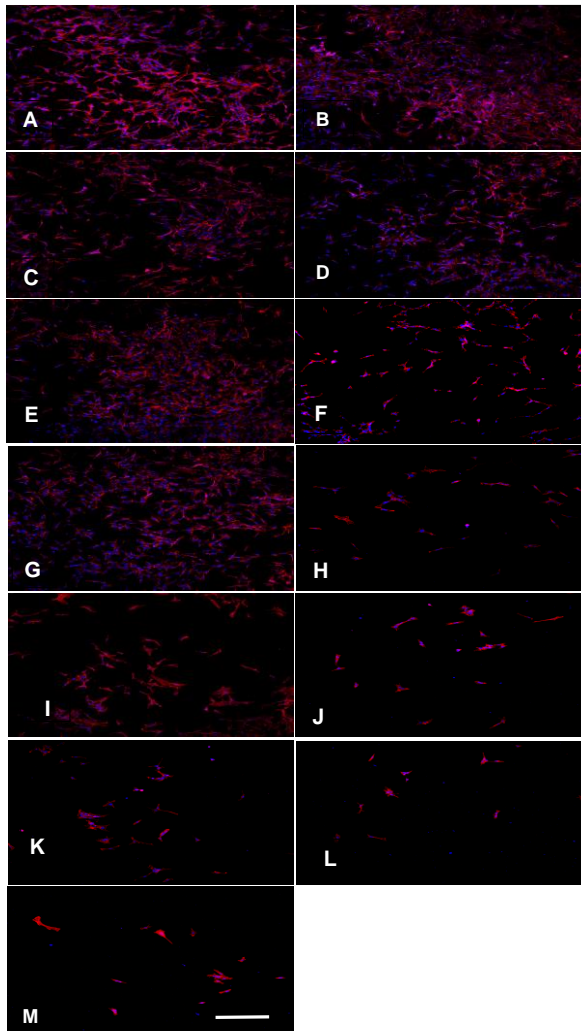


Figure 3.6c: Confocal Images on Day 5 (A) media, (B) HA, (C) AA, (D) 0.75mM Fe_AA, (E) 0.75 mM Fe_AA_HA, (F) 1.0 mM Fe_AA, (G) 1.0 mM Fe_AA_HA, (H) 1.25 mM Fe_AA, (I) 1.25 mM Fe_AA_HA, (J) 1.5 mM Fe_AA, (K) 1.5 mM Fe_AA_HA, (L) 3.0 mM Fe_AA, (M) 3.0 mM Fe_AA_HA

Scale bar = .90 μ m

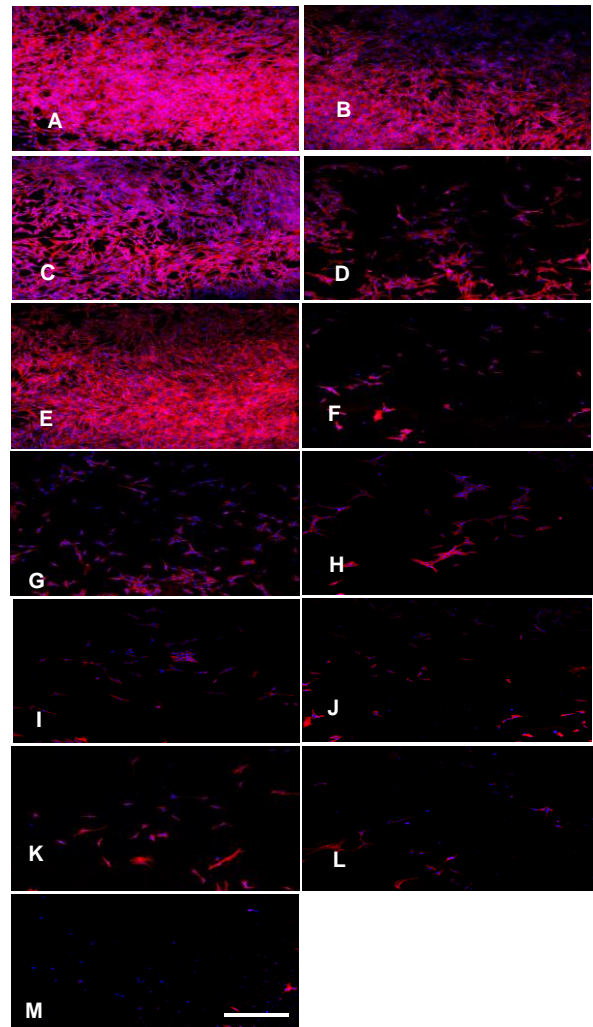


Figure 3.6d: Confocal Images on Day 7 (A) media, (B) HA, (C) AA, (D) 0.75mM Fe_AA, (E) 0.75 mM Fe_AA_HA, (F) 1.0 mM Fe_AA, (G) 1.0 mM Fe_AA_HA, (H) 1.25 mM Fe_AA, (I) 1.25 mM Fe_AA_HA, (J) 1.5 mM Fe_AA, (K) 1.5 mM Fe_AA_HA, (L) 3.0 mM Fe_AA, (M) 3.0 mM Fe_AA_HA.

Scale bar = 100 μ m

CellTiter-Blue assay provided an estimate of hNSC viability after exposure to iron (II)/ascorbate. The Cell-titer assay is a highly sensitive fluorescent assay in which the primary ingredient is a buffered solution of the indicator dye resazurin, which detects the metabolic activity of viable cells. The CellTiter-Blue reagent was diluted with hNSC culture medium in a 1:9 ratio (1.0 mL titer-blue: 9.0 mL medium) prior to adding to the cells. The 2h incubation period allowed the CellTiter to permeate the hNSC via the cell membrane. Viable cells are able to reduce resazurin (dark blue and non-fluorescent) to resofurin (bright pink and highly fluorescent), while non-viable cells lacked metabolic activity and as a result cannot reduce resazurin to give off a fluorescent signal. O'Brien et al. determined that resazurin reduces to resofurin inside the cell, probably by the action of several redox enzymes. They also determined that the resofurin dye could diffuse out of the cell into the surrounding medium where it can be detected using fluorescence spectroscopy.[146] At the end of the incubation period, the medium/Titer-Blue mixture was transferred from the cell culture to 96-multiwell plates compatible with the fluorescent microplate reader (SpectraMax, Molecular Devices) used to record fluorescent signals at excitation and emission wavelengths of 560 and 590 nm, respectively. **Figure 3.7** graphically illustrates the data from Titer- Blue viability assay after tracking the fluorescent response over 7 days.

On day zero, prior to adding treatment to the experimental groups, the fluorescent responses of all groups were within a narrow range of each other (~1000 -1100 nm; p-value = 0.39). On day one, the number of viable cells in each group increased compared to the signal on day 0 (p-value = 0.22). On day three, p-value analysis found that there were no statistical significance between the groups, since the p-values were greater than 0.05. On day 5, the viability of the cells in groups treated with 0.75 mM iron (II) in the presence and absence of HA were statistically significant (p-value =0.002).

3.3.5 Inhibition of Iron/Ascorbic Acid-Induced Lipid Peroxidation in hNSCs by HA

An evaluation of CD in cell lysate samples facilitated the determination of the extent of LPO in the hNSCs cultures. Culture the hNSCs in peptide pre-coated six-well plates to enhance cell adhesion. Incubate the cells until they are about 80% confluent and then add HA to assigned wells and incubated for 4 h. Subsequently, induce oxidative stress in the appropriate wells with a 40 mM iron (II) stock solution to obtain final iron (II) concentrations of 1.0 mM, 2.5 mM, and 5.0 mM, respectively. Add 50 mM ascorbic acid to the wells with the exception of the controls to ensure that iron (II) was recycled in solution. Further, incubate the cell samples for 2.0 h to allow time for free radical production and then wash them washed twice with 1.0 mL of PBS buffer. Add cold sterile water to each well and sonicate the cells for 1 minute at a power setting of 180 W. Sonicate the cells in short bursts (10 s sonication and 10 s rest for each cycle) and keep the sample on ice during the sonication process. Extract the lipids the cell lysate sample with a chloroform/methanol (2:1) mixture and dried under an atmosphere of nitrogen. Dissolve the residue in cyclohexane and the evaluate amount of CDs from cell content using a derivative spectrophotometric technique.

3.4 Discussion

3.4.1 Iron Chelation Efficiency of Hyaluronic Acid

Iron chelation is a viable theory to explain how HA provides neuroprotection and facilitates healing at injury sites, including CNS injuries, since it is an effective method for the removal of excess iron. Excess iron at the site of injury could be potentially hazardous in two ways: (1) Iron is an essential nutrient for the growth of pathogens and (2) iron is a catalyst in the Fenton reaction, which produces the highly reactive hydroxyl radical ($\bullet\text{OH}$). Even though iron is essential for both

pathogenic and human cell growth, some pathogens are more competitive for iron than human cells and as a result, pathogens proliferate could greatly inhibiting healing or regeneration.[146]

In this study, we determined the chelating efficiency of HA for iron. HA of varying molecular weights were utilized and the results showed that the chelation efficiency was independent of the size of the polymer. The chelation efficiency of HA was determined to be ~74%. The chelation efficiency of HA is independent of the molecular weight at a certain weight (in grams), the amount of effective chelating units (the disaccharide units) does not vary with different molecular weights.

[1] Mercê and co-workers proposed that in aqueous solution iron (III) complexes HA through both sub-units, the N-glucuronic acid and N-acetyl glucosamine, forming a complex with μ -oxo bridges.[147] The disaccharide units in HA are proposed to be a bidentate ligand combining with iron at the carboxylate group of the glucuronic unit and the acetamido group of the N-acetyl glucosamine unit. [148, 149] The N-acetyl glucosamine and D-glucuronic acid simultaneously link two HA chains to the metal.[147]

3.4.2 Inhibition of Iron/Ascorbate-induced Lipid Peroxidation of α -Linoleic acid by HA

LPO is the oxidative deterioration of unsaturated lipids and this process follows a free radical mechanism consisting of three distinct stages: initiation, propagation and, termination. Several agents initiates the *in vitro* oxidation of PUFA, including transition metals such as copper and iron, enzymes, the hydroxyl radical, and ionizing radiation.[150] LA was considered a good model for LPO because this PUFA represents a substantial portion of lipids in the human body and it constitutes the structural components of cell membranes.[151] The Iron (II)/ascorbate system can initiate LPO by grabbing an electron (via hydrogen abstraction) from the unsaturated lipid to produce a lipid free radical. The ascorbate, a reducing agent, is incorporated in the system

to ensure the availability of iron (II); it reduced the iron (III) formed back to iron (II).[152] In the case of LA, iron (II) gains an electron via hydrogen abstraction from carbon number eleven (C11) because it is positioned between the two double bonds, which makes it highly reactive. Resonance stabilizes the resulting lipid free radical wherein the radical may shift to C9 or C13 with the rearrangement of the carbon-carbon double bonds between carbons 10 and 11 and carbons 11 and 12, respectively. The resonant forms are energetically favorable and analysis of mixture from the oxidation of LA yields approximately equal amounts of C9 and C13 radicals with only trace amounts of the original C11 radical.[144, 153] This rearrangement results in CDs which serves as an indicator of oxidation and was estimated with UV-VIS spectroscopy.[144] The characteristic absorption band was observed at ~234 nm, indicative of CD monitored during spectroscopic analysis.[145] A comparison of **Figures 3a and 3b** shows that CD concentration are suppressed in the presence of HA. A suppression of CD concentration is related to a diminished rate of LPO. In fact, we believe that HA chelates iron (II), making it unavailable for the initiation of LPO of LA. **Figure 4** further illustrates the inhibitory effect of HA on LPO of LA; LPO of LA in the absence of HA produced a greater concentration of conjugated dienes when compared to LPO of LA in the presence of HA. After two hours, the rate of CD formation plateaued for HA-treated LA while the CD formation continued unabated for LA in the absence of HA. This shows that HA inhibits the LPO of LA possibly by chelating iron (II); making it less available for LPO and hence impedes CD production.

3.4.3 Inhibition of Iron/Ascorbic Acid-Induced Lipid Peroxidation in hNSCs by HA

Lipids are a principal structural and functional constituents of cells in biological systems, however, these macromolecules are predisposed to oxidation through a variety of pathways.[150]

LPO *in vivo* results in irreversible cellular and tissue damage and is linked with the physiology and pathology of various diseases including inflammation, aging, atherosclerosis, cardiovascular diseases, osteoarthritis, CNS injuries and a number of neurodegenerative diseases.[154-156] Lipids, especially, PUFA are susceptible to oxidation in the presence of metals like iron and copper; these metals act as initiators for LPO as well as the catalyst for the propagation steps of the chain reaction.[144]

In the present study, we evaluated the protective effect of HA on the extent of LPO induced in hNSCs by an iron (II)/ascorbate system. Cell lysates from hNSCs were considered an appropriate model for this evaluation since HA is widely distributed in the ECM of tissues, including neural tissues.[157] Furthermore, there is a high concentration of lipids in the tissues of the CNS which makes them highly susceptible to LPO.[154] Oxidative stress due to the overproduction of ROS and subsequent LPO during traumatic brain and spinal cord injuries is believed to play a crucial role in the secondary injury mechanism.[158] Thus, the inhibition of ROS production and LPO presents viable strategies for therapeutic interventions in CNS injuries.

CD accumulation estimated the extent of LPO and this was determined through UV-VIS spectroscopy. A number of scientists add 50-100 μM iron (II) in the presence of a reducing agent to initiate LPO *in vitro*. Iron (II) participates in electron transfer reaction with O_2 to form hydroxyl radicals (OH^\bullet). The OH^\bullet then attack lipids in the cell membrane forming lipid peroxides, which then stabilize themselves via the rearrangement of carbon-carbon double bonds to form CDs.[159] The results indicate a direct correlation between CD formation and iron (II) concentration. The increased level of iron in the system facilitated sustained lipid peroxidation and as a consequence, a higher concentration of CDs. However, cells exposed to an iron chelator, such as HA, showed a

decrease in CD formation in a concentration-dependent manner. The neuroprotection afforded by HA was at lower iron (II) concentrations. HA inhibits iron (II) / ascorbate-induced LPO by chelating the iron before it had a chance to oxidize the lipids found in the membranes of the hNSCs.

3.4.4 Influence of HA on Iron/Ascorbate-induced Oxidative Stress on the Viability of hNSCs.

The presence of iron at CNS injury amplifies oxidative stress and the consequences of this situation include proliferation, adaptation, cell injury, senescence, and cell death.[159] To protect the tissues at these injury sites it is fitting to design therapies that are directed towards the alleviation of oxidative stress. In this report, we studied the effect of HA on iron/ascorbate-induced oxidative stress on cell viability over a seven-day period. A sustained supply of iron (II) (0.75 - 3.000 mM) was maintained in the system by adding 50 mM ascorbic acid, a reducing agent, which reduces iron (III) to iron (II).[160]

The CellTiter-Blue assay evaluated the influence of iron (II)/ascorbate-induced oxidative stress on cell viability. The fluorescence produced is directly proportional to the number of viable cells, that is, there is a linear relationship between fluorescence and the number of cells.[161] Prior to treating the cells with iron (II)/ascorbate, the fluorescent response of all groups was with a very narrow range, between 1000-1100. This suggests that the number of viable cells in each well were nearly identical. On day one the fluorescent signal for all groups increased, with the exception of the group treated with 3.0 mM iron (II)/ascorbate. Increased fluorescence is indicative of cell proliferation and viability while the group with decreased fluorescent (3.0 mM iron (II)/ascorbate) suggest cell death. Groups pre-treated with HA prior to iron (II)/ascorbate had higher fluorescent signals that those not treated with HA as HA protected the cells from iron-induced oxidative stress either by acting as an iron chelator or as a free radical scavenger. However, the protection afforded

by HA varied in an iron (II) concentration dependent manner. The higher the concentration of iron (II) the lower the cell viability. Oxidative stress results when there is an imbalance between the production of free radicals and the ability of the cell to mitigate their harmful effects through neutralization by antioxidants. The groups treated with 3.0 mM iron (II) / ascorbate and iron (II) / ascorbate / HA showed fluorescent signal that was greatly attenuated, verifying the observations from optical imaging that 3.0 mM iron (II) is toxic to hNSCs. These cells had minimal or no metabolic activity and thus their inability to reduce resazurin to resofurin, the CellTiter-Blue reagent remained blue.

Confocal images indicate minimal mortality of hNSCs at all concentrations upon initial exposure to iron (II)/ascorbate whether in the presence or absence of HA. This suggests that the cells' antioxidant defense system was able to counteract the ROS produced by hNSCs exposed to iron (II)/ascorbate. Cell mortality increase in a concentration dependent matter upon further exposure of HA-treated hNSCs to iron (II)/ascorbate. At low concentrations of iron (II), for example 0.75 mM, the hNSCs continued to proliferate at a rate equivalent to the cells in the control groups. Yehuda and co-workers reported that brain cells function in an environment where the normal brain iron concentration is 0.73 mM.[162] Further, Zhou et al. and Halliwell et al. showed that under mild oxidative stress some cells are known to proliferate.[159, 163] Cells treated with 1.0 - 1.5 mM iron (II) in the presence of HA grew better than those treated with 1.0 - 1.5 mM iron (II) alone because HA chelated some of the iron (II) reducing its availability for ROS production. The cells treated with only 1.25-3.0 mM Fe^{2+} experienced higher mortality and growth inhibition due to more intensive ROS production. On day 7, the fluorescent signal of most groups showed a downward trend; the cells in the control groups and those treated with 0.75 mM iron (II) may have outgrown the capacity of the wells and since they have no more room to grow, the cells started

dying. Groups treated with 1.5 mM iron (II) decreased because of the accumulative effects of oxidative stress and the inability of HA to protect the cells from damages caused by ROS.

3.5 Conclusion

The results obtained in this study confirmed that HA is an efficient chelator of iron (II) and iron (III). It chelates iron (III) with an efficiency of ~74% *in vitro*. This study could signify an advancement in elucidating the precise function played by HA in healing and neuro-regeneration. Due to its fast bio-degradation rate in living tissues, its inhibitory effects on iron (II) /ascorbate-induced oxidative stress in hNSCs were short-lived. The half-life of HA in the body ranges from 12-72 hours regardless of its route of elimination.[164] When hNSCs were treated with 3.0 mM iron (II) / ascorbate and 3.0 mM iron (II) / ascorbate / HA, it was observed that the HA delayed the deleterious effects of oxidative stress by ~48 hours after which the cells suffered a similar fate to those treated with just 3.0 mM iron (II) / ascorbate. Cell death in the group treated with HA occurred because of the degradation of HA within 48 hours of the assay. The iron (II) chelated by HA was released and was able to participate in free radical production, which ultimately lead to oxidative stress. Modification of HA can alter its degradation rate and enable it to retain chelated metals for much longer periods. As a result, therapeutics systems based on HA could be a viable way of removing excess iron at the site of injury or disease that would mitigate against the buildup of ROS and the deleterious effects associated with oxidative stress.

CHAPTER 4

4 Synthesis and Characterization of Families of Iron Chelators-polymer Conjugates (ICCs) based on the Combination of three iron chelators and two polymers.

4.1 Introduction

Exposure to heavy metals is commonplace because they are ubiquitous in our environment.[165] The accumulation of heavy metals (lead, mercury, arsenic, cadmium, zinc, copper and iron) in the body can be toxic or even fatal.[166] Chelation therapy is the preferred medical treatment to mitigate against the toxic effects of these metals. This therapy uses chelating agents to bind to toxic metals having oxidation states of two or higher to form complexes which are readily eliminated from the body.[165, 167-169] Traditionally, chelation therapy treated heavy metal poisoning, but currently, some proponents of chelation therapy claim that it protects against major health problems including heart disease.[170-173] Heavy metals such as lead, cadmium, mercury and arsenic have no known physiological function but others like zinc, copper and iron are essential to maintain physiological function.[174, 175] For example, iron is essential for normal cellular function, but when homeostasis is disturbed can result in cell injury or death.[176] Iron is a known catalyst in the initiation of free radical reactions which produces oxy-radicals having the potential to damage cellular lipids, nucleic acids, proteins and carbohydrates.[177] Among chelation therapies, iron chelation therapy has emerged as the most interesting to researchers as well as clinicians. It is not just a treatment for iron over-load but as potential medicine for the treatment of hemorrhagic central nervous system (CNS) traumas.[178-180]

CNS injuries fall into two categories: primary and secondary injuries. Primary injuries are structural damages to the brain or spinal cord caused by the initial mechanical trauma while secondary injuries result from a complex cascade of pathophysiological and biochemical processes

initiated by the primary injury.[181, 182] Secondary injuries lead to oxidative stress and subsequent lipid membrane peroxidation which disrupts tissue homeostasis causing cellular injury and ultimately death.[183] Substantial evidence exists that iron plays an injurious role in the pathogenesis of CNS injuries.[22, 177, 184-190] MRI studies have shown increased levels of iron in the brain and spinal cord following TBI and SCI.[186, 188-191] Cellular damage from CNS injuries is capable of accelerating free radical reactions partly because hemorrhages and cell lysis are common events during trauma.[188, 192] The injured and lysed cells can extravasate their intracellular iron into the extracellular environment where it generates hydroxyl radicals ($\cdot\text{OH}$) to promote oxidative stress and apoptosis in the CNS. [193, 194]

With mounting evidence that iron plays a critical role in the secondary injury process of TBI and SCI, it is therefore feasible to hypothesize that a therapy that targets iron removal from the injury sites could be an effective neuroprotective treatment. To date, only a few studies have investigated the therapeutic efficacy of chelating iron in experimental TBI and SCI models.[179, 195-198] Currently, there are three food and drug administration (FDA) approved iron chelators for chelation therapy, these are deferoxamine (DFO), deferiprone (DFP) and deferasirox (DFX).[179, 199] Of these approved iron chelators, DFO has been the most studied in CNS injuries. Yao and coworkers used DFO to treat SCI in a rat model and found that the rats in the DFO group showed better hind limb recovery than in the SCI group. Additionally, they found that iron concentration was lower in the DFO group than in the SCI group after injury and that DFO increased survival of neurons and inhibited gliosis. They claimed that DFO promoted spinal cord repair by inhibiting ferroptosis, a novel iron-dependent cell death pathway. However, further clarification is needed to determine if ferroptosis represents the mechanism of action of DFO in SCI recovery.[194] Several other researchers have used DFO or DFO covalently modified with polymeric materials to treat

CNS injuries in rat models and each group has indicated improved functional as well as cognitive recovery with DFO.[42, 196, 200-203]

McTigue and coworkers conducted multiple studies to test the effectiveness of DFX on rats that received a moderate thoracic spinal contusion. In the first two studies, the rats received DFX for 7- or 14-days post-injury, this treatment yielded modest improvements in hind limb function, and tissue sparing improved minimally. They conducted further experiments to study chronic functional changes and to extend the treatment duration and observed that there were no significant improvements. However, when they increased DFX dosage two-fold significant morbidity and toxic side effects were reported.[179] Maher et al. performed *in vitro* experiments using deferiprone and its derivatives and showed that these compounds were able to reduce oxidative stress and prevent nerve cell death.[204]

Other experimental and clinical iron chelators used for CNS injures include *N,N'*-Di (2-hydroxybenzyl) ethylenediamine-*N,N'*-diacetic acid monohydrochloride (HBED), quercetin, curcumin, and minocycline.[197, 198, 205-207] Khalaf et al. induced TBI in mice using a controlled-cortical impact model and immediately subcutaneously injected the mice with HBED. They injected the mice again after a 12 hours interval, and injections were subsequently given twice daily until the end of the study three days later. Khalaf et al. evaluated the neurological behavior of the mice daily and quantified cortical injury volume, hemispheric enlargement and hippocampal swelling with cresyl violet. They used Perls' iron staining to assess the accumulation of iron and effects of HBED on iron accumulation and immunohistochemical staining to assess the markers for gliosis and oxidative stress and the effects of HBED on these markers. The data showed that HBED facilitated the recovery process following brain trauma by improving motor

functions and reducing the cortical injury volume, hippocampal swelling and total hemispheric injury volume by $36.6 \pm 6.8 \%$ ($p < 0.001$), $23.4 \pm 3.8\%$ ($p < 0.05$), and $13.3 \pm 2.7\%$ ($p < 0.01$), respectively. Khalaf et al. observed a reduction in microgliosis and oxidative stress markers in the impacted callosum area by $39.8 \pm 7.3 \%$ and by $80.5 \pm 0.8 \%$ ($p < 0.05$), respectively. They suggested a direct relationship between the reduction in cortical injury volume, hippocampal swelling and total hemispheric injury volume and the reduction in microgliosis and oxidative stress markers.[197] HBED facilitated the recovery process post TBI by binding to ferrous iron and inhibiting oxidative stress directly via its iron chelation properties. Alternatively, HBED is also a potent antioxidant, not only by chelating Fe^{2+} but also via donation of hydrogen (hydrogen abstraction).[208]

Schültke et al. tested whether or not quercetin would improve functional recovery after TSCI by decreasing secondary damages. To test this hypothesis they used 44 male Wistar rats in two experimental series. In the first animal experiment, Schültke et al subjected 28 rats to standardized spinal compression injury. The anesthetized animals underwent laminectomy at T6/T7 laminae and then subjected to an extradural 40 g clip compression for 5 seconds at T7.[209] Using a single blinded protocol, the rats were randomly assigned to four therapeutic groups ($n = 6$) and one control group ($n = 4$). The rats received different doses of quercetin (0, 5, 25, 50, 100 $\mu\text{mol/kg}$) or saline injection within the peritoneum 1 hour post injury, and 12 hours thereafter. In the second animal experiment, the researchers conducted a blind study in which they randomly assigned 16 rats to two therapeutic groups and a control group. They induced mid thoracic SCI in the rats following the same protocol used in the first animal study. Treatment with quercetin (therapeutic groups) and saline (control group) began 1-hour post injury and then every 12 hours for an interval of ten days. The rats in the first therapeutic group ($n = 4$) received a quercetin dosage of 2.5

$\mu\text{mol/kg}$ and those in the second therapeutic group ($n = 6$) received a quercetin dosage of $25 \mu\text{mol/kg}$ while rats in the control group ($n=6$) received physiological saline solution in weight adjusted dosages. They used Basso, Beattie and Bresnahan (BBB) ratings to evaluate motor function recovery weekly over the course of four weeks.[210]

The data revealed no significant improvement in functional outcome for the group treated with $2.5 \mu\text{mol/kg}$ quercetin but showed significantly better functional outcome for the groups receiving quercetin dosage between $5 \mu\text{mol}$ to $100 \mu\text{mol}$ quercetin/kg body weight. In this group, half or more of the animals walked, albeit with deficits whereas none of the animals in control group walked. There was no significant difference in functional outcome upon increasing the dosage from $5 - 100 \mu\text{mol/kg}$ nor was there a difference in animals treated for 4 or 10 days. The therapeutic outcome correlates to the efficient clearance of iron from the injury site, signifying that iron chelation is a possible mechanism whereby quercetin mitigate secondary damages.[198]

Curcumin is a well-known biphenolic phytochemical with a wide range of pharmacological activities. It possesses potent anti-oxidant, anti-inflammatory, and immunomodulatory effects and its neuroprotective effects in TBI and SCI are extensively studied.[211-216] Curcumin exerts neuroprotection via multiple mechanisms and pathways, which include the suppression of inflammatory reaction and lipid peroxidation, the modulation of oxidative stress, anti-apoptotic behavior, the upregulation of mitochondrial function and iron chelation.[217-220] For example, Lin et al. used the spinal cord hemisection injury model to investigate the neuroprotective effect of curcumin after SCI in rats. They randomly divided the rats into three groups (sham, vehicle and curcumin) and the sham operation consisted of only a laminectomy. The sham group received no medication; the vehicle group received 40 mg/kg of dimethyl sulfoxide (DMSO) once daily via

intraperitoneal injection; and the curcumin group received 40 mg/kg curcumin once daily starting 1 day before the hemisection surgery and continuing for 6 days via intraperitoneal injection. Lin et al used the BBB scale to observe and evaluate locomotor function and excluded rats with loss of locomotion in both hind limbs, indicating bilateral corticospinal tract transection, from the study. Compared to the vehicle group, the BBB scores for the curcumin treated group was significantly better indicating better functional outcomes. Immunohistochemistry of neuron-nuclear specific protein (NeuN) revealed substantive neuronal loss in the vehicle in contrast to the curcumin treated group, curcumin exerted its protective effects on the neurons after SCI. Additionally, in comparison to the vehicle group, curcumin significantly inhibited apoptosis after SCI ($P < 0.001$). Reversed transcription-polymerase chain reaction (RT-PCR) showed that curcumin significantly inhibited the expression of glial fibrillary acidic protein (GFAP). Lin et al. attributed the improvement in functional outcome to the ability of curcumin to inhibit astrocyte re-activation and prevent apoptosis and neuronal cell death.[215]

The multifunctionality of curcumin is due to its structure; it is an effective anti-oxidant and anti-inflammatory agent in TBI models because curcumin is a potent free radical scavenger.[220, 221] The free radical scavenging activity of curcumin arises from either the phenolic hydroxyl groups or from the methylene (CH_2) groups of the β -diketone moiety. These groups can donate electrons or hydrogen atoms to free radicals.[222] Curcumin also has the ability to chelate metal ions such as Cu^{2+} and Fe^{2+} , usually by way of the β -diketone or keto-enol moiety to generate metal–curcumin complexes. Metal chelation is an alternative possible mechanism by which curcumin exerts its neuroprotective effects.[219] Several researchers have demonstrated the therapeutic effect of curcumin via iron chelation in neurodegenerative diseases such as Alzheimer’s disease (AD) and

Parkinson's disease (PD).[219, 223-225] Even though this is viable therapeutic target for the treatment of TBI and SCI, to date there seemed to be no such account in the literature.

There are several limitations to the use of small molecule iron chelators in clinical applications. These limitations include poor aqueous solubility, permeability, and absorption, route of administration, bioavailability, short plasma half-life, rapid systemic elimination, fast metabolism, inactive metabolic products, toxicity, gastro-intestinal effects, and patients' adherence to therapy.[226] For example, the major challenge of iron chelation therapy with DFO is patients' adherence to therapy. During iron chelation therapy, patients receive DFO for 8-12 hours, 5 days/week via subcutaneous or intravenous injection due to its poor bioavailability and short plasma half-life (20-30 min). This treatment regimen is time-consuming, inconvenient, and painful for patients and frequently causes non-compliance.[227] Poor compliance may cause a gap in chelation coverage, during which labile plasma iron (LPI) levels can increase and cause further tissue damage.[228] Secondly, if administered as intravenous bolus, DFO can cause the rapid onset of acute hypertension, which in some cases can be deadly.[229-231] Further limitations of iron chelation therapy with DFO include rapid elimination via the kidney due to the short plasma half-life, growth retardation in children and adolescents, inefficient iron chelation, high cost, and allergic reactions.[226, 232, 233] DFO is an inefficient iron chelator, when administered only $\leq 5\%$ of the drug binds to iron.[229] DFO is a bacterial siderophore and its commercial production is via fermentation of a strain of *Streptomyces pilosus*. This production method contributes to the high cost of DFO and the allergic response experienced by some patients. The allergic response is potentially due to the presence of cytokines or other fermentation products still present following the purification process.[234]

Although DFP and DFX are orally active and patients have much better adherence to the treatment regimen, these iron chelators have some side effects and limitations. Adverse effects of DFP include agranulocytosis, neutropenia, arthropathy, gastrointestinal symptoms, increase of alanine transaminases (ALT) levels, and weight gain.[235] Agranulocytosis, severe neutropenia with absolute neutrophil count (ANC) $< 0.5 \times 10^9$ per liter, is the most consequential adverse health effect of chelation with DFP and its incidence vary from 0.5% - 3.6% of patients undergoing chelation therapy.[236-239] Agranulocytosis occurs three times as much in females (2.4%) than in males (0.8%) and this incidence was reported in whites, blacks and Asians.[239] Thus, it is highly recommended that all patients receiving DFP should monitor their blood ANC weekly to mitigate developing agranulocytosis and its possible complications and to discontinue treatment at the first sign of neutropenia or infection.[240] Less severe neutropenia (ANC $0.5 \times 10^9 - 1.5 \times 10^9$ per liter) is four times as frequent as agranulocytosis. Neutropenia affects up to 5% of patients and reports indicate that it occurs predominantly in younger patients and patients with intact spleens.[235, 241, 242] The onset of neutropenia (0 - 70 months) and agranulocytosis (0 - 19 month) may vary significantly but are both reversible when chelation therapy with DFP is discontinued; but the re-introduction of DFP may cause the reoccurrence of neutropenia.[235, 237, 243] Arthropathy is a frequently reported complication of iron chelation therapy with DFP.[240] The incidence of arthropathy varies from 2% - 30% among studies and is observed to affect mostly large joints such as the knee.[235, 244] Patients typically experience inflammation and/or pain, which generally resolves within days to weeks after DFP dose reduction or temporary discontinuation.[236, 240] The cause of joint discomfort during DFP therapy is unclear but some researchers have proposed iron deposition into the synovial fluid or high doses of DFP as possible causes.[245, 246] Patients on DFP therapy usually experience gastrointestinal symptoms such as

nausea, vomiting and abdominal pain during the early stages of treatment. These gastrointestinal symptoms are usually mild to moderate in severity, transient in nature, and normally resolve on their own. However, Cohen et al. reported that in a multicenter study consisting of 187 participants, 2% discontinued DFP treatment because of gastrointestinal symptoms.[238] Elevated liver enzymes is a concern for patients treated for iron overload as this indicates a medical condition like hepatitis or liver disease. Data from a number of clinical trials linked DFP with transient fluctuations in serum alanine transaminase (ALT) levels.[238, 240, 244, 247-250] Approximately 7% of patients experience fluctuating ALT levels during the first months of therapy but in the majority of patients, the levels returned to baseline values without DFP dose reduction or discontinuation of therapy.[251] In a multicenter trial consisting of 144 patients Maggio et al. reported that three patients (2%) developed transient elevated ALT levels that resulted in temporary withdrawal from treatment. These patients discontinued treatment because of the recurrence of elevated ALT levels and an additional ten patients recorded a mild increase in ALT levels, which subsequently returned to baseline values with dose reduction.[249] In a 4-year multicenter study, Cohen et al. observed that ALT values showed significant variation over the study period, not just in the first year. However, trend analysis did not show a marked increase in the percentage of patients with ALT levels greater than twice the upper limit of the reference range. In the first year of study, two patients withdrew due to elevated ALT levels but in the remaining three years, no one withdrew due to this reason.[248] In a previous multi-center study, Cohen et al. linked the elevated ALT levels to patients who were seropositive to hepatitis C. Approximately 85 % of patients manifesting elevated ALT levels had hepatitis C, a common infection among individuals treated for iron overload.[240] Olivier et al. conducted a small prospective study consisting of 21 patients on efficacy and safety of DFP and reported a reduction in serum ALT

levels regardless of the presence or absence of hepatitis C infection. Additionally, they observed that ALT levels increased in one patient who was seropositive for hepatitis C, and reported a decline in levels after discontinuing DFP treatment. They attributed the elevated ALT level to treatment with DFP.[250] In a multicenter study consisting of 167 patients, Al-Refaie et al. observed that 37 patients recorded elevated ALT levels. In the first six months of therapy 23% of patients had serum ALT levels greater than twice the upper limits of normal (ULN) but these values returned to baseline within twelve months of treatment with DFP.[238]

Adverse effects associated with DFX therapy include elevated creatinine and liver enzyme levels, GI symptoms and skin rashes.[226, 252-255] Typically, approximately one third of patients on DFX treatment experience mild dose-dependent elevated serum creatinine levels within a week of therapy or increasing DFX dosage. In most cases, the creatinine levels remained within the normal range but patients on DFX therapy need to monitor their kidney function monthly as an increase in serum creatinine levels is an indicator of renal problems.[226] In a phase III clinical trial Cappellini et al. observed that DFX-related ALT value elevation greater than twice ULN occurred in <1% of patients. In one case, the ALT value returned to baseline within a month while in another ALT values remained elevated to three times ULN four months after terminating DFX treatment.[252] Galanello et al conducted a phase II clinical evaluation of DFX in pediatric patients and observed that five patients (13%) developed elevated ALT levels >5 times ULN which resulted in treatment interruptions lasting 1-2 weeks. Treatment later resumed at the previous dosage without reoccurrence of ALT elevation.[253] The most common adverse event associated with DFX therapy is GI symptoms. Approximately 15% of patients experienced transient GI events including abdominal pain, diarrhea, constipation, nausea and vomiting. The symptoms usually persist for ≤ 8 days and resolve spontaneously without dose adjustment or discontinuation

of DFX.[254] Skin rash is one of the most commonly occurring adverse event related to DFX treatment.[256-258] For example, Atul Sharma et al. presented a case study of a thalassemia patient who initially underwent treatment for iron overload with DFP but developed DFP-induced arthropathy to the right knee and hip joint. In order to continue providing iron chelation therapy and to alleviate the pain and limping due to arthropathy, the patient switched to DFX after medical advice. Six days after commencing DFX treatment the patient noticed a pruritus (itchy) skin rash on the neck, which later spread downwards covering the entire body. Subsequent physical examinations and laboratory investigations did not show any abnormalities except for mild splenomegaly. Hemoglobin (Hb) test revealed low Hb levels but leukocyte and platelet counts along with liver and renal functions were within normal limits. Consequently, the patient discontinued DFX treatment and initiated antihistaminic therapy. The rashes subsided and the patient recovered nine days after stopping DFX therapy and initiating antihistaminics.[256]

The major factor that limits the use of small molecule chelators in the pharmaceutical industry and in clinical applications is poor bioavailability.[259, 260] The most influential factors affecting the bioavailability of small molecule chelators like quercetin and curcumin are poor aqueous solubility, permeability, and absorption, instability, rapid metabolism, and inactivity of metabolic products.[261-263] Since quercetin and curcumin cannot be produced in the human body, its intake is through the diet or via supplementation.[264] Naturally occurring quercetin exists as quercetin glycosides in fruits (citrus, apples, grapes, blueberries, cranberries, and dark cherries), vegetables (onions and green leafy vegetables such as kale, arugula, lettuce, spinach, and collard greens), drinks (green tea, black tea, and red wine), herbs (dill, chives, tarragon, oregano, tarragon, and fennel leaves), grains (buckwheat), and nuts (almond and pistachios).[265-267] Quercetin glycosides are quercetin molecules conjugated with sugar residues such as glucose, rhamnose and

rutinose. By contrast, commercial dietary supplements containing quercetin as an ingredient contain the free form of quercetin, called quercetin aglycone.[268]

The estimated daily intake of quercetin from fruits and vegetables expressed as aglycone equivalents are as high as 40 mg in diets lower in fruits and vegetables and as high as 250 mg in diets rich in fruits and vegetables.[264] On the other hand, the recommended daily dose for quercetin aglycone in dietary supplements is as high as 1000 mg (the most common dose being 500 mg). [264, 269]. When ingested, quercetin is primarily absorbed in the intestines and a small amount is absorbed in the stomach. The nature of the sugar residue attached to quercetin significantly influence the absorption efficiency of quercetin glycosides in the small intestine. Further, the deglycosylation of quercetin glycosides to quercetin aglycone via hydrolysis with lactase-phlorizin hydrolase (LPH) significantly increases the intestinal absorption of quercetin resulting in increased plasma concentrations and greater bioavailability.[270] Crespy et al. and Hollman et al. studied quercetin absorption *in vivo* and determined that the absorption of quercetin aglycone (24%) is more efficient than rutin (quercetin-3-O-glucose-rhamnose, 17%) but less efficient than quercetin glucosides (52%).[271, 272] Reportedly, rutin is hardly absorbed in the small intestine because of the lack of rutin-specific enzymes. However, rutin travels to the large intestines where it undergoes deglycosylation by enzymes expressed by the gut microbiota such as α -rhamnosidase and β -glucosidase.[273]

After absorption, quercetin undergoes phase I and II metabolism in the intestine and the liver. Phase I metabolism is mediated by cytochrome P450 (CYP450) and include reactions such as oxidation, reduction and hydrolysis, which facilitates further metabolism via the introduction of facile functional groups. Phase 1 metabolism has a minor impact on the overall metabolism of quercetin when compared to phase II metabolism.[274] The phase II metabolism of quercetin

mainly include conjugation reactions as methylation, glucuronidation and sulfation catalyzed by catechol-O-methyl-transferase, uridine-5'diphosphate glucuronosyl transferases (UGTs), and sulfotransferases (SULTs), respectively.[275] Since conjugation increase the hydrophilicity of quercetin phase II metabolites, these molecules are unable to cross the lipid bilayer of the membrane and must be transported to the gut lumen or the bloodstream via specific transporters. For example, ATP-binding cassettes (ABC) transporters, expressed on the intestinal epithelial cells, transport quercetin phase II metabolites into the gut lumen and bloodstream.[276, 277]

Quercetin and its gut metabolites reaches the liver through the portal vein and are exchanged from the bloodstream to hepatocytes via passive diffusion or by several types of transporters expressed on their basolateral and apical membranes.[278, 279] In the liver, quercetin and its metabolite will undergo further phase II metabolism involving glucuronidation, sulfation, and methylation, which facilitates excretion via bile, urine and feces.[280, 281] Organic anionic transports (OATs) located on the basolateral membrane of the renal proximal tubular cells and ABC efflux transporters located on the brush border membrane, synchronously promote the circulation of phase II quercetin conjugates from bloodstream to the kidney, where it is excreted in urine.[282]

Curcumin is a bright yellow pigment extracted from turmeric (*Curcuma longa*) and other members of the ginger family (*Zingiberaceae*). Curcumin is present in plants with other curcuminoids such as demethoxycurcumin, bis-demethoxycurcumin, and cyclo-curcumin.[283] Despite its efficacy and safety, debate persists about the therapeutic potential of curcumin because it displays poor pharmacokinetic profile after oral intake. Curcumin has relatively poor bioavailability in humans even when administered at high dosages.[260] Factors affecting the bioavailability of curcumin include poor aqueous solubility and chemical instability, relatively low

absorption by the small intestine and low serum levels, short plasma half-life and tissue circulation coupled with fast reductive and conjugative metabolism and rapid elimination from the body.[260, 284-286] Curcumin may bind to enterocyte proteins during intestinal absorption resulting in modification of its structure and further exacerbates the poor bioavailability of curcumin.[287] Evidence for the poor oral bioavailability of curcumin involves observations of extremely low serum levels, low tissue distribution and high fecal content after oral administration. In one study, Yang et al. compared the maximum serum levels of 10 mg/kg curcumin administered to rats intravenously and a 500 mg/kg dose administered orally. They observed that the intravenous administration yielded a maximum serum level of $0.36 \pm 0.05 \mu\text{g/mL}$ compared to a maximum serum level of $0.06 \pm 0.01 \mu\text{g/mL}$. [288] In other studies with rats, Maiti et al. and Marczylo et al. observed that an oral dose of 1 g/kg yielded a maximum serum level of $0.5 \mu\text{g/mL}$ after 45 minutes of administration and $6.5 \pm 4.5 \text{ nmol}$ after 50 minutes of administration, respectively.[289, 290] The absence or trace amounts of curcumin and its metabolites in portal blood and tissues is strong evidence for its poor intestinal absorption and low bioavailability.[291, 292] In one study, Ravindranath et al. orally administered 400 mg curcumin to rats and found that curcumin was absent in cardiac blood and only trace amounts ($<5 \mu\text{g/mL}$) was present in portal blood. Further, they reported negligible curcumin distribution ($<20 \mu\text{g/tissue}$) in the liver and kidney.[291] In another study, Garcea et al. investigated the detection of curcumin in hepatic tissues and portal blood and determined that only trace levels of curcumin and its metabolites were found in the liver and portal blood.[292] The elimination of ~90% of orally ingested curcumin via feces is additional evidence that supports curcumin's poor bioavailability.[293]

Approaches taken to improve the bioavailability of curcumin include the use of adjuvants, curcumin nanoparticles, curcumin phospholipid complex, liposomal curcumin, micellar curcumin,

and the use of structural analogs of curcumin. Animal and human studies show that adjuvants such as piperine combines with curcumin and inhibits hepatic and intestinal glucuronidation thereby increasing the bioavailability of curcumin. In one report, Shoba et al. combined piperine with curcumin and administered it to rat and healthy human volunteers. The oral administration of a 2g/kg curcumin to rats yielded a maximum serum curcumin level of $1.35 \pm 0.23 \mu\text{g/mL}$ at 0.83 h, while adding 20 mg/kg piperine to curcumin increased the serum concentration of curcumin transiently (1-2 h post drug). Further, the time of maximum concentration (T_{max}) at peak significantly, while elimination half-life and clearance decreased substantially resulting in a 154% increase in bioavailability. In the case of humans, oral ingestion of 2g /kg curcumin alone resulted in undetectable or negligible serum levels. The addition of 20 mg piperine significantly increased the serum levels and the bioavailability improved by 2000%.[294] Hence, piperine has a greater impact on the bioavailability of curcumin in humans than in rats. Shoba et al conducted another human volunteer trial to confirm the impact of piperine on the bioavailability of serum curcumin. This trial consisted of six healthy adult males, three of whom received 2g curcumin with 5 mg of piperine and the other three received curcumin without piperine. The serum bioavailability of curcumin increased in the presence of piperine but the bioavailability in tissues (e.g. liver, heart, etc.) did not significantly improve.[260] Other adjuvants showing a synergistic effect when combined with curcumin include quercetin, genistein, and essential oils such as eugenol and terpineol.[295-297]

Nanoparticle technology has emerged as a viable strategy used to improve the bioavailability of therapeutic agents. Reducing the size of therapeutic agents is known to improve their solubilization and this their bioavailability. In the case of lipophilic agents like curcumin, nanoparticle-based delivery systems are suitable because it alleviates the problem of low aqueous solubility. In one

study, Bisht et al. synthesized and characterized polymer-based curcumin nanoparticles, coined “nanocurcumin”. The nanoparticles (<100 nm in size) were reported to have similar *in Vitro* activities as that of curcumin when applied to cancer related applications using pancreatic cell lines. Similar to free curcumin, nanocurcumin inhibits the activation of the transcription factor NFκB and attenuates the steady state levels of pro-inflammatory cytokines like interleukins and TNF-R. In this work, the authors did not report on the *in vivo* effect of nanocurcumin in mice or its biodistribution to illustrate potential enhancement in the efficacy of nanocurcumin compared to free curcumin.[298] In another study, Ubeyitogullari et al. developed a novel method to produce food grade curcumin nanoparticles with reduced crystallinity as its high-crystallinity is known to affect its bioaccessibility. This method used nanoporous starch aerogels (NSAs) as a mold and supercritical carbon dioxide (SC-CO₂) to produce curcumin nanoparticles with average particle size 66 nm. In a simulated digestion, the low-crystallinity curcumin nanoparticles had significantly higher bioaccessibility compared to the bulk curcumin. The bioaccessibility of the bulk curcumin was ~4% while that of low-crystallinity curcumin nanoparticles was 173-fold higher than the bulk curcumin.[299]

Liposomes are extensively used delivery vehicles for drugs due to their capacity to encapsulate bioactive hydrophilic, amphiphilic, and lipophilic molecules into their inner aqueous phase or within lipid leaflets.[300] Since curcumin is a lipophilic molecule, liposomes can encapsulate it into its lipid bilayer and in so doing improve its aqueous solubility and bioavailability. The primary protocols used for curcumin’s encapsulation within liposomes include the thin film and ethanol injection methods.[301-308] The thin film method for the liposomal encapsulation of curcumin follows the method established by Zalloum et al. First, dissolve the phospholipid and curcumin in a 2:1 mixture of methanol and chloroform, then rotary evaporate the organic solvents. The dried

lipid film was further kept under vacuum to remove trace solvent and the resulting thin film hydrated in a buffer solution.[309] Researchers have used a number of techniques including centrifugation, microfluidization, and sonication to separate liposomal encapsulated curcumin from non-encapsulated curcumin.[301, 306, 308] The ethanol injection method involves dissolution of curcumin and the phospholipid in ethanol. Mix the resulting solution with di-ionized water and stir for several hours until the curcumin-encapsulated nanoliposomes spontaneously formed with the simultaneous evaporation of residual ethanol. After the initial liposomes formed via self-assembly with mild stirring, ultrasonic homogenization facilitated further size reduction. Centrifugation enabled the separation of liposomal encapsulated curcumin from non-encapsulated curcumin.[307]

Micellation of curcumin is another strategy used to improve the bioavailability of curcumin.[310-312] In one investigation, Schiborr et al compared the bioavailability of native curcumin and a liquid micellar curcumin formulation. The study group took the native curcumin and the liquid micellar curcumin formulation in random order, a single oral dose of 500 mg. They collected blood and urine samples from the study group, which they later analyzed for curcumin content. They collected the blood and urine samples before curcumin consumption and at 0.5, 1.0, 1.5, 2.0, 4.0, 6.0, 8.0 and 24.0 hours and at 6.0, 12.0 and 24.0 hours after oral curcumin intake for blood and urine, respectively. Based on the area under the plasma concentration-time curve (AUC), the bioavailability of the liquid micellar curcumin formulation was ~185-fold greater than the native curcumin.[310] In another study, Patil et al. prepared a novel curcumin-load mixed micelle (Cur-MM) composed of two surfactants, Pluronic F-127 (PF127) and Gelucire® 44/14 (GL44). The Cur-MM formulation exhibited a 55-fold better oral bioavailability when compared to the native curcumin.[311] Peng et al., prepared a sophorolipid-coated nanomicelle curcumin

formulation via a pH driven method. Both the in vitro and in vivo studies show that the bioavailability of sophorolipid coated curcumin nanomicelle improved ~3-4 fold.[312]

Another strategy used to improve the bioavailability of small molecule chelators such as curcumin, quercetin and 5-amino-8-hydroxyquinoline is the preparation of bioconjugates. For example, Dubey et al., Mishra et al., and Harish et al. improved the bioavailability of curcumin through bioconjugates design and synthesis.[313-315] Dubey et al. prepared monoester and diester bioconjugates of curcumin with valine and glycine; and valine, glutamic acid, and demethylenated piperic acid, respectively, via a novel solid phase synthesis method. They observed that the diesters of curcumin exhibited greater antimicrobial and antiproliferative activities than native curcumin due to their increased solubility, intestinal absorption, slower metabolism and increased bioavailability. Further, a comparison of the curcumin bioconjugates revealed that the monoesters of curcumin exhibited greatest antimicrobial activities. They attributed this enhanced antimicrobial activity to the free phenolic group in the monoesters of curcumin.[313] Mishra et al. prepared several mixed bioconjugates of curcumin from alanine, glycine, and piperic acid. They evaluated the bioconjugates for their antimicrobial and antifungal properties and compared them to cefepime and fluconazole, a popular antibacterial and antifungal drug on the market, respectively. They observed that 4,4'-di-O-(glycinoyl-di-N-piperoyl)-curcumin and 4,4'-di-acetyl-curcumin exhibited greater antimicrobial activities than cefepime while 4,4'-di-O-(glycinoyl-di-N-piperoyl)-curcumin and 4,4'-di-O-piperoyl curcumin possessed comparable antifungal properties to fluconazole. They attributed the improved antimicrobial and antifungal properties of these bioconjugates to improved bioavailability resulting from greater cellular uptake, improved aqueous solubility and reduced metabolism.[314] In another study, Harish et al. studied the effect of curcumin bioconjugates (di-demethylenated curcumin, di-valinoyl curcumin, and di-glutamoyl

curcumin) on glutathione (GSH) depletion mediated oxidative stress in a dopaminergic neuronal cell line. They observed that all three bioconjugates were either more potent or equal in potency when compared to curcumin in mitigating the GSH depletion mediated oxidative stress. Among the curcumin bioconjugates, di-glutamoyl curcumin showed substantial increase in GSH levels and greatly alleviated ROS production. The improved neuroprotection exhibited by the diester bioconjugates of curcumin result from (i) enhanced metabolic stability arising from the protection of phenolic hydroxyl groups thus delaying their glucuronidation, (ii) improved cellular uptake via amino acid carriers, and (iii) better stability due to increase hydrophilicity.[315]

In this chapter, we focus on the design, synthesis, spectral characterization, and *in vitro* assessment (using hNSCs) of iron chelators-polymer conjugates (ICCs) based on the combination of three small molecule iron chelators (curcumin, quercetin, and 5-amino-8-hydroxyquinoline) to two polymers, polyethylene glycol (PEG) and hyaluronic acid (HA). Each polymer component of the ICCs will play a critical role in promoting neuroprotection and neuroregeneration while the small molecule as well HA will be responsible for iron chelation at the CNS injury site. Hyaluronic acid is an attractive polymer for the design and synthesis of the ICCs because of its intrinsic functions in the human body such as cell adhesion regulation, morphogenesis, cellular differentiation, and modulation of inflammation.[115, 316, 317] Similarly, PEG as an ICC component also confers attractive properties that affects the pharmacokinetic of the drug. PEG promotes “stealth behavior” in drug delivery by prolonging blood circulation and effectively increases the likelihood that the drug reaches its intended site of action before the body identifies it as foreign and eliminates it.[318] PEGylating a drug results in higher physical and thermal stability because it reduces the rate of enzymatic degradation. Further, PEGylation prevents or extends renal clearance when the size of the conjugate is above the renal threshold. When attached

to a hydrophobic drug, PEG's hydrophilicity increases the solubility of the polymer conjugate in aqueous media. Due to high aqueous solubility of PEG, it has low intrinsic toxicity that renders it an ideal polymer for biological applications. Additionally, PEG exhibits high solubility in organic solvents and this allows easy chemical modifications to the end groups. PEG is a polymer with a low polydispersity index (PDI) and this a basic prerequisite for a polymer to have pharmaceutical applications. A low PDI value (PEG-4600, PDI=1.05) provides PEG with the ideal homogeneity to ensure reproducibility as in relates to body-residence time and immunogenicity. Lastly, PEG reduces aggregation of drugs *in vivo* as well as during storage via steric hindrance and/or masking of the charges facilitated by formation of "conformational clouds". The highly flexible linear polymer chains generates these conformational clouds, which prevents interactions with blood components as well as proteins. The diminished interaction with the body causes PEG to have antigenic properties.

4.2 Materials and Methods

All reagents were purchased from Sigma Aldrich Chemical Co. (St. Louis MO) or VWR International unless otherwise noted. The polymers used in the fabrication of polymer-modified iron chelators are hyaluronic acid (HA, 100 kDa) and polyethylen2e glycol (PEG, 4.6 kDa). Curcumin, quercetin hydrate and 5-amino-8-hydroxyquinoline are the iron chelators tethered to the polymers. Jones reagent (an acidified (H_2SO_4) solution of CrO_3), acetone (solvent) and isopropyl alcohol (free radical scavenger; quenched the reaction) facilitated the oxidation of the two hydroxyl groups on PEG to carboxylic acid. The reagents used to determine the number carboxylic groups per molecule of $HOOC-PEG-COOH$ were potassium (KOH) and potassium hydrogen phthalate (KHP). 1-ethyl-3-(3-dimethylaminopropyl) carbodiimide hydrochloride

(EDC) and N-hydroxysuccinimide (NHS) were the reagents used in the modification of the PEG with iron chelators (HOOC-PEG-chelator). Dicyclohexylcarbodiimide (DCC), 4-dimethylaminopyridine (DMAP) enabled the addition of HA-100 kDa to the HOOC-PEG-chelator via esterification of the carboxylic acid group on the PEG. DMSO is the solvent used in the reaction when the HA -100 kDa was added to the HOOC-PEG chelator. Iron (III) chloride hexahydrate ($\text{FeCl}_3 \cdot 6\text{H}_2\text{O}$), iron (II) chloride tetrahydrate ($\text{FeCl}_2 \cdot 4\text{H}_2\text{O}$), sodium citrate, hydroquinone, phenanthroline were the reagents used to obtain the iron chelation efficiency of HA, COOH-PEG-chelator, and HA-PEG-chelator. While α -linolenic acid (LA), sodium acetate, acetic acid, sulfuric acid (H_2SO_4), ascorbic acid (AA), Brij 35, dichloromethane (CH_2Cl_2), $\text{FeCl}_2 \cdot 4\text{H}_2\text{O}$ were the reagents used for the lipid peroxidation (LP) of linoleic acid. The cell culture surfaces used for adherent hNSCs were 250 mL cell culture flasks and 24 or 48-well plates for suspension culture purchased from Greiner Bio-One (Monroe, NC). The reagents used in the coating material for adhering hNSCs to cell culture surfaces are phosphate buffer saline (PBS), poly (vinyl alcohol-co-vinyl sulfone) (PVAVS) and proprietary integrin-based peptide coating. Accutase is the hNSC detachment reagent and butylated hydroxytoluene (BHT) is the antioxidant added to the cell lysate to protect the intact lipids from lipid peroxidation during storage. The non-toxic reagent used in the cell viability evaluation of hNSC was CellTiter-Blue purchased from Promega (Madison, WI).

4.2.1 Synthesis of the Oxidizing Agent (Jones Reagent)

The procedure used for the synthesis of Jones reagent was adapted from the procedure of Lele et al.[319] Dissolve seven grams (7.0 g) CrO_3 (0.07 mol) in 50 mL of distilled H_2O and stir the solution with a magnetic stirrer at 10 - 15°C (ice-water bath). Add dropwise 6.1 mL of concentrated H_2SO_4 to the solution containing the CrO_3 . When the addition is complete, stir the solution for an

additional 10 minutes and allow it to reach room temperature. Jones reagent prepared in this fashion was stored at room temperature and later used in the synthesis of poly (oxyethylene) - dicarboxylic acids (POE-dicarboxylic acid) from polyethylene glycol (4600 Da).

4.2.2 Synthesis of POE 4600-Dicarboxylic Acid

The procedure used to synthesize POE 4600-dicarboxylic acid (HOOH-PEG-COOH) was adapted from the procedure of Lele et al.[319] Place 4.6 g of PEG-4600 in a round bottom flask and add 40 mL of acetone. Heat the mixture to obtain a clear homogenous solution, allow the solution to come to room temperature. To this solution, add 1600 μ L Jones reagent dropwise; cover the reaction vessel in foil paper and stir at room temperature overnight. Add 10 mL of isopropyl alcohol (free radical scavenger) to quench the reaction.

Within minutes of adding Jones reagent to the reaction mixture, the solution changed to a blue-green color due to oxidation by-products (chromium salts), which precipitated out in the form of fine suspension in the acetone solution. To remove the chromium salt from the solution, add 0.92 g of activated charcoal to the solution and stir with a magnetic stirrer for 2 hours. Centrifuge the solution to obtain a clear colorless acetone solution. Use a rotary evaporator to extract the acetone from the product. Remove any residual acetone left on the product with forced air and dissolve the resulting white solid in water, freeze and later lyophilize or dry in a vacuum oven.

4.2.3 Estimation of Carboxylic Groups per PEG Molecule

The number of carboxyl group per PEG molecule was determined from an acid-base titration between HOOC-PEG-COOH and KOH. Potassium hydrogen phthalate (KHP), a primary standard was used in the standardization of KOH and the resulting concentration determined as 0.0696 M. Then, combine and dissolve 0.5000 g HOOC-PEG-COOH and 20 mL of deionized H₂O in an

Erlenmeyer flask. Add two drops of phenolphthalein indicator to the mixture in the Erlenmeyer flask and titrate against KOH until the colorless to faint pink colored endpoint occurred. The number of carboxylic acid per PEG molecule was determined from **Equation 4.1**, where V_{KOH} is

$$\text{Number of COOH Groups} = \frac{V_{(\text{KOH})} M_{(\text{KOH})} M_{\text{wt}(\text{HOOC-PEG-COOH})}}{W_{(\text{HOOC-PEG-COOH})}} \quad \text{eqn. 4.1}$$

the volume of KOH in liters, M_{KOH} is the concentration of KOH, $M_{\text{wt}(\text{HOOC-PEG-COOH})}$ is the molecular weight of the polymer and $w_{(\text{HOOC-PEG-COOH})}$ is the mass of the polymer used in the titration.

4.2.4 Iron Chelation Efficiency of Small Molecule Iron Chelators

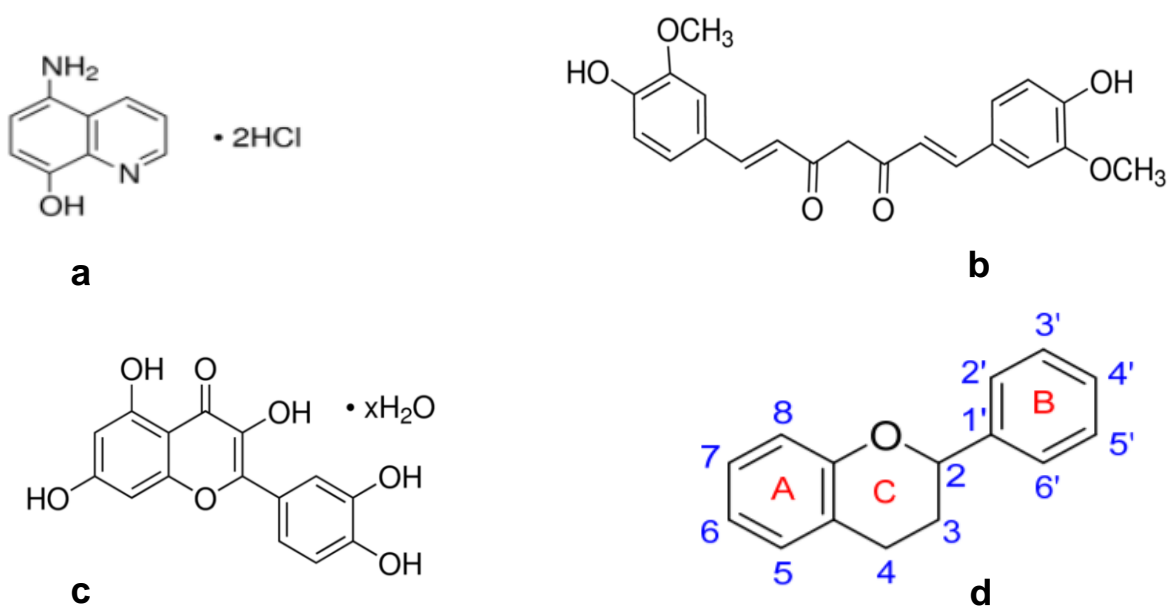
First, prepare a series of acidified iron (III) standards ranging in concentration from 14.2 μM to 114.0 μM . Use hydroquinone to reduce the iron (III) in solution to iron (II) by adjusting the pH to 3.5 with sodium citrate. Add a solution of 1, 10-phenanthroline to the solution and allow the orange-red complex to develop. Analyze the solution with UV-visible spectroscopy and prepare the calibration curve for iron (III) from the absorbance maximum of each spectrum.

Prepare chelator-iron (III) complexes by mixing 28.30 μM iron (III) solution (in excess) with each iron chelator, 5-amino-8-hydroxyquinoline, quercetin, and curcumin, respectively. Leave the solutions under magnetic stirring to facilitate complex formation and determine the amount of unreacted iron (III) in the sample. Use hydroquinone to reduce the unreacted iron (III) in the solution containing the chelator-iron (III) complex to iron (II) by adjusting the pH to 3.5 with sodium citrate. Add a solution of 1, 10-phenanthroline to the solution and allow the orange-red complex to develop. To access the iron chelation efficiency of the small molecule iron chelators,

analyze the solutions with UV-visible spectroscopy and the previous prepared iron (III) calibration curve.

4.2.5 Synthesis of Iron Chelator Modified POE-4600-Carboxylic Acid

The iron chelators used to modify POE 4600-dicarboxylic acid were 5-amino-8-hydroxyquinoline dihydrochloride, curcumin and quercetin hydrate. Consequently, three different families of iron chelator modified-polymers resulted from the conjugation namely quinolines, curcuminoids and flavonoids. **Scheme 4.1** shows the different iron chelators used in the polymer conjugation.



Scheme 4.1: Structural representation of the iron chelators used in polymer conjugation (a) 5-amino-8-hydroxyquinoline dihydrochloride (b) curcumin (c) quercetin hydrate and (d) flavonoid ring numbering system.

4.2.5.1 Synthesis of 5-amino-8-hydroxyquinoline Modified POE 4600-carboxylic Acid

The procedure used in the synthesis of 5-amino-8-hydroxyquinoline (5A8HQ) modified POE 4600-dicarboxylic acid (HOOC-PEG-5A8HQ) was adapted from the procedure of Kichler et al. [320] The method in brief, thoroughly dissolve 1000 mg HOOC-PEG-HOOC (217 μmol) and 15 mg NHS (130 μmol) in 80 mL de-ionized H_2O under stirring at room temperature. Then add 25.0 mg solid EDC (130 μmol) to the mixture this was allowed to stir for 2 hours to activate the carboxylic group of POE 4600-dicarboxylic acid. After the time elapsed, add 30.3 mg 5-amino-8-hydroxyquinoline pre-dissolved in 10 mL of de-ionized H_2O to the mixture. Stir the solution for 48 hours, then transfer the solution to 3500 MWCO dialysis tubes and dialyze exhaustively against deionized water. After dialysis, the samples were frozen and solvent eliminated by lyophilization. The HOOC-PEG-5A8HQ conjugate obtained was brownish red in color.

4.2.5.2 Synthesis of Curcumin Modified POE 4600-carboxylic Acid

The curcumin modified POE 4600-dicarboxylic acid (HOOC-PEG-Cur) was prepared from a procedure adapted from Manju et al.[321] Combine 3.0 g HOOC-PEG-COOH (652 μmol) with 300 mL of a 1:1 (V/V) DMSO/ H_2O mixture. Then add 0.1614 g DCC (782 μmol) and 0.0955 g DMAP (782 μmol) dissolved in 5 mL of DMSO, respectively, to the mixture. Stir the solution for 1 hour to activate the carboxylic group of HOOC-PEG-COOH. Add 0.2402 g curcumin (652 μmol) dissolved in 50 mL of DMSO slowly to the mixture under an atmosphere of nitrogen (N_2). Stir the mixture with a magnetic stir bar at a temperature of 60-65°C overnight. Dialyze the resultant solution was for 24 hours against DMSO and against de-ionized water for 72 hours using a dialysis membrane (MWCO: 3500 Da) to remove any unbound entities. HOOC-PEG-Cur conjugates were

initially frozen at -80°C , lyophilized and stored under refrigeration. The HOOC-PEG-Cur conjugate obtained was yellow in color.

4.2.5.3 Synthesis of Quercetin Modified POE 4600-carboxylic Acid

The quercetin modified POE 4600-dicarboxylic acid (HOOC-PEG-Quer) was prepared from a procedure adapted from Manju et al.[321] Add 5 g HOOC-PEG-COOH (1.09 mmol) with 300 mL of a 1:1 (V/V) DMSO/H₂O mixture. Then add 0.3364 g DCC (1.63 mmol) and 0.1991 g DMAP (1.63 mmol) dissolved in 5 mL of DMSO, respectively, to the mixture. Stir the solution for 1 hour to activate the carboxylic group of HOOC-PEG-COOH. Add 0.3285 g curcumin (1.09 mmol) dissolved in 50 mL of DMSO slowly to the mixture under an atmosphere of nitrogen (N₂). Stir the mixture with a magnetic stir bar at a temperature of 60-65°C overnight. Dialyze the resultant solution for 24 hours against DMSO and against de-ionized water for 72 hours using a dialysis membrane (MWCO: 3500 Da) to remove any unbound entities. HOOC-PEG-Quer conjugates were initially frozen at -80°C , lyophilized and stored under refrigeration. The HOOC-PEG-Quer conjugate obtained was pale-yellow in color.

4.2.6 Synthesis of Hyaluronic Acid Modified HOOC-PEG-Chelator.

The method used by Manju et al was adapted for the synthesis of hyaluronic acid modified HOOC-PEG-chelators.[321] Since all three families used the same method, a brief description of the procedure for HA modified with HOOC-PEG-5A8HQ is given. Combine 0.5 g HOOC-PEG-5A8HQ (109 μmol) in a 1:1 (V/V) of DMSO/H₂O mixture. Then add 0.0269 g DCC (130 μmol) and 0.0159 g DMAP (130 μmol) dissolved in 5 mL of DMSO, respectively, to the mixture. Stir the solution for 1 hour to activate the carboxylic group of HOOC-PEG-5A8HQ. Add 0.1744 g HA-100 kDa (1.09 mmol) dissolved in 40 mL of DMSO slowly to the mixture under an atmosphere

of nitrogen (N₂). Stir the mixture with a magnetic stir bar at a temperature of 60-65°C overnight. Dialyze the resultant solution was for 24 hours against DMSO and against de-ionized water for 72 hours using a dialysis membrane (MWCO: 14,500 Da) to remove any unbound entities. HA-PEG-5A8HQ conjugates were initially frozen at -80°C, lyophilized and stored under refrigeration. The HA-PEG-5A8HQ conjugate obtained was dark brown in color. The HA-PEG-Cur and HA-PEG-Quer similarly synthesized were yellow and pale yellow in color.

4.2.7 Characterization of HOOC-PEG-Chelator and HA-PEG-Chelator Conjugates.

FTIR spectra of the produced conjugates (HOOC-PEG-chelator and HA-PEG-chelator) were acquired using a Nicolet iS10 Fourier transform infrared spectrometer from Thermo Scientific. All recorded spectra were in the wave number range 4000-400 cm⁻¹.

4.2.8 The inhibition of Lipid Peroxidation of Linoleic Acid by HA and HA-PEG-Chelator

The micelle model of LPO used in this work was adapted from the procedure of Sy and coworkers.[142] The method in brief, the micelle working solution contained 250 µL of 56 mM α-LA and 2.0 mL of a 40.0 mM stock solution of 30% (w/w) Brij 35 in CH₂Cl₂. To test the influence of HA and/or HA-PEG-chelator on the LPO of α-LA, add 0.0200 g HA and/or HA-PEG-chelator were dissolved in 250 µL of H₂O to the micelle solution. Vortex the samples using a vortex mixer for 30 seconds to disperse the fatty acid. Remove the CH₂Cl₂ under reduced pressure (N₂) and dissolve the dried viscous residue in 20.0 mL of aqueous 0.2 M acetate buffer. Cover the sample vial with foil paper to protect it from light. Prepare three replicate samples for the LPO experiment. First, cover the vials with foil paper, add 250 µL of micelle solution to each vial and

dilute to 5 mL with sodium acetate buffer. A sample blank was prepared using 5 mL of 0.2 M sodium acetate buffer. Initiate oxidation in the samples by adding 400 μL of 1 mM Fe^{2+} solution acidified with 0.1 M H_2SO_4 and 1 mM AA. Add a magnetic stirrer to each vial, stir the solution at 37°C, and follow the LPO of the samples by monitoring the concentration of the CDs every 0.5 h by UV-VIS spectroscopy at 234 nm

4.2.9 Cell Culture

This study used human neural stem cells (hNSCs) purchased from Millipore Sigma (Billerica, MA). The stem cell is an immortalized human neural progenitor cell line derived from the ventral mesencephalon region of human fetal brain and immortalized by retroviral transduction with the v-myc oncogene. The hNSCs were cultured in and maintained in DMEM/F12 basal medium (Thermo Fisher Scientific, MA, USA) supplemented with 20 ng ml^{-1} basic fibroblast growth factor (FGF-2, Peprotech, Rocky Hill, NJ) and 20 ng ml^{-1} epidermal growth factor (EGF, Peprotech). Culture flask and well plates (24 or 48-well plates) pre-treated with PVAVS and proprietary integrin-based peptides were the surfaces used for adherent hNSC culture. First, add PVAVS to the surfaces for 5 minutes, and then rinse with PBS. The PVAVS formed a thin layer of hydrogel containing disulfide linkages on the cell culture surfaces, which facilitated the adhesion of the integrin-based peptides to the surface. The integrin-based peptides remained on the cell culture surfaces for 90 minutes under incubation conditions. After the incubation period, remove the peptide solution from the cell culture surfaces and rinse with PBS. The surfaces are now ready for the culture of adherent hNSC.

Add the culture medium to the cell culture container: 10-12 mL in the 250 mL flasks, 500 μL per well in 24 well plates and 250 μL per well in the 48-well plates. Rapidly thaw cryo-preserved

hNSCs in a 37°C water bath, ensuring that the cap of the cryo vial is above the water. Once thawed, spray the vial with 70% alcohol and wipe with Kim wipe, transfer the cells to a 15 mL conical centrifuge flask and add 10 mL of complete media. Centrifuge at 220 RCF (relative centrifugal force) for 5 minutes and remove the supernatant to eliminate the DMSO. Re-suspend the cells in 1-5 mL complete media and gently mix by micro pipetting the solution up and down to break up cell aggregates into small clusters. Transfer the cells to the pre-treated flasks or well plates and incubate at 37°C and humidified air with 5% CO₂. Feed the cells within 24 hours of passaging and every 48 hours thereafter. The cells used in this study did not exceed the tenth generation of passaging.

4.2.10 Inhibition of Iron (II)/Ascorbic Acid-Induced Lipid Peroxidation in hNSCs by HA and HA-PEG-Chelator

An evaluation of CDs in cell lysate samples facilitated the determination of the extent of LPO in the hNSCs cultures. The cultured hNSCs adhered to the surface of six-well plates pre-coated with an integrin-based sulfur-cross-linked peptides designed to enhance cell adhesion. Add HA and/or Ha-PEG-Chelator solution to the appropriate wells and incubate for 4 h, when the cells attained 80% confluence. The subsequent addition of 40 mM stock Fe²⁺ solution to the appropriate wells induced oxidative stress to obtain a final iron (II) concentration of 1.0 mM, 2.5 mM, and 5.0 mM, respectively. Add 50 mM ascorbic acid to the wells with the exception of the controls to ensure that iron (II) was recycled in solution. Further, incubate the cell samples for another 2.0 h to allow time for free radical production, and then wash twice with 1.0 mL of PBS buffer. Add cold sterile water to each well and sonicate the cells for 1 minute at a power setting of 180 W. Sonicate the cells in short bursts (10 s sonication and 10 s rest for each cycle) and keep the sample on ice during the sonication process. A chloroform/methanol (2:1) mixture facilitated

the extraction of lipids from the cell lysate and subsequently dried the samples under an atmosphere of nitrogen. Dissolve the residue in cyclohexane and use a derivative spectrophotometric (UV-VIS) to evaluate the amount of CDs from the cell content.

4.2.11 Influence of HA and/or HA-PEG-Chelator on Iron (II)/Ascorbate-induced Oxidative Stress on the Viability of hNSCs.

CellTiter Blue assay facilitated the determination of the effect of HA and HA-PEG-chelator on the viability of hNSCs following iron (II)-induced oxidative stress. Culture adherent hNSCs in 24 or 48-well plates at a seeding density of 7,500 or 4000 cells per well, respectively and incubate for 16-24 h. On Day 0, when the cells firmly attach, replace the culture medium with 500 μ L (24-well plate) or 250 μ L (48-well plate) of CellTiter Blue Solution (CellTiter Blue and medium in a ratio of 9:1). Incubate the cells for 2 h, after the incubation period remove the CellTiter Blue solution from the 24 or 48-well plate and add at least four 100 μ L amounts of each group to 96-wellplates and obtain fluorescence readings at 560 nm/590 nm (excitation/emission wavelength) using a microplate reader (SpectraMax, Molecular Devices). Prior to CellTiter Blue assay, on days 1, 3, 5 and 7, add fresh medium with and without HA and/or HA-PEG-Chelator (1.0 mg/mL in each well) to the assigned wells and incubate for 4 h. Subsequently, add Fe^{2+} (0.75 mM, 1.0 mM, 1.25 mM, 1.5 mM and 3.0 mM) and 50 mM AA to the assigned wells. Add media only (Do not add iron) to the wells assigned to the three control groups containing media only, HA and or HA-PEG-chelator and AA, respectively. Incubate the well plates for an additional 2 h for free radical production. At the end of the incubation period, aspirate the medium and add fresh media. The next day, evaluate the viability of the cells via CellTiter Blue assay.

4.2.12 Histochemical staining with Fluorescent Phallotoxin and DAPI to determine morphology of hNSC via Confocal Microscopy.

Each day, after the CellTiter Blue viability assay, fix and stain the adherent hNSC grown in monolayer in the well plates with actin and DAPI dyes and later examine their morphology via confocal microscopy.

4.2.12.1 Fix Adherent hNSCs with 4% Paraformaldehyde Solution in PBS

First, make 250 mL of 16% paraformaldehyde (PFA) stock solution using the procedure described herein. Add 160 mL 1x PBS to a 600 mL glass beaker in a water bath, with stirring in a ventilated hood. Ensure that the temperature of the water bath remain under 70°C to prevent the evaporation of the PFA. Allow the PFA (stored in the refrigerator) to come to room temperature and then add 40 g of the powder to the heated PBS solution. The powder will not immediately dissolve; slowly increase the pH by adding 1 M NaOH dropwise from a pipette until the solution clears. Once the PFA dissolves, cool and filter the solution and adjust the volume to 250 mL with 1x PBS in the fume hood. Re-check the pH and adjust it with small amounts of dilute HCl to pH 7.4 if needed. The solution is aliquoted and frozen (-80°C) and can be stored for at least 5 years.

Fix the hNSCs with a 4% PFA working solution. This solution is prepared using the procedure described herein. Pipette 8 mL of 16% PFA stock solution in a 50 mL tube with 32 mL 1x PBS and mix well. Aspirate cell culture medium from the well plates and wash the well by adding 250 µL (48-well plate) or 500 µL of 4% PFA solution per well. Aspirate the PFA, and add the same volume of PFA solution to each well and incubate at room temperature for 25 minutes. After the time has elapsed, aspirate the PFA solution and wash the cells with PBS at least three times. Wrap the fixed cells in parafilm and store at 2-8°C and use within six (6) months.

4.2.12.2 Staining hNSCs with Actin Dye (Phalloidin-iFluor 555 conjugate) and DAPI Dye.

Permeabilize hNSCs prior to staining with actin dye by adding 0.1 % triton x-100 in PBS to the well plates for 5 minutes. Wash three times with PBS; wait 5 minutes between each wash. Additionally, pre-incubate fixed/permeabilized hNSCs with PBS containing 1% BSA for 25 minutes prior to adding actin dye as this reduces background staining. Warm the vial with phalloidin conjugate to room temperature and centrifuge briefly before use. Prepare a 1x phalloidin conjugate working solution by adding 1 μ L of the supplied stock solution (1000x phalloidin conjugate in DMSO) to 1 mL of PBS containing 1% BSA. Add the staining solution to the well plates containing the fix/permeabilized cells and incubate for 20 minutes at 37°C. To avoid evaporation, keep the well plates covered during the incubation. Rinse gently with PBS twice to remove excess phalloidin conjugates before imaging under the microscope.

Perform 4',6-diamidino-2-phenylindole (DAPI) staining after all other staining. First, prepare the 5mg/mL DAPI stock solution (14.3 mM for the dihydrochloride or 10.9 mM for the dilactate) by dissolving the content of one vial (10 mg) in 2 mL de-ionized water or dimethylformamide (DMF). Equilibrate the sample briefly by adding PBS to the wells for about 3 minutes. Dilute the DAPI stock solution to 300 nM in PBS; remove the PBS from the well plates and DAPI solution ensuring that the cells are completely covered. Incubate for 5 minutes, and then rinse the sample several times in PBS. Add PBS to the wells; view the samples using a fluorescent microscope with appropriate filters. Wrap the sample with parafilm wrap and store the sample at 2-8°C for a short time if additional microscopic analysis is required.

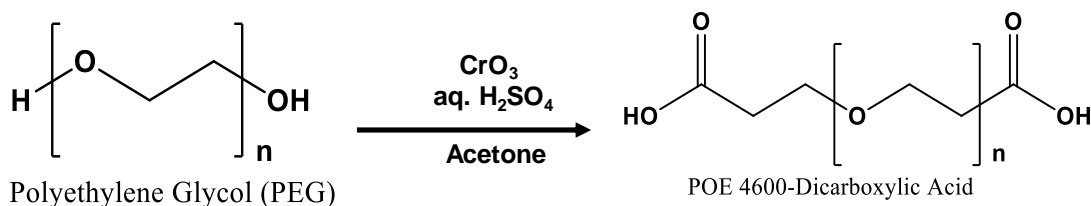
4.2.13 Statistical Analysis

All data in this study are presented as mean \pm SD. Data were analyzed in excel and p-values obtained from the data regression analysis tool

4.3 Results

4.3.1 Oxidation of Terminal Hydroxyl Groups of Polyethylene Glycol (PEG)

Polyethylene glycol is an inert amphiphilic polymer that requires activation with reactive functionalities (amine, ester, aldehyde, carboxylic acid, etc.,) prior to conjugation. Using a direct oxidation method, we replaced the inert hydroxyl end groups with reactive carboxyl functional groups. The oxidation of PEG 4600 occurred at room temperature using Jones Reagent, which consisted of stoichiometric amounts CrO_3 with respect to the hydroxyl groups. **Scheme 4.2** illustrates the oxidation of terminal hydroxyl groups of PEG to carboxyl groups. As the oxidation reaction progressed, a pale blue-green colored chromium salt formed as fine suspension in the acetone solution. Adding activated charcoal to the reaction mixture ensured the removal of all chromium salt from the reaction mixture during centrifugation. The clear colorless supernatant, containing POE 4600-dicarboxylic acid and acetone was rotary evaporated to remove the acetone. Rotary evaporation of the clear acetone solution yielded a viscous liquid. After removing any residual acetone with forced air, dissolving in water, and lyophilizing, a white powder was the final product. Acid-base titration and FTIR spectroscopy verified the presence of carboxyl group in the prepared POE 4600-dicarboxylic acid.



Scheme 4.2: Synthesis of POE 4600-Dicarboxylic Acid using Jones Reagent

4.3.2 Estimation of Carboxylic Groups per PEG Molecule

The number of carboxyl group per PEG molecule was determined from an acid-base titration between HOOC-PEG-COOH and KOH using phenolphthalein as an indicator. After standardizing the KOH with KHP, the molarity of KOH was determined as 0.0696 M. The reaction stoichiometry is 1 mole HOOC-PEG-COOH to 2 mole KOH, and the amount HOOC-PEG-COOH used in the chemical reaction was 0.5000 g. The actual amount of HOOC-PEG-COOH that reacted in the acid-base reaction is 0.4802 g or a percent yield of 96.0% using the reaction stoichiometry and pH curve. This percent yield translated to an acid value of 1.92 (~2), that is ~2 carboxyl groups per HOOC-PEG-COOH molecule. Alternatively, the number of carboxyl group per PEG molecule can be determined using equation **eqn. 1** and the titration curve shown in **Figure 4.1**. FTIR characterization of the PEG and product (HOOC-PEG-COOH) collected after oxidation with Jones reagent yielded the FTIR spectra depicted in **Figure 4.2**. This characterization corroborated the presence of carboxylic group in the sample. The peak at $\sim 1720 \text{ cm}^{-1}$ is indicative of the C=O group in a carboxylic acid such as HOOC-PEG-COOH.

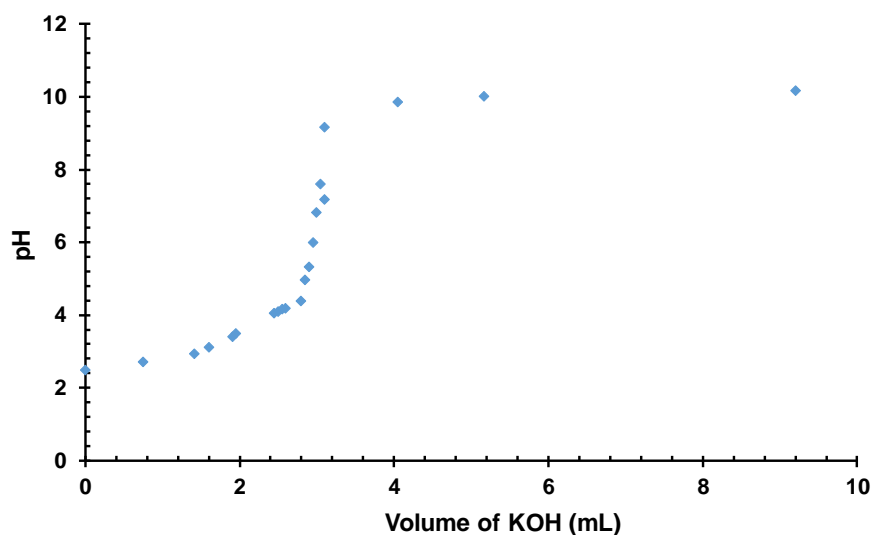


Figure 4.1: Acid-Base Titration of HOOC-PEG-COOH with KOH to Determine the Number of Carboxylic Acid Group per PEG Molecules.

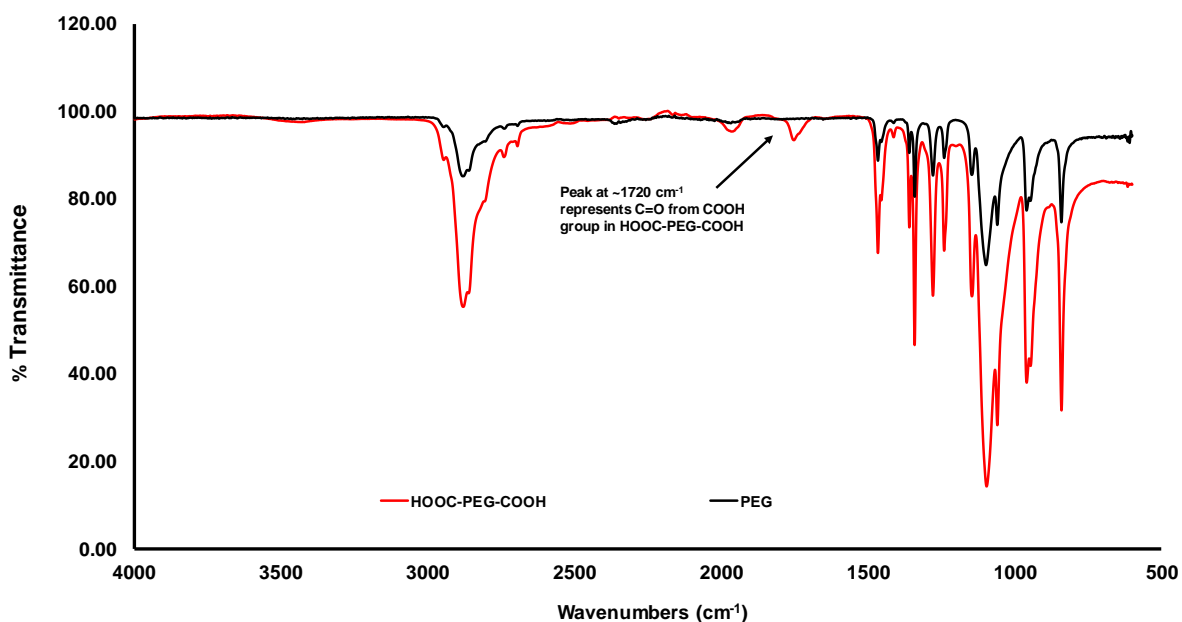


Figure 4.2: FTIR Characterization of PEG 4600 (PEG) and 4600-Dicarboxylic Acid (HOOC-PEG-COOH). The black arrow indicates the peak that represents the C=O group in carboxylic acids such as HOOC-PEG-COOH.

4.3.3 Iron Chelation Efficiency of Small Molecule Iron Chelators

The iron chelation efficiency of the small molecule iron chelators were determined by UV-vis spectrometry. We adopted the same approach used in chapter 3 to find the iron chelation efficiency

of 5A8HQ, Quer, and Cur. **Table 4.1** shows the iron chelation efficiency of the chelators using the absorption maximum of the UV-vis spectra, the iron (III) calibration curve, **Figure 3.1** and **Equation 3.1** from the previous chapter.

Table 4.1: Iron Chelation Efficiency of Small Molecule Iron Chelators

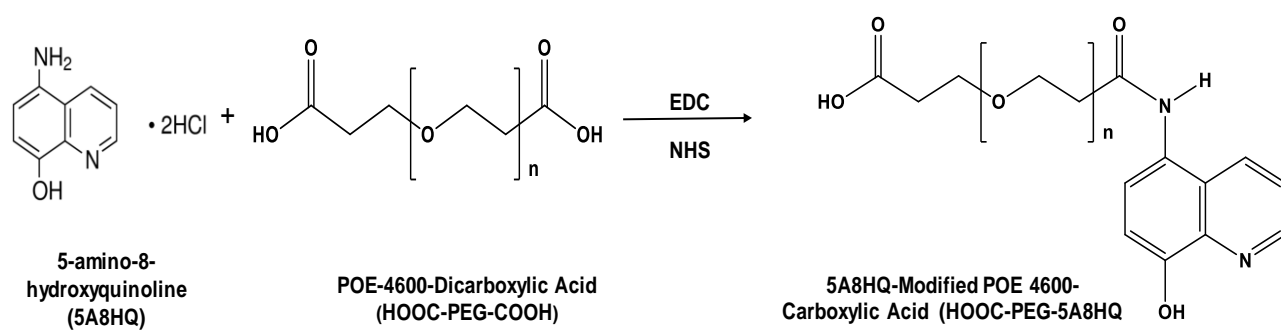
Small Molecule Iron Chelator	Initial [Fe ³⁺] before complex formation (μM)	Abs. of Fe (II) Phenanthroline complex after complexation with chelator	[Fe ³⁺] used in Fe ²⁺ - phenanthroline complex (μM)	Actual [Fe ³⁺] used to complex iron chelator	Iron Chelation Efficiency (%)
5A8HQ	28.3	0.052	7.71	20.59	72.7
Quercetin	28.3	0.043	6.26	21.74	76.8
Curcumin	28.3	0.035	4.97	23.33	83.3

4.3.4 Synthesis of Iron Chelator Modified POE-4600-Carboxylic Acid

Bioconjugation of the iron chelators with activated PEG occurred via EDC-NHS or DCC/DMAP coupling.

4.3.4.1 Synthesis of 5-amino-8-hydroxyquinoline Modified POE 4600-carboxylic Acid

The synthesis of 5A8HQ modified POE 4600-carboxylic (5A8HQ-PEG-COOH) acid occurred via EDC-NHS coupling. **Scheme 4.3** depicts the EDC/NHS conjugation of HOOC-PEG-COOH to 5A8HQ. An amide bond formation is the result of EDC/NHS conjugation. After purification and lyophilization, a pale brown powdery sample resulted. Verification that the amide functional group formed in the product resulted from a comparison of the FTIR spectra of 5A8HQ-PEG-COOH, PEG and HOOC-PEG-COOH, shown in **Figure 4.3**. The peak at ~1650 cm⁻¹, observed in 5A8HQ-PEG-COOH, represents the C=O found in amides. This peak was absent in the PEG and HOOC-PEG-COOH, indicating that the EDC/NHS-mediated Bioconjugation was successful.



Scheme 4.3: Synthesis of 5A8HQ-modified 4600 carboxylic acid via EDC/NHS mediated bioconjugation.

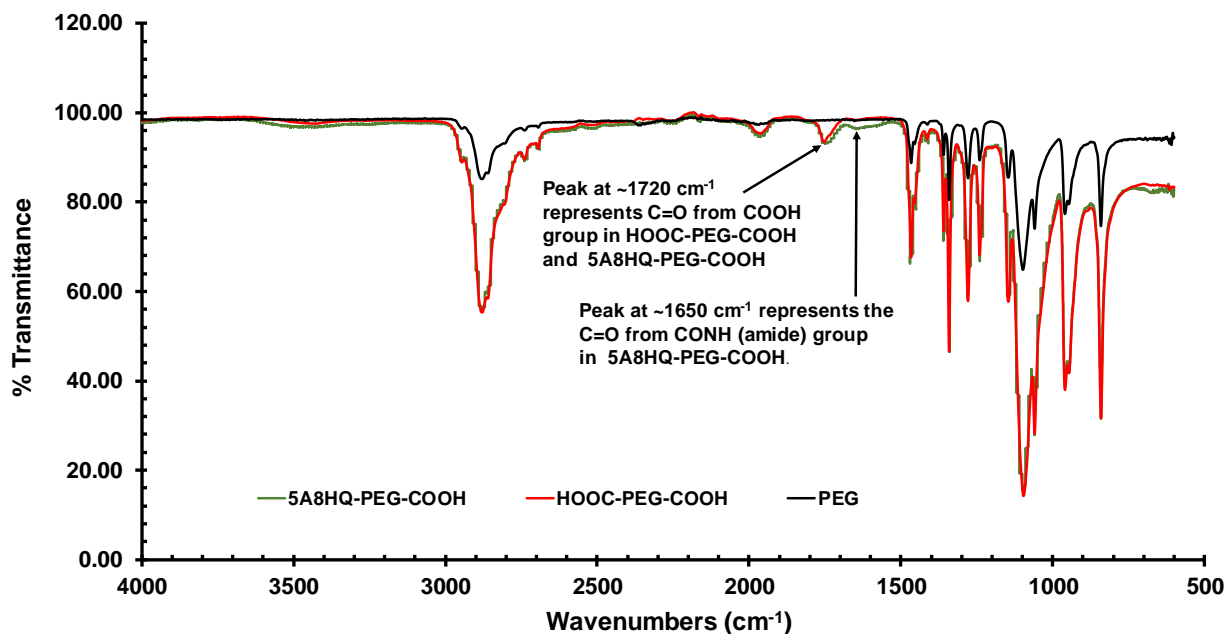
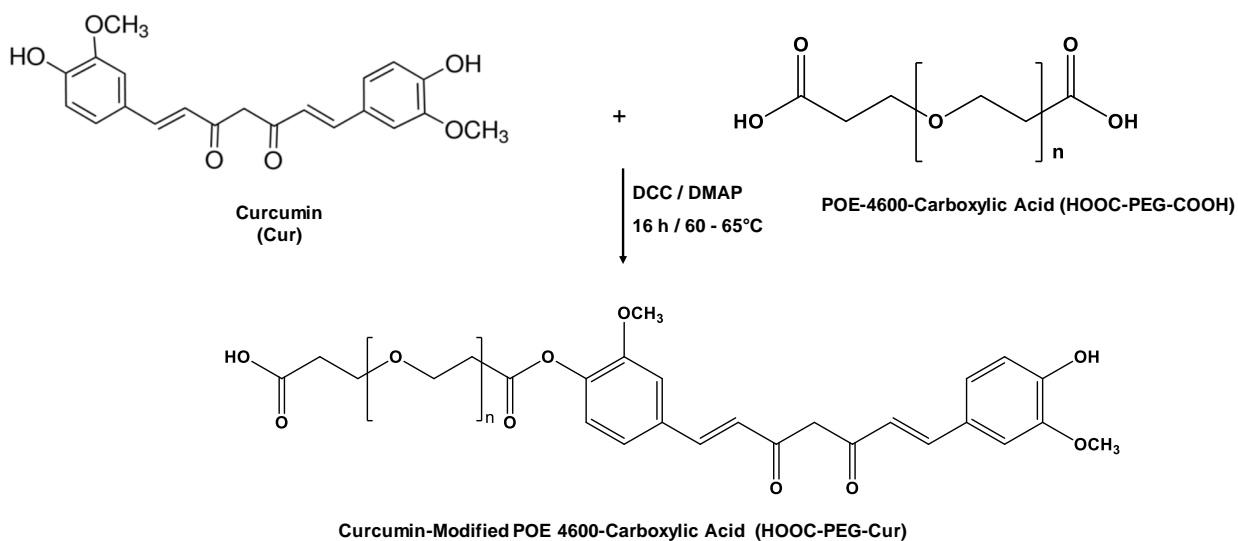


Figure 4.3: FTIR characterization of PEG 4600 (PEG), POE 4600-dicarboxylic acid (HOOC-PEG-COOH), and 5-amino -8-hydroxyquinoline-modified POE 4600-carboxylic acid (5A8HQ-PEG-COOH).

4.3.4.2 Synthesis of Curcumin Modified POE 4600-carboxylic Acid

The synthesis of Curcumin modified POE 4600-carboxylic (Cur-PEG-COOH) acid occurred via DCC-DMAP coupling, where DCC is the coupling agent and DMAP is the catalyst. **Scheme 4.4** depicts the DCC/DMAP conjugation of HOOC-PEG-COOH to curcumin. An ester bond formation is the result of DCC/DMAP conjugation. After purification and lyophilization, a yellow powdery sample resulted. Verification that the ester functional group formed in the product resulted from a comparison of the FTIR spectra of Cur-PEG-COOH, PEG and HOOC-PEG-COOH, shown in **Figure 4.4**. The peak at $\sim 1750\text{ cm}^{-1} - 1735\text{ cm}^{-1}$, observed in Cur-PEG-COOH, represents the C=O found in ester and the COOH bond of HOOC-PEG-COOH. This peak was absent in the PEG, indicating that the EDC/NHS-mediated and DCC/DMAP Bioconjugation were successful.



Scheme 4.4: Synthesis of Curcumin-Modified POE 4600-Carboxylic Acid via DCC/DMAP Esterification

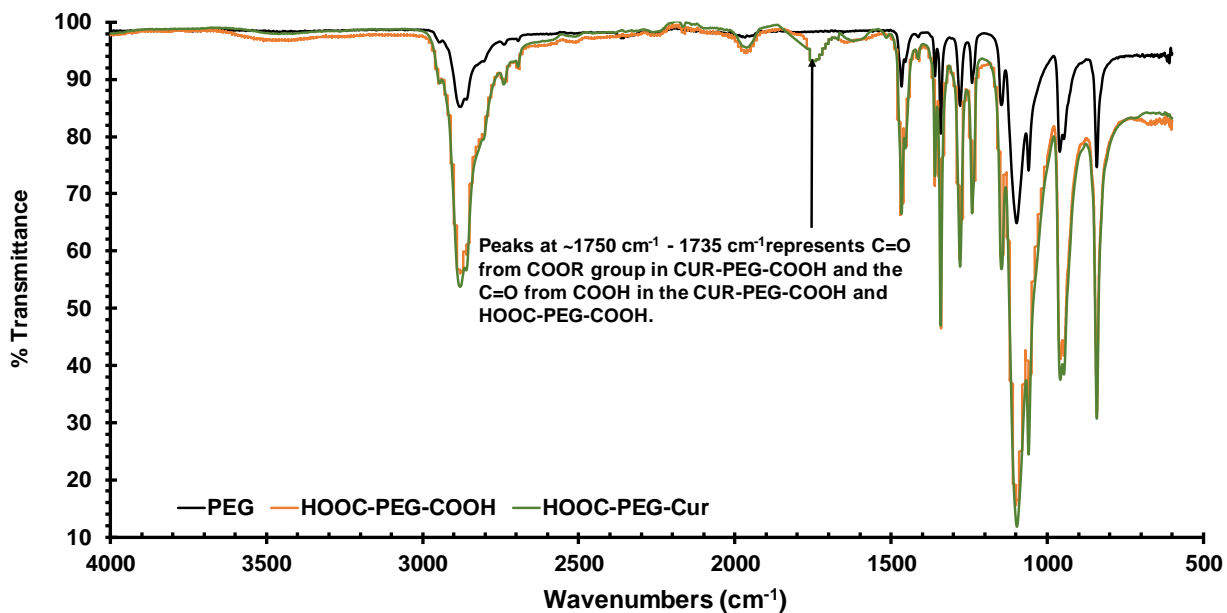
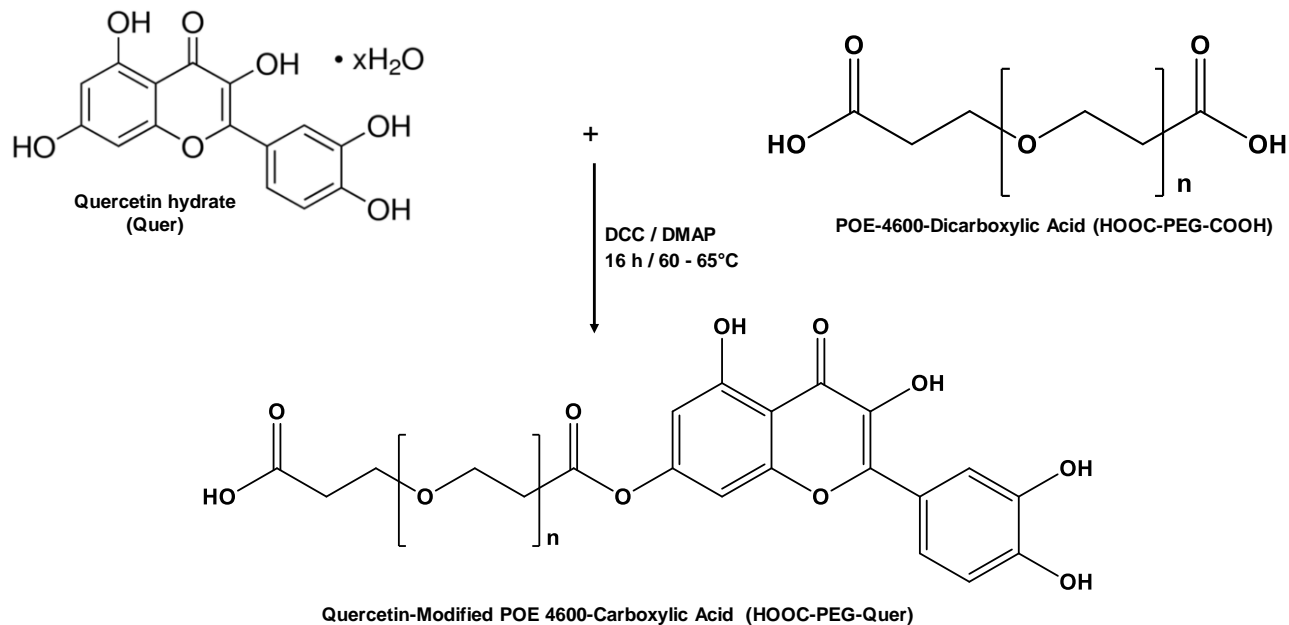


Figure 4.4: FTIR Characterization of PEG 4600 (PEG), POE 4600-Dicarboxylic Acid (HOOC-PEG-COOH), and Curcumin-Modified POE 4600-Carboxylic Acid (HOOC-PEG-Cur)

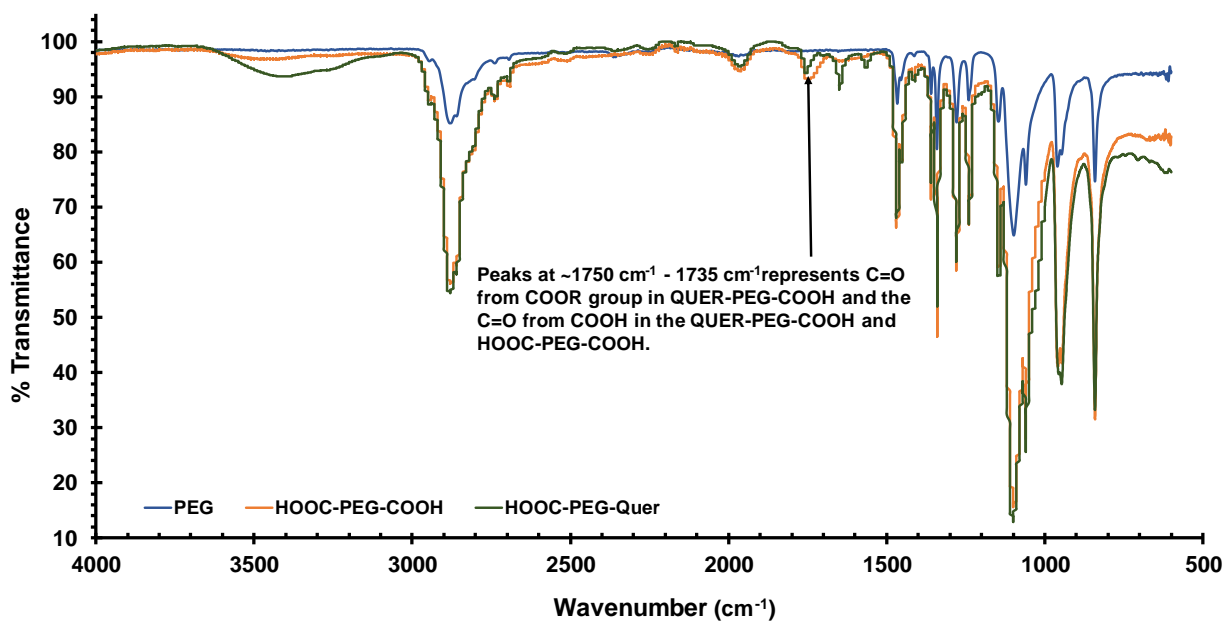
4.3.4.3 Synthesis of Quercetin Modified POE 4600-carboxylic Acid

The synthesis of quercetin modified POE 4600-carboxylic (Quer-PEG-COOH) acid occurred via DCC-DMAP coupling, where DCC is the coupling agent and DMAP is the catalyst. **Scheme 4.5** depicts the DCC/DMAP conjugation of HOOC-PEG-COOH to quercetin. An ester bond formation is the result of DCC/DMAP conjugation. After purification and lyophilization, a pale yellow powdery sample resulted. Verification that the ester functional group formed in the product resulted from a comparison of the FTIR spectra of Quer-PEG-COOH, PEG and HOOC-PEG-COOH, shown in **Figure 4.5**. The peak at $\sim 1750\text{ cm}^{-1} - 1735\text{ cm}^{-1}$, observed in Quer-PEG-COOH, represents the C=O found in ester and the COOH bond of HOOC-PEG-COOH. This peak was

absent in the PEG, indicating that the EDC/NHS-mediated and DCC/DMAP Bioconjugation were successful.



Scheme 4.5: Synthesis of Quercetin-Modified POE 4600-Carboxylic Acid via DCC/DMAP Esterification

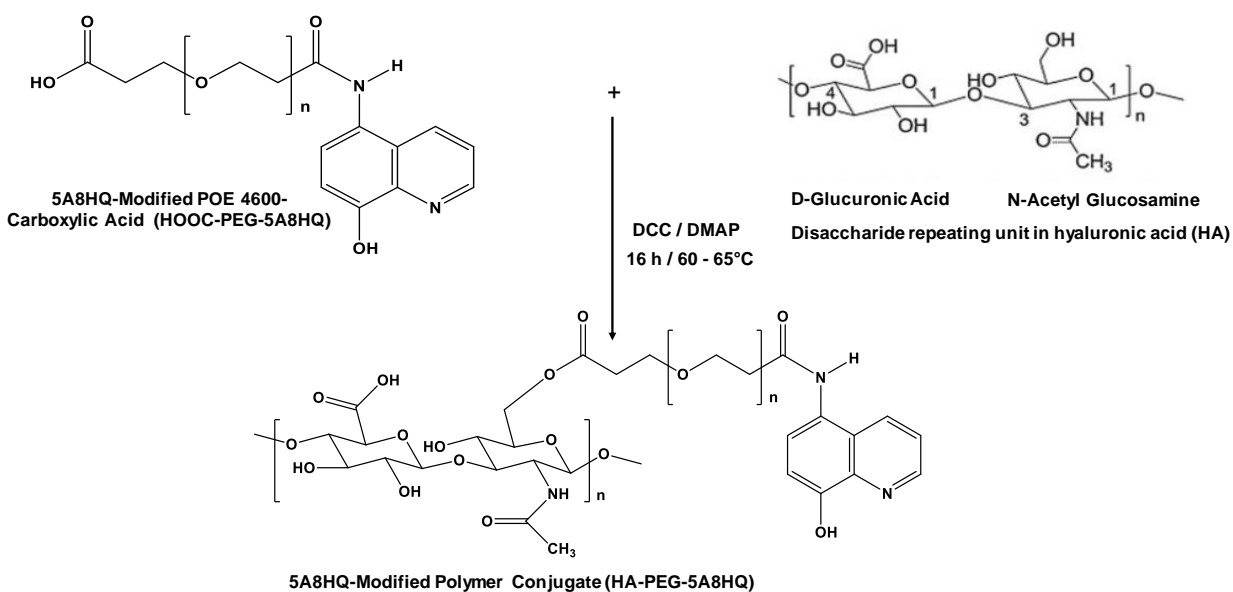


4.3.5 Synthesis of Hyaluronic Acid Modified HOOC-PEG-Chelator.

Synthesis of hyaluronic acid modified HOOC-PEG-Chelator occurred via DCC/DMAP coupling.

4.3.5.1 Synthesis of Hyaluronic Acid Modified HOOC-PEG-5A8HQ.

Synthesis of HA modified HOOC-PEG-5A8HQ occurred via the direct conjugation of the carboxyl groups of HOOC-PEG-COOH and the hydroxyl groups on the N-acetyl glucosamine unit of HA using DMAP as a catalyst and DCC as the coupling agent as shown in **Scheme 4.6**. The product, HA-PEG-5A8HQ was confirmed by FTIR spectroscopy as illustrated in **Figure 4.6**. A broad band around 3290 cm^{-1} represents the OH groups in HA and 8-hydroxyquinoline portions of the bioconjugate. The peak at 1720 cm^{-1} represents the C=O group of the ester linkage in HA-PEG-5A8HQ and the C=O from the carboxyl group in HOOC-PEG-COOH, 5A8HQ-PEG-COOH, and HA-PEG-5A8HQ. The peak at around 1640 cm^{-1} represents C=O stretching vibrations (C=O) from the secondary amide bond formed from the acetamido moiety on the N-acetyl glucosamine within the HA-PEG-5A8HQ conjugate.



Scheme 4.6: Synthesis of 5A8HQ-modified Polymer Conjugate

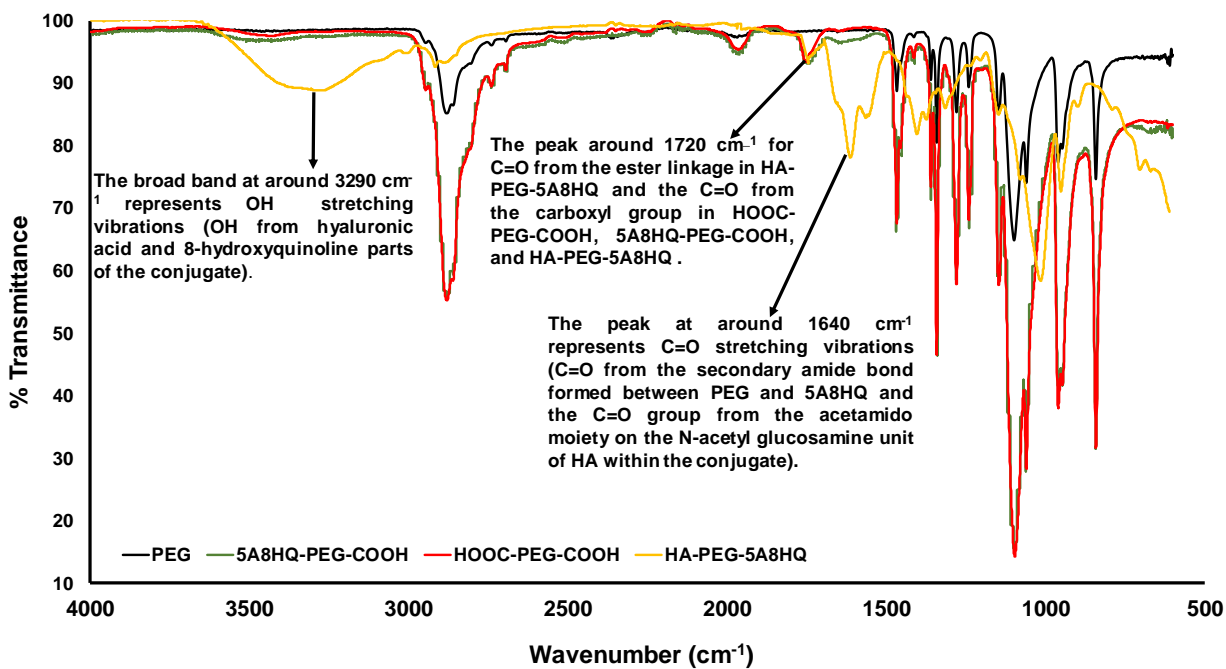
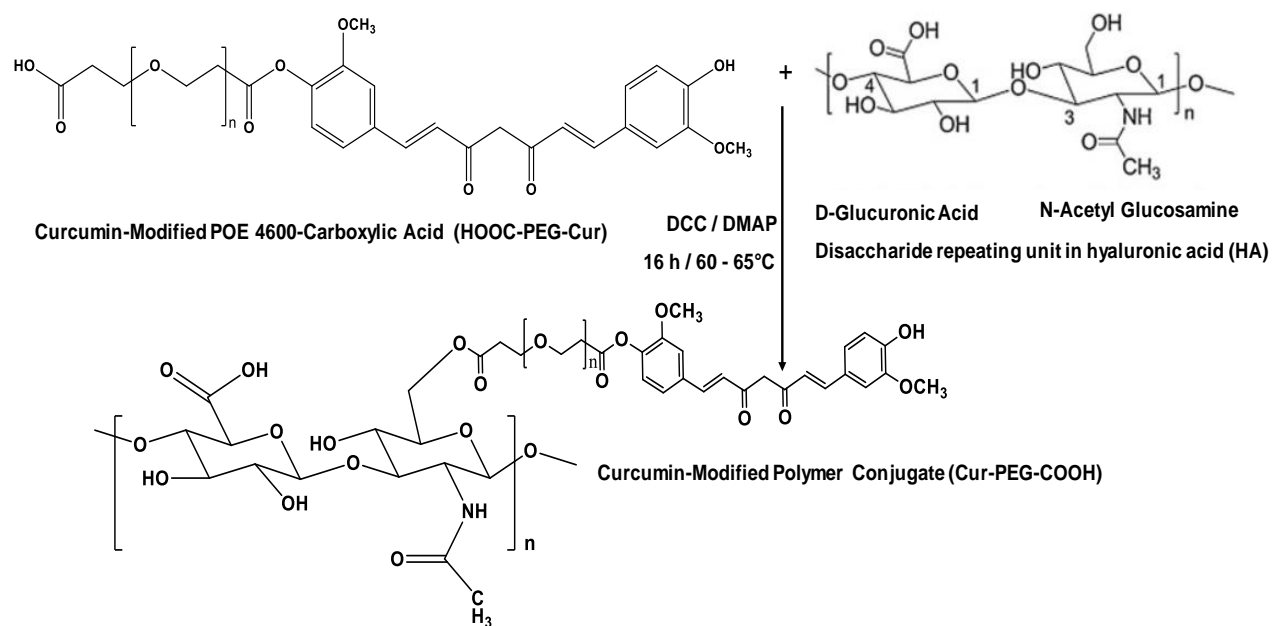


Figure 4.6: FTIR characterization of PEG 4600 (PEG), POE 4600 dicarboxylic acid (HOOC-PEG-COOH), 5-amino-8-hydroxyquinoline modified POE 4600 carboxylic acid (5A8HQ-PEG-COOH) and HA modified 5-amino-8-hydroxyquinoline POE 4600 (HA-PEG-5A8H)

4.3.5.2 Synthesis of Hyaluronic Acid Modified HOOC-PEG-Cur.

Synthesis of HA modified HOOC-PEG-Cur occurred via the direct conjugation of the carboxyl groups of HOOC-PEG-Cur and the hydroxyl groups on the N-acetyl glucosamine unit of HA using DMAP as a catalyst and DCC as the coupling agent as shown in **Scheme 4.7**. The product, HA-PEG-Cur was confirmed by FTIR spectroscopy as illustrated in **Figure 4.7**. The broad band at around 3310 cm^{-1} represents OH stretching vibrations from the hyaluronic acid and phenolic hydroxyl group on curcumin in the bioconjugate. The peak at around 1740 cm^{-1} represents C=O from the ester linkage in HA-PEG-Cur and the C=O from the carboxyl group in HOOC-PEG-COOH, Cur-PEG-COOH, and HA-PEG-Cur. The peak at around 1640 cm^{-1} represents C=O stretching vibrations from the acetamido moiety on the N-acetyl glucosamine unit of HA and the C-O stretching frequency of the diketo functionality of curcumin within the conjugate.



Scheme 4.7: Synthesis of Curcumin-Modified Polymer Conjugate

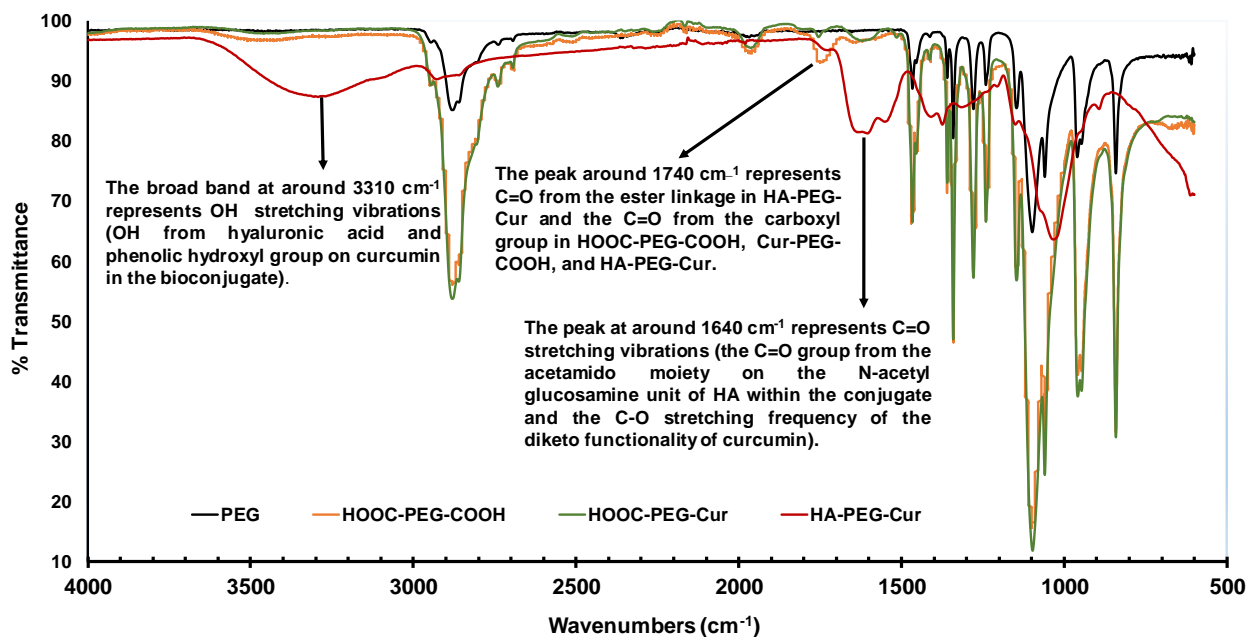
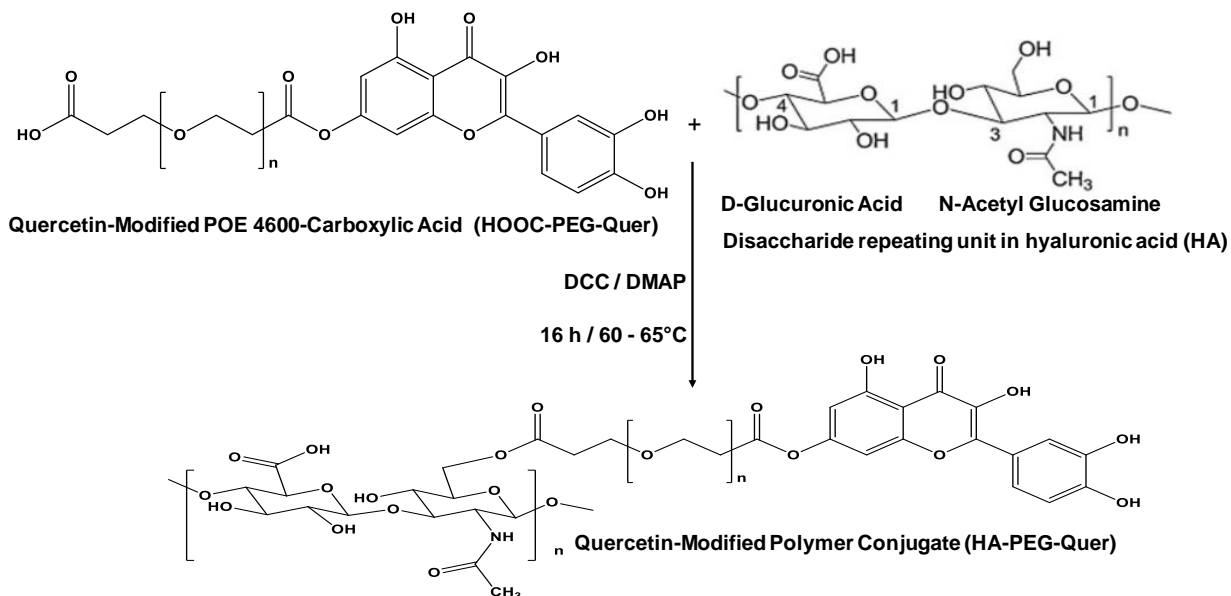


Figure 4.7: FTIR characterization of PEG 4600 (PEG), POE 4600 dicarboxylic acid (HOOC-PEG-COOH), curcumin modified POE 4600 carboxylic acid (Cur-PEG-COOH) and HA modified curcumin POE 4600 (HA-PEG-Cur).

4.3.5.3 Synthesis of Hyaluronic Acid Modified HOOC-PEG-Quer

Synthesis of HA modified HOOC-PEG-QUER occurred via the direct conjugation of the carboxyl groups of HOOC-PEG-COOH and the hydroxyl groups on the N-acetyl glucosamine unit of HA using DMAP as a catalyst and DCC as the coupling agent as shown in **Scheme 4.8**. The product, HA-PEG-5A8HQ was confirmed by FTIR spectroscopy as illustrated in **Figure 4.7**. The broad band around 3280 cm^{-1} represents the OH stretching vibrations in HA and the phenolic OH groups and the OH group on the γ -pyrone ring on curcumin in the of curcumin in the conjugate. The peak around 1740 cm^{-1} represents C=O from the ester linkage in HA-PEG-Quer and the C=O from the carboxyl group in HOOC-PEG-COOH, Quer-PEG-COOH, and HA-PEG-Quer. The peaks around 1640 cm^{-1} represents C =O stretching vibrations from the acetamido moiety on the

N-acetyl glucosamine unit of HA, the carboxylic acid of HA and the C=O (ketone group) on the γ -pyrone moiety.



Scheme 4.8: Synthesis of Quercetin-Modified Polymer Conjugate (HA-PEG-Quer)

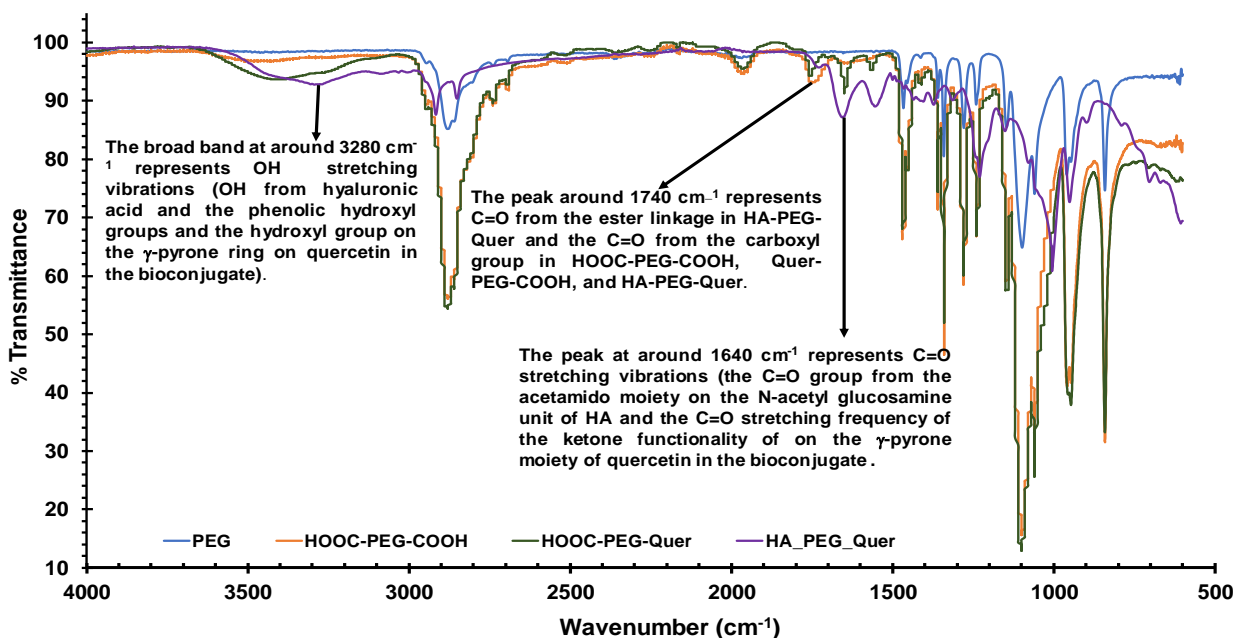


Figure 4.8: FT IR Characterization of PEG 4600 (PEG), POE 4600-Dicarboxylic Acid (HOOC-PEG-COOH), Quercetin-Modified POE 4600-Carboxylic Acid (HOOC-PEG-Quer), and Quercetin-Modified Polymer Conjugate (Quer-PEG-HA).

4.3.6 Inhibition of Iron/Ascorbate-Induced Lipid Peroxidation of α -Linoleic Acid by HA, HA-PEG-5A8HQ, HA-PEG-Cur, and HA-PEG-Quer.

Iron (II) /ascorbate-induced LPO was carried out on LA in the micelle model. Oxidation of LA results in the formation of CDs which serves as an indicator of oxidation and can be estimated with UV-VIS spectroscopy.[144] UV-VIS spectroscopic monitoring of LPO in the absence and presence of HA, HA-PEG-5A8HQ, HA-PEG-Cur, and HA-PEG-Quer are shown in **Figures 4.9, 4.10, 4.11 and 4.12**, respectively. The characteristic absorption band was observed at ~234 nm, indicative of CDs monitored during spectroscopic analysis.[145] The amounts of CD produced during LPO of LA for all sample increased over the time span of the experiment. The UV-vis spectra for the LPO of LA in the presence and absence of HA, HA-PEG-5A8HQ, HA-PEG-Cur and HA-PEG-Quer shows the greatest difference in CD signal immediately after the addition of iron (II) to the solution. In general, the absorbance signal for the other time points had smaller gaps as time increased. Further, the propagation rates for LPO in the presence of HA, HA-PEG-5A8HQ, HA-PEG-Cur and HA-PEG-Quer were lower than in the control (LPO of LA). In fact, HA, HA-PEG-5A8HQ, HA-PEG-Cur and HA-PEG-Quer inhibited LPO for each measurement taken when compared to the control.

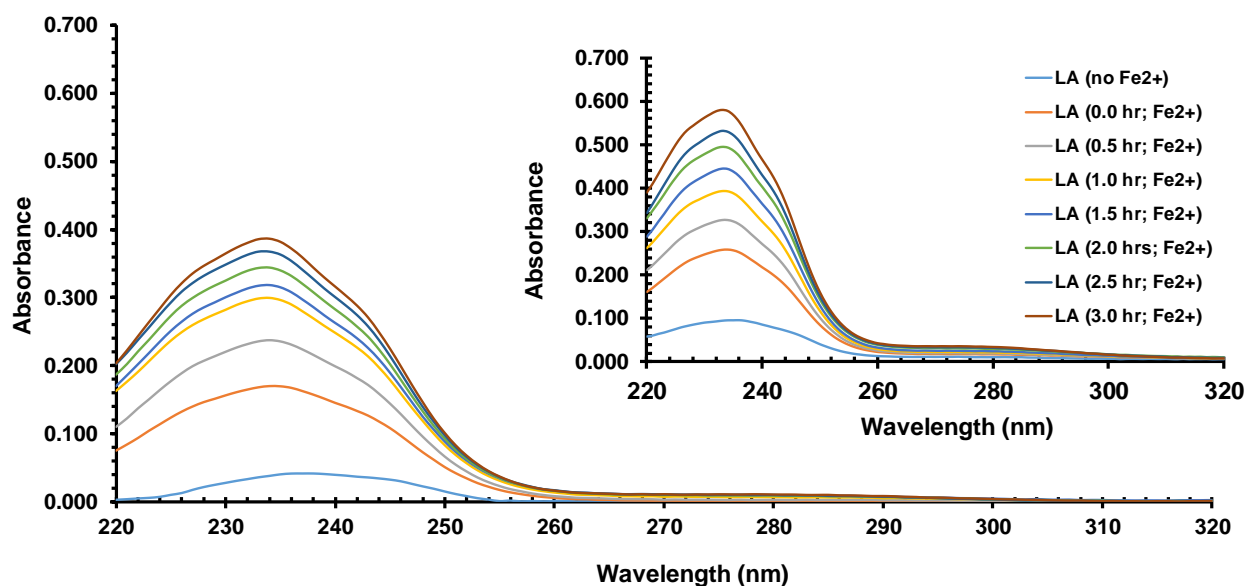


Figure 4.9: Inhibition of the lipid peroxidation of α -linoleic acid by HA (inset lipid peroxidation of linoleic acid without HA). Lipid Peroxidation was measured in terms of CDs at half hour intervals spanning a time of three hours.

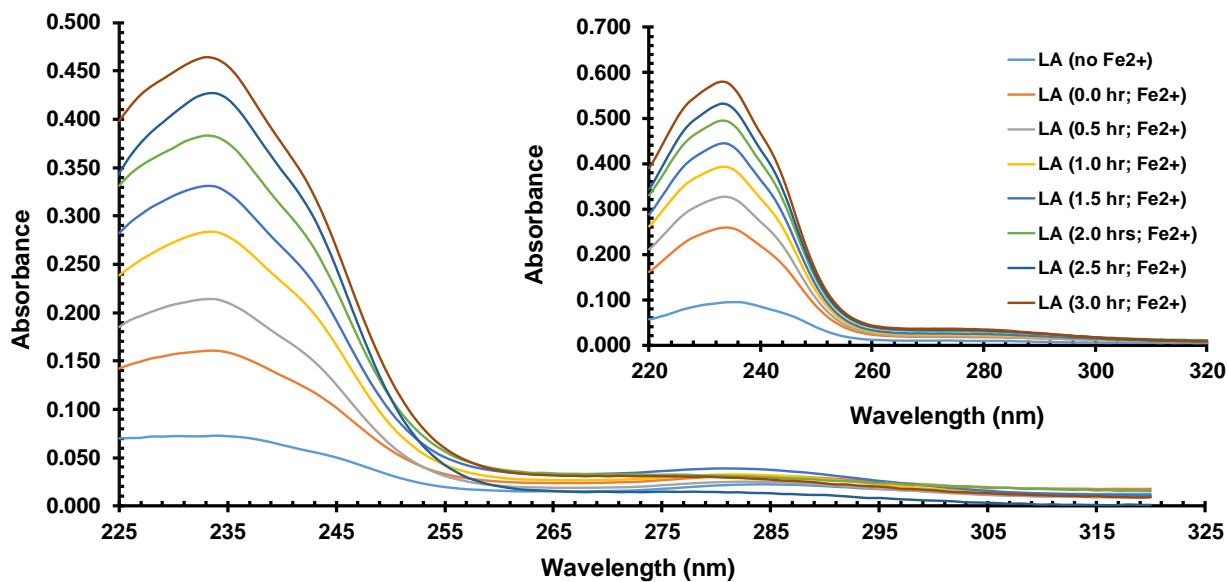


Figure 4.10: Inhibition of the lipid peroxidation of α -linoleic acid by HA-PEG-5A8HQ (Inset: Lipid peroxidation of α -linoleic acid without HA-PEG-5A8HQ). Lipid peroxidation was measured in terms of CDs at half hour intervals spanning a time of three hours.

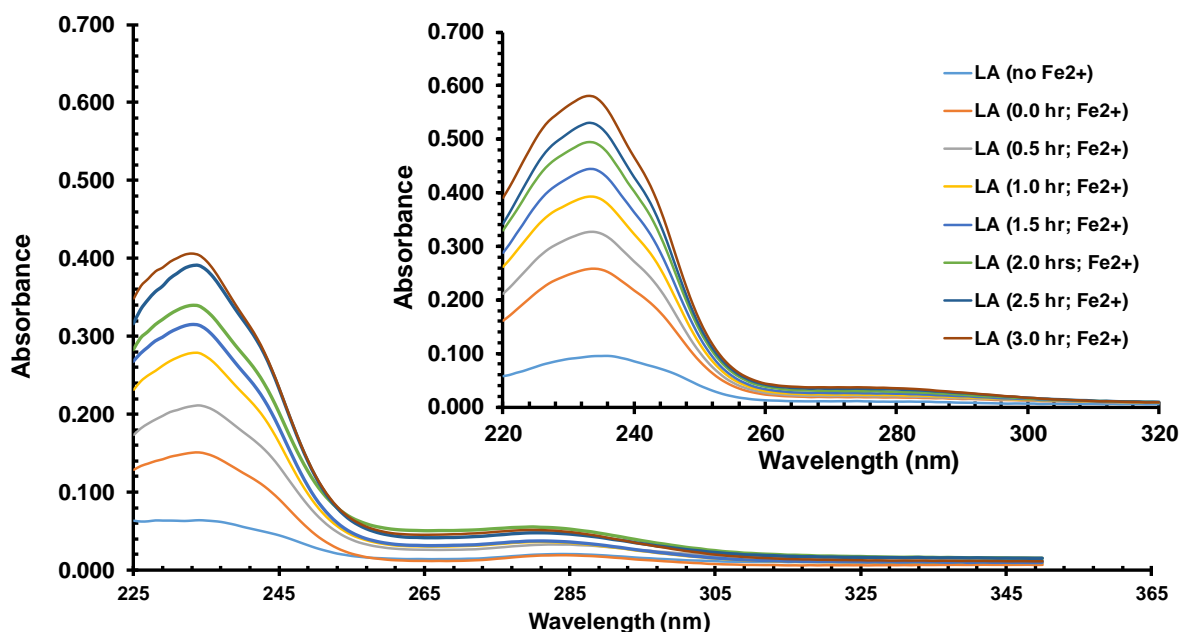


Figure 4.11: Inhibition of the lipid peroxidation of α -linoleic acid by HA-PEG-Cur (Inset: Lipid peroxidation of α -linoleic acid without HA-PEG-Cur). Lipid peroxidation was measured in terms of CDs at half hour intervals spanning a time of three hours.

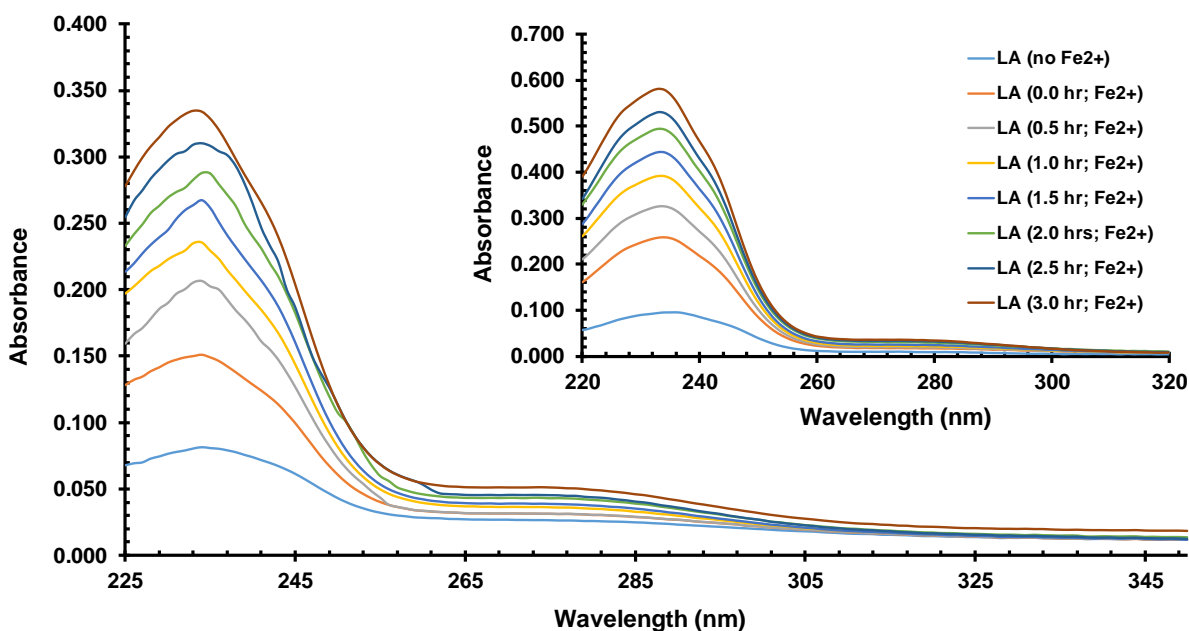


Figure 4.12: Inhibition of the lipid peroxidation of α -linoleic acid by HA-PEG-Quer (Inset: Lipid peroxidation of α -linoleic acid without HA-PEG-Quer). Lipid peroxidation was measured in terms of CDs at half hour intervals spanning a time of three hours.

The kinetic curves plotted from the spectroscopic data obtained for LPO of LA in the presence and absence of HA, HA-PEG-5A8HQ, HA-PEG-Cur, and HA-PEG-Quer further illustrates the

inhibitory effect of HA and its conjugated derivatives. **Figure 4.13** compares the rate of formation of CDs in the presence and absence of HA and its derivatives. The kinetic curves show that CDs formed rapidly in the first 30 minutes of the experiment for HA-, HA-PEG-5A8HQ-, HA-PEG-Cur-, and HA-PEG-Cur-treated LA and LA. The rate of CD formation plateaued for HA-, and HA-PEG-Cur-treated LA while the rate of CD formation continued unabated for LA in the absence of HA. CDs accumulated all the was observed for HA-PEG-Quer even though during the time of the experiment, the rate of CD formation did not show any sign of achieving steady state for HA-PEG-Quer and HA-PEG-5A8HQ. However, LA treated with HA and its derivatives produced CDs at a lower rate than the untreated LA.

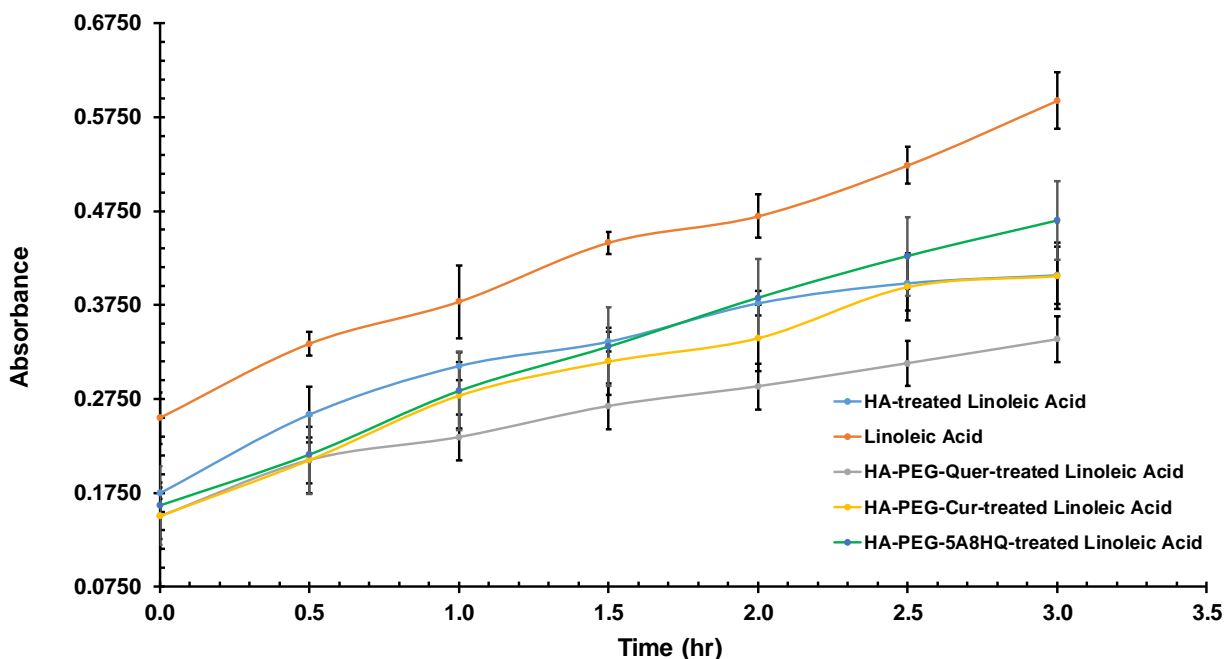


Figure 4.13: Kinetic curves for conjugated diene formed during iron/ascorbate-induced lipid peroxidation of LA in the presence and absence of HA.

4.3.7 Influence of HA, HA-PEG-5A8HQ, HA-PEG-Cur, and HA-PEG-Quer on Iron/Ascorbate-induced Oxidative Stress on the Viability of hNSC.

The effect of HA, HA-PEG-5A8HQ, HA-PEG-Cur, and HA-PEG-Quer on iron (II)/ascorbate-induced oxidative stress on cell viability was investigated over a seven-day period. To achieve iron (II)/ascorbate-induced oxidative stress, we treated the cells with iron (II) solutions having concentrations within the range 0.75 - 3.00 mM and 50 mM ascorbic acid. Initial exposure of cells to iron (II)/ascorbate did not produce a noticeable difference between the groups, shown in **Figures 4.14a, b, c, and d**. However, repeated exposure of hNSCs to iron/ascorbate-induced oxidative stress resulted in higher mortality and growth inhibition in cells, especially the untreated cells (no HA or HA-derivatives). On Day 1, the confocal images (**Figure 4.15a, b, c, and d**) for each group show that the cells began sprouting neurite outgrowths and there are more cells in the wells containing the control groups and those pre-treated with HA and its derivatives. On average, the cells in all wells looked healthy and remained adherent to the surface of the well plate. The fluorescent signal obtained from the CellTiter Blue assay and the confocal images indicate that the cells pre-treated with quercetin proliferated at a faster rate than cells pre-treated with HA, HA-PEG-5A8HQ, and HA-PEG-Cur.

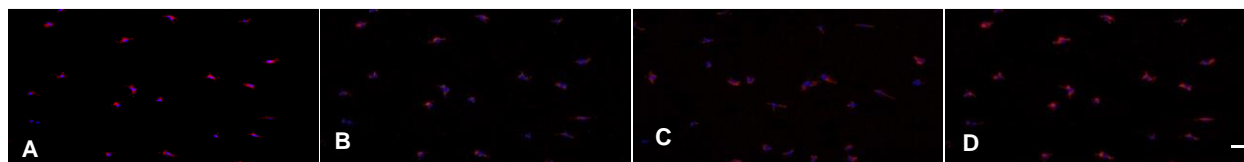
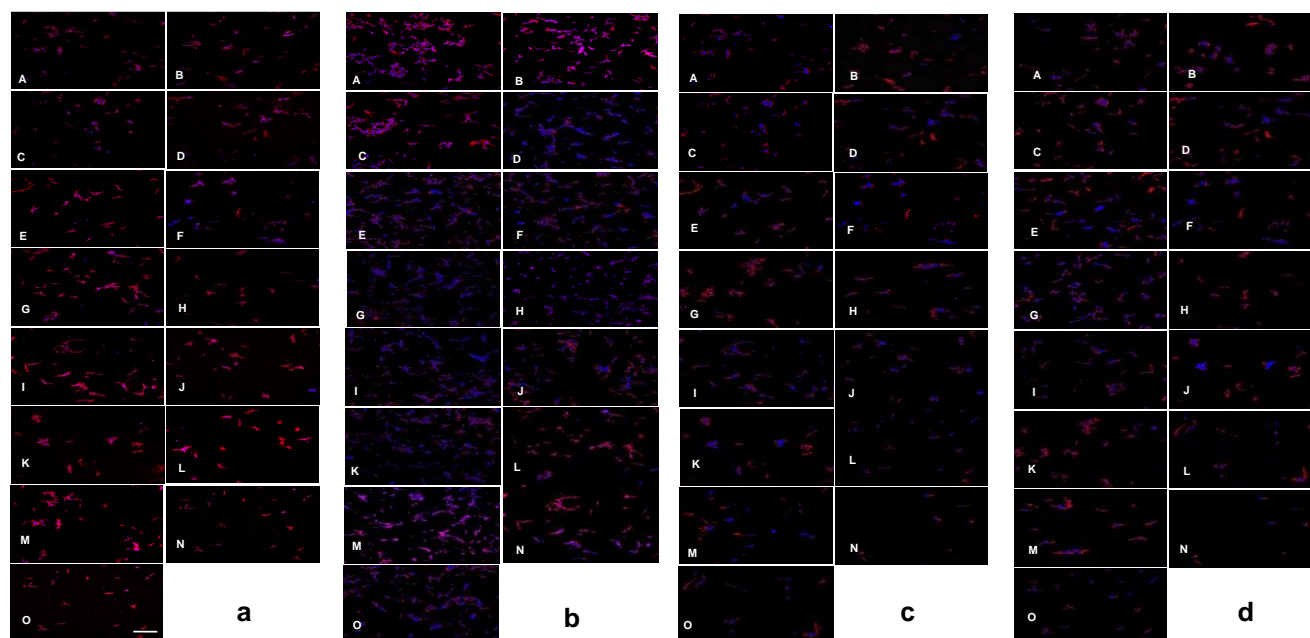
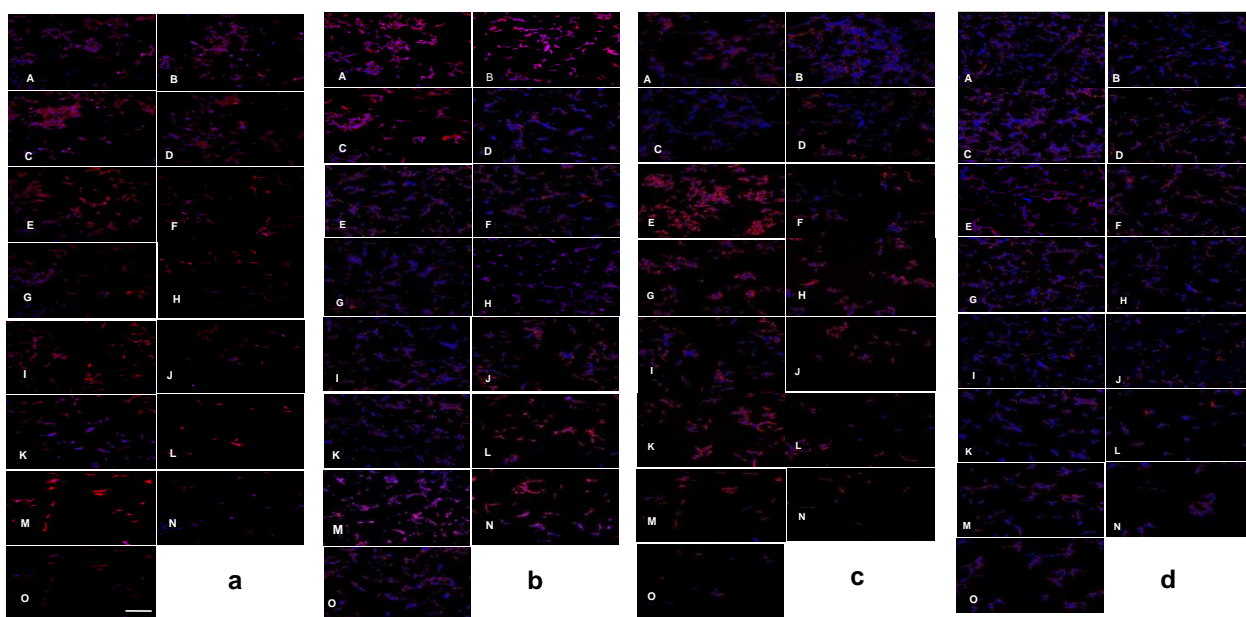


Figure 4.14: Confocal Images on Day 0. The images for the different groups were roughly identical for cells treated with and without (A) HA, (B), HA-PEG-5A8HQ, (C) HA-PEG-Cur, and (D) HA-PEG-Quer. Scale bar = 50 μ m



Figures 4.15a (HA), b (5A8HQ), c (Cur), and d (Quer): Confocal images on Day 1 for (A) media, (B) HA, (C) AA, (D) 0.75mM Fe_AA, (E) 0.75 mM Fe_AA_HA, (F) 1.0 mM Fe_AA, (G) 1.0 mM Fe_AA_HA, (H) 1.25 mM Fe_AA, (I) 1.25 mM Fe_AA_HA, (J) 1.5 mM Fe_AA, (K) 1.5 mM Fe_AA_HA, (L) 1.75 mM Fe_AA, (M) 1.75 mM Fe_AA_HA, (N) 2.00 mM Fe_AA, and (O) 2.00 mM Fe_AA_HA. Scale bar = 70 μ m

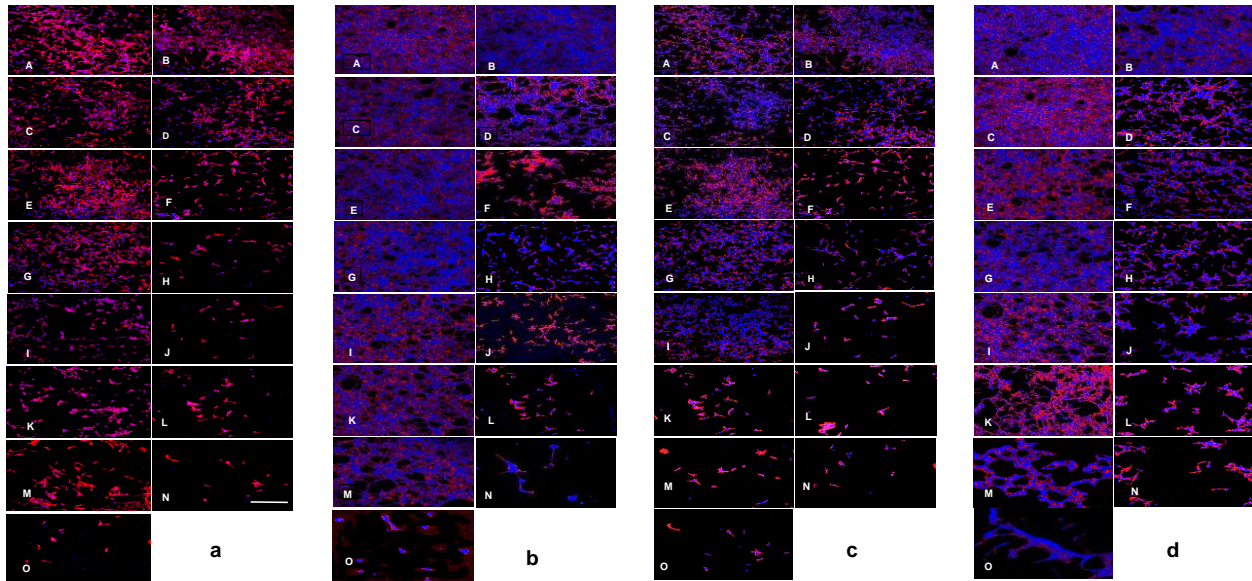
Figures 4.16a, b, c, and d show that on day 3, the cells formed an interconnected network as their neurite outgrowths increased. The control and cells treated with 0.75 mM iron (II) with/without HA and its derivatives continued to proliferate more rapidly than all other groups. Cells proliferated more in the groups pre-treated with HA, HA-PEG-5A8HQ, HA-PEG-Cur, and HA-PEG-Quer than those that were not. The rate of proliferation is dependent on the concentration of iron (II), with cells treated with lower iron (II) concentration growing at a faster rate. Similarly, the mortality rate is dependent on the concentration of iron (II), the cells treated with 1.75 mM and 2.00 mM iron (II) experienced the highest mortality as seen in **Figures 4.16a and c**.



Figures 4.16a (HA), b (5A8HQ), c (Cur), and d (Quer): Confocal images on day 3 (A) media, (B) HA, (C) AA, (D) 0.75mM Fe_AA, (E) 0.75 mM Fe_AA_HA, (F) 1.0 mM Fe_AA, (G) 1.0 mM Fe_AA_HA, (H) 1.25 mM Fe_AA, (I) 1.25 mM Fe_AA_HA, (J) 1.5 mM Fe_AA, (K) 1.5 mM Fe_AA_HA, (L) 1.75 mM Fe_AA, (M) 1.75 mM Fe_AA_HA, (N) 2.00 mM Fe_AA, and (O) 2.00 mM Fe_AA_HA. **Scale bar = 80 μ m**

Figures 4.17a, b, c, and d show that on day 5, the trend in proliferation and mortality are similar to those described on day 3. In **Figure 4.17a**, the control groups, cells treated with 0.75 mM and cells pre-treated with HA and 1.00 mM iron (II) were 70-80% confluent. **Figure 4.17c** showed a similar trend, except that cells treated with 1.00 mM and 1.25 mM iron (II) in the presence of HA-PEG-Cur were about 70-80% confluent as well. Additionally, cells treated with 0.75 mM iron (II) with HA and HA-PEG-Cur showed excellent proliferation rates, while those cells treated with higher iron (II) concentrations experience cell death in an iron (II) concentration-dependent manner. **Figures 4.17b** and **d** showed that the control groups and cells treated with 0.75 -1.00 mM iron (II) in the presence of HA-PEG-5A8HQ and HA-PEG-Quer were almost confluent. The cells treated with 1.25 -1.75 mM iron (II) in the presence of HA-PEG-Cur and those treated with 1.25 -

1.50 mM iron (II) in the presence of HA-PEG-Quer were ~80 % confluent. Additionally, the wells treated with 0.75 -2.00 mM iron (II) in the absence of HA-PEG-5A8HQ and HA-PEG-Quer experienced cell death in an iron (II) concentration-dependent manner, with a direct proportional relationship between cell death and an increase in iron (II) concentration.



Figures 4.17a (HA), b (5A8HQ), c (Cur), and d (Quer): Confocal Images on Day 5 (A) media, (B) HA, (C) AA, (D) 0.75mM Fe_AA, (E) 0.75 mM Fe_AA_HA, (F) 1.0 mM Fe_AA, (G) 1.0 mM Fe_AA_HA, (H) 1.25 mM Fe_AA, (I) 1.25 mM Fe_AA_HA, (J) 1.5 mM Fe_AA, (K) 1.5 mM Fe_AA_HA, (L) 1.75 mM Fe_AA, (M) 1.75 mM Fe_AA_HA, (N) 2.00 mM Fe_AA, and (O) 2.00 mM Fe_AA_HA. Scale bar= 120 μ m

On day 7, Figure 4.18a and c show that the control groups and cells treated with 0.75 mM iron (II) were fully confluent while all other groups experience cell death. As the iron (II) concentration increases, the higher degree of cell death. Figures 4.18b and d show that cells in the control groups and those in the presence of HA-PEG-5A8HQ or HA-PEG-Quer were fully confluent, except for group treated with 2.00 mM iron (II) and 1.50 - 2.00 Mm iron (II) in the case of HA-PEG-5A8HQ and HA-PEG-Quer, respectively. Cells treat with iron (II) experienced cell death in an iron (II)

concentration dependent manner. As the iron (II) concentration increases, the cells lose their fluids to extra cellular environment, shrink in size and in some case possibly die.

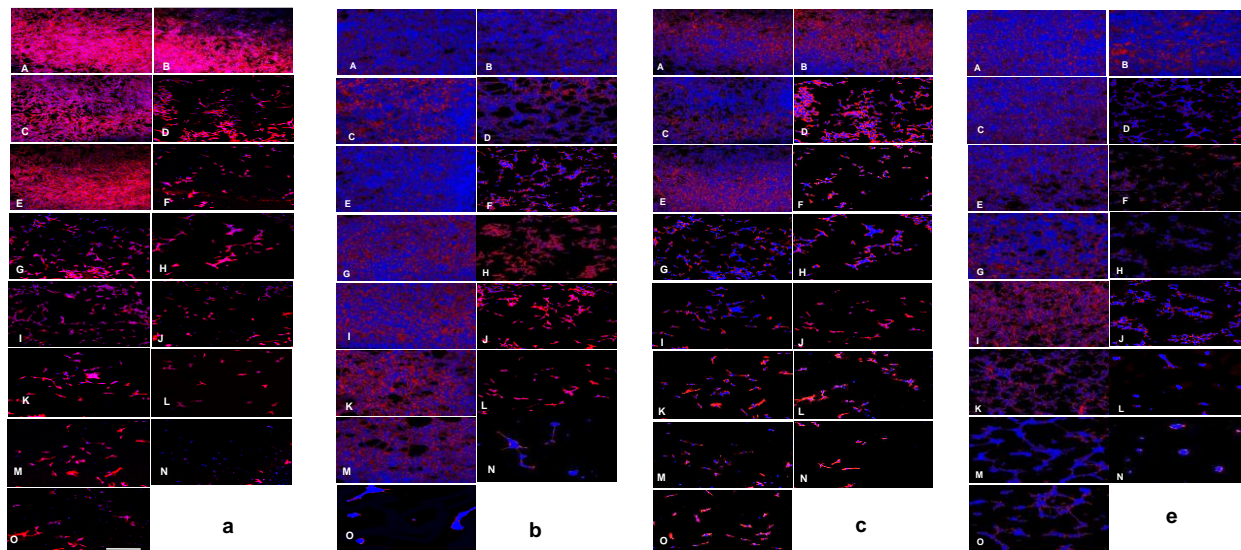


Figure 4.18a (HA), b (5A8HQ), c (Cur), and d (Quer): Confocal Images on Day 7 (A) media, (B) HA, (C) AA, (D) 0.75mM Fe_AA, (E) 0.75 mM Fe_AA_HA, (F) 1.0 mM Fe_AA, (G) 1.0 mM Fe_AA_HA, (H) 1.25 mM Fe_AA, (I) 1.25 mM Fe_AA_HA, (J) 1.5 mM Fe_AA, (K) 1.5 mM Fe_AA_HA, (L) 1.75 mM Fe_AA, (M) 1.75 mM Fe_AA_HA, (N) 2.00 mM Fe_AA and (O) 2.00 mM Fe_AA_HA. Scale bar= 210 μ m.

Figures 4.19a, b, c, and d show the results of the CellTiter-Blue viability assay for hNSC after exposure to iron (II)/ascorbate-induced oxidative stress in the presence and absence of HA, HA-PEG-5A8HQ, HA-PEG-Cur, and HA-PEG-Quer. The CellTiter-Blue reagent was diluted with hNSC culture medium in a 1:9 ratio (1.0 mL titer-blue: 9.0 mL medium) prior to adding to the cells. The CellTiter-Blue reagent permeated the cells over a 2 h interval while they incubated at 37°C in humidified air with 5% CO₂. Viable cells reduced resazurin (dark blue and non-fluorescent) to resofurin (bright pink and highly fluorescent), while non-viable cells lacked metabolic activity and as a result cannot reduce resazurin to give off a fluorescent signal. At the end of the incubation period, we transferred the medium/CellTiter-Blue mixture from the well plates with hNSC culture to 96-multiwell plates compatible with the fluorescent microplate reader

(SpectraMax, Molecular Devices). The microplate reader recorded fluorescent signals at excitation and emission wavelengths of 560 and 590 nm, respectively.

On day zero, prior to adding treatment to the experimental groups, the fluorescent responses of all groups were within a narrow range of each other (~1000 - 2000 relative fluorescence units), except for the negative control. On day one, the fluorescent signals of the different groups increased to ~3000 – 6000 relative fluorescence units, with the exception of the negative control. The fluorescent signals for the groups treated with 0.75 -1.25 mM iron (II) in the presence and absence of HA (iron (II)/ascorbate/with and without HA) (**Figure 4.19a**) were ~22% lower than the fluorescent signal in the control groups. While the groups treated with 1.50 - 2.00 mM iron (II)/ascorbate/with and without HA showed fluorescent signals 59 - 65 % lower than the control groups. The fluorescent signal for the groups treated with 0.75 -1.25 mM iron (II)/ascorbate/HA-PEG-5A8HQ were almost identical to the control groups while the groups treated with 1.50 - 2.00 mM iron (II)/ascorbate/HA-PEG-5A8HQ recorded fluorescent signals ~45 - 49% lower than the control groups (**Figure 4.19b**). The fluorescent signals for cells treated with 0.75 -1.25 mM iron (II)/ascorbate/HA-PEG-Cur were identical to those of the control groups but cells treated with 0.75 - 1.25 mM and 1.50 mM - 2.00 mM iron (II)/without HA-PEG-Cur recorded fluorescent signals ~24% and 43% lower than the fluorescent intensity of the control groups, respectively (**Figure 4.19c**). **Figure 4.19d** shows greater fluorescent signals (~12%) for the cells treated with 0.75 - 2.00 mM iron (II)/ascorbate / HA-PEG-Quer compared to the control groups but the groups treated with 0.75 - 1.25 mM iron (II)/ascorbate/ without HA-PEG-Quer and 1.50 - 2.00 mM iron (II)/ascorbate/ without HA-PEG-Quer recorded 26 % and 45 % lower fluorescent signals than the control groups respectively.

On day 3 as shown in **Figure 4.19 a, b, c and d** the control groups increased in fluorescent intensity more than 2-fold compared to day 1. The fluorescent intensities of groups treated with 0.75 mM iron (II)/ascorbate/without (HA and its derivatives) increased by ~12% for HA, HA-PEG-5A8HQ, HA-PEG-Cur, HA-PEG-Quer compared the response recorded on day 1. Additionally, the groups treated with 1.00 mM - 2.00 mM iron (II) ascorbate/without HA and its derivatives decreased in fluorescent signal by 9 - 49 % compared to day 1. The fluorescent intensities of groups treated with 0.75 - 2.00 mM iron (II) /ascorbate/HA increased slightly compared with the responses recorded on day 1. The groups treated with 0.75 - 1.75 mM iron (II)/ascorbate/HA-PEG-5A8HQ recorded nearly identical fluorescent signals, an increase of 29% over that of day 1 and cells treated with 2.00 mM iron (II) / ascorbate / HA declined in fluorescent intensity when compared to the fluorescent intensity on day 1, a decline of ~40%. The fluorescent intensity of groups treated with 0.75 - 2.00 mM iron (II) /HA-PEG-Cur increased ~62 - 102 % and the groups treated with 0.75 -1.25 mM iron (II)/ascorbate/HA-PEG-Quer increased from 34 - 51% from the signals recorded on day1. Further, the groups treated with 1.50 -1.75 mM iron (II)/ascorbate/HA-PEG-Quer recorded constant fluorescent signals when compared to day 1 and the groups treated with 2.00 mM iron (II)/ascorbate/ HA-PEG-Quer decreased in fluorescent intensity by 17%.

On day 5 as shown in **Figures 4.19a, b, c, and d**, the fluorescent signal of the control groups and 0.75 mM iron (II)/ascorbate/without HA and its derivatives increased by ~15% and ~30%, respectively compared to the intensities on day 3. Meanwhile, groups treated with 1.00 mM - 2.00 mM iron (II)/ascorbate/without HA and its derivatives show a decrease in fluorescent intensity from 5 - 30%. The groups treated with 0.75 - 1.75 mM iron (II)/ascorbate/HA, 0.75-1.75 iron (II)/ascorbate/HA-PEG-5A8HQ, 0.75-1.75 mM iron (II)/ascorbate/HA-PEG-Quer increased in

fluorescent intensity by 58 - 122%, 53 - 78%, and 7 - 25% compared to the signals recorded on day 3, respectively. The fluorescent signal increased for groups treated with 0.75 – 1.25 mM iron (II)/ascorbate by 5 – 17% and decrease for groups treated with 1.50 - 1.75 mM iron (II)/ascorbate by 6 - 30%, respectively when compared to day 3. The group treated with 2.00 mM/ascorbate /HA-derivatives remained constant for each group from day 3 to day 5.

The fluorescent intensities of the control groups increased by ~16% from day 5 to day 7, while the groups treated with 0.75 mM iron (II)/ascorbate/without HA or HA-derivatives decreased by ~46%. The groups treated with 1.00 -2.00 iron (II)/ascorbate/without HA or HA-derivatives did not undergo any significant changes from day 5 to day 7. The fluorescent intensities of groups treated with 0.75 - 1.50 mM iron (II)/ascorbate/HA or HA-PEG-Cur increased by 6 - 26 % compared to day 5. The fluorescent intensity of groups treated with 0.75 -1.25 mM iron (II)/ascorbate/HA-PEG-5A8HQ increased by 17 - 49% on day 7 compared to day 5, while the fluorescent intensity of groups treated with 1.50 - 1.75 mM iron (II)/ascorbate/HA-PEG-5A8HQ decreased by 5% and 12%, respectively. The fluorescent intensity of the groups treated with 2.00 mM iron (II)/ascorbate/HA-PEG-5A8HQ remained constant from day 5 to day 7. The fluorescent intensities of the groups treated with 1.00 mM iron (II)/ascorbate/HA-PEG-5A8HQ remained the same on day 7 compared to day 5.

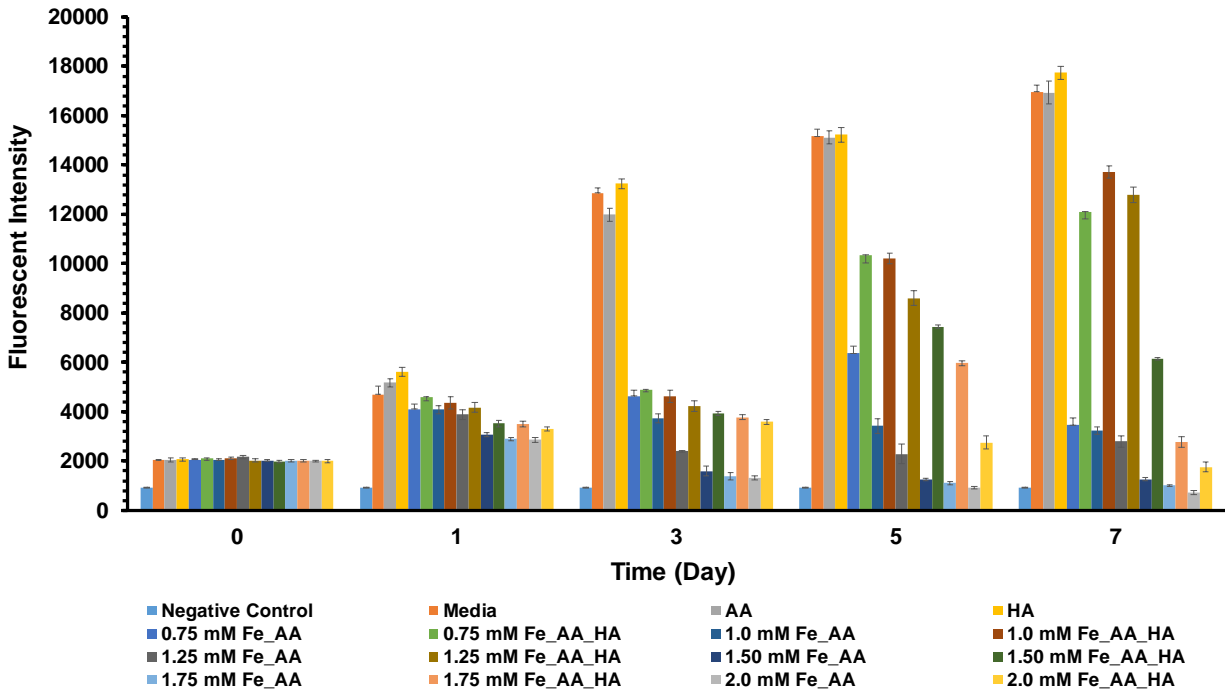


Figure 4.19a: Viability of hNSCs (CellTiter Blue Assay) with and without HA

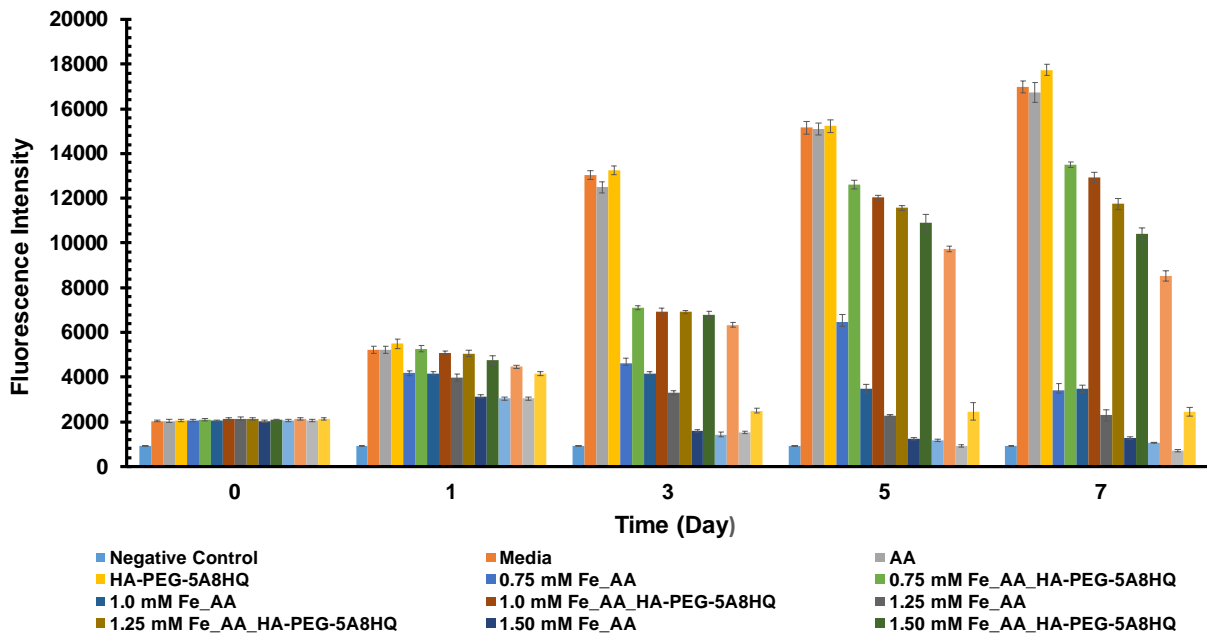


Figure 4.19b: Viability of hNSCs (CellTiter Blue Assay) with and without HA-PEG-5A8HQ

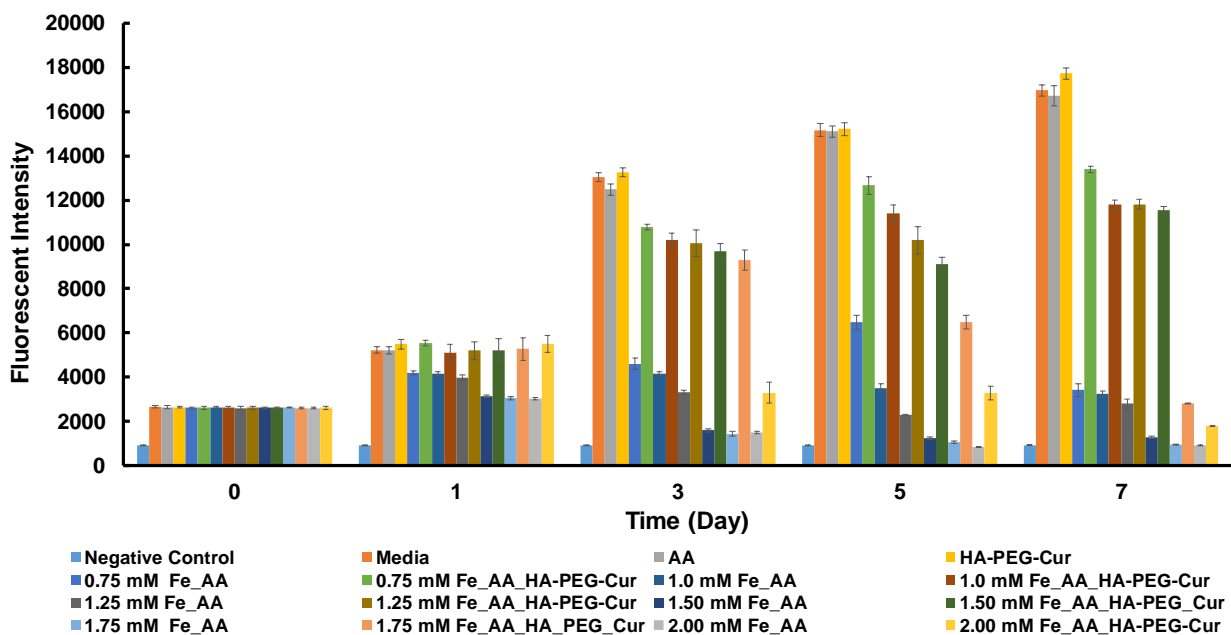


Figure 4.19c: Viability of hNSCs (CellTiter Blue Assay) with and without HA-PEG-Cur

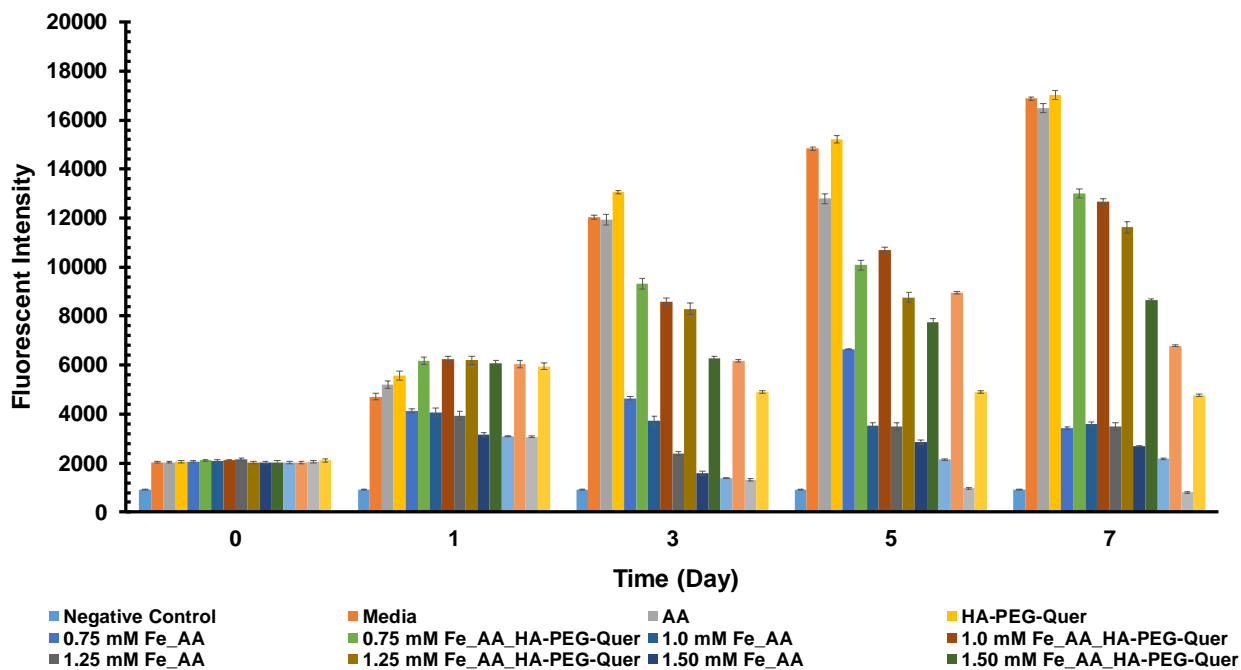


Figure 4.19d: Viability of hNSCs (CellTiter Blue Assay) with and without HA-PEG-Quer

4.4 Discussion

4.4.1 Synthesis and Characterization of HOOC-PEG-COOH

In this study, we prepared the di-carboxyl functionalized PEG via oxidation of the terminal hydroxyl groups of PEG using Jones reagent as the oxidant and acetone as the solvent. Acetone is an excellent solvent for this reaction because the greenish-blue chromium salts formed after oxidation forms a precipitate in acetone.[319] The reaction required stoichiometric amounts of CrO_3 (Jones reagent) to the terminal hydroxyl groups on PEG. Use of excess CrO_3 results in difficulty separating accumulated Cr (IV) from the product, even after multiple washes. This imparts a hint of greenish-blue to the product due to the presence of the Cr (IV) impurity.[322] The chromium salt in the reaction mixture was not easily removed by filtration, consequently centrifugation of the sample facilitated its removal. The product was isolated from the supernatant via concentration under vacuum and any trace chromium salt eliminated from the product via adsorption on activated charcoal. Customarily, organic chemists use activated charcoal to eliminate colored impurities from crude organic reaction products.[323] The carboxyl functionalized PEG was synthesized because the carboxyl functionality couples easily with polymers and small molecules containing amine or hydroxyl functional groups to form amides or esters using coupling agents such as water-soluble EDC/NHS or water insoluble DCC/DMAP.[324, 325]

To provide validation that HOOC-PEG-COOH formed via oxidation of PEG with Jones reagent, we characterized the sample using acid-base titration and FTIR spectroscopy. The acid-base titration of HOOC-PEG-COOH with KOH estimated the carboxylic groups per PEG molecule and FTIR spectroscopy determined the functional groups present in the starting material (PEG) and the product (HOOC-PEG-COOH). **Figure 4.1** shows the acid-base titration curve of HOOC-PEG-

COOH with KOH used to determine the number of carboxyl group per PEG molecule. Titration analysis and **Equation 4.1** indicated 1.92-carboxyl groups per PEG molecule, a good approximation of the theoretical value (2-carboxylic groups per PEG molecule). **Figure 4.2** shows a comparison of the FTIR characterization of PEG and HOOC-PEG-COOH. The peak at 1720 cm^{-1} is present in the spectrum of HOOC-PEG-COOH and absent in the spectrum of PEG. The peak at 1720 cm^{-1} is the characteristic transmittance signal for the C=O group present in the carboxyl group. The results from these characterizations provide evidence for the formation of HOOC-PEG-COOH.

4.4.2 Iron Chelation Efficiency of Small Molecule Iron Chelators

Iron chelation therapy originates in the treatment of iron-overload syndromes and the gold standard of care for this purpose is FDA-approved iron chelator, DFO. The clinical care of iron overload now extends to the FDA-approved orally administered iron chelators, DFX and DFP. DFX and DFO enhances the pharmacological properties relative to DFO and improve patients' adherence to therapy. Currently, iron chelation therapy extends to the treatment of diseases and injuries characterized by oxidative stress such as cardiovascular disease (CVD), neurodegenerative diseases, stroke, TBI, SCI, atherosclerosis, and cancer. While iron is not the root cause of these diseases, it plays a critical role in disease progression via promotion of cellular growth and proliferation or through participation in redox reactions, which catalyzes the formation of ROS and increases oxidative stress.[326]

In this study, we determined the chelating efficiency of three small molecule iron chelators, 5-amino-8-hydroxyquinoline (5A8HQ), curcumin (Cur) and quercetin (Quer) for iron. Table 4.1 shows the iron chelation efficiency of the small molecule iron chelators. The results show that the

iron chelation efficiencies for 5A8HQ, Cur and Quer are 72.7%, 76.8% and 83.3 % respectively. Similar to other 8-hydroxyquinoline derivatives, the iron chelation ability of 5A8HQ arise from two electron donor sites in the molecule, the N atom located on the pyridine ring and the phenolate oxygen.[327] Thus, 5A8HQ is a bidentate chelator, reacting with iron in a 3:1 stoichiometric ratio. The chelation ability of Cur arise from two electron donor sites in the molecule, the β -diketone group, a known bidentate chelator of iron, with a formation constant of 10^{22} M^{-1} .[328] The complexation mechanism of Quer with iron was studied with first principle density function theory (DFT) and the bonding energies identifies several iron binding sites in the Quer molecule. The highest binding energy identifies the 3-hydroxy-4-carbonyl group on the C-ring as the most likely chelation site for iron, followed by the 4-carbonyl-5-hydroxy on the C- and A-rings, respectively, and the 3-4-hydroxyl groups on the B-ring. Quer can form complexes with iron in a 2:1 stoichiometric ratio (more thermodynamically stable) and in a 3:1 ratio to saturate all binding sites on iron (six binding sites on iron).[329] The results obtained for the iron chelation efficiency for the small molecule chelators fits well with number of electron donor sites in the molecule. Quer has the greatest potential for binding iron due to its multiple electron donor sites and consequently has the highest iron chelation efficiency. The iron chelation efficiency of Cur is slightly higher than 5A8HQ and this difference could be due to the difference in structures of the molecules. 5A8HQ is a planar aromatic molecule consisting of fused heterocyclic rings (a benzene ring and a pyridine ring) and curcumin is a symmetrical molecule consisting of two planar aromatic rings separated by a seven-carbon linker consisting of α,β -unsaturated β -diketone moiety. The electron-donor sites in curcumin are found on the linker and maybe more readily available to iron.

4.4.3 Synthesis and Characterization of Iron Chelator Modified POE-4600-Carboxylic Acid.

In this work we PEGylated three small molecule iron chelators, 5-amino-8-hydroxyquinoline (5A8HQ), curcumin (Cur), and quercetin (Quer) via zero-length crosslinkers, EDC/NHS or DCC/DMAP. These compounds facilitate the conjugation of two molecules by forming a bond containing no additional atoms. PEGylation of the highly hydrophilic 5A8HQ occurred via EDC/NHS coupling as depicted in **Scheme 4.3**. This reaction follows a two-step mechanism; first EDC activates the carboxylate group on HOOC-PEG-COOH to form the N-hydroxysuccinimide ester (NHS ester). Then the highly nucleophilic primary amine on the 5A8HQ attacks the carbonyl group of the NHS ester to yield a stable amine bond and the NHS leaves. The NHS is water-soluble and dialysis in copious amounts of water facilitates its elimination from the reaction mixture, leaving only the product.[330]

Due to the limited water-solubility of Cur and Quer, PEGylation occurred via Steglich esterification reaction with DCC/DMAP as depicted in **Schemes 4.4 and 4.5**, respectively. Cur has two potential sites for conjugation with HOOC-PEG-COOH, the two phenolic OH groups. Choice of solvent system required a delicate balance between the hydrophilicity of the HOOC-PEG-COOH and the hydrophobicity of Cur or Quer and the coupling agent. The solvent system that works is a 1:1(v/v) mixture of H₂O/DMSO; it was able to dissolve the HOOC-PEG-COOH and Cur. The mechanism of Steglich esterification the use of DMAP as a catalyst, which accelerates the DCC-activated esterification of the carboxylic acid (HOOC-PEG-COOH) with the phenolic OH group on Cur. First, DCC and HOOC-PEG-COOH forms an O-acylisourea intermediate. The alcohol adds to the activated carboxylic acid in the presence of DMAP to form the ester and dicyclohexyl urea.[325, 331] Dialysis in DMSO for 24 h and then against DI water

for 72 h facilitate the removal of the dicyclohexyl urea (side product) and any unbounded entities. Quer has five hydroxyl groups in its structure; they are located at positions 5 and 7 on A-ring, position 3 on the C-ring, and positions 3 and 4 on the B-ring. The likelihood of conjugation with HOOC-PEG-COOH is greatest with the OH in position 7 on the A-ring or position 4 on the B-ring. The mechanism for Steglich esterification with DCC/DMAP for Quer and HOOC-PEG-COOH follows the same path as described for Cur and HOOC-PEG-COOH.

Figures 4.3, 4.4, and 4.5 shows the FTIR characterization of HOOC-PEG-5A8HQ, HOOC-PEG-Cur and HOOC-PEG-Quer, respectively. The conjugation between 5A8HQ and HOOC-PEG-COOH resulted in the formation of a secondary amide linkage. In **Figure 4.3**, peak at ~ 1720 cm^{-1} is representative of the C=O (carbonyl group) in the COOH groups of HOOC-PEG-HOOC and HOOC-PEG-5A8HQ. This peak is absent from the FTIR spectrum of PEG as it does not contain a COOH group. The peak at ~ 1650 is representative of the C=O group in the HOOC-PEG-5A8HQ, but absent in the FTIR spectrum of PEG and HOOC-PEG-COOH. The peak at ~ 1650 infers that the amide bond formation occurred during the EDC/NHS coupling of HOOC-PEG-COOH and 5A8HQ.[332]

The Steglich esterification between HOOC-PEG-COOH and Cur or HOOC-PEG-COOH and Quer via DCC/DMAP coupling agents yield an ester linkage in the conjugate formed. The FTIR spectrum for HOOC-PEG-Cur and HOOC-PEG-Quer in **Figures 4.4 and 4.5** show a peak at 1750 cm^{-1} , representative of the C=O group in HOOC-PEG-Cur and HOOC-PEG-Quer. The peak for the C=O for the carboxylic acid is around that region as well, hence a peak for the HOOC-PEG-COOH. The peak at 1750 indicate the formation of the ester linkage during the DCC/DMAP esterification reaction.[333]

4.4.4 Synthesis of Hyaluronic Acid Modified HOOC-PEG-Chelator

Schemes 4.6, 4.7, and 4.8 shows the modification HOOC-PEG-5A8HQ, HOOC-PEG-Cur, and HOOC-PEG-Quer with HA via Steglich esterification with DCC/DMAP to yield HA-PEG-5A8HQ, HA-PEG-Cur and HA-PEG-Quer. An ester linkage joins the HA to HOOC-PEG-chelator via the condensation reaction of OH group on HA and COOH group on HOOC-PEG-chelator. Even though the small molecule are potent iron chelators, the poor bioavailability of Cur and Quer and the high toxicity of 5A8HQ warrants their conjugation to polymeric materials like HA to improve their water solubility, plasma half-life and reduce their metabolism and elimination from the body.[321, 334, 335]

Figures 4.6, 4.7, and 4.8 shows the FTIR spectrum for HA-PEG-5A8HQ, HA-PEG-Cur, and HA-PEG-Quer, respectively. The broad peak in **Figures 4.6, 4.7, and 4.8** around 3290 cm^{-1} , 3310 cm^{-1} , and 3280 cm^{-1} is representative of the OH groups in HA-PEG-5A8HQ, HA-PEG-Cur and HA-PEG-Quer, respectively. The peak at 1740 cm^{-1} represents the C=O group of the ester linkage in HA-PEG-5A8HQ, HA-PEG-Cur, and HA-PEG-Quer. Additionally, this peak could also represent the C=O from the carboxyl group in HOOC-PEG-COOH, HOOC-PEG-Chelator (5A8HQ, Cur, and Quer), and HA-PEG-Chelator (5A8HQ, Cur, and Quer). The peak at around 1640 cm^{-1} represents C=O stretching vibrations from the secondary amide bond formed between HOOC-PEG-COOH and 5A8HQ and the C=O group from the acetamido moiety on the N-acetyl glucosamine unit of HA within the conjugate. In the case of Cur, the peak at around 1640 cm^{-1} represents C=O stretching vibrations (the C=O group from the acetamido moiety on the N-acetyl glucosamine unit of HA within the conjugate and the C=O stretching frequency of the diketo functionality of curcumin). As it relates to Quer, the peak at around 1640 cm^{-1} represents C=O stretching vibrations (the C=O group from the acetamido moiety on the N-acetyl glucosamine unit

of HA and the C=O stretching frequency of the ketone functionality of on the γ -pyrone moiety of quercetin in the bioconjugate). The identified peaks, especially the one at 1740 cm^{-1} representative of the ester linkage, indicate that the covalent conjugation between HA and HOOC-PEG-Chelator is successful.

4.4.5 Inhibition of Iron/Ascorbate-Induced Lipid Peroxidation of α -Linoleic Acid by HA, HA-PEG-5A8HQ, HA-PEG-Cur, and HA-PEG-Quer.

Lipids are a class of water-insoluble macromolecules, which include fats, and oils (Triglycerides), phospholipids, waxes and steroids. Lipids are essential to health and wellbeing but a buildup in the blood stream could pose a threat contribute your health, contributing to atherosclerosis and cardiovascular disease.[336] Lipids and lipid intermediates are a principal component of the structural and functional constituents of cells in biological systems, including the cells in the CNS.[337] However, these macromolecules are predisposed to oxidation through a variety of pathways including metal-dependent Fenton oxidation, enzyme-catalyzed oxidation, cell-dependent oxidation via a diversity of O_2^- and H_2O_2 -generating oxidases, and oxidation by NO-derived reactive species.[338] LPO *in vivo* results in irreversible cellular and tissue damage and is linked with the physiology and pathology of various diseases including inflammation, aging, atherosclerosis, cardiovascular diseases, osteoarthritis, CNS injuries and a number of neurodegenerative disease.[339-342] Lipids, especially, PUFAs like LA are susceptible to oxidation in the presence of metals like iron and copper; these metals act as initiators for LPO as well as the catalyst for the propagation steps of the chain reaction.[343, 344]

In the present study, we evaluated the inhibitory effect of HA and its derivatives (HA-PEG-5A8HQ, HA-PEG-Cur, and HA-PEG-Quer) on the extent of LPO in LA via iron (II)/ascorbate system using the micelle model.

Oxidation of LA results in the formation of CDs, which allows the spectroscopic monitoring of un-inhibited and inhibited lipid peroxidation of LA via UV-VIS spectroscopy. [144] Conjugated dienes are compounds that contain two carbon-carbon double bond separated by a single bond. UV-VIS spectroscopic monitoring of LPO in the absence and presence of HA, HA-PEG-5A8HQ, HA-PEG-Cur, and HA-PEG-Quer are shown in **Figures 4.9, 4.10, 4.11 and 4.12**, respectively. The characteristic absorption band was observed at ~234 nm, indicative of CDs monitored during spectroscopic analysis.[145] Each spectrum shows the accumulation of CDs over the times span of the experiment and the production of CDs was greatest for the LPO of LA without HA or its derivatives. The UV-vis spectra for the LPO of LA in the presence and absence of HA, HA-PEG-5A8HQ, HA-PEG-Cur and HA-PEG-Quer shows the greatest difference in CD signal immediately after the addition of iron (II) to the solution. Iron (II) initiated the oxidation of LA and the models containing HA, HA-PEG-5A8HQ, HA-PEG-Cur, and HA-PEG-Quer showed a slower rate of CD accumulation indicating that HA and its derivatives inhibited LPO of LA. In general, the absorbance signal for the other time points had smaller gaps as time increased showing the consumption of LA and accumulation of CDs.

The kinetic curves for LPO of LA in the presence and absence of HA, HA-PEG-5A8HQ, HA-PEG-Cur, and HA-PEG-Quer further illustrates the inhibitory effect of HA and its conjugated derivatives. **Figure 4.13** compares the rate of formation of CDs in the presence and absence of HA and its derivatives. The kinetic curves show that CDs formed rapidly in the first 30 minutes of the experiment for HA-, HA-PEG-5A8HQ-, HA-PEG-Cur-, and HA-PEG-Cur-treated LA and LA. The rate of CD formation plateaued for HA-, and HA-PEG-Cur-treated LA while the rate of CD formation continued unabated for LA in the absence of HA. During the time of the experiment, the rate of CD formation did not show any sign of achieving steady state for HA-PEG-5A8HQ and

HA-PEG-Quer. However, LA treated with HA and its derivatives produced CDs at a lower rate than the untreated LA.

LPO follows a free radical mechanism consisting of three distinct stages: initiation, propagation and, termination. In the model demonstrated here, iron (II) initiates LPO of LA by grabbing an electron (via hydrogen abstraction) from the unsaturated lipid to produce a lipid free radical. The ascorbate, a reducing agent, is incorporated in the system to ensure the availability of iron (II); it reduced the iron (III) formed back to iron (II).[152] In the case of LA, iron (II) gains an electron via hydrogen abstraction from carbon number eleven (C11) because it is positioned between the two double bonds, which makes it highly reactive. The resulting lipid free radical gains stability by forming resonance structures wherein the radical may shift to C9 or C13 with the rearrangement of the carbon-carbon double bonds between C10 & C11 and C11 & C12, respectively.[159] The results indicate a direct correlation between CD accumulation and LA consumption. The increased level of iron in the system facilitated sustained lipid peroxidation and consequently the, accumulation of CDs. However, exposure of LA to HA and its derivatives, showed a decrease in CD accumulation indicating that the molecules inhibits LPO of LA by one or multiple mechanisms. HA and its derivatives are iron potent iron chelators and the most like mechanism by which they inhibited LPO of LA is by chelating iron before it induced LPO of LA. HA and its derivatives are good antioxidants or free radical scavengers, they can inhibit LPO by donating an electron to the free radical reducing its capacity to cause oxidative stress.

LA is an appropriate model for this evaluation since it is the most abundant PUFA in mammals and its LPO products dominate.[345] Furthermore, there is a high concentration of lipids in the tissues of the CNS, which makes them highly susceptible to LPO.[346] Oxidative stress due to the

overproduction of ROS and subsequent LPO during traumatic brain and spinal cord injuries is believed to play a crucial role in the secondary injury mechanism.[158, 347] Thus, the inhibition of ROS production and LPO presents viable strategies for therapeutic interventions in CNS injuries.

4.4.6 Influence of HA, HA-PEG-5A8HQ, HA-PEG-Cur, and HA-PEG-Quer on Iron/Ascorbate-induced Oxidative Stress on the Viability of hNSC.

There is mounting evidence that accumulation of iron at CNS injury sites plays a deleterious role in TBI and SCI pathogenesis. Iron accumulation in the brain can occur by hemorrhage or micro-hemorrhage, heme-bound deposition or independently as labile iron (no-heme bound). The presence of excess iron at CNS injury sites amplifies oxidative stress, a disturbance in the balance between the production of free radicals (reactive oxygen species or reactive nitrogen species) and antioxidant defenses. The consequences of oxidative stress are DNA damage, cell injury, senescence, and cell death.[159] To protect the tissues at CNS injury sites it is fitting to design therapies that are directed towards the alleviation of oxidative stress. In this chapter, we studied the effect of HA and its derivatives on iron/ascorbate-induced oxidative stress on cell viability over a seven-day period using the CellTiter Blue assay. To initiate iron/ascorbate-induced oxidative stress, we added iron in the concentration range 0.75 - 2.00 mM to the medium used for culturing hNSCs. A sustained supply of iron (III) was maintained in the system by adding 50 mM ascorbic acid, a reducing agent, which reduces iron (III) to iron (II).[160]

The CellTiter Blue assay uses a fluorometric method to estimate the number of viable cells present in multi-well plates. In this assay, the indicator dye resazurin measures the metabolic capacity of cells, an indicator of cell viability. Viable cells has the ability to reduce resazurin into resofurin, a high fluorescent compound. Nonviable cells rapidly lose metabolic capacity, and do

not reduce the indicator dye, generating no fluorescent signal. Figures **4.14**, **4.15a, b, c, and d** - **4.19a, b, c, and d** shows the fluorescence intensities of hNSCs over seven days. The fluorescence produced in the CellTiter Blue assay is directly proportional to the number of viable cells, that is, there is a linear relationship between fluorescence and the number of cells.[161] Prior to treating the cells with iron (II)/ascorbate, the fluorescent response of all groups almost the same. This suggests that the number of viable cells in each well were nearly identical. On day 1, the fluorescent signal for all groups increased, with the control groups showing the highest fluorescent intensities and groups treated with HA, HA-PEG-5A8HQ, HA-PEG-Cur and HA-PEG-Quer showing slightly higher fluorescence intensities than the groups not treated with HA and its derivatives. Fluorescent intensities increased for the control groups and the groups treated with H and its derivatives over days 3, 5 and 7 while fluorescent intensities decreased or remained constant in for groups not treated with the absence of HA and its derivatives. Cells treated with 0.75 -1.25 mM iron (II) resisted the iron (II)-induced oxidative stress up day 3, but the accumulation of iron in the cells caused an increased in oxidative stress and subsequent cell damage and death. Increased fluorescence is indicative of cell proliferation and viability; while the group with decreased fluorescent suggest senescence and cell death. Groups pre-treated with HA and its derivatives prior to iron (II)/ascorbate had higher fluorescent signals than those not treated. The results that HA and its derivatives protected the cells from iron-induced oxidative stress. They achieved this either by acting as an iron chelator or as a free radical scavenger. However, the protection afforded by HA and its derivatives varied in an iron (II) concentration dependent manner. The higher the concentration of iron (II) the lower the cell viability. Oxidative stress results when there is an imbalance between the production of free radicals and the ability of the cell to mitigate their harmful effects through neutralization by antioxidants. The groups treated with 2.0 mM iron (II) /

ascorbate and iron (II) / ascorbate / HA or HA derivatives, the cells could not resist the induced oxidative stress and the antioxidant or iron chelation capacity of HA or its derivatives were not enough to provide protection from oxidative stress beyond day 3. The decrease in fluorescent signal validated the observations from optical imaging that 2.0 mM iron (II) is toxic to hNSCs. These cells had minimal or no metabolic activity and thus lost their inability to reduce resazurin to resofurin and the CellTiter-Blue reagent remained blue.

Confocal images indicate minimal mortality of hNSCs at all concentrations upon initial exposure to iron (II)/ascorbate in the presence or absence of HA and its derivatives. This suggests that the cells' anti-oxidative defense system was able to counteract the ROS produced by hNSCs exposed to iron (II)/ascorbate or there simply was enough accumulated iron to cause cellular damage. Cell mortality increase in an iron (II) concentration dependent manner upon further exposure of HA-treated hNSCs to iron (II)/ascorbate. At low concentrations of iron (II), for example 0.75 mM, the hNSCs continued to proliferate at a rate equivalent to the cells in the control groups. Yehuda and co-workers reported that brain cells function in an environment where the normal brain iron concentration is 0.73 mM.[162] Further, Zhou et al. and Halliwell et al. showed that under mild oxidative stress some cells are known to proliferate.[159, 163] Cells treated with 1.00 - 1.50 mM iron (II) in the presence of HA and its derivatives grew better than those treated with 1.00 - 1.50 mM iron (II) alone because HA and its derivatives chelated or scavenged the iron (II), reducing its availability for ROS production. The cells treated with only 1.25 - 2.0 mM Fe²⁺ experienced higher mortality and growth inhibition due to more intensive ROS production. On day 7, the fluorescent signal of most groups showed a downward trend; the cells in the control groups and those treated with 0.75 mM iron (II) may have outgrown the capacity of the wells and since they have no more room to grow, the cells started dying. Groups treated with 1.50 and 1.75 mM iron (II) decreased

because of the accumulative effects of oxidative stress and the inability of HA and its derivatives to protect the cells from damages caused by ROS.

4.5 Conclusion

Besides surgery and cell therapy, biomaterials have the greatest potential to impact improvement, regeneration and restoration of the CNS injury site. Among all the biomaterials, HA shows tremendous promise in neural regeneration because it is ubiquitous in ECM of the mammalian body, including the brain and spinal cord, and it has unique biochemical and biological properties. For example, the role of HA in the brain extends beyond space filling, hydration and matrix formation. It interacts with cells via HA receptors such CD 44, RHAMM and TLR4 to influence cellular processes such as cell adhesion, migration, proliferation, differentiation, axon guidance, angiogenesis, inflammation, wound repair, and morphogenesis.[348]

The work presented in this chapter examined HA, HA-PEG-5A8HQ, HA-PEG-Cur, and HA-PEG-Quer for their potential as iron chelators, their ability to provide neuroprotection and healing in the injured CNS using hNSCs as an *in vitro* model. We found that HA and its derivatives are highly biocompatible with hNSCs, potent iron chelators and good inhibitors of LPO and oxidative stress. The data collected indicate that HA-PEG-Quer is a better iron chelator than HA, HA-PEG-5A8HQ, and HA-PEG-Cur due to the fact that this flavonoid has multiple-electron donor sites in the molecule compared to HA and its other derivatives. The iron chelation efficiency of HA-PEG-Quer was determined as ~83% in comparison to HA, HA-PEG-5A8HQ, and HA-PEG-Cur with iron chelation efficiency of ~74%, ~73% and ~77%, respectively.

The performance of HA-PEG-Quer was superior to HA, HA-PEG-5A8HQ, and HA-PEG-Cur in preventing LPO, oxidative stress and thus providing neuroprotection for hNSC. HA-PEG-Quer

inhibited LPO of LA at almost twice the rate of LPO of LA without lipid peroxidation inhibitor and 1.5 time the rate in the presence of HA-PEG-5A8HQ. In the cell viability assay, the cells were more viable in HA-PEG-Quer over a longer period of time and the confocal images show that proliferated faster when treated with HA-PEG-Que. All around, the performance of HA-PEG-5A8HQ and HA-PEG-Cur were better than HA and the data gathered in this investigation indicate that all there HA derivatives have the potential to affect changes at the CNS injury site.

CHAPTER 5

5 Engineering Injectable Iron Chelation-bound hydrogels (ICH) Scaffolds as a Permissive Niche for Neural Stem Cell Growth, Viability and Proliferation.

5.1 Introduction

Sustaining a traumatic CNS injury (SCI, TBI, or stroke) or receiving a diagnosis of CNS neurodegenerative disorder such as Alzheimer's, Parkinson's, or Huntington's disease is life altering, debilitating or even fatal. Despite the millions of dollars and the extensive research efforts allocated to developing efficacious treatments, there are still no curative therapies to improve or restore the CNS after damage from injury or disease. In the case of traumatic injuries to the CNS such as TBI and SCI, there is loss of parenchymal mass resulting in disruption of neural tissue architecture. Furthermore, the formation of glial scars and cystic cavities interferes with axonal and neurite outgrowths inducing permanent neurological deficits and disabilities. The fundamental obstacles impeding regeneration and full functional and cognitive recovery from CNS damage are (i) the reduced regenerative capacity of the mammalian brain and spinal cord, compared to other organs (skin, liver, lung, and bone), (ii) scar and cystic cavity formation, and (iii) disrupted vasculature that cuts off the blood flow to tissues.

Currently, the treatment modalities for CNS injuries include the use of pharmacological agents and stem cell therapy. Therapy utilizing pharmacological agents focus on reducing the cascade of events that occur after injury and preserving the function of remaining nervous tissues while ignoring the regeneration or replacement of the damaged or necrotic tissues.[349] Additionally, pharmacological intervention is hindered by our limited understanding of the complex and dynamic processes occurring at the injury site, the inability to deliver some therapeutic agents

across the blood-brain barrier (BBB), and translational challenges in moving therapies from preclinical studies to clinics.[350] W.M. Pardridge highlighted the disparity between the design of drugs that target the BBB and the progress made in molecular neuroscience. He postulated that advances in molecular neuroscience could provide a wealth of information useful to the design of drugs that target the BBB. Currently, the majority of pharmacological agents developed for the injured brain are not able to cross the BBB; ~100% of large-molecule drugs and ~98% of small-molecule drugs do not cross the BBB. To mitigate this critical and wide-scale problem in the development of pharmacological agents that target the BBB, Pardridge proposed building BBB drug targeting technology around a knowledge base of the endogenous transporters within the brain capillary endothelium, which forms the BBB in vivo.[351]

The translation of CNS therapies from laboratory to clinical application is very challenging and failure could cost millions of dollars. For example, more than 30 clinical trials for pharmacological agents to treat TBI have failed.[352] Progesterone, a naturally occurring hormone was one of those pharmacological agents that showed promising neuroprotective effects in animal model for TBI.[353] Progesterone reduces glutamate excitotoxicity, membrane lipid peroxidation, apoptotic pathways and diffuse axonal injury.[354-357] Two randomized, double-blinded, placebo-controlled, phase II clinical trials for progesterone showed positive trends towards improvement in outcomes by progesterone treatment.[358, 359] Progesterone therapy progressed to phase III clinical trials, where two multi-center studies occurred. However, the ProTECT and SyNaPSe trial had negative outcomes; they terminated the ProTECT trial because of lack of data supporting the effectiveness of the therapy and they cited the complexity and variability of the injury and the multi injury mechanism at work as the principal factor for the negative outcome of the SyNaPSe trial.[360, 361]

A key reason for the failure of past and present CNS therapies is limited understanding of the inherent properties of neural parenchyma. Evidence suggests that human parenchyma possess inadequate progenitor neural cells and mature neural cells regenerate, proliferate, and migrate at very slow rate. Additionally, the biochemical microenvironment of the neural parenchyma is quite complex, especially after a CNS injury.[362] It is clear that improvements and potentially a cure for CNS injuries require a combination approach to overcome the challenges previously cited, one involving stem cell therapy and neural tissue engineering. Indeed, stem cell therapy is a crucial step towards replacing the damaged and necrotic tissues caused by the initial injury and the subsequent secondary injury sequelae. Stem cells are capable of restoring the damaged nervous structures because of their ability to self-renew, proliferate and differentiate into new nervous tissues producing the three lineage of neural cells (neurons, astrocytes, and oligodendrocytes).[363-365]

The clinical translation of stem cell therapy for human TBI and SCI are ongoing but there remains some obstacle to the success of this approach. These include unification of the delivery approach, correlation of stem cells with tumor formation, limited knowledge of the mechanism through which stem cells target specific tissues and the dosage required for specific transplanted stem cells to produce neural cell lines in sufficient quantities to replace damage tissues and promote full functional recovery.[366, 367] The website, <http://clinicaltrials.gov>, publishes clinical trials for TBI and SCI using stem cell/progenitor cells as therapy. [368-372] Zhang et al. used a combined procedure to deliver autologous bone marrow-derived mesenchymal stromal cells (BM-MSCs) to seven TBI patients. First, they directly infused between 10^7 - 10^9 cells into the injured area during cranial operation, and then they intravenously delivered a second dose of 10^8 - 10^{10} cells. They used the Barthel Index (BI) to assess neurologic functions of patients over a six

months period and found that these functions significantly improved at the end of this assessment. Additionally, they evaluated the safety profile of the therapy and found no BMM-MSC-related adverse effects.[368] Cox et al. treated ten pediatric patients with severe TBI using autologous bone marrow mononuclear cells (BM-MNCs, $\sim 6 \times 10^6$ cells /kg body weight) via intravenous delivery. In this clinical trial, he assessed the feasibility and safety of the treatment. They assessed the safety of the treatment by monitoring systemic and cerebral hemodynamics during bone marrow (BM) harvest and BM-MNCs-related toxicity by a number of organ function test. Further, they assessed the neurologic functions of the children one and six months post injury. All patients survived the treatment and assessment interval; they found no BM harvest-related fluctuations of systemic or cerebral hemodynamics and there were no BM-MNC-related toxicity as determined by organ tests (lungs, liver and kidney). Additionally, seven patients exhibited significant improvement in their Glasgow Outcome Scores (GOS) while three patients exhibited moderate to severe TBI.[369] Wang et al. investigated the impact of human umbilical cord mesenchymal stem cell (hUC-MSC) transplantation in patients with sequelae TBI. They infused the patients in the stem cell group with 1×10^7 hUC-MSCs via lumbar puncture at 3-4 or 4-5 intervertebral space and administered the treatment four times over an interval of 5-7 days. Wang et al. used the Fugl-Meyer Assessments (FMA) and Functional Independence Measures (FIM) to assess patients before and at 6 months after transplant. The FMA and FIM results revealed improved motor functions and patient self-care score at six months for those treated with hUC-MSCs, respectively. Patients in the control group demonstrated no significant improvement at the end of the assessment period. [370] Tian et al. evaluated the therapeutic effect and safety of autologous BM-MSC therapy in ninety-seven TBI patients (24 in a persistent vegetative state (PVS) and 73 with disturbance motor activity) in the subarachnoid space via lumbar puncture. They observed that

39.2% of patients exhibited improvement in brain function two weeks after transplant and 45.8 % of patients with PVS showed post therapeutic improvement in consciousness. More than one third (37%) of patients with motor activity dysfunction began to show improvement in motor functions within this period. Additionally, they found the time elapsed prior to treatment and the age of patient affected the outcome of the BM-MSC therapy.[371] In another clinical trial (phase I and II) for adult patients with acute severe TBI (after a 36 h time window of treatment), Cox et al. transplanted patients with autologous BM-MNC. Twenty-five (25) patients received a dose escalation (6, 9, and 12 x10⁶ cells/kg body weight) of BM-MNC and subsequently monitored for harvest/infusion related hemodynamic changes, infusional toxicity and adverse events. The patients experienced no adverse events related to harvest/infusion but there was a mild pulmonary toxicity associated with the higher dose. Additionally, they observed that inflammatory cytokine levels attenuated after infusion with BM-MNC.[372] Sharma et al. conducted a phase 1 clinical trial in which they investigated the effect of stem cell therapy on common symptoms in patients with chronic TBI. They intrathecally administered autologous BM-MNC to fourteen (14) patients and followed up with them at 1 week, 3 months, and 6 months after intervention. They assessed the study outcomes with the FIM scale, the SF-8 Health Survey Scoring and the Disability Rating scale. These scores showed a positive shift in scores at the end of the six-month assessment period. Patients exhibited functional (motor activities, balance, posture, etc.) and cognitive (memory, speech, communication, etc.) improvements. [373]

The classification of the clinical trials published for the treatment of SCI with stem cells are as follows: (i) acute (cell transplantation within a few days of injury) (ii) sub-acute (cell transplantation within six months of injury), and (iii) chronic (transplantation > six months from the injury).[367] Xiao et al. transplanted human umbilical cord MSCs loaded on a collagen

scaffold, named NeuroRegen, into the injury site of two patients with acute SCI. One patient suffered injury in the cervical region of the spine (C4) and the other patient at the thoracic level (T11). Xiao et al used the ASIA Impairment Scale, MRI and nerve electrophysiology to assess the severity of the injuries. Both patients received a diagnosis of complete SCI, a score of A on the ASIA scale, and MRI scans corroborated this result. The MRI scan of the patient with C4 injured showed abnormal MRI signal at C4 segment and the patient with T11 SCI showed a discontinuity in the spinal cord at T11 segment. The patient with C4 injury lost voluntary movements of the muscle below the injury and had no sensory response to deep anal pressure, while the patient with T11 injury experienced loss of sensation and movement below T11 and no voluntary anal contraction as well as no sensory response to deep anal pressure. Electrophysiology showed disruption of neural conduction below the level of the injury in both patient. The patients underwent standard rehabilitation after surgery and the ASIA impairment scale used to evaluate the severity of their injury each month and their nerve electrophysiology was evaluated at 2, 4, 6, and 12 months. Both patients experienced improvement in function after the surgery; they both regained some sensory function at 2 months and the 6-month assessment the sensation level increased to S2 level at the left side and T10 at the right side in the C4 patient. At the 6-month assessment, the sensory score of the T11 patient increased from 72 to 84 in the left and right side. At the 12-month assessment, the injury status of both patients improved from ASIA A complete injury to ASIA C incomplete injury. This improvement was tangible as the C4 patient was now able to raise is lower leg against gravity in the wheel chair and wiggle his toes under control while the T11 patient could walk with the hip under the help of brace. They experienced improvement in neural conduction; the C4 and T11 patient regained nerve conduction in the right lower extremity after 6 months.[374]

Hur et al. intrathecally transplanted autologous adipose-derived mesenchymal stem cells (ADMSCs) in the injury site of 14 sub-acute (the duration of the impairment 3-28 months) SCI patients with ASIA Impairment scores of A(12 patients), B (1 patient), and D (1 patient). Six patients suffered cervical injuries, one patient had cervico-thoracic injury, 6 patients suffered thoracic injuries and 1 at lumbar level. ASIA Impairment scale, MRI and nerve electrophysiology assessed the recovery outcomes of patients. The ASIA motor scores improved for 5 patients and voluntary contraction improved for 2 patients. Ten patients experience an increase in ASIA sensory score recovery but one patient showed degeneration.[375]

Vaquero et al intrathecally administered three doses of autologous mesenchymal stromal cells (100×10^6 MSCs) to patients with chronic SCI with varied degrees of severity and tracked their progress for 10 months immediately after the first treatment. In this phase II, clinical trial patients they evaluated efficacy of the treatment on nine patients and evaluated safety of the treatment on 11 patients. The used various clinical scales (ASIA Impairment Scales to assess SCI severity, Ashworth and Penn scales to evaluate spasticity and spasm, and the VAS scale to measure neuropathic pain), along with neurophysiological, urodynamic and neuroimaging before and after treatment to assess recovery outcomes. The treatment progressed without adverse events to MSCs treatment and patients showed varied improvement in sensitivity, motor function, spasticity and spasm, neuropathic pain, bladder and bowel function, and sexual function. During the course of the follow-up, three patients improved their ASIA grades from A, B, and C, to B, C, and D, respectively. After 10 months, ~60% of the patients showed improved sensory and motor functions and ~44% exhibited improved voluntary muscle contraction.[376]

Although the results were positive and promising, these improvements were not optimal, and additional studies are required to establish cell therapy as standard of care in TBI and SCI. To date, stem cell therapy has failed to realize full functional recovery in TBI and SCI patients because some of the inhibitory factors of central nervous system (CNS) regeneration still persists. Thus, a combinatorial approach that seeks to build on the gains of cell therapy and integrates several components to conquer all of the inhibitory factors to brain regeneration and spinal cord repair is required to remedy this situation.[107, 377] NTE fits this criteria; its goal is to replace or regrow damaged or necrotic tissues by using cells, biomaterial scaffolds and bioactive molecules.[378] Numerous reports have cited low stem cell survival and engraftment after transplantation and inhospitable microenvironment as challenges to the success of cell therapy.[379-381] Biomaterial scaffolds can ameliorate these situation by providing neuroprotection to the transplanted cells, act as a supportive matrix for cell infiltration and a conduit for nutrient transport to and from the lesion site.[382] Since the scaffold is integral for regenerative success and complete functional recovery, care must be taken in developing material-based strategies to mitigate against the inhibitory microenvironment at the lesion site. Attributes that are considered critical in this regards are: (1) choice of biomaterial, (2) ability to tune the biomechanical and chemical properties to mimic those of the native brain, (3) interconnected pore structures, (4) non-immunogenicity, and (5) scaffold should be reproducible and cost effective.[383] Ultimately, the designed scaffold should mimic the specific requirements of the brain or spinal cord.

The most common strategy used in NTE is a top-down approach in which a biocompatible and biodegradable scaffold serve as temporary ECM support for cells (until they create their own ECM) and controlled release carrier for therapeutics and bioactive molecules. Numerous types of scaffolds using natural or synthetic polymers can be fabricated using this approach.[383]

Architectural forms of scaffolds include nanofibers, sintered matrixes, nanofoams, nanotubes and hydrogels. In recent times, research interest in hydrogels as suitable scaffolds for NTE has increased because hydrogels are highly hydrophilic and biocompatible three-dimensional injectable constructs which can be tuned to provide suitable chemical, mechanical and spatial microenvironment comparable to the native brain tissues.[384] Woerly et al. are among the first researchers who attempted to study the effect of implanting hydrogels together with living cells in the brain. First, they encapsulated brain cells within poly-[N-(2-hydroxypropyl)-methacrylamide]-based hydrogel matrices for 1-6 days *in vitro*. Hydrogel containing Schwann cells were implanted into the rat cortex and results suggested that it promoted cellular and axonal growth *in vivo*, with the polymer.[385] Duan et al. fabricated a sodium hyaluronate collagen hydrogel and loaded it with basic fibroblast growth factor (bFGF), a system collectively referred to as bFGF-controlled release system (CRS). They found that NSCs 3D-cultured on the bFGF-CRS were induced to differentiate into a high percentage (82%) of mature neurons at 14 days *in vitro*. In TBI rat model (groups: sham, water- soluble bFGF, CRS and bFGF-CRS), NSCs were engrafted into the lesion cavity. One-month post injury, fluorescent microscopy of excised rat brains revealed that bFGF-CRS provided an optimal microenvironment, which promoted NSCs survival, differentiation and synaptogenesis between newly formed neurons and those in the host brain. Morris water maze (MWM) test showed that only the bFGF-CRS group recovered cognitive functions 30 days post-transplant.[386] Fons et al. used glial-derived neurotrophic factor (GDNF) entrapped within gelatin-based injectable hydrogel matrix to stimulate the migration of endogenous NPCs from the SVZ to the lesion site. GDNF entrapped within the porous hydrogel helped to block glial scar formation and one week post implant significantly more NPCs surrounded the implant in comparison to the lesion alone controls, indicating that the migration of NPCs are enhanced when

GDNF is incorporated. However, cells did not reach the lesion site over the time frame in which migration effect was observed, the cell disappeared 21 days post implant.[387]

Despite the promising results obtained from *in vitro* studies and animal models, there are still no clinical trials for NTE with hydrogels at this time and still no cure for TBI, indicating that there still remain some challenges to its clinical translation. Even though injectable hydrogels have met the need for providing a less invasive strategy for the delivery of therapeutics, preventative measures must be taken to ensure that biomaterials do not swell after injection. This swelling could compress neural tissues and cause further tissue and functional loss.[388] Further, there might be some challenges with scalability from animal models to clinical translation. For example, integration of the hydrogel biomechanical properties with the spatiotemporal controls of signaling molecules and important ECM components.[389]

Another challenge to clinical translation of NTE with hydrogel is the impact of iron overload at the injury site. Iron overload is a documented condition in TBI and stem cell transplantation and it may increase toxicity and infection events at the TBI lesion site making the environment inhospitable to regeneration.[141, 390-393] With the exception of certain species of bacteria, iron is an essential nutrient for all living organisms and plays a crucial role in normal brain functioning as iron is necessary for oxygen transport, oxidative metabolism and it is a co-factor in the production of neurotransmitters and myelin. In the normal brain, iron homeostasis is tightly regulated and is accomplished by four classes of compounds: (1) iron-containing proteins, (2) heme proteins, (3) iron-sulfur enzymes and (4) iron-containing enzymes.[394] A dysfunction in iron regulation in the brain may result from iron deficiency or overload. Iron deficiency may cause changes in these different proteins and their functions, but iron overload is harmful due to its

catalytic activities in the formation of highly reactive oxygen species (ROS) leading to oxidative stress. Additionally, this high availability of free iron could increase the microbial growth as it is an essential nutrient for all pathological micro-organism.[395]

At least 75% of the body's iron content is found within erythrocytes bound to oxygen-carrying heme proteins which include hemoglobin. The remaining 25 % of iron is "non-heme" iron bound to plasma transport protein called transferrin and plasma storage protein called ferritin.[396] The normal brain has a relatively high concentration of iron (second only to the liver) consistent with its high oxidative metabolic activities and high energy demands. It is possible for certain regions of the brain (substantia nigra and globus pallidus) to have iron content that exceeds hepatic levels.[397] Despite stringent regulation of iron in the brain, conditions such as TBI-induced intracranial hemorrhage (ICH) may induce iron release from transferrin and ferritin due to a decrease in pH and the release of iron from heme due to hemoglobin extravasation.[398, 399] These events may lead to iron overload at the TBI lesion site with a large increase in chelatable free iron, which is too large to be sequestered by ferritin within cells. If this chelatable iron pool is left unchecked could lead to significant cellular damage.[141, 400] Iron toxicity arising from oxidative stress results from Fenton Chemistry where iron reacts with reactive oxygen intermediates, including hydrogen peroxide (H_2O_2) and superoxide anion (O_2^-) to produce ROS such as hydroxyl free radical. Since the brain has relatively low antioxidant defenses it is especially susceptible to oxidative damage which will lead to cell death and degeneration.[401] In support of this hypothesis, Zhang et al. and Willmore et al. performed *in vitro* and *in vivo* studies, respectively, that indicate that exposure of neuronal cells to iron induces lipid peroxidation leading to loss of cell viability through apoptosis.[402, 403] Further, another group of researchers showed

that iron-induced free radical production and neurodegeneration were attenuated by supplying deferoxamine, an iron chelator, in rat hippocampal neurons.[404]

In this work, we aim to investigate and ameliorate the impact of iron overload on NTE. We will employ iron chelators tethered to injectable hydrogel scaffolds as a controlled release drug to modulate the iron concentration in the TBI lesion while providing neuroprotection. We strongly envision that, this NTE therapy will alleviate the toxic and infectious events at the TBI lesion site as well as attenuating the production of excess free radical and related secondary injury. Further, we expect this NTE strategy to promote full functional recovery in CCI TBI rat model via improved cell survival and engraftment, migration, differentiation and integration within the host tissues.

5.2 Materials and Methods

All reagents were purchased from Sigma Aldrich Chemical Co. (St. Louis MO) or VWR International unless otherwise noted. The reagents used to prepare thiolated-HA (HA-SH) and thiolated –HA-PEG-chelator (5A8HQ, Cur, and Quer) were HA (80-100 kDa), HA-PEG-chelator (~80 - 100 kDa), 1.0 M NaOH, 1.0 M HCl, HCl solution (pH 3.5) cysteine hydrochloride monohydrate or L-cysteine, EDC, and NHS and 100 mM NaCl. The HA-SH and HS-HA-PEG-chelator were purified using dialysis tube with 14, 500 MWCO. The reagents used for quantifying the free sulfhydryl groups in the HA-SH and HS-HA-PEG-chelator were 0.1 M sodium phosphate, 1 mM EDTA, cysteine hydrochloride monohydrate, DTNB (Ellman's reagent solution; 5,5'-dithio-bis-(2 -nitrobenzoic acid). The materials used to prepare the injectable hydrogels were HA-SH, The cell culture surfaces used for adherent hNSCs were 250 mL cell culture flasks and 24 or 48-well plates for suspension culture purchased from Greiner Bio-One (Monroe, NC). The reagents

used in the coating material for adhering hNSCs to cell culture surfaces are phosphate buffer saline (PBS), poly (vinyl alcohol-co-vinyl sulfone) (PVAVS) and proprietary integrin-based peptide coating. The hNSC culture media consisted of DMEM/F12 solution and supplements. Accutase is the hNSC detachment reagent and PBS used for rinsing. The non-toxic reagent used in the cell viability evaluation of hNSC was CellTiter-Blue purchased from Promega (Madison, WI).

5.2.1 Synthesis of thiolated HA and HA-PEG-Chelator

The method used by Bian et al was adapted for the synthesis of HA-SH and HS-HA-PEG-chelators.[405] In brief, thoroughly dissolve 400 mg HA or HA-PEG-Chelator and 230 mg NHS (2mmol) in 80 mL of DI water under magnetic stirring at room temperature. Then, add 383 mg (2 mmol) EDC in the solid form into the reaction solution and allow to react for 2h to activate the carboxylic groups of HA or HA-PEG-chelator. After this time interval, dissolve 121.2 mg L-cysteine (1 mM) dissolved in 10 mL DI water and it slowly to the reaction mixture. Adjust the pH of the reaction mixture to 4.75 by adding 1.0 M NaOH or 1.0 HCl and allow the reaction solution to stir for 24 h. Subsequently, transfer the reaction solution to 14500 MWCO dialysis tubing and every two hours against dilute HCl solution (pH 3.5) containing 100 mM NaCl for 48 h. The acidified solution was initially frozen at -80, lyophilized to produce HA-SH or HS-HA-PEG-chelator and stored under refrigeration.

5.2.2 Quantitating Sulfhydryl Groups Using a Cysteine Standard

The method used by Ellman was adapted for quantitating the sulfhydryl groups on HA-SH and HS-HA-PEG-chelators.[405] In brief, prepare standard solutions of cysteine hydrochloride monohydrate at concentrations of 0 -1.5 mM in 0.1 M sodium phosphate, containing 1mM EDTA, known as the reaction buffer. Then prepare 7 test tubes, each with 50 μ L of Ellman's reagent

solution and 2.5 mL of reaction buffer. Add 250 μ L of each standard or unknown (sample) to the separate test tubes prepared in the previous step. Mix and incubate at room temperature for 15 minutes, allowing the orange-yellow color to develop. Measure the absorbance at 412 nm and plot the values obtained for the standards to generate a standard curve. Finally, determine the experimental sample concentration from this curve.

5.2.3. Preparation of PEGTA Cross-linked HA-SH or HS-HA-PEG-Chelator Injectable Hydrogels

Chemically cross-linked hydrogels were prepared by combining 8-arm PEGTA and HA-SH or HS-HA-PEG-chelator. To determine the influence of concentration on hydrogel properties, 8-arm PEGTA solutions of different concentrations (1.0%, 1.5%, 2.0%, 4.0% and 6.0 %) were mixed with HA-SH of different concentrations (1.0%, 1.5%, 2.0%, 4.0%, and 6.0%) in a ratio of 1:1, respectively to create hydrogels with concentrations of 0.5%, 0.75 %, 1.0%, 2.0% and 3.0 %). For example, to prepare a hydrogel with a concentration of 3.0% (w/v), first dissolve 18 mg PEGTA in 300 μ L PBS solution (6.0 % w/v). Then dissolve 18 mg HA-SH in 300 μ L PBS solution (6.0% w/v) and combine it with the previously prepared PEGTA solution. Homogenize the solutions and determine the time for hydrogel formation.

5.2.3 The Gelation time of HA-SH or HS-HA-PEG-Chelator hydrogel.

The method for determining the gelation time of HA-SH or HS-HA-PEG-chelator was adapted from the work of Bian et al.[405] A vial inverting method facilitated the determination of the solution-gel transition, that is, a state in which the vial content is flowable to one that is non-flowable. Pour freshly prepared HA-SH or HS-HA-chelator solution into a vial, invert it and incubate at 37°C and check regularly to confirm gel formation. Gel formation occurs when there is absence of fluidity over a 60 s period during tube inversion.

5.2.4 Cell Culture (2D- and 3D-Culture)

The human neural stem cells (hNSCs) used for 2D cell culture was purchased from Millipore Sigma (Billerica, MA). The stem cell is an immortalized human neural progenitor cell line derived from the ventral mesencephalon region of human fetal brain and immortalized by retroviral transduction with the v-myc oncogene. The hNSCs were cultured in and maintained in DMEM/F12 basal medium (Thermo Fisher Scientific, MA, USA) supplemented with 20 ng ml⁻¹ basic fibroblast growth factor (FGF-2, Peprotech, Rocky Hill, NJ) and 20 ng ml⁻¹ epidermal growth factor (EGF, Peprotech). For 2D-culture, well plates (24 or 48-well plates) pre-treated with PVAVS and proprietary integrin-based peptides were the surfaces to which the hydrogel precursor solution was added. First, add PVAVS to the surfaces for 5 minutes, and then rinse with PBS. The PVAVS formed a thin layer of hydrogel containing disulfide linkages on the cell culture surfaces, which facilitated the adhesion of the integrin-based peptides to the surface. The integrin-based peptides remained on the cell culture surfaces for 90 minutes under incubation conditions. After the incubation period, remove the peptide solution from the cell culture surfaces and rinse with PBS. Add the hydrogel precursor solution to a little more (500 µL) than desired amount of culture media containing the proprietary integrin-based peptide, mix well, and sterilize by filtering with a 0.45-micron syringe filter. Add the appropriate amounts of hNSCs to the mixture of media and hydrogel precursor solution; gently mix by micro pipetting the solution up and down to break up cell aggregates into small clusters. Add 500 µL of media containing 1 x 10⁴ cells per well in 24-well plate. Then incubate at 37°C and humidified air with 5% CO₂ and check at regular time intervals to time when the solution gels. Feed the cells within 24 hours of passaging and every 48 hours thereafter. The cells used in this study did not exceed the tenth generation of passaging.

In the case of 3D-culture, to avoid precipitation of cells onto the surface of plate during the hydrogel formation, coat the plate with hydrogels prior to adding the hydrogel precursor solution, media, and hNSCs. 500 μ L of media containing 1.0×10^4 cells per well in 24 well plates were seeded on the top of pre-formed hydrogels and incubate for 24 h. CellTiter Blue assay facilitated the determination of the effect of hydrogel on hNSC viability and proliferation. On Day 0 (24 hr later), replace the culture medium with 500 μ L of CellTiter Blue solution (CellTiter Blue and medium in a ratio of 9:1) without disrupting the hydrogel. Incubate the cells for 2 h, after the incubation period remove the CellTiter Blue solution from the 24-well plate, and add at least four 100 μ L amounts of each group to 96-well plates and obtain fluorescence readings at 560 nm/590 nm (excitation/emission wavelength) using a microplate reader (SpectraMax, Molecular Devices). Rinse the 24-well plates containing the cells and hydrogel with PBS to remove CellTiter Blue solution, add fresh hNSC media to the wells and incubate. Repeat the same procedure on days 1-7.

5.2.5 Statistical Analysis

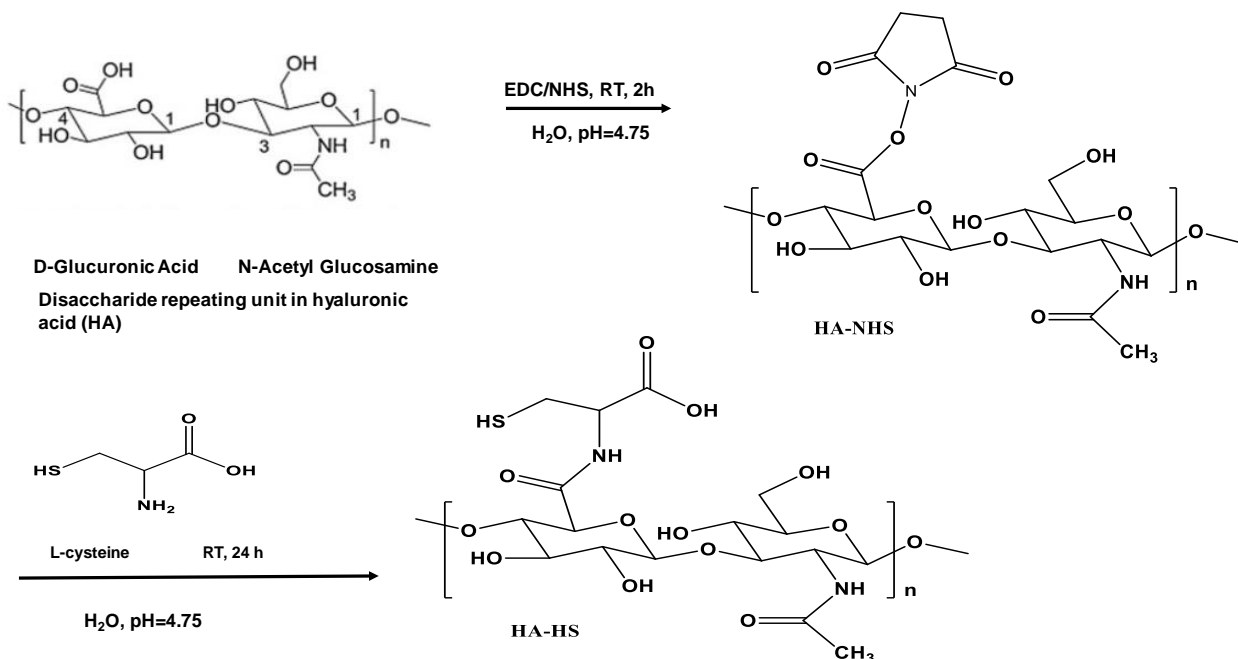
All data in this study are presented as mean \pm SD. Data were analyzed in excel and p-values obtained from the data regression analysis tool

5.3 Results

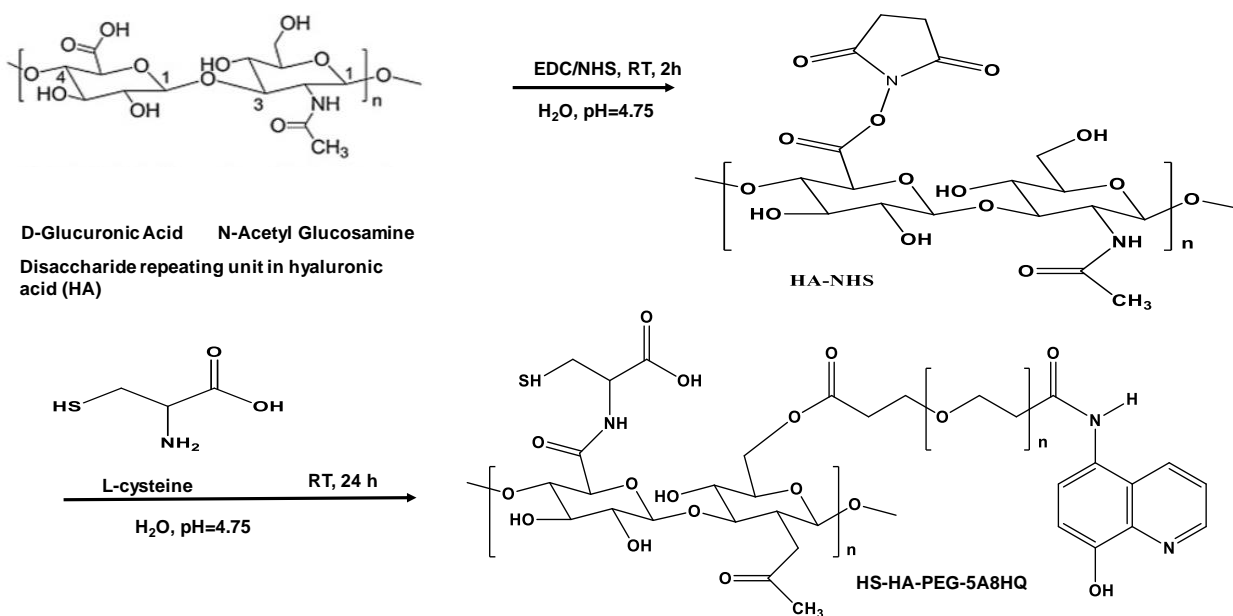
5.3.1 Synthesis of thiolated HA and HA-PEG-Chelator

Schemes 5.1 and 5.2 (a, b, and c) depicts the synthesis of HA-SH and HS-HA-PEG-chelator prepared from HA or HA-PEG-Chelator and L-cysteine. Initially, EDC a condensing agent, activating the carboxyl groups of HA to reacts with NHS to yield HA-NHS active ester. Cysteine,

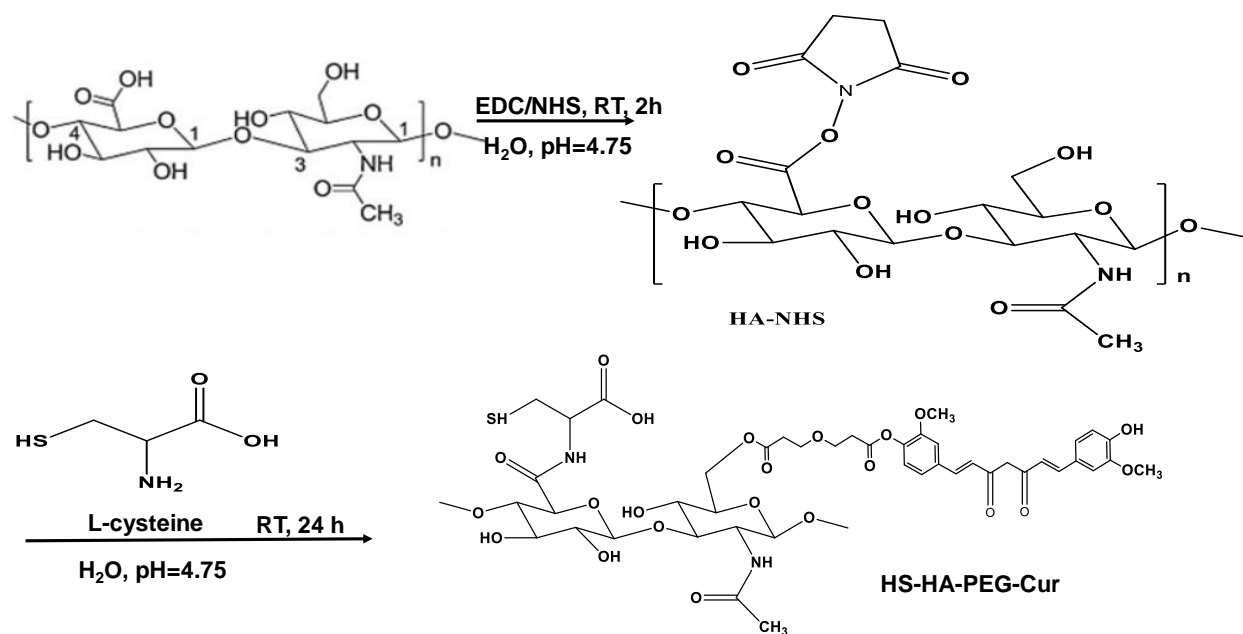
an amine nucleophile readily attacks the C=O group of the ester and NHS rapidly leaves and the result is the formation of an amide bond.



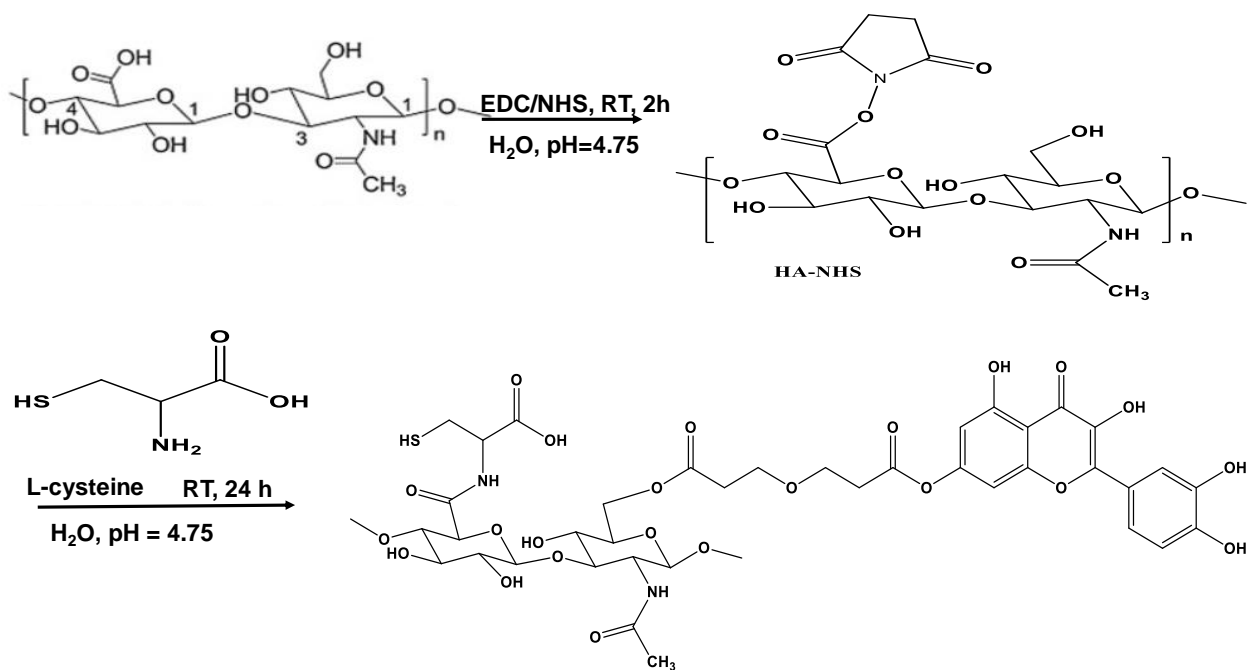
Scheme 5.1: Synthesis schematic of thiolated hyaluronic acid (HS-HA) via EDC/NHS coupling reaction.



Scheme 5.2a: Synthesis of thiolated HA-PEG-5A8HQ (HS-HA-PEG-5A8HQ) via EDC/NHS reaction.



Scheme 5.2b: Synthesis schematic of thiolated HA-PEG-Cur (HS-HA-PEG-Cur) via EDC/NHS reaction.



Scheme 5.2c: Synthesis schematic of thiolated HA-PEG-Quer (HS-HA-PEG-Quer) via EDC/NHS reaction

Figure 5.1 depicts the FTIR spectra for cysteine, HA, and HA-SH. The peak representing the SH stretching vibration was observed in the spectrum for cysteine and HA-SH at 2540 cm^{-1} , but not in HA. The SH peak was less intense in the HA-SH than in the cysteine. Additionally, the NH stretch for the amine group (3150 cm^{-1}) in cysteine is weaker and sharper compared to the OH stretching (3260 cm^{-1}) vibrations in hyaluronic acid and its derivatives. Both the NH and OH stretching vibrations appear in the same region of the IR spectrum, between $3300\text{--}3000\text{ cm}^{-1}$. The spectrum of HA-SH a weak peak at 1720 cm^{-1} and a shoulder at $\sim 3100\text{ cm}^{-1}$ representing the C=O stretch and the NH stretch of the amide functional group formed between HA and cysteine following EDC/NHS coupling reaction, respectively. NH bending vibrations are seen in cysteine, HA, and HA-SH between 1650 cm^{-1} - 1580 cm^{-1} .

FTIR characterization of cysteine, hyaluronic acid ((HA 100 kDa), and thiolated hyaluronic acid (HA-SH)

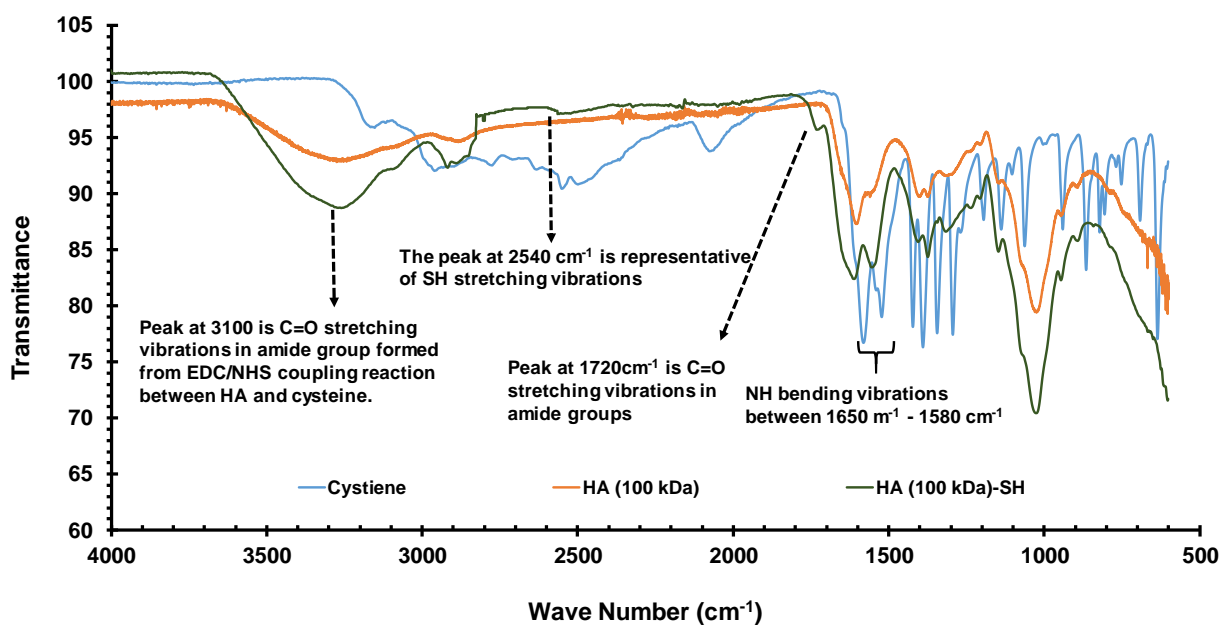


Figure 5.1: FTIR characterization of cysteine, hyaluronic acid ((HA 100 kDa), and thiolated hyaluronic acid (HA-SH).

Figures 5.2 (a, b, and c) show the FTIR spectra for HS-HA-PEG-5A8HQ, HS-HA-PEG-Cur, and HS-HA-PEG-Quer, respectively. The FTIR spectrum for each of these thiolated polymer-conjugates showed a less intense peak at 2540 cm^{-1} , when compared to that of L-cysteine. Additionally, they show the C=O stretching peak at between $1720\text{ cm}^{-1} - 1740\text{ cm}^{-1}$ due to amide formation in the conjugates and the intense signal between $1650\text{ cm}^{-1} - 1580\text{ cm}^{-1}$ representing the NH bending vibrations. HS-HA-PEG-5A8HQ shows a more pronounced amide C=O signal than the other two conjugates, because two amide functionalities are in this structure.

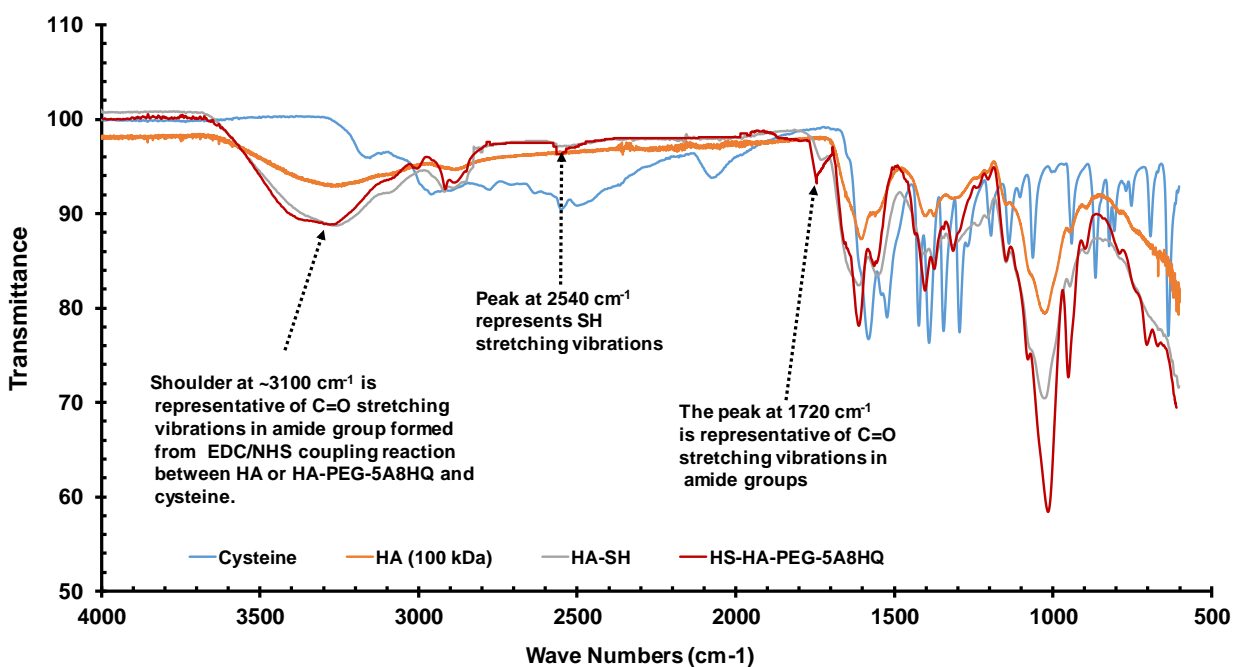


Figure 5.2a: FTIR characterization of cysteine, hyaluronic acid (HA 100 kDa), thiolated hyaluronic acid (HA-SH), and thiolated HA-PEG-5A8HQ (HS-HA-PEG-5A8HQ).

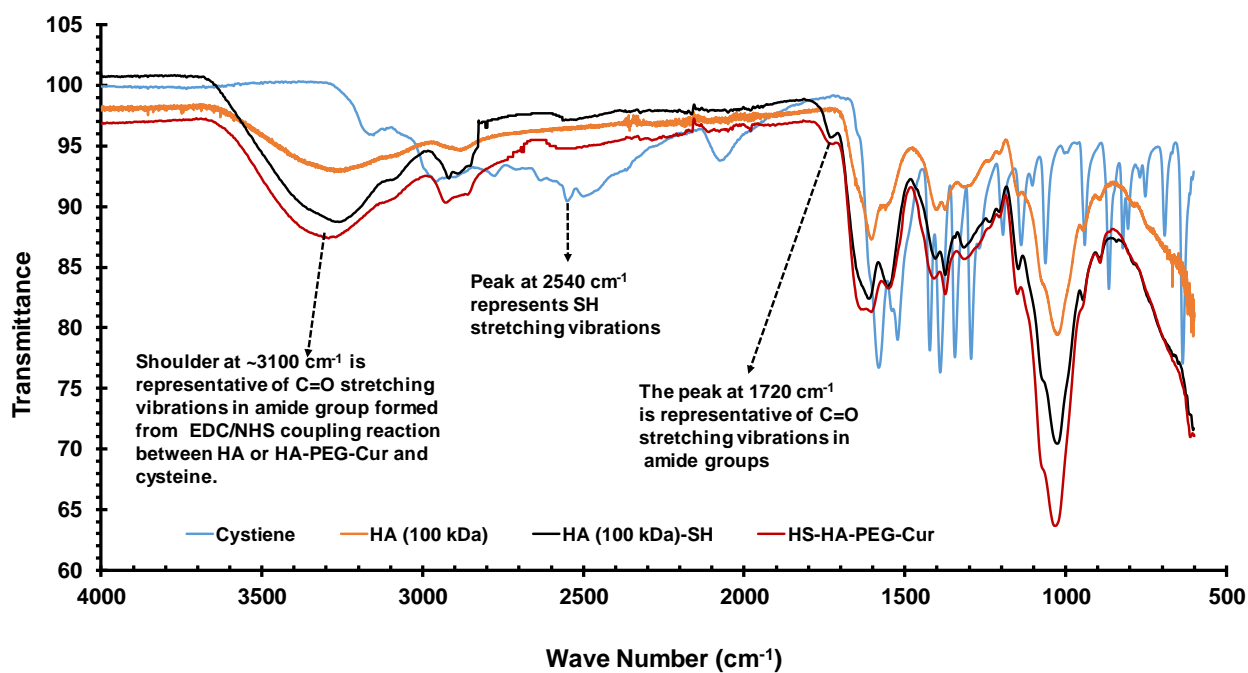


Figure 5.2b: FTIR characterization of cysteine, hyaluronic acid (HA 100 kDa), thiolated hyaluronic acid (HA-SH), and thiolated HA-PEG-Cur (HS-HA-PEG-Cur)

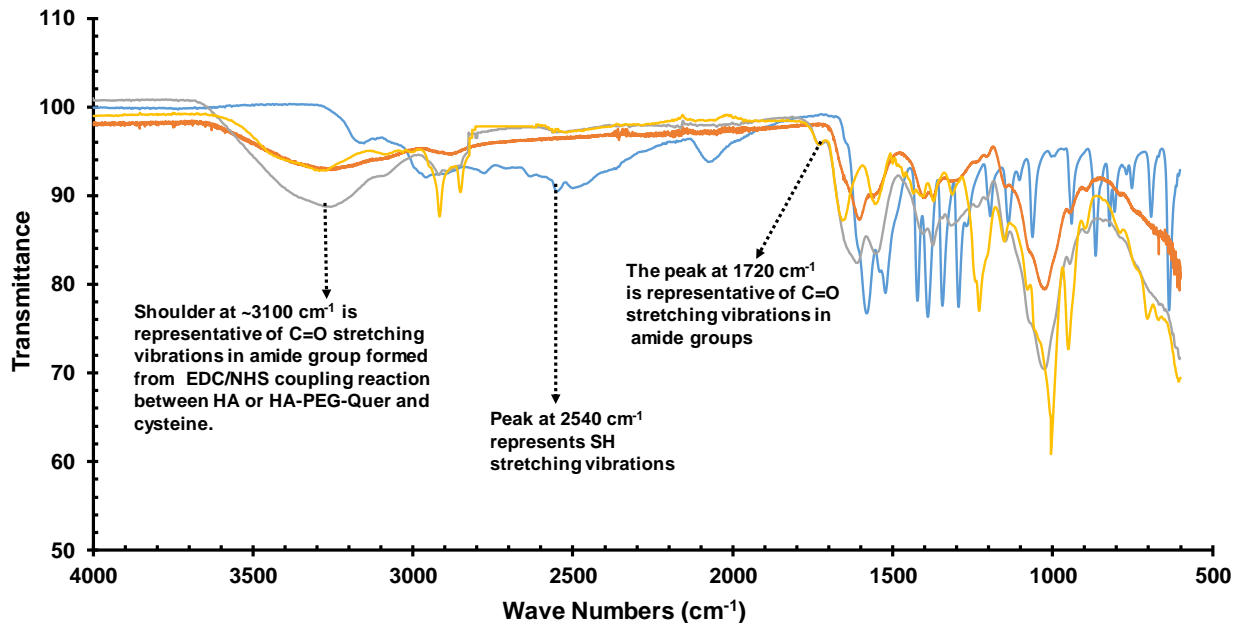


Figure 5.2c: FTIR characterization of cysteine, hyaluronic acid (HA 100 kDa), thiolated hyaluronic acid (HA-SH), and thiolated HA-PEG-Quer (HS-HA-PEG-Quer).

5.3.2 Quantitating Sulfhydryl Groups Using a Cysteine Standard

The Ellman's assay as previously described was the method used to quantify the amount of free thiol groups in HA-SH and HS-HA-PEG-chelator. **Figure 5.3** shows the calibration curve prepared from cysteine standards (0.0 mM -1.50 mM) and the UV-vis spectra of these standards. The absorbance of the samples (HA-SH and HS-HA-PEG-chelators), done in triplicates, were compared to the calibration curve to evaluate the concentration of the free thiol groups. The average concentration of the free thiol groups in HA-SH from the calibration curve is 0.234 ± 0.002 mM, as the average sample absorbance is 0.1360 ± 0.0007 . The percentage free thiol group in the sample is ~23% since the sample preparation involved 1.00 mM L-cysteine. The average concentration of free thiol groups in HS-HA-PEG-5A8HQ, HS-HA-PEG-Cur, and HS-PEG-Quer are 0.155 ± 0.002 mM, 0.161 ± 0.003 mM, and 0.159 ± 0.004 mM, respectively. The corresponding percentage free thiol groups in the sample are 15.5%, 16.1%, and 15.9 % for HS-HA-PEG-5A8HQ, HS-HA-PEG-Cur, and HS-PEG-Quer, respectively. **Figure 5.4** shows a comparison of free thiol groups in HA-SH, HS-HA-PEG-5A8HQ, HS-HA-PEG-Cur, and HS-HA-PEG-Quer. The control, prepared by omitting the EDC/NHS during the coupling reaction, resulted in negligible amounts of thiol groups (15. compared to the samples that underwent EDC/NHS coupling).

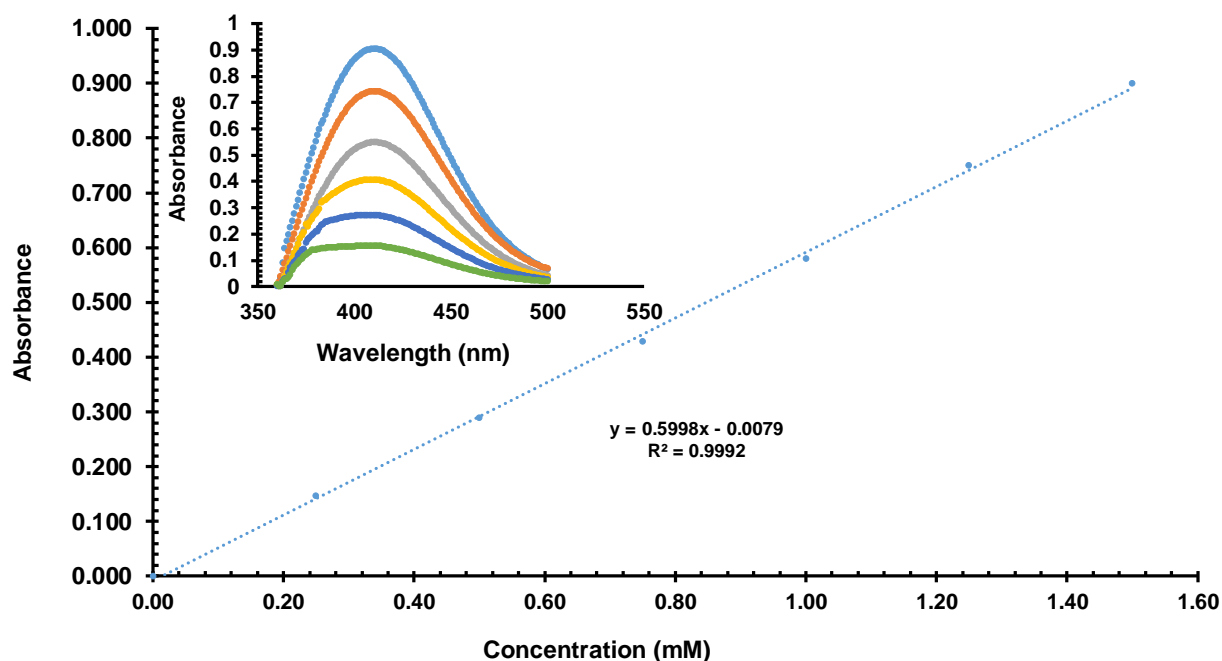


Figure 5.3: Calibration curve for cysteine prepared via Ellman's assay (inset: UV-vis spectra for cysteine standards used to prepare the calibration curve).

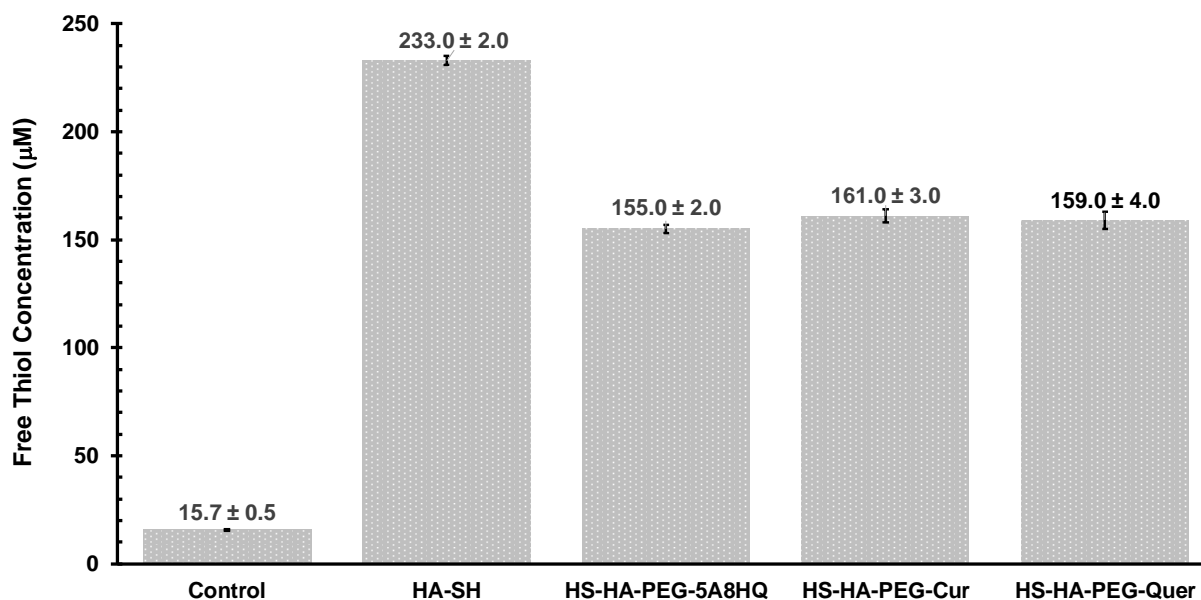
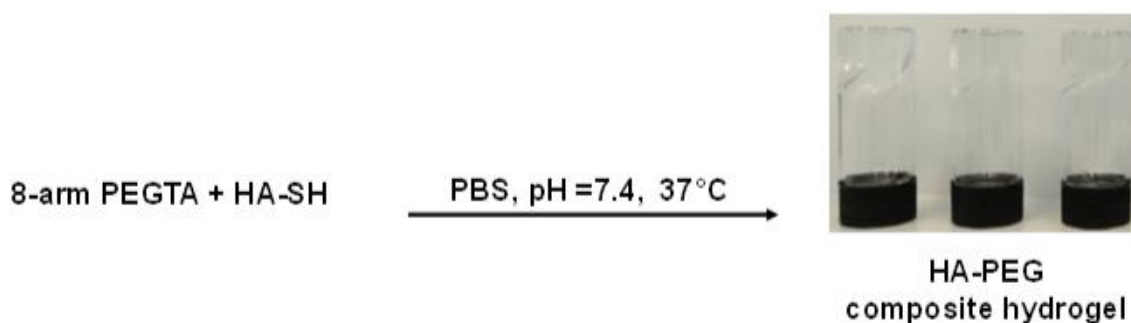


Figure 5.4: Ellman's Assay of lyophilized HA-SH, HS-HA-PEG-5A8HQ, HS-HA-PEG-Cur, and HS-HA-PEG-Quer. Columns represent mean \pm S.D; $n=3$. The control group, omitted EDC/NHS from the coupling reaction

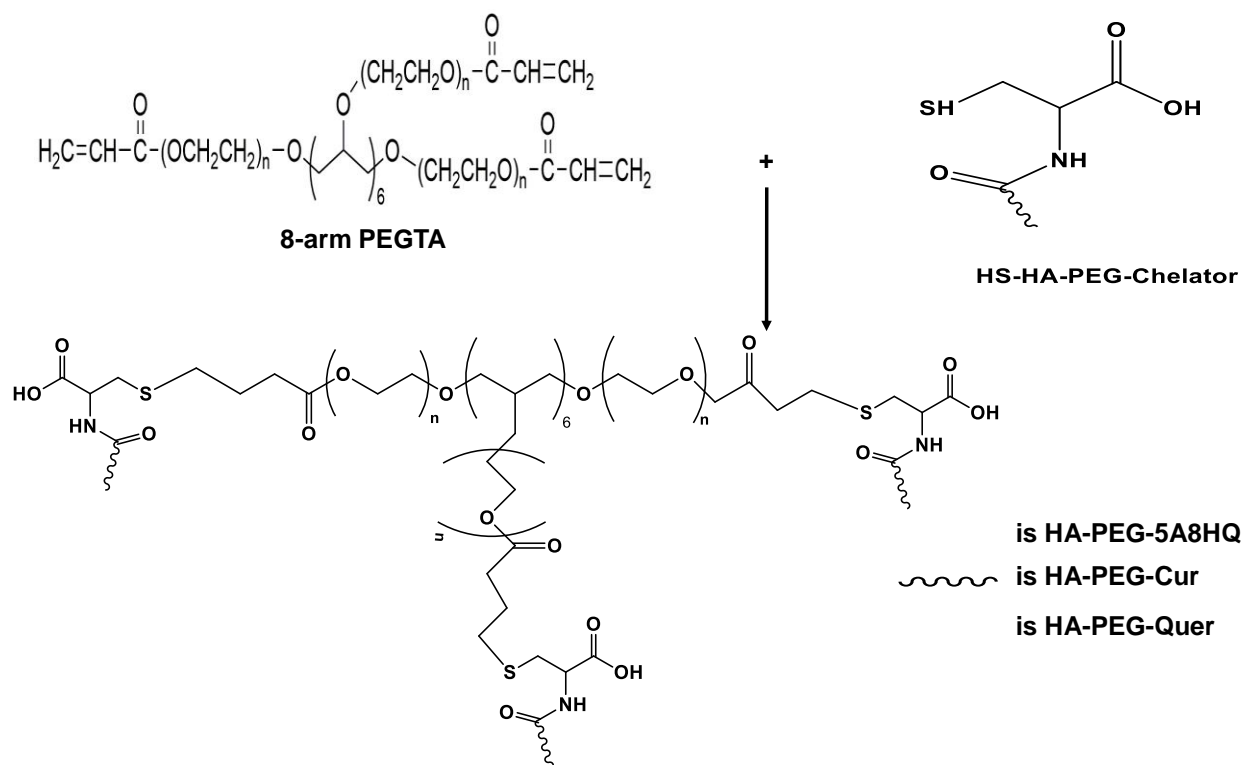
5.3.3 Preparation of PEGTA Cross-linked HA-SH or HS-HA-PEG-Chelator Injectable Hydrogels via Thiol-Acrylate Michael Addition

Schemes 5.3 and **5.4** depicts the Michael addition reaction between HA-SH and 8-arm PEGTA in PBS at 37 °C to yield a chemically cross-linked HA-PEG composite hydrogels. The polymer concentration used in the synthesis was the total dry weight of both PEG-TA and HA-SH per volume of buffer. The vial inversion method ascertained the gelation time of the hydrogels and Tables 5.1 and 5.2 show the gelation times of the HA-SH/PEGTA Hydrogel systems, respectively.



Scheme 5.3: Formation of the HA-PEG composite hydrogel vial the Michael addition reaction between HA-SH and 8-arm –PEGTA.

The gelation time for the hydrogel polymer systems decrease with an increase in polymer concentration or with an increase in the hydrogel precursor solution. The gelation time for hydrogel-precursor solution concentration of 0.75, 1.0, 2.0, and 3.0 are were a bit longer in the HS-HA-PEG-Cur/PEGTA system than it was in the HA-SH/PEGTA system.



Scheme 5.4: Formation of the HA-PEG composite hydrogel via the Michael addition reaction between HA-SH and 8-arm-PEG-TA.

Table 5.1: Gelation times for the HA-SH/PEGTA polymer system. Gelation us determine with the inverted via method.

Concentration of HA-SH (% w/v)	Concentration PEGTA (% w/v)	Concentration of Hydrogel Precursor Solution (% w/v)	Hydrogel Gelation Time (min)
1.50	1.50	0.75	65
2.00	2.00	1.00	40
4.00	4.00	2.00	25
6.00	6.00	3.00	18

Table 5.2: Gelation times for the HS-HA-PEG-Cur/PEGTA Polymer System. Gelation us determine with the inverted via method.

Concentration of HS-HA-PEG-Cur (% w/v)	Concentration PEGTA (% w/v)	Concentration of Hydrogel Precursor Solution (% w/v)	Hydrogel Gelation Time (min)
1.50	1.50	0.75	68
2.00	2.00	1.00	46
4.00	4.00	2.00	28
6.00	6.00	3.00	22

5.3.4 2D- and 3D-cell Culture on HA-S-PEGTA and PEGTA-S-HA-PEG-Cur Hydrogels

The hNSCs showed excellent biocompatibility with HA-S-PEGTA and PEGTA-S-HA-PEG-Cur hydrogel systems in 2D-cell culture. These hydrogel systems were the substrate for hNSCs in adherent 2D-cultured for at least a week. **Figure 5.5 (Left)** is a representative illustration of the morphological features of the hNSCs grown on HA-SH/PEGT and HS-HA-PEG-Cur/PEGTA hydrogels. On Day 0, the hNSCs formed an adherent monolayer on the surface of the hydrogel and the neurite outgrowths are at a minimal. On Days 1, 3, 5, and 7 the neurite extensions increase, forming neural networks with greater interconnectivity between hNSCs as time progressed. Additionally, the number of cells in the well increased exponentially as time progressed, as shown in **Figures 5.6 (Left)**. On average, the optical images and the viability assay indicate that the hNSCs reproduced rapidly between days 1 and 7. Additionally, the viability assay indicate that the adherent hNSC grew faster on the HS-HA-PEG-Cur/PEGTA hydrogel. By day 7, the cells in the well plate were at least 80 – 90% confluent for both hydrogel system.

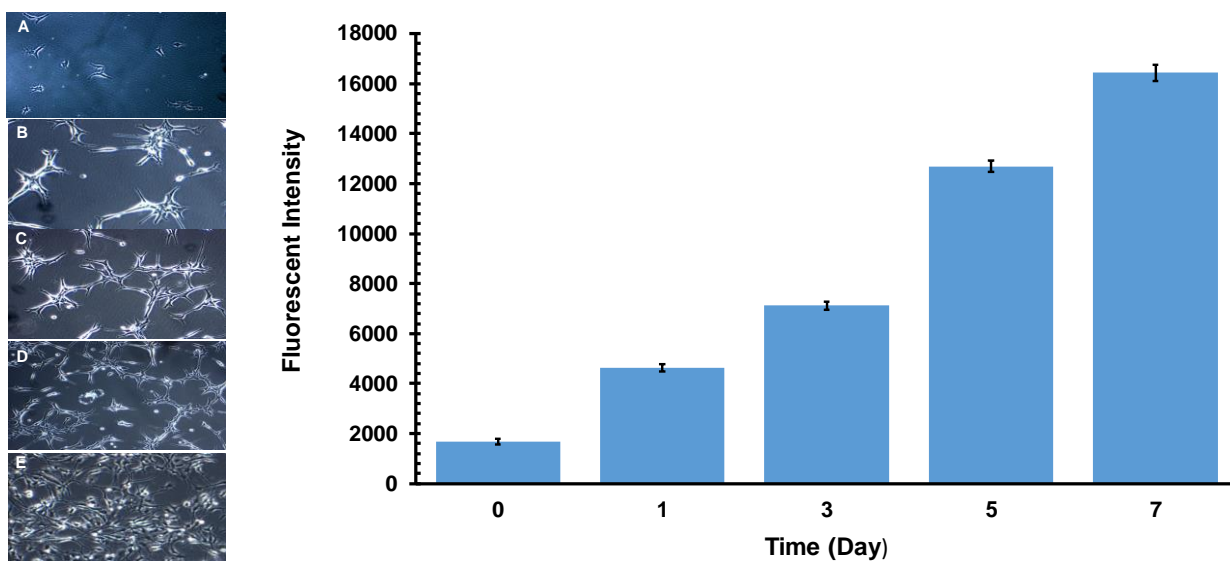


Figure 5.5: (Left) Morphological features of the hNSCs grown on HA-SH/PEGTA hydrogel (2D-cell culture) on (A) day 0, (B) day 1, (C) day 3, (D) day 5, and (E) Day 7. (Right) Viability of hNSCs on HA-SH/PEGTA hydrogel in 2D-cell culture

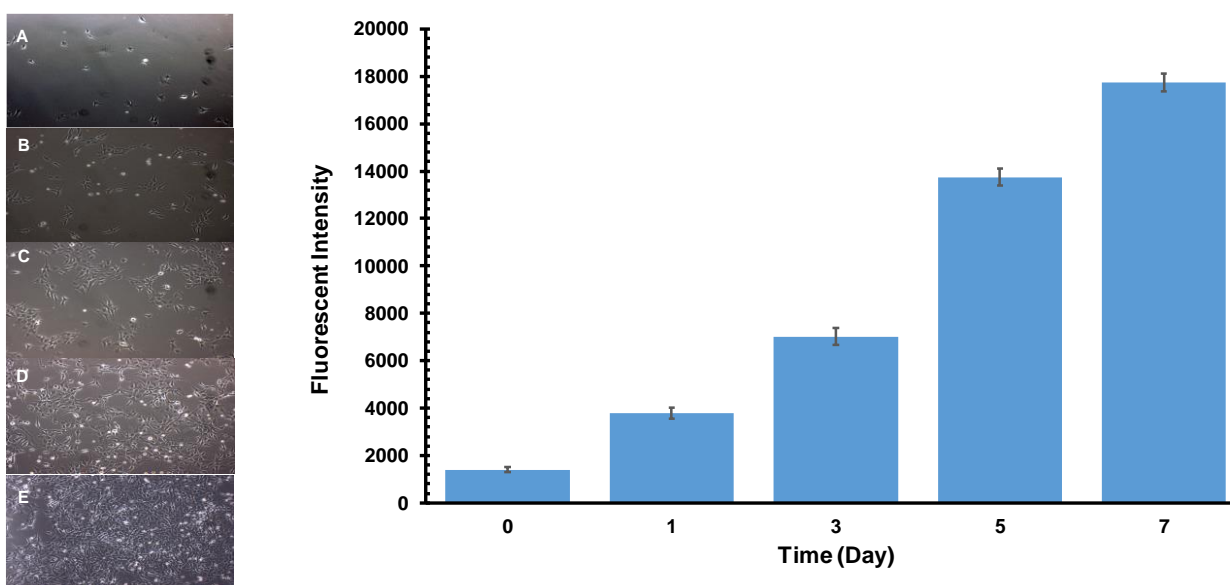


Figure 5.6: (Left) Morphological features of hNSCs grown on HS-HA-PEG-Cur/PEGTA hydrogel (3D-cell culture) on (A) day 0, (B) day 1, (C) day 3, (D) day 5, and (E) day 7. (Right) Viability of hNSC on HS-HA-PEG-Cur/PEGTA hydrogel in 2D-cell culture.

Figures 5.5a and 5.6a shows the growth of neurospheroids, three-dimensional aggregation of hNSCs, inside of HA-SH/PEGTA and HS-HA-PEG-Cur/PEGTA hydrogels, respectively, during 3D-cell culture. As time progressed, the spheroids increased in size, but they are not uniform. On days 0 and 1, the neurospheroids are isolated but as time progressed, they begin to cluster and on day 5, the extension of neurite processes between adjacent neurospheroids are visible. **Figures 5.5b and 5.6b** shows the results of the CellTiter Blue viability assay, which indicates the hNSC-derived neurospheroids are biocompatible with the HA-HS/PEGTA and HS-HA-PEG-Cur/PEGTA hydrogels. The fluorescent signal increased as time progressed, indicating that the number or/and size of neurospheroids are increasing.

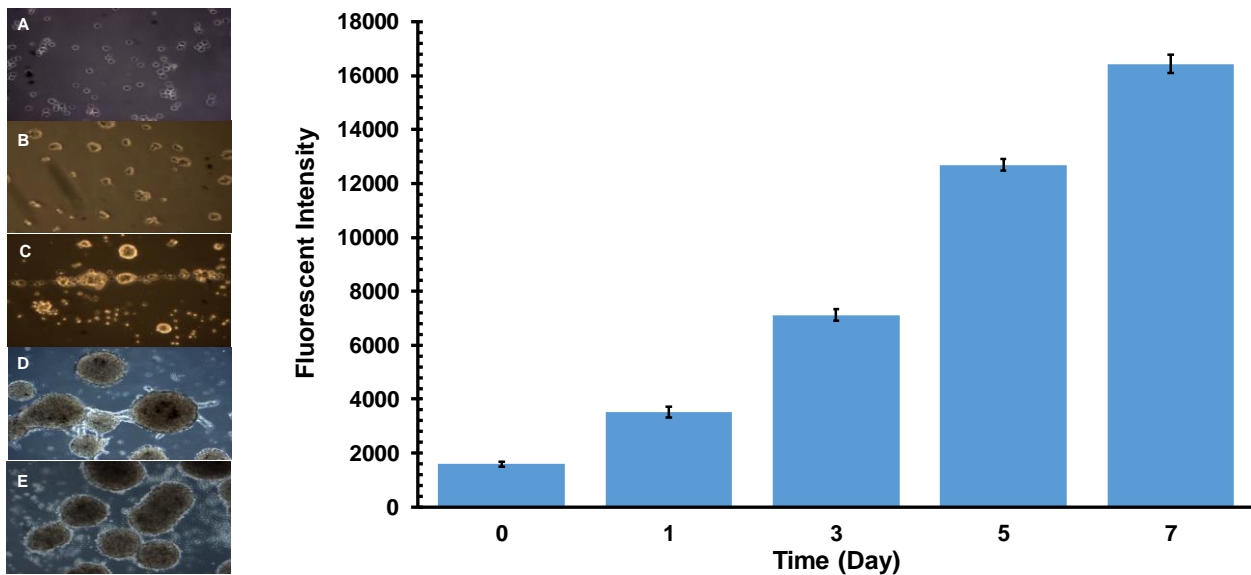


Figure 5.7: (Left) Morphological features of neurospheroids grown inside HA-SH/PEGTA hydrogel (3D-cell culture) on (A) day 0, (B) day 1, (C) day 3, (D) day 5, and (E) day 7. (Right) Viability of neurospheroids inside HA-SH/PEGTA Hydrogel in 3D-cell culture

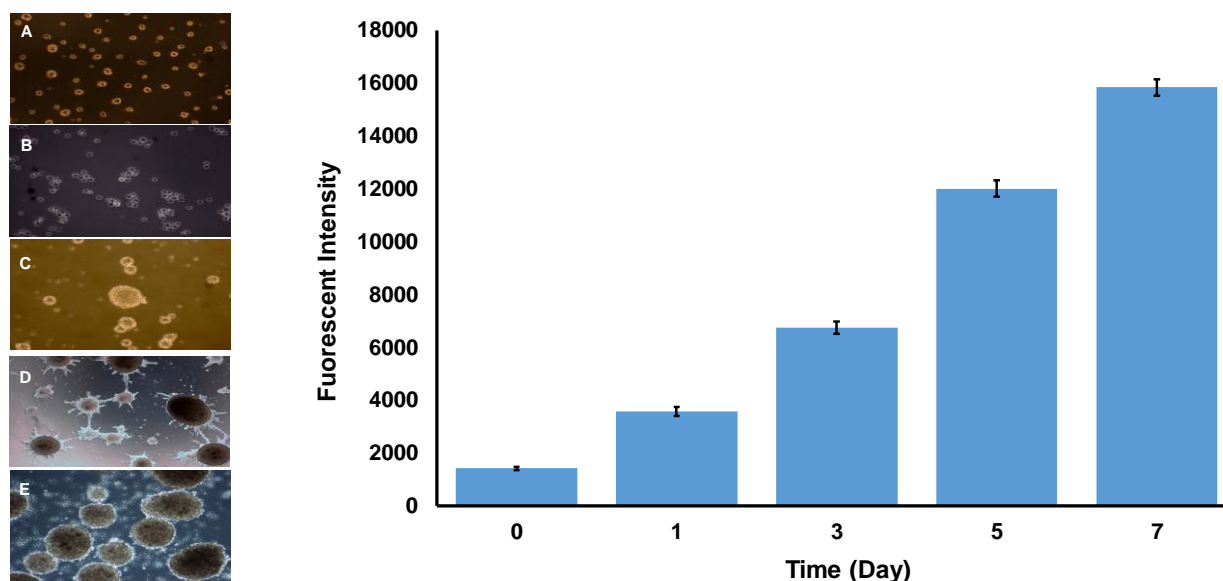


Figure 5.8: (Left) Morphological features of neurospheroids grown inside of HS-HA-PEG-Cur on (A) day 0, (B) day 1, (C) day 3, (D) day 5, and (E) day 7. (Right) The viability of neurospheroids inside HS-HA-PEG-Cur/PEGTA hydrogel in 3D-cell culture

5.4 Discussion

5.4.1 Thiolated HA-SH/PEGTA and HS-HA-PEG-Cur/PEGTA Hydrogels.

A versatile and facile synthesis protocol of thiolated HA and HA-PEG-chelators is illustrated in **Figures 5.1 and 5.2 (a, b, and c)**. This two-step, zero-length crosslinking procedure uses EDC/NHS coupling to mediate the conjugation between HA or HA-PEG-Chelator and cysteine forming a bond that contains no additional atoms. First, the water-soluble carbodiimide forms an O-acylisourea active intermediate with the carboxylate group on HA or HA-PEG-Chelator, which is later, converted to an active ester functionality using NHS. The nucleophilic amine functionality on the cysteine attacks the carbonyl group on the NHS-ester; the NHS rapidly leaves and creates a stable amine bond between the carbonyl and the amine groups.[330] Adding cysteine via the formation of the amide bond allows thiolation of HA (HA-SH) or HA-PEG-Chelator (HS-HA-**No table of figures entries found.**PEG-Chelator). Even though EDC/NHS coupling reaction is highly efficient and usually increase the yield of the product, potential side reactions can occur.

Competing reactions include the reaction of thiol (SH) and hydroxyl (OH) groups with the NHS-ester to form thioester or ester. Fortunately, the products formed from the side reaction are relatively unstable compared to the amide bond.

HA-SH and HS-HA-PEG-chelator were purified of any by-products or unreacted starting material using dialysis. The samples were dialyzed against copious amounts of dilute aqueous HCl solution (pH 3.5), which prevented the formation of disulfide bonds (S-S) via the reaction of thiol groups with each other.[406]

5.4.2 Quantitating Sulfhydryl Groups Using a Cysteine Standard

The degree of thiol substitution determined from Ellman's test in the HA-HS is about 23%, while that in the HS-HA-PEG-5A8HQ, HS-HA-PEG-Quer, and HS-HA-PEG-Cur are 15.5 %, 15.9, and 16.1 %, respectively. Ellman's reagent, 5,5'-dithio-bis-(2-nitrobenzoic acid) abbreviated DTNB react with the free thiol groups in the sample to form a mixed disulfide and 2-nitro-5-thiobenzoic acid (TNB). TNB is a chromophore as a high molar extinction ($14,150 \text{ M}^{-1} \text{ cm}^{-1}$) coefficient in the visible range (412 nm).[407] UV analysis of the reaction product at 412 nm and by comparison to cysteine standard calibration curve led to the quantitative determination of the free thiol group in the thiolated samples. A major factor that could cause the degree of thiol substitution in the sample to be underestimated is oxidation of thiol groups to S-S bonds.[406]

5.4.3 HA-S-PEGTA and PEGTA-S-HA-PEG-Cur Injectable Hydrogels

In spite of the attractive attributes of native HA, its poor biomechanical properties when isolated from the other components of the ECM and its rapid degradation via hyaluronidase limits its application in bioengineering and medicine.[408] However, thiolated hyaluronic acid (HA-SH) cross-linked with polyethylene glycol tetra-acrylate is a HA-based hydrogel with the attractive

properties of the native hyaluronic acid and the improved mechanical properties. Michael thiol-acrylate addition reaction between HA-SH and PEGTA facilitates *in situ* gelation. The HA-SH is the Michael donor and the PEGTA, which contains the α,β -unsaturated carbonyl, is the Michael acceptor. The first step in the reaction mechanism is the formation of a thiolate anion (SH^-), a strong nucleophile. The Michael addition reaction is a special case of conjugate (1, 4) addition, in which the SH^- anion attacks the β -carbon of the α,β -unsaturated carbonyl in PEGTA.[409] **Schemes 5.3** and **5.4** depicts the Michael addition reaction between HA-SH and 8-arm PEGTA in PBS at 37 °C to yield a chemically cross-linked HA-S-PEGTA composite hydrogels.

The gelation time for the hydrogels prepared from the 2% w/v precursor hydrogel solution are 25 min and 28 min for HA-S-PEGTA and PEGTA-S-HA-PEG-Cur, respectively. The gelation periods are long enough to enable easy handling during sterilization in 2D- and 3D-cell culture and allow efficient encapsulation of the cells inside the hydrogel in 3D-cell culture. The gelation time is also appropriate for *in vivo* studies as well, because it enables easy handling during injection yet rapid enough to facilitate the efficient encapsulation of cells for transplantation. Additionally, a gelation time less than 30 min is rapid enough to enhance retention at the injection site, prevent leakage into surrounding tissues from the injection sites, and prevent dilution with body fluids prior to gelation.

5.4.4 2D- and 3D-cell Culture on HA-S-PEGTA and PEGTA-S-HA-PEG-Cur Hydrogels

The *in vitro* cell model selected to test the biocompatibility of the hydrogels is hNSCs and the viability of hNSCs assessed via CellTiter blue assay. Cells cultured on the surface of the hydrogel (2D-cell culture) maintained their viability over a seven-day period. The adherent cells were between 80-90% confluence on day 7 as seen optical image labeled E of **Figures 5.3a and 5.4a**.

Although the hNSCs showed excellent biocompatibility on both the HA-S-PEGTA and PEGTA-S-HA-PEG-Cur hydrogels, the hNSC showed slightly better viability with the PEGTA-S-HA-Cur hydrogel as shown in **Figures 5.3a and 5.4b**. The main difference between these hydrogel systems is the presence of curcumin (Cur) on the PEGTA-S-PEG-Cur hydrogel. Examination of the cytotoxicity of free Curcumin on hNSCs as well as on hepatic stellate cells (HSCs) show a decreased in cell viability with increasing curcumin concentration. However, when conjugated to polymers such as HA and/or PEG, the conjugate shows increased viability.[410]

Both HA and PEG are known to reduce cytotoxicity and extend the plasma half-life of small molecule drugs. For example, Xu et al. prepared and investigated PEGylated DFO for improving the cytotoxicity and stability in an experimental stroke model. They found that PEGylated DFO exhibited significantly lower cytotoxicity (~85% or greater viable cells than DFO at all equivalent concentrations) and a 20-fold stability when compared to DFO.[411] Greco et al. prepared and investigated the effect of hyaluronan-carnosine conjugates (HyCar (200)14 and HyCar (700)35) on amyloid- β - ($A\beta$)-induced toxicity. To assess the cytotoxicity of $A\beta_{42}$ at different levels of oligomerization they used undifferentiated SH-SY5Y as an *in vitro* model via the MTT assay. The cells were pre-incubated with $A\beta_{42}$ for 6, 24, and 48 h, and some cells treated with the HyCar conjugates. The results show a decrease in SH-SY5Y cell viability after treatment with pre-incubated $A\beta_{42}$ alone. However, the result show a significant increase in cell viability when treated with the HyCar conjugates, which could be attributed to a decrease in $A\beta_{42}$ and thus a reduction in the $A\beta$ -induced cell toxicity.[412]

Cell cultures are very important for testing biocompatibility of biomaterials and drugs. However, the popular *in vitro* 2D-cell culture model does not mimic the natural cell environment and growing

cells on flat 2D-surfaces as monolayers may alter their metabolism, functions, and drastically reduce cell-cell and cell-extracellular matrix interaction.[413] A much better *in vitro* model is 3D-cell culture because all cells live in 3D environment in the body. This 3D environment is important for growth and metabolism since cells can interact with neighboring cells and the extracellular matrix.[414] The physiology and morphology of cells in 3D-cell cultures are different from cells in 2D cultures and may have different responses to drugs and their cytotoxic effects.[415] **Figures 5.3a and 5.4a**, and **Figures 5.5a and 5.6** a shows the morphological difference of hNSC culture via 2D and 3D-cell culture, respectively.

3D-cell cultures more precisely mimic the natural cellular environment and have the ability to self-assemble and form spheroids. Spheroids are cell aggregates that self-assemble in an environment that prevents attachment to flat surfaces.[416] Encapsulation of cells inside hydrogels provides one method for culturing cells into spheroids. Successful NTE in CNS injuries is largely dependent on the survival of the transplanted stem cells. In this work, we investigated the survival of hNSCs in HA-S-PEGTA and PEGTA-S-HA-PEG-Cur injectable hydrogels. The gelation times for HA-S-PEGTA and PEGTA-S-HA-PEG-Cur injectable hydrogels are 25 and 28 min, respectively. These gelation times should be long enough for mixing and injecting of cells without the clogging of the syringe needle or micropipette tips and short enough to prevent leakage of fluids into the host tissue parenchyma. **Figures 5.5a and 5.6b** shows the neurospheres grown inside the HA-S-PEGTA and PEGTA-S-HA-PEG-Cur hydrogels. The size of the neurospheres depends on seeding concentration; the greater the number of hNSCs seeded inside the hydrogels the larger the size of the neurospheres.[417] The growth of the neurospheroids in the hydrogels emphasizes the key role hyaluronic acid plays in mediating cell survival and proliferation. The neuroprotective effect of the hydrogel scaffolds for hosting the encapsulated hNSCs stems from

the shielding effect of HA and PEG. Fabricating the hydrogels from an ECM component, HA, provides a good representation of a natural *in vivo* milieu for the encapsulated hNSCs while PEG improves the biocompatibility of the hydrogel with hNSC.

5.5 Conclusion

Michael-type addition reaction between thiolated-hyaluronic acid based polymers and PEGTA resulted in the fabrication of HA-S-PEGTA and PEGTA-S-HA-PEG-chelator (5A8HQ, Cur, and Quer) hydrogels. We demonstrated that this crosslinking reaction forms hydrogels that are biocompatible with hNSCs in 2D- and 3D-cell cultures. The preliminary data obtained from the system are encouraging and shows that the design and fabrication of these systems are conducive to the proliferation of hNSCs in 2D and 3D-cell culture. The gelation times of these hydrogels are 25 min for HS-S-PEGTA and 28 min for PEGTA-S-HA-PEG-cur. In the *in vitro* experiments conducted so far, the gelation times were long enough to facilitate mixing of the hNSC into the hydrogel precursor material without the clogging of the syringe needles or micropipette tips. Additionally, the gelation time must be short enough to prevent leakage into the host parenchyma. Knowledge of the latter will manifest during the *in vivo* animal studies.

The hydrogel properties needs optimization before their use as scaffolds for loading hNSCs into the CNS injury site and as a mimic of the ECM in the injury microenvironment. One way of optimizing the hydrogel properties is by varying the degree of thiol substitution in the thiolated-HA or by varying the concentrations of the hydrogel precursor materials. This will affect the biomechanical properties of the hydrogel such as porosity, stiffness (elastic modulus), loss modulus and viscosity. By varying these parameters, we hope to tune the hydrogel mechanical

properties to mimic that of the brain or spinal cord. These bioengineered materials will provide an initial cue for cells to maintain their programmed functions and coordinate the regeneration of neural tissues.

Chapter 6

6 Conclusions and Future Directions

6.1 Conclusions

The significance and major impact of this work resides with the development of a biomaterial scaffold that meets the three most important criteria for CNS regeneration. CNS regeneration requires cellular components, growth and differentiation factors, and a scaffold matrix. The designed injectable iron-chelating hydrogels prepared in chapter five, shows that it is biocompatible with hNSCs in both 2D- and 3D-cell culture. Additionally, the hydrogel will encapsulate hNSC, differentiation, and growth factors and enable their delivery to the site of CNS injury. Further, it will fill the lesion site or cavity in severe injuries and mimic the biomechanical microenvironment of the host, providing a site for cellular attachment, growth, differentiation, and revascularization. This injectable hydrogel

will help to bridge the gap between in vitro and in vivo research and provide a reliable platform to answer some of the most pressing research questions.

6.1.1 Chapter 3

Chapter 3 is an interrogation of HA, a natural glycosaminoglycan. We investigated the iron-chelating abilities of HA and found that it is a potent iron chelator with an iron chelation efficiency of ~74%. HA showed the effect of its antioxidant and iron chelating properties when iron (II)/ascorbate-induced LPO in LA in the micelle model, and hNSC lysate, and iron (II)/ascorbate-induced oxidative stress in HA. The data showed that HA inhibited the LPO in both cases and inhibited oxidative stress in hNSCs. In the micelle model, we UV-Vis spectroscopy to monitored the accumulation of CDs and found that HA inhibited LPO of LA in comparison to LPO in untreated-LA. In the case of hNSC, we followed CD formation using a second derivative UV-Vis spectroscopic method and found that HA inhibited iron (II)/ascorbate-induced LPO of hNSC lysates. Less conjugated CDs formed in HA-treated hNSCs when compared to untreated cells. CellTiter-Blue assay analysis shows higher fluorescent signals for HA-treated hNSCs when compared to untreated cells. Further, the findings this chapter were useful in the design of the iron-chelating polymer-conjugates studied chapters 5.

6.1.2 Chapter 4

The work in chapter 4 developed from the worked in chapter 3. We synthesized and characterized three families of Iron-chelating polymer-conjugates. In the design of the iron-chelating polymer conjugates we used HA as the polymer material due to its attractive attributes including its iron chelating abilities. We used three different small molecule chelators: (i) 5A8HQ, (ii) Cur, and (iii) Quer. PEG was used as a spacer or linker between the chelators and HA. The components of the

iron-chelating polymer conjugates work synergistically to make them more attractive. First, the small molecule iron-chelators possess poor oral bioavailability, which limits their use in clinical application. Attaching the polymer material to the chelators extends their plasma half-life and improve their bioavailability. 5A8HQ is cytotoxic to hNSCs and by covalently bonding with the polymeric materials, its biocompatibility is drastically improved. We interrogated these iron-chelating polymer conjugates in a similar fashion to HA and found that they too inhibit iron (II)/ascorbate-induced LPO of LA and iron (II)/ascorbate-induced oxidative stress in hNSC. HA-PEG-Quer had the greatest inhibitory effect on LPO and oxidative stress because it is a more potent chelator and free-radical scavenger than the other iron-chelating polymer conjugates.

6.1.3 Chapter 5

The precursor materials used to prepare the injectable iron-chelating hydrogel were the iron-chelating polymer conjugates interrogated in chapter 4 and PEGTA. Michael-type addition reaction between thiolated-hyaluronic acid based polymers and PEGTA resulted in the fabrication of HA-S-PEGTA and PEGTA-S-HA-PEG-chelator (5A8HQ, Cur, and Quer) hydrogels. We demonstrated that this crosslinking reaction forms hydrogels that are biocompatible with hNSCs in 2D- and 3D-cell cultures. The preliminary data obtained from the system are encouraging and shows that the design and fabrication of these systems are conducive to the proliferation of hNSCs in 2D and 3D-cell culture. The gelation times of these hydrogels are 25 min for HS-S-PEGTA and 28 min for PEGTA-S-HA-PEG-cur. In the *in vitro* experiments conducted so far, the gelation times were long enough to facilitate mixing of the hNSC into the hydrogel precursor material without the clogging of the syringe needles or micropipette tips. Additionally, the gelation time must be

short enough to prevent leakage into the host parenchyma. Knowledge of the latter will manifest during the *in vivo* animal studies.

The hydrogel properties need optimization before their use as scaffolds for loading hNSCs into the CNS injury site and as a mimic of the ECM in the injury microenvironment. One way of optimizing the hydrogel properties is by varying the degree of thiol substitution in the thiolated-HA or by varying the concentrations of the hydrogel precursor materials. This will affect the biomechanical properties of the hydrogel such as porosity, stiffness (elastic modulus), loss modulus and viscosity. By varying these parameters, we hope to tune the hydrogel mechanical properties to mimic that of the brain or spinal cord. These bioengineered materials will provide an initial cue for cells to maintain their programmed functions and coordinate the regeneration of neural tissues.

6.2 Future Works

6.2.1 Hydrogel Optimization Study

Since specific aim #3 (work in chapter 5) was incomplete, in the future, completion of specific aim #3 is the initial step. Completion of specific aim #3 requires the following investigations:

Michael-type addition reaction between thiolated-hyaluronic acid based polymers and PEGTA resulted in the fabrication of HA-S-PEGTA and PEGTA-S-HA-PEG-chelator (5A8HQ, Cur, and Quer) hydrogels. We demonstrated that this crosslinking reaction forms hydrogels that are biocompatible with hNSCs in 2D- and 3D-cell cultures. The preliminary data obtained from the system are encouraging and shows that the design and fabrication of these systems are conducive to the proliferation of hNSCs in 2D and 3D-cell culture. The gelation times of these hydrogels are 25 min for HS-S-PEGTA and 28 min for PEGTA-S-HA-PEG-cur. In the *in vitro* experiments

conducted so far, the gelation times were long enough to facilitate mixing of the hNSC into the hydrogel precursor material without the clogging of the syringe needles or micropipette tips. Additionally, the gelation time must be short enough to prevent leakage into the host parenchyma. Knowledge of the latter will manifest during the *in vivo* animal studies.

The hydrogel properties need optimization before their use as scaffolds for loading hNSCs into the CNS injury site and as a mimic of the ECM in the injury microenvironment. One way of optimizing the hydrogel properties is by varying the degree of thiol substitution in the thiolated-HA or by varying the concentrations of the hydrogel precursor materials. This will affect the biomechanical properties of the hydrogel such as porosity, stiffness (elastic modulus), loss modulus and viscosity. By varying these parameters, we hope to tune the hydrogel mechanical properties to mimic that of the brain or spinal cord. These bioengineered materials will provide an initial cue for cells to maintain their programmed functions and coordinate the regeneration of neural tissues.

6.2.1.1 Varying the Degrees of Thiol Substitution.

Degree of thiol substitution affects hydrogel properties in several ways. Increased thiol substitution decreases the gelation time of the hydrogel by increasing the chance for thiol groups to react with PEGTA. On the other hand, excessive thiol groups may cause the gel to solidify too quickly upon contact, which makes mixing hNSCs and injecting the gel to the damaged area very difficult. Fast gelation also may cause overheating and unreacted thiol groups may involve series of unknown biochemical reactions. Evaluation of the mechanical property, morphology, swelling ratio and degradation behavior at various thiol substitutions are required to optimize the hydrogel system.

6.2.1.2 The Effect of Varying the Concentrations of the Hydrogel Precursors.

The precursor concentration affects the performance of the hydrogel system in many ways. Higher precursor concentrations reduce gelation time, creates stronger physical support, and higher chelating capacity. By contrast, lower precursor concentration decreases the rigidity of the hydrogel, lower swelling ratio, producing less heat during gelation process, and increases hNSC loading rates. A series of precursor pairs at various concentrations will be prepared to optimize the concentration by carefully studying the gelation time, heat generation, iron chelating capacity, mechanical property, swelling ratio, and hNSC loading capacity.

6.2.2 In vivo evaluation of the therapeutic effect of bioengineered injectable hydrogel optimized for pediatric mice brain tissue.

Induce the CCI model in pediatric rats by first administering anesthesia and performing craniectomy, a round opening made to expose the dura mater. The impact system uses an actuator and has some parameters that must be set prior to the impact to the rat's skull. Set the velocity of the actuator to 3.5 m/s, impact depth of 2 mm and install a 5 mm impactor tip. Position the tip over the open skull area and adjust it so that it is parallel to the surface of impact. Determine the zero point and set it by lowering the actuator until it just touches the area assigned for impact. Set the appropriate deformation depth for moderate TBI. Evaluate of the impact of injectable hydrogels on vascular regeneration in the pediatric rat brain after a CCI-induced focal injury by the following steps:

1. Determining if the ICH optimized for the pediatric rat brain will promote angiogenesis and neuronal cell growth in vivo. Randomly assign the animals used in this experiment to five groups: (1) Sham, (2) TBI only, (3) TBI treated with ICH 2 days post injury (dpi), (4) TBI treated with ICH 7 dpi and (5) TBI treated with ICH 14 dpi (n=5 group at each specified time

point). To evaluate the therapeutic time window and impact of the ICH in promoting angiogenesis and rebuilding the vascular network treat the animals in groups 3-5 with the ICH via injection into the cortical lesion site. Evaluate vascularization at the injury site weekly, for one month, and use hematoxylin and eosin (H&E) stains to histochemically examine and assess the cortical lesion volume. Further, conduct immunostaining with vascular endothelial marker (RECA-1) and angiogenesis marker (VEGF) on a second set of sections to examine the vascular network. Use laser scanning confocal microscopy to stack and digitally reconstruct 3D projections of RECA-1 positive vascular endothelial cells. Characterize microvascular permeability and stability on brain sections by using markers for endothelial tight junction and adherens junction including zonula occludens-1 (ZO-1) and VE-cadherin. Quantify the immuno-stained cells/vessels throughout the lesion site and determine if remodeling the injured environment will fuel endogenous NSCs migration to the lesion site. To map the migration of newly formed neurons to the lesion site, conduct DCX staining for new migrating neurons and dual labeling of BrdU with DCX or NeuN for mature neurons.

2. To evaluate the impact of hydrogels, loaded with CSPG- and type IV collagen-antagonists, on glial scar reduction, enhancement of neural structural repair and endogenous neurogenesis use this study, para-nitrophenyl- β -D-xylopyranoside (PNPX), chondroitinase ABC (ChABC) and CSPG antagonistic agents to block the biosynthesis of CSPGs then suppress the formation of glial scar in the TBI lesion. Further, use PNPX and ChABC to assess the ability of the injectable ICH loaded to facilitate repair, survival and integration of the transplanted NSCs. Further, we will use ethyl-3,4-dihydroxybenzoate (EDHB a prolyl hydroxylase inhibitor), 2,2-bipyridyl and cAMP to suppress fibrotic scar formation by inhibiting type IV collagen biosynthesis and fibroblast proliferation. Pediatric rats in animal groups 3-5 will be injected

with hydrogel loaded with bioactive molecules at 2, 7 and 14 dpi, respectively. The animals will be sacrificed; brain tissue spanning the lesion site will be sectioned and processed for H&E staining to determine lesion volume and determine vasculature formation weekly for a month.. Additionally, brain sections will be immune-stained with RECA-1, VEGF, markers for glial scar (CSPG, collagen IV and GFAP), neurons (MAP2, β -III tubulin, neurofilament H-200), oligodendrocytes (Oligo2), myelination (MBP), and microglia (Iba1). Map axonal sprouting by silver staining and assess migration of endogenous NSCs as previously described. Use laser scanning confocal microscopy to reconstruct 3D projections of RECA-1 positive vascular endothelial cells. Quantify immunostaining by stereological cell quantifying methods or densitometry analysis.

3. To determine the fate of transplanted mNSCs seeded on injectable hydrogels implanted in injured rat brains, place the animals randomly animals groups. In this study the groups are: (1) TBI + mNSCs only, (2) TBI + ICH and mNSCs (3) TBI + ICH with mNSCs + BDNF/GDNF, (4) TBI + ICH with PNPX/ChABC/EDHB/2,2-bipyridyl/cAMP, and (5) TBI + ICH with mNSCs + BDNF/GDNF + PNPX/ChABC/EDHB/2,2-bipyridyl/cAMP. Subject the rats to moderate CCI and randomly assigned to the groups described above. Inject the optimally designed hydrogel loaded with mNSCs (5.0×10^5 cells) and biomolecules into the lesion site of the animals at the required concentration at the post injury times assigned in previous experiments. To evaluate the viability of transplanted cells, multi-photon images of mNSCs will be taken of live animals using a Zeiss multiphoton microscope over 2 week intervals (2, 4 and 6 weeks) after injection and MRA will be performed to determine vasculature formation in the injury site. Permeated animal to determine the fate of the transplanted NSCs including survival, differentiation and possible tumor formation. Use fluorescent microscopy to examine

sections encompassing the graft, followed by immunostaining for green fluorescent protein positive (GFP+) cells. Characterize the fate of the transplanted cells with double labeling for GFP+ cell type specific including neuronal markers, synaptic markers, glial markers, etc. Sox 2, Nestin and Musashi1 are identifiable markers if the transplanted cells retain immature NSCs property. Assess the association of grafted cell to blood vessels and glial scars by RECA-1, VEGF, CSPG and collagen IV with GFP staining and stain sections with proliferation marker Ki67 to detect the presence of mitotic activity. Compare the total number of surviving cells, percentages of cells expressing each marker from each animal group

References

1. Prins, M., et al., *The pathophysiology of traumatic brain injury at a glance*. Disease models & mechanisms, 2013. **6**(6): p. 1307-1315.

2. Schmidt, O.I., et al., *The role of neuroinflammation in traumatic brain injury*. European Journal of Trauma, 2004. **30**(3): p. 135-149.
3. Oyinbo, C.A., *Secondary injury mechanisms in traumatic spinal cord injury: a nugget of this multiply cascade*. Acta Neurobiol Exp., 2011. **71**: p. 281–299.
4. Fehlings, M.G., et al., *Essentials of spinal cord injury: basic research to clinical practice*. 2013, Denver Colorado: Thieme Medical Publishers Inc. .
5. Barbeau, H., et al., *Tapping into spinal circuits to restore motor function*. Brain Research Reviews, 1999. **30**(1): p. 27-51.
6. Tran, A.P., P.M. Warren, and J. Silver, *The biology of regeneration failure and success after spinal cord injury*. Physiological reviews, 2018. **98**(2): p. 881-917.
7. Dyck, S.M. and S. Karimi-Abdolrezaee, *Chondroitin sulfate proteoglycans: key modulators in the developing and pathologic central nervous system*. Experimental neurology, 2015. **269**: p. 169-187.
8. Alizadeh, A. and S. Karimi-Abdolrezaee, *Microenvironmental regulation of oligodendrocyte replacement and remyelination in spinal cord injury*. The Journal of physiology, 2016. **594**(13): p. 3539-3552.
9. Alizadeh, A., S.M. Dyck, and S. Karimi-Abdolrezaee, *Myelin damage and repair in pathologic CNS: challenges and prospects*. Frontiers in molecular neuroscience, 2015. **8**: p. 35.
10. Couillard-Despres, S. and M. Vogl, *Pathophysiology of traumatic spinal cord injury.*, in *Neurological aspects of spinal cord injury*, N. Weidner, R. Rupp, and K.E. Tansey, Editors. 2017, Springer International Publishing: Switzerland.
11. Koyanagi, I., C.H. Tator, and E. Theriault, *Silicone rubber microangiography of acute spinal cord injury in the rat*. Neurosurgery, 1993. **32**(2): p. 260-268.

12. Tator, C.H. and I. Koyanagi, *Vascular mechanisms in the pathophysiology of human spinal cord injury*. Journal of neurosurgery, 1997. **86**(3): p. 483-492.
13. Agrawal, S.K. and M.G. Fehlings, *Mechanisms of secondary injury to spinal cord axons in vitro: role of Na⁺, Na (+)-K (+)-ATPase, the Na (+)-H⁺ exchanger, and the Na (+)-Ca²⁺ exchanger*. Journal of Neuroscience, 1996. **16**(2): p. 545-552.
14. Kase, C.S., *Cerebellar hemorrhage*. Intracerebral hemorrhage, 1994: p. 425-443.
15. Xi, G., R.F. Keep, and J.T. Hoff, *Erythrocytes and delayed brain edema formation following intracerebral hemorrhage in rats*. Journal of neurosurgery, 1998. **89**(6): p. 991-996.
16. Thompson, K.J., S. Shoham, and J.R. Connor, *Iron and neurodegenerative disorders*. Brain research bulletin, 2001. **55**(2): p. 155-164.
17. Siesjö, B., C.-D. Agardh, and F. Bengtsson, *Free radicals and brain damage*. Cerebrovascular and brain metabolism reviews, 1989. **1**(3): p. 165-211.
18. Xi, G., R.F. Keep, and J.T. Hoff, *Pathophysiology of brain edema formation*. Neurosurgery Clinics, 2002. **13**(3): p. 371-383.
19. Huang, F.-P., et al., *Brain edema after experimental intracerebral hemorrhage: role of hemoglobin degradation products*. Journal of neurosurgery, 2002. **96**(2): p. 287-293.
20. Wu, J., et al., *Oxidative brain injury from extravasated erythrocytes after intracerebral hemorrhage*. Brain research, 2002. **953**(1-2): p. 45-52.
21. Rathore, K.I., et al., *Ceruloplasmin protects injured spinal cord from iron-mediated oxidative damage*. Journal of Neuroscience, 2008. **28**(48): p. 12736-12747.
22. Liu, D., et al., *Spinal cord injury increases iron levels: catalytic production of hydroxyl radicals*. Free Radical Biology and Medicine, 2003. **34**(1): p. 64-71.
23. Hershko, C., *Mechanism of iron toxicity*. Food and nutrition bulletin, 2007. **28**(4_suppl4): p. S500-S509.

24. Tanaka, Y. and K. Ohno, *Chronic subdural hematoma—an up-to-date concept*. Journal of medical and dental sciences, 2013. **60**(2): p. 55-61.
25. Walcott, B.P., et al., *Bilateral hemicraniectomy in non-penetrating traumatic brain injury*. Journal of Neurotrauma, 2012. **29**(10): p. 1879-1885.
26. Osteen, C., C. Giza, and D. Hovda, *Injury-induced alterations in N-methyl-D-aspartate receptor subunit composition contribute to prolonged 45calcium accumulation following lateral fluid percussion*. Neuroscience, 2004. **128**(2): p. 305-322.
27. Bareyre, F.M., et al., *Alterations in ionized and total blood magnesium after experimental traumatic brain injury: relationship to neurobehavioral outcome and neuroprotective efficacy of magnesium chloride*. Journal of neurochemistry, 1999. **73**(1): p. 271-280.
28. McINTOSH, T.K., et al., *Magnesium deficiency exacerbates and pretreatment improves outcome following traumatic brain injury in rats: 31P magnetic resonance spectroscopy and behavioral studies*. Journal of neurotrauma, 1988. **5**(1): p. 17-31.
29. Hoane, M.R., *Treatment with magnesium improves reference memory but not working memory while reducing GFAP expression following traumatic brain injury*. Restorative neurology and neuroscience, 2005. **23**(2): p. 67-77.
30. Zhou, F., et al., *Changes of mGluR4 and the effects of its specific agonist L-AP4 in a rodent model of diffuse brain injury*. Journal of clinical neuroscience, 2003. **10**(6): p. 684-688.
31. Mukhin, A., L. Fan, and A.I. Faden, *Activation of metabotropic glutamate receptor subtype mGluR1 contributes to post-traumatic neuronal injury*. Journal of Neuroscience, 1996. **16**(19): p. 6012-6020.
32. Zhang, C., et al., *Riluzole attenuates cortical lesion size, but not hippocampal neuronal loss, following traumatic brain injury in the rat*. Journal of neuroscience research, 1998. **52**(3): p. 342-349.

33. Sun, F.-Y. and A.I. Faden, *Neuroprotective effects of 619C89, a use-dependent sodium channel blocker, in rat traumatic brain injury*. Brain research, 1995. **673**(1): p. 133-140.
34. Limbrick Jr, D., S. Sombati, and R. DeLorenzo, *Calcium influx constitutes the ionic basis for the maintenance of glutamate-induced extended neuronal depolarization associated with hippocampal neuronal death*. Cell Calcium, 2003. **33**(2): p. 69-81.
35. Okiyama, K., et al., *(S)-emopamil attenuates acute reduction in regional cerebral blood flow following experimental brain injury*. Journal of neurotrauma, 1994. **11**(1): p. 83-95.
36. Okiyama, K., et al., *Evaluation of a novel calcium channel blocker, (S)-emopamil, on regional cerebral edema and neurobehavioral function after experimental brain injury*. Journal of neurosurgery, 1992. **77**(4): p. 607-615.
37. Maeda, T., S.M. Lee, and D.A. Hovda, *Restoration of cerebral vasoreactivity by an L-type calcium channel blocker following fluid percussion brain injury*. Journal of neurotrauma, 2005. **22**(7): p. 763-771.
38. Floyd, R.A., *Antioxidants, oxidative stress, and degenerative neurological disorders*. Proceedings of the Society for Experimental Biology and Medicine, 1999. **222**(3): p. 236-245.
39. Marklund, N., *The role of reactive oxygen species in traumatic brain injury: Experimental studies in the rat*. 2001, Acta Universitatis Upsaliensis.
40. Jacobsen, E.J., et al., *Novel 21-aminosteroids that inhibit iron-dependent lipid peroxidation and protect against central nervous system trauma*. Journal of medicinal chemistry, 1990. **33**(4): p. 1145-1151.
41. Althaus, J.S., et al., *The use of salicylate hydroxylation to detect hydroxyl radical generation in ischemic and traumatic brain injury*. Molecular and chemical neuropathology, 1993. **20**(2): p. 147-162.

42. PANTER, S.S., J.M. BRAUGHLER, and E.D. HALL, *Dextran-coupled deferoxamine improves outcome in a murine model of head injury*. Journal of neurotrauma, 1992. **9**(1): p. 47-53.
43. Wada, K., et al., *Early treatment with a novel inhibitor of lipid peroxidation (LY341122) improves histopathological outcome after moderate fluid percussion brain injury in rats*. Neurosurgery, 1999. **45**(3): p. 601-608.
44. Adibhatla, R.M., J. Hatcher, and R. Dempsey, *Citicoline: neuroprotective mechanisms in cerebral ischemia*. Journal of neurochemistry, 2002. **80**(1): p. 12-23.
45. Dempsey, R.J. and V.L.R. Rao, *Cytidinediphosphocholine treatment to decrease traumatic brain injury—induced hippocampal neuronal death, cortical contusion volume, and neurological dysfunction in rats*. Journal of neurosurgery, 2003. **98**(4): p. 867-873.
46. Oliver, C., et al., *Oxidative damage to brain proteins, loss of glutamine synthetase activity, and production of free radicals during ischemia/reperfusion-induced injury to gerbil brain*. Proceedings of the National Academy of Sciences, 1990. **87**(13): p. 5144-5147.
47. Marklund, N., et al., *α -phenyl-tert-N-butyl nitron (PBN) improves functional and morphological outcome after cortical contusion injury in the rat*. Acta neurochirurgica, 2001. **143**(1): p. 73-81.
48. Kontos, H.A. and E.P. Wei, *Superoxide production in experimental brain injury*. Journal of neurosurgery, 1986. **64**(5): p. 803-807.
49. Gahm, C., S. Holmin, and T. Mathiesen, *Nitric oxide synthase expression after human brain contusion*. Neurosurgery, 2002. **50**(6): p. 1319-1326.
50. Dhillon, H., et al., *Regional levels of free fatty acids and Evans blue extravasation after experimental brain injury*. Journal of neurotrauma, 1994. **11**(4): p. 405-415.

51. DASH, P.K., S.A. MACH, and A.N. MOORE, *Regional expression and role of cyclooxygenase-2 following experimental traumatic brain injury*. Journal of neurotrauma, 2000. **17**(1): p. 69-81.
52. Kunz, T., et al., *Cyclooxygenase-2, prostaglandin synthases, and prostaglandin H2 metabolism in traumatic brain injury in the rat*. Journal of neurotrauma, 2002. **19**(9): p. 1051-1064.
53. Raghupathi, R., *Cell death mechanisms following traumatic brain injury*. Brain pathology, 2004. **14**(2): p. 215-222.
54. Kerr, J.F., A.H. Wyllie, and A.R. Currie, *Apoptosis: a basic biological phenomenon with wideranging implications in tissue kinetics*. British journal of cancer, 1972. **26**(4): p. 239-257.
55. ZIPFEL, G.J., et al., *Neuronal apoptosis after CNS injury: the roles of glutamate and calcium*. Journal of neurotrauma, 2000. **17**(10): p. 857-869.
56. McEwen, B.S., *Steroid hormone actions on the brain: when is the genome involved?* Hormones and behavior, 1994. **28**(4): p. 396-405.
57. Kazanis, I., et al., *Alterations in IGF-I, BDNF and NT-3 levels following experimental brain trauma and the effect of IGF-I administration*. Experimental neurology, 2004. **186**(2): p. 221-234.
58. Kimonides, V., et al., *Dehydroepiandrosterone (DHEA) and DHEA-sulfate (DHEAS) protect hippocampal neurons against excitatory amino acid-induced neurotoxicity*. Proceedings of the National Academy of Sciences, 1998. **95**(4): p. 1852-1857.
59. Singh, P.L., et al., *Current therapeutic strategies for inflammation following traumatic spinal cord injury*. Neural Regeneration Research, 2012. **7**(23): p. 1812.
60. Dario, A. and G. Tomei, *A benefit-risk assessment of baclofen in severe spinal spasticity*. Drug safety, 2004. **27**(11): p. 799-818.

61. Schumacher, M.A., A.I. Basbaum, and W. Way, *Basic and clinical pharmacology*. Opioid analgesics and antagonists, 12th ed. New York, USA: McGraw-Hill, 2012: p. 542-3.
62. Mashkouri, S., et al., *Utilizing pharmacotherapy and mesenchymal stem cell therapy to reduce inflammation following traumatic brain injury*. *Neural Regeneration Research*, 2016. **11**(9): p. 1379.
63. Antonucci, I., et al., *Amniotic fluid stem cells: a promising therapeutic resource for cell-based regenerative therapy*. *Current pharmaceutical design*, 2012. **18**(13): p. 1846-1863.
64. Wislet-Gendebien, S., et al., *Adult bone marrow: which stem cells for cellular therapy protocols in neurodegenerative disorders?* *Journal of Biomedicine and Biotechnology*, 2012. **2012**.
65. Weston, N.M. and D. Sun, *The potential of stem cells in treatment of traumatic brain injury*. *Current neurology and neuroscience reports*, 2018. **18**(1): p. 1-10.
66. Huang, L., et al., *Stem cell therapy for spinal cord injury*. *Cell Transplantation*, 2021. **30**: p. 0963689721989266.
67. Rosenfeld, J.V., et al., *Early management of severe traumatic brain injury*. *The Lancet*, 2012. **380**(9847): p. 1088-1098.
68. Galgano, M., et al., *Traumatic brain injury: current treatment strategies and future endeavors*. *Cell transplantation*, 2017. **26**(7): p. 1118-1130.
69. Wilson, J.R., N. Forgione, and M.G. Fehlings, *Emerging therapies for acute traumatic spinal cord injury*. *Cmaj*, 2013. **185**(6): p. 485-492.
70. Ng, S.Y. and A.Y.W. Lee, *Traumatic brain injuries: pathophysiology and potential therapeutic targets*. *Frontiers in cellular neuroscience*, 2019. **13**: p. 528.
71. Xiong, Y., A. Mahmood, and M. Chopp, *Emerging treatments for traumatic brain injury*. *Expert opinion on emerging drugs*, 2009. **14**(1): p. 67-84.

72. Diaz-Arrastia, R., et al., *Pharmacotherapy of traumatic brain injury: state of the science and the road forward: report of the Department of Defense Neurotrauma Pharmacology Workgroup*. Journal of neurotrauma, 2014. **31**(2): p. 135-158.
73. Hugenholtz, H., et al., *High-dose methylprednisolone for acute closed spinal cord injury- only a treatment option*. Canadian journal of neurological sciences, 2002. **29**(3): p. 227-235.
74. Baskin, D.S., et al., *The effect of long-term high-dose naloxone infusion in experimental blunt spinal cord injury*. Journal of spinal disorders, 1993. **6**(1): p. 38-43.
75. Bracken, M.B., et al., *A randomized, controlled trial of methylprednisolone or naloxone in the treatment of acute spinal-cord injury: results of the Second National Acute Spinal Cord Injury Study*. New England Journal of Medicine, 1990. **322**(20): p. 1405-1411.
76. Bracken, M.B., et al., *Administration of methylprednisolone for 24 or 48 hours or tirilazad mesylate for 48 hours in the treatment of acute spinal cord injury: results of the Third National Acute Spinal Cord Injury Randomized Controlled Trial*. Jama, 1997. **277**(20): p. 1597-1604.
77. Fehlings, M.G., C.H. Tator, and R.D. Linden, *The effect of nimodipine and dextran on axonal function and blood flow following experimental spinal cord injury*. Journal of neurosurgery, 1989. **71**(3): p. 403-416.
78. Bose, B., J.L. Osterholm, and M. Kalia, *Ganglioside-induced regeneration and reestablishment of axonal continuity in spinal cord-transected rats*. Neuroscience letters, 1986. **63**(2): p. 165-169.
79. Teng, Y.D., et al., *Basic fibroblast growth factor increases long-term survival of spinal motor neurons and improves respiratory function after experimental spinal cord injury*. Journal of Neuroscience, 1999. **19**(16): p. 7037-7047.
80. Fehlings, M.G., et al., *Riluzole for the treatment of acute traumatic spinal cord injury: rationale for and design of the NACTN Phase I clinical trial*. Journal of Neurosurgery: Spine, 2012. **17**(Suppl1): p. 151-156.

81. Grossman, R., M. Fehlings, and R. Frankowski. *A phase I multicenter trial to investigate the safety and pharmacokinetics profile of riluzole in the treatment of traumatic spinal cord injury*. in *Proceedings of the Society for Neuroscience 12 meeting*. 2012.
82. Festoff, B.W., et al., *Minocycline neuroprotects, reduces microgliosis, and inhibits caspase protease expression early after spinal cord injury*. *Journal of neurochemistry*, 2006. **97**(5): p. 1314-1326.
83. Casha, S., et al., *Results of a phase II placebo-controlled randomized trial of minocycline in acute spinal cord injury*. *Brain*, 2012. **135**(4): p. 1224-1236.
84. Fehlings, M.G., et al., *A phase I/IIa clinical trial of a recombinant Rho protein antagonist in acute spinal cord injury*. *Journal of neurotrauma*, 2011. **28**(5): p. 787-796.
85. Badhiwala, J.H., J.R. Wilson, and M.G. Fehlings, *Global burden of traumatic brain and spinal cord injury*. *The Lancet Neurology*, 2019. **18**(1): p. 24-25.
86. Freund, P., et al., *Anti-Nogo-A antibody treatment enhances sprouting of corticospinal axons rostral to a unilateral cervical spinal cord lesion in adult macaque monkey*. *Journal of Comparative Neurology*, 2007. **502**(4): p. 644-659.
87. Wang, J. and D.D. Pearse, *Therapeutic hypothermia in spinal cord injury: the status of its use and open questions*. *International journal of molecular sciences*, 2015. **16**(8): p. 16848-16879.
88. ALBIN, M.S., et al., *Localized Spinal Cord Hypothermia:—anesthetic effects and application to spinal cord injury*. *Anesthesia & Analgesia*, 1967. **46**(1): p. 8-17.
89. Albin, M.S., et al., *Study of functional recovery produced by delayed localized cooling after spinal cord injury in primates*. *Journal of neurosurgery*, 1968. **29**(2): p. 113-120.
90. Ducker, T.B. and H.F. Hamit, *Experimental treatments of acute spinal cord injury*. *Journal of neurosurgery*, 1969. **30**(6): p. 693-697.

91. Salzano Jr, R.P., et al., *Regional deep hypothermia of the spinal cord protects against ischemic injury during thoracic aortic cross-clamping*. The Annals of thoracic surgery, 1994. **57**(1): p. 65-71.
92. Tabayashi, K., et al., *Protection from postischemic spinal cord injury by perfusion cooling of the epidural space*. The Annals of thoracic surgery, 1993. **56**(3): p. 494-498.
93. King, C., et al., *Brain temperature profiles during epidural cooling with the ChillerPad in a monkey model of traumatic brain injury*. Journal of neurotrauma, 2010. **27**(10): p. 1895-1903.
94. Rokkas, C.K., et al., *Profound systemic hypothermia inhibits the release of neurotransmitter amino acids in spinal cord ischemia*. The Journal of thoracic and cardiovascular surgery, 1995. **110**(1): p. 27-35.
95. Rose, W.W., et al., *Protective effect of hypothermia and left heart bypass on spinal ischemia in the dog*. Archives of Surgery, 1997. **132**(6): p. 633-640.
96. Ueno, T., et al., *Protection against ischemic spinal cord injury: one-shot perfusion cooling and percutaneous topical cooling*. Journal of vascular surgery, 1994. **19**(5): p. 882-887.
97. Yu, C.G., et al., *Beneficial effects of modest systemic hypothermia on locomotor function and histopathological damage following contusion-induced spinal cord injury in rats*. Journal of Neurosurgery: Spine, 2000. **93**(1): p. 85-93.
98. Dietrich, W.D., et al., *Post-traumatic brain hypothermia reduces histopathological damage following concussive brain injury in the rat*. Acta neuropathologica, 1994. **87**(3): p. 250-258.
99. Bramlett, H.M., et al., *Posttraumatic brain hypothermia provides protection from sensorimotor and cognitive behavioral deficits*. Journal of neurotrauma, 1995. **12**(3): p. 289-298.

100. Dietrich, W.D. and H.M. Bramlett, *Therapeutic hypothermia and targeted temperature management in traumatic brain injury: Clinical challenges for successful translation*. Brain research, 2016. **1640**: p. 94-103.
101. Zhou, Y., et al., *Advance of stem cell treatment for traumatic brain injury*. Frontiers in cellular neuroscience, 2019. **13**: p. 301.
102. Walker, P.A., et al., *Progenitor cell therapy for the treatment of central nervous system injury: a review of the state of current clinical trials*. Stem cells international, 2010. **2010**.
103. Sun, D., *The potential of neural transplantation for brain repair and regeneration following traumatic brain injury*. Neural regeneration research, 2016. **11**(1): p. 18.
104. Bonilla, C. and M. Zurita, *Cell-Based Therapies for Traumatic Brain Injury: Therapeutic Treatments and Clinical Trials*. Biomedicines, 2021. **9**(6): p. 669.
105. Rodriguez, A.L., D.R. Nisbet, and C.L. Parish, *The potential of stem cells and tissue engineered scaffolds for repair of the central nervous system*, in *Stem Cells and Cancer Stem Cells, Volume 4*. 2012, Springer. p. 97-111.
106. Kim, K. and G. Evans, *Tissue engineering: the future of stem cells*. Topics in tissue engineering, 2005. **2**: p. 1-21.
107. Wang, X., et al., *Hyaluronic acid-based scaffold for central neural tissue engineering*. Interface Focus, 2012. **2**(3): p. 278-291.
108. Potts, M.B., et al., *Traumatic injury to the immature brain: inflammation, oxidative injury, and iron-mediated damage as potential therapeutic targets*. NeuroRx, 2006. **3**(2): p. 143-153.
109. Garton, T., et al., *Brain iron overload following intracranial haemorrhage*. Stroke and Vascular Neurology, 2016: p. e000042.
110. Wang, L.-F., et al., *Male-specific alleviation of iron-induced striatal injury by inhibition of autophagy*. PloS one, 2015. **10**(7): p. e0131224.

111. Tanida, I., T. Ueno, and E. Kominami, *LC3 and Autophagy*. Autophagosome and Phagosome, 2008: p. 77-88.
112. Wang, L.-F., et al., *Knockout of ho-1 protects the striatum from ferrous iron-induced injury in a male-specific manner in mice*. Scientific reports, 2016. **6**.
113. Necas, J., et al., *Hyaluronic acid (hyaluronan): a review*. Veterinarni medicina, 2008. **53**(8): p. 397-411.
114. Toole, B.P., S. Ghatak, and S. Misra, *Hyaluronan oligosaccharides as a potential anticancer therapeutic*. Current pharmaceutical biotechnology, 2008. **9**(4): p. 249-252.
115. Solis, M.A., et al., *Hyaluronan regulates cell behavior: a potential niche matrix for stem cells*. Biochemistry research international, 2012. **2012**.
116. Toole, B.P., *Hyaluronan: from extracellular glue to pericellular cue*. Nature Reviews Cancer, 2004. **4**(7): p. 528.
117. Rooney, P., et al., *The role of hyaluronan in tumour neovascularization*. International Journal of Cancer, 1995. **60**(5): p. 632-636.
118. Margolis, R., et al., *Glycosaminoglycans of brain during development*. Biochemistry, 1975. **14**(1): p. 85-88.
119. Ikeda, Y. and D.M. Long, *The molecular basis of brain injury and brain edema: the role of oxygen free radicals*. Neurosurgery, 1990. **27**(1): p. 1-11.
120. Bains, M. and E.D. Hall, *Antioxidant therapies in traumatic brain and spinal cord injury*. Biochimica et Biophysica Acta (BBA)-Molecular Basis of Disease, 2012. **1822**(5): p. 675-684.
121. Myint, P., et al., *The reactivity of various free radicals with hyaluronic acid: steady-state and pulse radiolysis studies*. Biochimica et Biophysica Acta (BBA)-General Subjects, 1987. **925**(2): p. 194-202.

122. Laurent, T.C., U. Laurent, and J. Fraser, *Functions of hyaluronan*. Annals of the rheumatic diseases, 1995. **54**(5): p. 429.
123. Laurent, T.C., U.B. Laurent, and J.R.E. Fraser, *The structure and function of hyaluronan: an overview*. Immunology and cell biology, 1996. **74**(2): p. a1-a7.
124. Ke, C., et al., *Antioxidant activity of low molecular weight hyaluronic acid*. Food and chemical toxicology, 2011. **49**(10): p. 2670-2675.
125. Wakao, N., et al., *Hyaluronan oligosaccharides promote functional recovery after spinal cord injury in rats*. Neuroscience letters, 2011. **488**(3): p. 299-304.
126. Wang, J., et al., *Hyaluronan tetrasaccharide in the cerebrospinal fluid is associated with self-repair of rats after chronic spinal cord compression*. Neuroscience, 2012. **210**: p. 467-480.
127. Wang, J., et al., *Hyaluronan tetrasaccharide exerts neuroprotective effect and promotes functional recovery after acute spinal cord injury in rats*. Neurochemical research, 2015. **40**(1): p. 98-108.
128. Torigoe, K., et al., *Hyaluronan tetrasaccharide promotes regeneration of peripheral nerve: in vivo analysis by film model method*. Brain research, 2011. **1385**: p. 87-92.
129. Andrews, N.C., *Iron homeostasis: insights from genetics and animal models*. Nature Reviews Genetics, 2000. **1**(3): p. 208.
130. Kushchayev, S.V., et al., *Hyaluronic acid scaffold has a neuroprotective effect in hemisection spinal cord injury*. Journal of Neurosurgery: Spine, 2016. **25**(1): p. 114-124.
131. Pakulska, M.M., B.G. Ballios, and M.S. Shoichet, *Injectable hydrogels for central nervous system therapy*. Biomedical materials, 2012. **7**(2): p. 024101.
132. Tian, W., et al., *Hyaluronic acid hydrogel as Nogo-66 receptor antibody delivery system for the repairing of injured rat brain: in vitro*. Journal of Controlled Release, 2005. **102**(1): p. 13-22.

133. Park, J., et al., *Nerve regeneration following spinal cord injury using matrix metalloproteinase-sensitive, hyaluronic acid-based biomimetic hydrogel scaffold containing brain-derived neurotrophic factor*. Journal of Biomedical Materials Research Part A, 2010. **93**(3): p. 1091-1099.
134. Wang, Y., et al., *Combination of hyaluronic acid hydrogel scaffold and PLGA microspheres for supporting survival of neural stem cells*. Pharmaceutical research, 2011. **28**(6): p. 1406.
135. Pan, L., et al., *Viability and differentiation of neural precursors on hyaluronic acid hydrogel scaffold*. Journal of neuroscience research, 2009. **87**(14): p. 3207-3220.
136. Demopoulos, H., et al., *Further studies on free-radical pathology in the major central nervous system disorders: effect of very high doses of methylprednisolone on the functional outcome, morphology, and chemistry of experimental spinal cord impact injury*. Canadian journal of physiology and pharmacology, 1982. **60**(11): p. 1415-1424.
137. Demopoulos, H., et al., *Oxygen free radicals in central nervous system ischemia and trauma*. Pathology of oxygen, 1982: p. 127-155.
138. Ortega, B.D., H.B. Demopoulos, and J. Ransohoff, *Effect of antioxidants on experimental cold-induced cerebral edema*, in *Steroids and Brain Edema*. 1972, Springer. p. 167-175.
139. Greenwald, R.A. and W.W. Moy, *Effect of oxygen-derived free radicals on hyaluronic acid*. Arthritis & Rheumatism: Official Journal of the American College of Rheumatology, 1980. **23**(4): p. 455-463.
140. Halliwell, B. and J. Gutteridge, *Oxygen toxicity, oxygen radicals, transition metals and disease*. Biochemical journal, 1984. **219**(1): p. 1.
141. Gaasch, J.A., et al., *Brain iron toxicity: differential responses of astrocytes, neurons, and endothelial cells*. Neurochemical research, 2007. **32**(7): p. 1196-1208.

142. Sy, C., et al., *Inhibition of iron-induced lipid peroxidation by newly identified bacterial carotenoids in model gastric conditions: comparison with common carotenoids*. Food & function, 2013. **4**(5): p. 698-712.
143. Atkins, R.C., *Colorimetric determination of iron in vitamin supplement tablets. A general chemistry experiment*. Journal of chemical education, 1975. **52**(8): p. 550.
144. Shahidi, F. and Y. Zhong, *Lipid oxidation and improving the oxidative stability*. Chemical Society Reviews, 2010. **39**(11): p. 4067-4079.
145. Corongiu, F.P. and A. Milia, *An improved and simple method for determining diene conjugation in autoxidized polyunsaturated fatty acids*. Chemico-biological interactions, 1983. **44**(3): p. 289-297.
146. Davoodi, S.H., et al., *The dual nature of iron in relation to cancer: a review*. Iranian Journal of Cancer Prevention, 2016. **9**(6).
147. Mercê, A.L.R., et al., *Aqueous and solid complexes of iron (III) with hyaluronic acid: potentiometric titrations and infrared spectroscopy studies*. Journal of inorganic biochemistry, 2002. **89**(3): p. 212-218.
148. Balogh, G.T., et al., *Effect of different metal ions on the oxidative damage and antioxidant capacity of hyaluronic acid*. Archives of biochemistry and biophysics, 2003. **410**(1): p. 76-82.
149. Nieto, J., C. Peniche-Covas, and J. Del Bosque, *Preparation and characterization of a chitosan-Fe (III) complex*. Carbohydrate Polymers, 1992. **18**(3): p. 221-224.
150. Yin, H., L. Xu, and N.A. Porter, *Free radical lipid peroxidation: mechanisms and analysis*. Chemical reviews, 2011. **111**(10): p. 5944-5972.
151. Spiteller, G., *Linoleic acid peroxidation—the dominant lipid peroxidation process in low density lipoprotein—and its relationship to chronic diseases*. Chemistry and physics of lipids, 1998. **95**(2): p. 105-162.

152. Elmagirbi, A., H. Sulistyarti, and A. Atikah, *Study of ascorbic acid as iron (III) reducing agent for spectrophotometric iron speciation*. The Journal of Pure and Applied Chemistry Research, 2012. **1**(1): p. 11-17.
153. Porter, N.A., S.E. Caldwell, and K.A. Mills, *Mechanisms of free radical oxidation of unsaturated lipids*. Lipids, 1995. **30**(4): p. 277-290.
154. Adibhatla, R.M. and J.F. Hatcher, *Role of lipids in brain injury and diseases*. Future lipidology, 2007. **2**(4): p. 403-422.
155. Adibhatla, R.M. and J.F. Hatcher, *Lipid oxidation and peroxidation in CNS health and disease: from molecular mechanisms to therapeutic opportunities*. Antioxidants & redox signaling, 2010. **12**(1): p. 125-169.
156. Adibhatla, R.M. and J. Hatcher, *Altered lipid metabolism in brain injury and disorders, in Lipids in health and disease*. 2008, Springer. p. 241-268.
157. Costa, C., et al., *Mapping of aggrecan, hyaluronic acid, heparan sulphate proteoglycans and aquaporin 4 in the central nervous system of the mouse*. Journal of chemical neuroanatomy, 2007. **33**(3): p. 111-123.
158. Hall, E.D. and J.E. Springer, *Neuroprotection and acute spinal cord injury: a reappraisal*. NeuroRx, 2004. **1**(1): p. 80-100.
159. Halliwell, B. and J. Gutteridge, *Oxidative stress and redox regulation: adaptation, damage, repair, senescence and death*. 2015, Oxford University Press, Oxford, UK. p. 199-284.
160. Du, J., J.J. Cullen, and G.R. Buettner, *Ascorbic acid: chemistry, biology and the treatment of cancer*. Biochimica et Biophysica Acta (BBA)-Reviews on Cancer, 2012. **1826**(2): p. 443-457.
161. Riss, T.L., et al., *Cell viability assays*, in *Assay Guidance Manual [Internet]*. 2016, Eli Lilly & Company and the National Center for Advancing Translational Sciences.

162. Yehuda, S. and D.I. Mostofsky, *Iron deficiency and overload: from basic biology to clinical medicine*. 2010: Springer Science & Business Media.
163. Zhou, X., et al., *Signaling in H₂O₂-induced increase in cell proliferation in Barrett's esophageal adenocarcinoma cells*. Journal of pharmacology and experimental therapeutics, 2011. **339**(1): p. 218-227.
164. Perkins, K.L., et al., *Brain extracellular space, hyaluronan, and the prevention of epileptic seizures*. Reviews in the neurosciences, 2017. **28**(8): p. 869-892.
165. Sears, M.E., *Chelation: harnessing and enhancing heavy metal detoxification—a review*. The Scientific World Journal, 2013. **2013**.
166. Fu, Z. and S. Xi, *The effects of heavy metals on human metabolism*. Toxicology mechanisms and methods, 2020. **30**(3): p. 167-176.
167. Kim, J.-J., Y.-S. Kim, and V. Kumar, *Heavy metal toxicity: An update of chelating therapeutic strategies*. Journal of Trace elements in Medicine and Biology, 2019. **54**: p. 226-231.
168. Flora, S., M. Mittal, and A. Mehta, *Heavy metal induced oxidative stress & its possible reversal by chelation therapy*. Indian Journal of Medical Research, 2008. **128**(4): p. 501.
169. Flora, S.J. and V. Pachauri, *Chelation in metal intoxication*. International journal of environmental research and public health, 2010. **7**(7): p. 2745-2788.
170. NE, C., C. CN, and M. RE, *The in vivo dissolution of metastatic calcium; an approach to atherosclerosis*. The American journal of the medical sciences, 1955. **229**(2): p. 142-149.
171. Clarke, C., N. Clarke, and R. Mosher, *Treatment of angina pectoris with disodium ethylene diamine tetraacetic acid*. The American journal of the medical sciences, 1956. **232**(6): p. 654-666.
172. Behrouzi, B., et al., *Action of iron chelator on intramyocardial hemorrhage and cardiac remodeling following acute myocardial infarction*. Basic research in cardiology, 2020. **115**(3): p. 1-18.

173. Zlatanova, I., et al., *Iron regulator hepcidin impairs macrophage-dependent cardiac repair after injury*. *Circulation*, 2019. **139**(12): p. 1530-1547.
174. Crichton, R.R., *Metal Toxicity - An Introduction*, in *Metal chelation in medicine* R.R. Crichton, R.J. Ward, and R.C. Hider, Editors. 2016, Royal Society of Chemistry. p. 1-23.
175. Prashanth, L., et al., *A review on role of essential trace elements in health and disease*. *Journal of dr. ntr university of health sciences*, 2015. **4**(2): p. 75.
176. Cronin, S.J., et al., *The role of iron regulation in immunometabolism and immune-related disease*. *Frontiers in molecular biosciences*, 2019. **6**: p. 116.
177. Britton, R.S., K.L. Leicester, and B.R. Bacon, *Iron toxicity and chelation therapy*. *International journal of hematology*, 2002. **76**(3): p. 219-228.
178. Sripetchwandee, J., et al., *Combined therapy of iron chelator and antioxidant completely restores brain dysfunction induced by iron toxicity*. *PLoS One*, 2014. **9**(1): p. e85115.
179. Sauerbeck, A., et al., *Systemic iron chelation results in limited functional and histological recovery after traumatic spinal cord injury in rats*. *Experimental neurology*, 2013. **248**: p. 53-61.
180. McTigue, D.M., *Targeted Iron Chelation Will Improve Recovery after Spinal Cord Injury*. 2014, Ohio State University Research Foundation Columbus United States.
181. Sekhon, L.H. and M.G. Fehlings, *Epidemiology, demographics, and pathophysiology of acute spinal cord injury*. *Spine*, 2001. **26**(24S): p. S2-S12.
182. Werner, C. and K. Engelhard, *Pathophysiology of traumatic brain injury*. *BJA: British Journal of Anaesthesia*, 2007. **99**(1): p. 4-9.
183. Hall, E.D., et al., *Lipid peroxidation in brain or spinal cord mitochondria after injury*. *Journal of bioenergetics and biomembranes*, 2016. **48**(2): p. 169-174.
184. Núñez, M.T., et al., *Iron toxicity in neurodegeneration*. *Biometals*, 2012. **25**(4): p. 761-776.

185. Daglas, M. and P.A. Adlard, *The involvement of iron in traumatic brain injury and neurodegenerative disease*. *Frontiers in neuroscience*, 2018. **12**: p. 981.
186. Raz, E., et al., *Brain iron quantification in mild traumatic brain injury: a magnetic field correlation study*. *American journal of neuroradiology*, 2011. **32**(10): p. 1851-1856.
187. Lu, L., et al., *Iron deposition is positively related to cognitive impairment in patients with chronic mild traumatic brain injury: assessment with susceptibility weighted imaging*. *BioMed research international*, 2015. **2015**.
188. Nisenbaum, E.J., D.S. Novikov, and Y.W. Lui, *The presence and role of iron in mild traumatic brain injury: an imaging perspective*. *Journal of neurotrauma*, 2014. **31**(4): p. 301-307.
189. Babadjouni, R.M., et al., *Neuroprotective strategies following intraparenchymal hemorrhage*. *Journal of neurointerventional surgery*, 2017. **9**(12): p. 1202-1207.
190. Robicsek, S.A., et al., *Blood-related toxicity after traumatic brain injury: potential targets for neuroprotection*. *Molecular neurobiology*, 2019: p. 1-20.
191. Ziegler, G., et al., *Progressive neurodegeneration following spinal cord injury: implications for clinical trials*. *Neurology*, 2018. **90**(14): p. e1257-e1266.
192. Donovan, V., et al., *Computational analysis reveals increased blood deposition following repeated mild traumatic brain injury*. *NeuroImage: Clinical*, 2012. **1**(1): p. 18-28.
193. Garton, T., et al., *Brain iron overload following intracranial haemorrhage*. *Stroke and vascular neurology*, 2016. **1**(4): p. 172-184.
194. Yao, X., et al., *Deferoxamine promotes recovery of traumatic spinal cord injury by inhibiting ferroptosis*. *Neural regeneration research*, 2019. **14**(3): p. 532.
195. Meng, F.X., J.M. Hou, and T.S. Sun, *Effect of oxidative stress induced by intracranial iron overload on central pain after spinal cord injury*. *Journal of orthopaedic surgery and research*, 2017. **12**(1): p. 1-10.

196. Zhang, L., et al., *Deferoxamine attenuates iron-induced long-term neurotoxicity in rats with traumatic brain injury*. Neurological Sciences, 2013. **34**(5): p. 639-645.
197. Khalaf, S., et al., *Unique properties associated with the brain penetrant iron chelator HBED reveal remarkable beneficial effects after brain trauma*. Journal of neurotrauma, 2019. **36**(1): p. 43-53.
198. Schültke, E., et al., *Quercetin promotes functional recovery following acute spinal cord injury*. Journal of neurotrauma, 2003. **20**(6): p. 583-591.
199. Baksi, A.J. and D.J. Pennell, *Randomized controlled trials of iron chelators for the treatment of cardiac siderosis in thalassaemia major*. Frontiers in pharmacology, 2014. **5**: p. 217.
200. Long, D.A., et al., *Deferoxamine improves spatial memory performance following experimental brain injury in rats*. Brain research, 1996. **717**(1-2): p. 109-117.
201. Zhao, J., et al., *Deferoxamine attenuates acute hydrocephalus after traumatic brain injury in rats*. Translational stroke research, 2014. **5**(5): p. 586-594.
202. Wang, K., et al., *HIF-1 α and VEGF Are Involved in Deferoxamine-Ameliorated Traumatic Brain Injury*. Journal of Surgical Research, 2019.
203. Shi, J., et al., *Attenuation of white matter damage following Deferoxamine treatment in rats after spinal cord injury*. World neurosurgery, 2019.
204. Maher, P. and G.J. Kontoghiorghes, *Characterization of the neuroprotective potential of derivatives of the iron chelating drug deferiprone*. Neurochemical research, 2015. **40**(3): p. 609-620.
205. Zhang, L., et al., *Minocycline attenuates neurological impairment and regulates iron metabolism in a rat model of traumatic brain injury*. Archives of biochemistry and biophysics, 2020. **682**: p. 108302.

206. He, J., et al., *Minocycline attenuates neuronal apoptosis and improves motor function after traumatic brain injury in rats*. *Experimental Animals*, 2021: p. 21-0028.
207. Kumar, P., et al., *Cur (Que) min: A neuroactive permutation of Curcumin and Quercetin for treating spinal cord injury*. *Medical hypotheses*, 2014. **82**(4): p. 437-441.
208. Samuni, A.M., et al., *Multifunctional antioxidant activity of HBED iron chelator*. *Free Radical Biology and Medicine*, 2001. **30**(2): p. 170-177.
209. KAMENCIC, H., et al., *Promoting glutathione synthesis after spinal cord trauma decreases secondary damage and promotes retention of function*. *The FASEB Journal*, 2001. **15**(1): p. 243-250.
210. Basso, D.M., M.S. Beattie, and J.C. Bresnahan, *A sensitive and reliable locomotor rating scale for open field testing in rats*. *Journal of neurotrauma*, 1995. **12**(1): p. 1-21.
211. Wu, A., Z. Ying, and F. Gomez-Pinilla, *Dietary curcumin counteracts the outcome of traumatic brain injury on oxidative stress, synaptic plasticity, and cognition*. *Experimental neurology*, 2006. **197**(2): p. 309-317.
212. Zhang, N., et al., *Effect of curcumin on acute spinal cord injury in mice via inhibition of inflammation and TAK1 pathway*. *Pharmacological Reports*, 2017. **69**(5): p. 1001-1006.
213. Kim, K.-T., et al., *The neuroprotective effect of treatment with curcumin in acute spinal cord injury*. *Neurologia medico-chirurgica*, 2014: p. oa. 2013-0251.
214. Liu, X., et al., *Therapeutic effect of curcumin and methylprednisolone in the rat spinal cord injury*. *The Anatomical Record*, 2018. **301**(4): p. 686-696.
215. Lin, M.-S., et al., *Curcumin provides neuroprotection after spinal cord injury*. *Journal of Surgical Research*, 2011. **166**(2): p. 280-289.
216. Huang, T., et al., *Curcumin mitigates axonal injury and neuronal cell apoptosis through the PERK/Nrf2 signaling pathway following diffuse axonal injury*. *Neuroreport*, 2018. **29**(8): p. 661.

217. Marchiani, A., et al., *Curcumin and curcumin-like molecules: from spice to drugs*. Current medicinal chemistry, 2014. **21**(2): p. 204-222.
218. Sahebkar, A., et al., *Effect of curcuminoids on oxidative stress: A systematic review and meta-analysis of randomized controlled trials*. Journal of Functional Foods, 2015. **18**: p. 898-909.
219. Baum, L. and A. Ng, *Curcumin interaction with copper and iron suggests one possible mechanism of action in Alzheimer's disease animal models*. Journal of Alzheimer's disease, 2004. **6**(4): p. 367-377.
220. Farkhondeh, T., et al., *Impact of curcumin on traumatic brain injury and involved molecular signaling pathways*. Recent patents on food, nutrition & agriculture, 2020. **11**(2): p. 137-144.
221. Malik, P. and T.K. Mukherjee, *Structure-function elucidation of antioxidative and prooxidative activities of the polyphenolic compound curcumin*. Chinese Journal of Biology, 2014. **2014**.
222. Priyadarsini, K.I., et al., *Role of phenolic OH and methylene hydrogen on the free radical reactions and antioxidant activity of curcumin*. Free Radical Biology and Medicine, 2003. **35**(5): p. 475-484.
223. Rao, M., *Curcuminoids as potent inhibitors of lipid peroxidation*. Journal of pharmacy and pharmacology, 1994. **46**(12): p. 1013-1016.
224. Dairam, A., et al., *Antioxidant and iron-binding properties of curcumin, capsaicin, and S-allylcysteine reduce oxidative stress in rat brain homogenate*. Journal of agricultural and food chemistry, 2008. **56**(9): p. 3350-3356.
225. Du, X.-X., et al., *Curcumin protects nigral dopaminergic neurons by iron-chelation in the 6-hydroxydopamine rat model of Parkinson's disease*. Neuroscience bulletin, 2012. **28**(3): p. 253-258.

226. Poggiali, E., et al., *An update on iron chelation therapy*. *Blood Transfusion*, 2012. **10**(4): p. 411.
227. Nisbet-Brown, E., et al., *Effectiveness and safety of ICL670 in iron-loaded patients with thalassaemia: a randomised, double-blind, placebo-controlled, dose-escalation trial*. *The Lancet*, 2003. **361**(9369): p. 1597-1602.
228. Borgna-Pignatti, C., et al., *Cardiac morbidity and mortality in deferoxamine-or deferipronetreated patients with thalassemia major*. *Blood* 2006; *107*: 3733-7. Letters to the Editor.
229. Bergeron, R.J., J. Wiegand, and G.M. Brittenham, *HBED ligand: preclinical studies of a potential alternative to deferoxamine for treatment of chronic iron overload and acute iron poisoning*. *Blood, The Journal of the American Society of Hematology*, 2002. **99**(8): p. 3019-3026.
230. Lee, P., et al., *Intravenous infusion pharmacokinetics of desferrioxamine in thalassaemic patients*. *Drug metabolism and disposition*, 1993. **21**(4): p. 640-644.
231. Whitten, C.F., et al., *Studies in acute iron poisoning. I. Desferrioxamine in the treatment of acute iron poisoning: clinical observations, experimental studies, and theoretical considerations*. *Pediatrics*, 1965. **36**(3): p. 322-335.
232. Dragsten, P.R., et al., *First human studies with a high-molecular-weight iron chelator*. *Journal of Laboratory and Clinical Medicine*, 2000. **135**(1): p. 57-65.
233. Hallaway, P.E., et al., *Modulation of deferoxamine toxicity and clearance by covalent attachment to biocompatible polymers*. *Proceedings of the National Academy of Sciences*, 1989. **86**(24): p. 10108-10112.
234. Surapolchai, P., *Anaphylactic reaction with subsequent desensitisation: case report*. *Reactions*, 2015. **1556**: p. 105-20.

235. Piga, A., et al., *Deferiprone*. Annals of the New York Academy of Sciences, 2010. **1202**(1): p. 75-78.
236. Ceci, A., et al., *The safety and effectiveness of deferiprone in a large-scale, 3-year study in Italian patients*. British journal of haematology, 2002. **118**(1): p. 330-336.
237. Al-Refaie, F., B. Wonke, and A. Hoffbrand, *Deferiprone-associated myelotoxicity*. European journal of haematology, 1994. **53**(5): p. 298-301.
238. Al-Refaie, F., et al., *Results of long-term deferiprone (L1) therapy: a report by the International Study Group on Oral Iron Chelators*. British journal of haematology, 1995. **91**(1): p. 224-229.
239. Tricta, F., et al., *Deferiprone-induced agranulocytosis: 20 years of clinical observations*. American journal of hematology, 2016. **91**(10): p. 1026-1031.
240. Cohen, A.R., et al., *Safety profile of the oral iron chelator deferiprone: a multicentre study*. British journal of haematology, 2000. **108**(2): p. 305-312.
241. Hider, R.C. and A.V. Hoffbrand, *The role of deferiprone in iron chelation*. New England Journal of Medicine, 2018. **379**(22): p. 2140-2150.
242. Hsieh, M.M., et al., *Prevalence of neutropenia in the US population: age, sex, smoking status, and ethnic differences*. Annals of internal medicine, 2007. **146**(7): p. 486-492.
243. Hoffbrand, A.V., A. Cohen, and C. Hershko, *Role of deferiprone in chelation therapy for transfusional iron overload*. Blood, 2003. **102**(1): p. 17-24.
244. Bartlett, A., A. Hoffbrand, and G. Kontoghiorghes, *Long-term trial with the oral iron chelator 1, 2-dimethyl-3-hydroxypyrid-4-one (L1) II. Clinical observations*. British Journal of Haematology, 1990. **76**(2): p. 301-304.
245. Agarwal, M., et al., *Long-term assessment of efficacy and safety of L1, an oral iron chelator, in transfusion dependent thalassaemia: Indian trial*. British journal of haematology, 1992. **82**(2): p. 460-466.

246. Berkovitch, M., et al., *Arthropathy in thalassaemia patients receiving deferiprone*. The Lancet, 1994. **343**(8911): p. 1471-1472.
247. El Alfy, M., et al., *The safety, tolerability, and efficacy of a liquid formulation of deferiprone in young children with transfusional iron overload*. Journal of pediatric hematology/oncology, 2010. **32**(8): p. 601-605.
248. Cohen, A.R., et al., *Safety and effectiveness of long-term therapy with the oral iron chelator deferiprone*. Blood, 2003. **102**(5): p. 1583-1587.
249. Maggio, A., et al., *Deferiprone versus deferoxamine in patients with thalassemia major: a randomized clinical trial*. Blood Cells, Molecules, and Diseases, 2002. **28**(2): p. 196-208.
250. Olivieri, N.F., et al., *Iron-chelation therapy with oral deferiprone in patients with thalassemia major*. New England Journal of Medicine, 1995. **332**(14): p. 918-922.
251. Galanello, R., *Deferiprone in the treatment of transfusion-dependent thalassemia: a review and perspective*. Therapeutics and clinical risk management, 2007. **3**(5): p. 795.
252. Cappellini, M.D., et al., *A phase 3 study of deferiasirox (ICL670), a once-daily oral iron chelator, in patients with β -thalassemia*. Blood, 2006. **107**(9): p. 3455-3462.
253. Galanello, R., et al., *Phase II clinical evaluation of deferiasirox, a once-daily oral chelating agent, in pediatric patients with beta-thalassemia major*. haematologica, 2006. **91**(10): p. 1343-1351.
254. Piga, A., et al., *Randomized phase II trial of deferiasirox (Exjade, ICL670), a once-daily, orally-administered iron chelator, in comparison to deferoxamine in thalassemia patients with transfusional iron overload*. haematologica, 2006. **91**(7): p. 873-880.
255. Vichinsky, E., et al., *A randomised comparison of deferiasirox versus deferoxamine for the treatment of transfusional iron overload in sickle cell disease*. British journal of haematology, 2007. **136**(3): p. 501-508.

256. Sharma, A., E. Arora, and H. Singh, *Hypersensitivity reaction with deferasirox*. Journal of pharmacology & pharmacotherapeutics, 2015. **6**(2): p. 105.
257. Ohshita, A., et al., *A maculopapular-type eruption associated with deferasirox administration*. Journal of the American Academy of Dermatology, 2013. **69**(5): p. e265-e267.
258. Isik, P., et al., *Type-I hypersensitivity reaction secondary to deferasirox intake*. International Journal of Hematology & Oncology, 2010. **20**: p. 42-44.
259. Rich, G.T., et al., *Towards an understanding of the low bioavailability of quercetin: a study of its interaction with intestinal lipids*. Nutrients, 2017. **9**(2): p. 111.
260. Anand, P., et al., *Bioavailability of curcumin: problems and promises*. Molecular pharmaceutics, 2007. **4**(6): p. 807-818.
261. B Mythri, R. and M. M Srinivas Bharath, *Curcumin: a potential neuroprotective agent in Parkinson's disease*. Current pharmaceutical design, 2012. **18**(1): p. 91-99.
262. Batiha, G.E.-S., et al., *The pharmacological activity, biochemical properties, and pharmacokinetics of the major natural polyphenolic flavonoid: quercetin*. Foods, 2020. **9**(3): p. 374.
263. Guillermo Gormaz, J., S. Quintremil, and R. Rodrigo, *Cardiovascular disease: a target for the pharmacological effects of quercetin*. Current topics in medicinal chemistry, 2015. **15**(17): p. 1735-1742.
264. Andres, S., et al., *Safety aspects of the use of quercetin as a dietary supplement*. Molecular nutrition & food research, 2018. **62**(1): p. 1700447.
265. Dabeek, W.M. and M.V. Marra, *Dietary quercetin and kaempferol: Bioavailability and potential cardiovascular-related bioactivity in humans*. Nutrients, 2019. **11**(10): p. 2288.
266. David, A.V.A., R. Arulmoli, and S. Parasuraman, *Overviews of biological importance of quercetin: A bioactive flavonoid*. Pharmacognosy reviews, 2016. **10**(20): p. 84.

267. Lesser, S. and S. Wolfram, *Oral bioavailability of the flavonol quercetin a review*. Current Topics in Nutraceutical Research, 2006. **4**(3/4): p. 239.
268. Kelly, G.S., *Quercetin*. Alternative medicine review, 2011. **16**(2): p. 172-195.
269. FDA. *GRAS Notice for high purity quercetin*. 2010; Available from: <https://www.fda.gov/downloads/Food/IngredientsPackagingLabeling/GRAS/NoticeInventory/UCM269540.pdf>.
270. Arts, I.C., et al., *The type of sugar moiety is a major determinant of the small intestinal uptake and subsequent biliary excretion of dietary quercetin glycosides*. British Journal of Nutrition, 2004. **91**(6): p. 841-847.
271. Crespy, V., et al., *Quercetin, but not its glycosides, is absorbed from the rat stomach*. Journal of agricultural and food chemistry, 2002. **50**(3): p. 618-621.
272. Hollman, P.C., et al., *Absorption of dietary quercetin glycosides and quercetin in healthy ileostomy volunteers*. The American journal of clinical nutrition, 1995. **62**(6): p. 1276-1282.
273. Cermak, R., et al., *In vitro degradation of the flavonol quercetin and of quercetin glycosides in the porcine hindgut*. Archives of animal nutrition, 2006. **60**(2): p. 180-189.
274. Zhou, S., et al., *Drug bioactivation covalent binding to target proteins and toxicity relevance*. Drug metabolism reviews, 2005. **37**(1): p. 41-213.
275. Zhang, L., Z. Zuo, and G. Lin, *Intestinal and hepatic glucuronidation of flavonoids*. Molecular pharmaceutics, 2007. **4**(6): p. 833-845.
276. Dreiseitel, A., et al., *Berry anthocyanins and anthocyanidins exhibit distinct affinities for the efflux transporters BCRP and MDRI*. British journal of pharmacology, 2009. **158**(8): p. 1942-1950.
277. Hribar, U. and N. Poklar Ulrih, *The metabolism of anthocyanins*. Current drug metabolism, 2014. **15**(1): p. 3-13.

278. Chandra, P. and K.L. Brouwer, *The complexities of hepatic drug transport: current knowledge and emerging concepts*. *Pharmaceutical research*, 2004. **21**(5): p. 719-735.
279. Wong, C.C., et al., *Carrier-mediated transport of quercetin conjugates: Involvement of organic anion transporters and organic anion transporting polypeptides*. *Biochemical pharmacology*, 2012. **84**(4): p. 564-570.
280. Williamson, G., et al., *Human metabolic pathways of dietary flavonoids and cinnamates*. *Biochemical Society Transactions*, 2000. **28**(2): p. 16-22.
281. Liu, Y., et al., *Enteric disposition and recycling of flavonoids and ginkgo flavonoids*. *The Journal of Alternative & Complementary Medicine*, 2003. **9**(5): p. 631-640.
282. Wong, C.C., et al., *Flavonoid conjugates interact with organic anion transporters (OATs) and attenuate cytotoxicity of adefovir mediated by organic anion transporter 1 (OAT1/SLC22A6)*. *Biochemical pharmacology*, 2011. **81**(7): p. 942-949.
283. Dei Cas, M. and R. Ghidoni, *Dietary curcumin: correlation between bioavailability and health potential*. *Nutrients*, 2019. **11**(9): p. 2147.
284. Hewlings, S.J. and D.S. Kalman, *Curcumin: A review of its effects on human health*. *Foods*, 2017. **6**(10): p. 92.
285. Toden, S. and A. Goel, *The holy grail of curcumin and its efficacy in various diseases: is bioavailability truly a big concern?* *Journal of restorative medicine*, 2017. **6**(1): p. 27.
286. Wahlang, B., Y.B. Pawar, and A.K. Bansal, *Identification of permeability-related hurdles in oral delivery of curcumin using the Caco-2 cell model*. *European Journal of Pharmaceutics and Biopharmaceutics*, 2011. **77**(2): p. 275-282.
287. Heger, M., et al., *The molecular basis for the pharmacokinetics and pharmacodynamics of curcumin and its metabolites in relation to cancer*. *Pharmacological reviews*, 2014. **66**(1): p. 222-307.

288. Yang, K.-Y., et al., *Oral bioavailability of curcumin in rat and the herbal analysis from Curcuma longa by LC–MS/MS*. Journal of chromatography B, 2007. **853**(1-2): p. 183-189.
289. Maiti, K., et al., *Curcumin–phospholipid complex: preparation, therapeutic evaluation and pharmacokinetic study in rats*. International journal of pharmaceutics, 2007. **330**(1-2): p. 155-163.
290. Marczylo, T.H., et al., *Comparison of systemic availability of curcumin with that of curcumin formulated with phosphatidylcholine*. Cancer chemotherapy and pharmacology, 2007. **60**(2): p. 171-177.
291. Ravindranath, V. and N. Chandrasekhara, *Absorption and tissue distribution of curcumin in rats*. Toxicology, 1980. **16**(3): p. 259-265.
292. Garcea, G., et al., *Detection of curcumin and its metabolites in hepatic tissue and portal blood of patients following oral administration*. British journal of cancer, 2004. **90**(5): p. 1011-1015.
293. Metzler, M., et al., *Curcumin uptake and metabolism*. Biofactors, 2013. **39**(1): p. 14-20.
294. Shoba, G., et al., *Influence of piperine on the pharmacokinetics of curcumin in animals and human volunteers*. Planta medica, 1998. **64**(04): p. 353-356.
295. Cruz–Correa, M., et al., *Combination treatment with curcumin and quercetin of adenomas in familial adenomatous polyposis*. Clinical Gastroenterology and Hepatology, 2006. **4**(8): p. 1035-1038.
296. Verma, S.P., E. Salamone, and B. Goldin, *Curcumin and genistein, plant natural products, show synergistic inhibitory effects on the growth of human breast cancer MCF-7 cells induced by estrogenic pesticides*. Biochemical and biophysical research communications, 1997. **233**(3): p. 692-696.

297. Fang, J.-Y., et al., *Efficacy and irritancy of enhancers on the in-vitro and in-vivo percutaneous absorption of curcumin*. Journal of pharmacy and pharmacology, 2003. **55**(5): p. 593-601.
298. Bisht, S., et al., *Polymeric nanoparticle-encapsulated curcumin ("nanocurcumin"): a novel strategy for human cancer therapy*. Journal of nanobiotechnology, 2007. **5**(1): p. 1-18.
299. Ubeyitogullari, A. and O.N. Ciftci, *A novel and green nanoparticle formation approach to forming low-crystallinity curcumin nanoparticles to improve curcumin's bioaccessibility*. Scientific Reports, 2019. **9**(1): p. 1-11.
300. Lila, A.S.A. and T. Ishida, *Liposomal delivery systems: design optimization and current applications*. Biological and pharmaceutical bulletin, 2017. **40**(1): p. 1-10.
301. Chen, X., et al., *The stability, sustained release and cellular antioxidant activity of curcumin nanoliposomes*. Molecules, 2015. **20**(8): p. 14293-14311.
302. Jin, H.-H., Q. Lu, and J.-G. Jiang, *Curcumin liposomes prepared with milk fat globule membrane phospholipids and soybean lecithin*. Journal of dairy science, 2016. **99**(3): p. 1780-1790.
303. Liu, Y., et al., *Temperature-dependent structure stability and in vitro release of chitosan-coated curcumin liposome*. Food research international, 2015. **74**: p. 97-105.
304. Hasan, M., et al., *Chitosan-coated liposomes encapsulating curcumin: Study of lipid-polysaccharide interactions and nanovesicle behavior*. RSC advances, 2016. **6**(51): p. 45290-45304.
305. Niu, Y., et al., *Temperature-dependent stability and DPPH scavenging activity of liposomal curcumin at pH 7.0*. Food Chemistry, 2012. **135**(3): p. 1377-1382.
306. Huang, Q., et al., *Coating of carboxymethyl dextran on liposomal curcumin to improve the anticancer activity*. RSC advances, 2014. **4**(103): p. 59211-59217.

307. Shin, G.H., et al., *Preparation of chitosan-coated nanoliposomes for improving the mucoadhesive property of curcumin using the ethanol injection method*. Journal of agricultural and food chemistry, 2013. **61**(46): p. 11119-11126.
308. Wei, X.-Q., et al., *Improving the stability of liposomal curcumin by adjusting the inner aqueous chamber pH of liposomes*. ACS omega, 2020. **5**(2): p. 1120-1126.
309. Zalloum, N., D. Biloti, and F. Pessine, *Spectrofluorimetry and chemometrics for investigation of norfloxacin distribution in multilamellar liposomes*. Applied spectroscopy, 2005. **59**(8): p. 1032-1036.
310. Schiborr, C., et al., *The oral bioavailability of curcumin from micronized powder and liquid micelles is significantly increased in healthy humans and differs between sexes*. Molecular nutrition & food research, 2014. **58**(3): p. 516-527.
311. Patil, S., et al., *Enhanced oral bioavailability and anticancer activity of novel curcumin loaded mixed micelles in human lung cancer cells*. Phytomedicine, 2015. **22**(12): p. 1103-1111.
312. Peng, S., et al., *Enhancement of curcumin bioavailability by encapsulation in sophorolipid-coated nanoparticles: An in vitro and in vivo study*. Journal of agricultural and food chemistry, 2018. **66**(6): p. 1488-1497.
313. Dubey, S.K., et al., *Design, synthesis and characterization of some bioactive conjugates of curcumin with glycine, glutamic acid, valine and demethylenated piperic acid and study of their antimicrobial and antiproliferative properties*. European journal of medicinal chemistry, 2008. **43**(9): p. 1837-1846.
314. Mishra, S., et al., *Design, development and synthesis of mixed bioconjugates of piperic acid–glycine, curcumin–glycine/alanine and curcumin–glycine–piperic acid and their antibacterial and antifungal properties*. Bioorganic & medicinal chemistry, 2005. **13**(5): p. 1477-1486.
315. Harish, G., et al., *Bioconjugates of curcumin display improved protection against glutathione depletion mediated oxidative stress in a dopaminergic neuronal cell line:*

- implications for Parkinson's disease*. Bioorganic & medicinal chemistry, 2010. **18**(7): p. 2631-2638.
316. Toole, B.P. *Hyaluronan in morphogenesis*. in *Seminars in cell & developmental biology*. 2001. Elsevier.
317. Petrey, A.C. and C.A. de la Motte, *Hyaluronan, a crucial regulator of inflammation*. *Frontiers in immunology*, 2014. **5**: p. 101.
318. Knop, K., et al., *Poly (ethylene glycol) in drug delivery: pros and cons as well as potential alternatives*. *Angewandte chemie international edition*, 2010. **49**(36): p. 6288-6308.
319. Lele, B. and M. Kulkarni, *Single step room temperature oxidation of poly (ethylene glycol) to poly (oxyethylene)-dicarboxylic acid*. *Journal of applied polymer science*, 1998. **70**(5): p. 883-890.
320. Kichler, A., et al., *Intranasal gene delivery with a polyethylenimine-PEG conjugate*. *Journal of Controlled Release*, 2002. **81**(3): p. 379-388.
321. Manju, S. and K. Sreenivasan, *Conjugation of curcumin onto hyaluronic acid enhances its aqueous solubility and stability*. *Journal of colloid and interface science*, 2011. **359**(1): p. 318-325.
322. Fishman, A., A. Acton, and E. Lee-Ruff, *A Simple Preparation of PEG-Carboxylates by Direct Oxidation*. *Synthetic communications*, 2004. **34**(12): p. 2309-2312.
323. Mohammad-Khah, A. and R. Ansari, *Activated charcoal: preparation, characterization and applications: a review article*. *Int J Chem Tech Res*, 2009. **1**(4): p. 859-864.
324. Sehgal, D. and I.K. Vijay, *A method for the high efficiency of water-soluble carbodiimide-mediated amidation*. *Analytical biochemistry*, 1994. **218**(1): p. 87-91.
325. Neises, B. and W. Steglich, *Simple method for the esterification of carboxylic acids*. *Angewandte Chemie International Edition in English*, 1978. **17**(7): p. 522-524.

326. Hatcher, H.C., et al., *Synthetic and natural iron chelators: therapeutic potential and clinical use*. *Future medicinal chemistry*, 2009. **1**(9): p. 1643-1670.
327. Prachayasittikul, V., et al., *8-Hydroxyquinolines: a review of their metal chelating properties and medicinal applications*. *Drug design, development and therapy*, 2013. **7**: p. 1157.
328. Jiao, Y., et al., *Iron chelation in the biological activity of curcumin*. *Free Radical Biology and Medicine*, 2006. **40**(7): p. 1152-1160.
329. Ren, J., et al., *Complexation of flavonoids with iron: structure and optical signatures*. *The Journal of Physical Chemistry B*, 2008. **112**(6): p. 1845-1850.
330. Hermanson, G.T., *Bioconjugate techniques*. 3rd ed. 2013: Academic press.
331. Valiulin, R., *Organic Chemistry: 100 Must-Know Mechanisms*, in *Organic Chemistry: 100 Must-Know Mechanisms*. 2020, De Gruyter.
332. Smith, B.C., *Organic nitrogen compounds, VII: Amides—the rest of the story*. 2020.
333. Smith, B.C., *IR Spectral Interpretation Workshop The C=O Bond, Part VI: Esters and the Rule of Three*. *Spectroscopy*, 2018. **33**: p. 20-3.
334. Pang, X., et al., *Hyaluronic acid-quercetin conjugate micelles: synthesis, characterization, in vitro and in vivo evaluation*. *Colloids and Surfaces B: Biointerfaces*, 2014. **123**: p. 778-786.
335. Cherdtrakulkiat, R., et al., *Derivatives (halogen, nitro and amino) of 8-hydroxyquinoline with highly potent antimicrobial and antioxidant activities*. *Biochemistry and biophysics reports*, 2016. **6**: p. 135-141.
336. Natesan, V. and S.-J. Kim, *Lipid Metabolism, Disorders and Therapeutic Drugs—Review*. *Biomolecules & therapeutics*, 2021. **29**(6): p. 596.
337. Bruce, K.D., A. Zsombok, and R.H. Eckel, *Lipid processing in the brain: a key regulator of systemic metabolism*. *Frontiers in endocrinology*, 2017. **8**: p. 60.

338. O'Donnell, V.B. and B.A. Freeman, *Interactions between nitric oxide and lipid oxidation pathways: implications for vascular disease*. *Circulation research*, 2001. **88**(1): p. 12-21.
339. Gianazza, E., et al., *Lipid peroxidation in atherosclerotic cardiovascular diseases*. *Antioxidants & Redox Signaling*, 2021. **34**(1): p. 49-98.
340. Gianazza, E., et al., *Lipoxidation in cardiovascular diseases*. *Redox biology*, 2019. **23**: p. 101119.
341. Shen, L., et al., *Ferroptosis in acute central nervous system injuries: the future direction?* *Frontiers in cell and developmental biology*, 2020. **8**: p. 594.
342. Abusarah, J., et al., *An overview of the role of lipid peroxidation-derived 4-hydroxynonenal in osteoarthritis*. *Inflammation Research*, 2017. **66**(8): p. 637-651.
343. Bondet, V., M.-E. Cuvelier, and C. Berset, *Behavior of phenolic antioxidants in a partitioned medium: Focus on linoleic acid peroxidation induced by iron/ascorbic acid system*. *Journal of the American Oil Chemists' Society*, 2000. **77**(8): p. 813-819.
344. Beker, B.Y., et al., *Antioxidant protective effect of flavonoids on linoleic acid peroxidation induced by copper (II)/ascorbic acid system*. *Chemistry and Physics of Lipids*, 2011. **164**(8): p. 732-739.
345. Jira, W., et al., *Strong increase in hydroxy fatty acids derived from linoleic acid in human low density lipoproteins of atherosclerotic patients*. *Chemistry and physics of lipids*, 1998. **91**(1): p. 1-11.
346. Haag, M., *Essential fatty acids and the brain*. *The Canadian Journal of Psychiatry*, 2003. **48**(3): p. 195-203.
347. Ismail, H., et al., *Traumatic brain injury: oxidative stress and novel anti-oxidants such as mitoquinone and edaravone*. *Antioxidants*, 2020. **9**(10): p. 943.
348. Moshayedi, P. and S.T. Carmichael, *Hyaluronan, neural stem cells and tissue reconstruction after acute ischemic stroke*. *Biomatter*, 2013. **3**(1): p. e23863.

349. van den Bergh, W., *Pharmacotherapy of traumatic brain injury*.
350. Loane, D.J. and A.I. Faden, *Neuroprotection for traumatic brain injury: translational challenges and emerging therapeutic strategies*. Trends in pharmacological sciences, 2010. **31**(12): p. 596-604.
351. Pardridge, W.M., *Blood-brain barrier drug targeting: the future of brain drug development*. Molecular interventions, 2003. **3**(2): p. 90.
352. Hack, D., *TBI clinical trials: past, present, and future*. Bridge Natl Acad Eng, 2016. **46**(1): p. 34-8.
353. Roof, R.L. and E.D. HALL, *Gender differences in acute CNS trauma and stroke: neuroprotective effects of estrogen and progesterone*. Journal of neurotrauma, 2000. **17**(5): p. 367-388.
354. Smith, S., *Progesterone administration attenuates excitatory amino acid responses of cerebellar Purkinje cells*. Neuroscience, 1991. **42**(2): p. 309-320.
355. Roof, R.L., S.W. Hoffman, and D.G. Stein, *Progesterone protects against lipid peroxidation following traumatic brain injury in rats*. Molecular and chemical neuropathology, 1997. **31**(1): p. 1-11.
356. Djebaili, M., et al., *The neurosteroids progesterone and allopregnanolone reduce cell death, gliosis, and functional deficits after traumatic brain injury in rats*. Journal of neurotrauma, 2005. **22**(1): p. 106-118.
357. O'Connor, C.A., et al., *Effects of progesterone on neurologic and morphologic outcome following diffuse traumatic brain injury in rats*. Experimental Neurology, 2007. **205**(1): p. 145-153.
358. Wright, D.W., et al., *ProTECT: a randomized clinical trial of progesterone for acute traumatic brain injury*. Annals of emergency medicine, 2007. **49**(4): p. 391-402. e2.

359. Xiao, G., et al., *Improved outcomes from the administration of progesterone for patients with acute severe traumatic brain injury: a randomized controlled trial*. *Critical care*, 2008. **12**(2): p. 1-10.
360. Stein, D., *Progesterone in the treatment of acute traumatic brain injury: a clinical perspective and update*. *Neuroscience*, 2011. **191**: p. 101-106.
361. Stein, D.G. and D.W. Wright, *Progesterone in the clinical treatment of acute traumatic brain injury*. *Expert opinion on investigational drugs*, 2010. **19**(7): p. 847-857.
362. Anderson, M.A., et al., *Required growth facilitators propel axon regeneration across complete spinal cord injury*. *Nature*, 2018. **561**(7723): p. 396-400.
363. Gage, F.H. and S. Temple, *Neural stem cells: generating and regenerating the brain*. *Neuron*, 2013. **80**(3): p. 588-601.
364. Blurton-Jones, M., et al., *Neural stem cells improve cognition via BDNF in a transgenic model of Alzheimer disease*. *Proceedings of the National Academy of Sciences*, 2009. **106**(32): p. 13594-13599.
365. Suksuphew, S. and P. Noisa, *Neural stem cells could serve as a therapeutic material for age-related neurodegenerative diseases*. *World journal of stem cells*, 2015. **7**(2): p. 502.
366. Gennai, S., et al., *Cell-based therapy for traumatic brain injury*. *British journal of anaesthesia*, 2015. **115**(2): p. 203-212.
367. Yamazaki, K., et al., *Clinical trials of stem cell treatment for spinal cord injury*. *International Journal of Molecular Sciences*, 2020. **21**(11): p. 3994.
368. Zhang, Z.X., et al., *A combined procedure to deliver autologous mesenchymal stromal cells to patients with traumatic brain injury*. *Cytotherapy*, 2008. **10**(2): p. 134-139.
369. Cox Jr, C.S., et al., *Autologous bone marrow mononuclear cell therapy for severe traumatic brain injury in children*. *Neurosurgery*, 2011. **68**(3): p. 588-600.

370. Wang, S., et al., *Umbilical cord mesenchymal stem cell transplantation significantly improves neurological function in patients with sequelae of traumatic brain injury*. Brain research, 2013. **1532**: p. 76-84.
371. Tian, C., et al., *Autologous bone marrow mesenchymal stem cell therapy in the subacute stage of traumatic brain injury by lumbar puncture*. Exp Clin Transplant, 2013. **11**(2): p. 176-81.
372. Cox Jr, C.S., et al., *Treatment of severe adult traumatic brain injury using bone marrow mononuclear cells*. Stem Cells, 2017. **35**(4): p. 1065-1079.
373. Sharma, A., et al., *Cell therapy attempted as a novel approach for chronic traumatic brain injury—a pilot study*. SpringerPlus, 2015. **4**(1): p. 1-8.
374. Xiao, Z., et al., *Significant improvement of acute complete spinal cord injury patients diagnosed by a combined criteria implanted with neuroregen scaffolds and mesenchymal stem cells*. Cell Transplantation, 2018. **27**(6): p. 907-915.
375. Hur, J.W., et al., *Intrathecal transplantation of autologous adipose-derived mesenchymal stem cells for treating spinal cord injury: a human trial*. The Journal of Spinal Cord Medicine, 2016. **39**(6): p. 655-664.
376. Vaquero, J., et al., *Intrathecal administration of autologous mesenchymal stromal cells for spinal cord injury: Safety and efficacy of the 100/3 guideline*. Cytotherapy, 2018. **20**(6): p. 806-819.
377. Carballo-Molina, O.A. and I. Velasco, *Hydrogels as scaffolds and delivery systems to enhance axonal regeneration after injuries*. Frontiers in cellular neuroscience, 2015. **9**.
378. Zhang, T., et al., *Three-dimensional gelatin and gelatin/hyaluronan hydrogel structures for traumatic brain injury*. Journal of bioactive and compatible polymers, 2007. **22**(1): p. 19-29.
379. Molcanyi, M., et al., *Trauma-associated inflammatory response impairs embryonic stem cell survival and integration after implantation into injured rat brain*. Journal of neurotrauma, 2007. **24**(4): p. 625-637.

380. Suuronen, E.J., et al., *Tissue-engineered injectable collagen-based matrices for improved cell delivery and vascularization of ischemic tissue using CD133+ progenitors expanded from the peripheral blood*. *Circulation*, 2006. **114**(1 suppl): p. I-138-I-144.
381. Xiong, Y., et al., *Delayed transplantation of human marrow stromal cell-seeded scaffolds increases transcallosal neural fiber length, angiogenesis, and hippocampal neuronal survival and improves functional outcome after traumatic brain injury in rats*. *Brain research*, 2009. **1263**: p. 183-191.
382. Willerth, S.M. and S.E. Sakiyama-Elbert, *Approaches to neural tissue engineering using scaffolds for drug delivery*. *Advanced drug delivery reviews*, 2007. **59**(4): p. 325-338.
383. Nair, L.S., *Injectable hydrogels for regenerative engineering*. 2015: World Scientific.
384. Subramanian, A., U.M. Krishnan, and S. Sethuraman, *Development of biomaterial scaffold for nerve tissue engineering: Biomaterial mediated neural regeneration*. *Journal of biomedical science*, 2009. **16**(1): p. 108.
385. Woerly, S., G.W. Plant, and A.R. Harvey, *Cultured rat neuronal and glial cells entrapped within hydrogel polymer matrices: a potential tool for neural tissue replacement*. *Neuroscience letters*, 1996. **205**(3): p. 197-201.
386. Duan, H., et al., *Functional hyaluronate collagen scaffolds induce NSCs differentiation into functional neurons in repairing the traumatic brain injury*. *Acta biomaterialia*, 2016. **45**: p. 182-195.
387. Fon, D., et al., *Effects of GDNF-Loaded Injectable Gelatin-Based Hydrogels on Endogenous Neural Progenitor Cell Migration*. *Advanced healthcare materials*, 2014. **3**(5): p. 761-774.
388. Donaghue, I.E., et al., *Cell and biomolecule delivery for tissue repair and regeneration in the central nervous system*. *Journal of Controlled Release*, 2014. **190**: p. 219-227.

389. Li, X., et al., *Engineering neural stem cell fates with hydrogel design for central nervous system regeneration*. Progress in polymer science, 2012. **37**(8): p. 1105-1129.
390. Strasser, S., et al., *Iron overload in bone marrow transplant recipients*. Bone marrow transplantation, 1998. **22**(2).
391. Storey, J.A., et al., *The transplant iron score as a predictor of stem cell transplant survival*. Journal of hematology & oncology, 2009. **2**(1): p. 44.
392. Majhail, N., H. Lazarus, and L. Burns, *Iron overload in hematopoietic cell transplantation*. Bone marrow transplantation, 2008. **41**(12): p. 997.
393. Altes, A., et al., *Early clinical impact of iron overload in stem cell transplantation. A prospective study*. Annals of hematology, 2007. **86**(6): p. 443-447.
394. Piñero, D.J. and J.R. Connor, *Iron in the brain: an important contributor in normal and diseased states*. The Neuroscientist, 2000. **6**(6): p. 435-453.
395. Bullen, J., *The significance of iron in infection*. Reviews of infectious diseases, 1981. **3**(6): p. 1127-1138.
396. Gerlach, M., et al., *Altered brain metabolism of iron as a cause of neurodegenerative diseases?* Journal of neurochemistry, 1994. **63**(3): p. 793-807.
397. Schenck, J.F. and E.A. Zimmerman, *High-field magnetic resonance imaging of brain iron: birth of a biomarker?* NMR in Biomedicine, 2004. **17**(7): p. 433-445.
398. Ying, W., et al., *Acidosis potentiates oxidative neuronal death by multiple mechanisms*. Journal of neurochemistry, 1999. **73**(4): p. 1549-1556.
399. Andrews, N.C. and P.J. Schmidt, *Iron homeostasis*. Annu Rev Physiol, 2007. **69**: p. 69-85.
400. Breuer, W., E. Greenberg, and Z.I. Cabantchik, *Newly delivered transferrin iron and oxidative cell injury*. FEBS letters, 1997. **403**(2): p. 213-219.

401. Ward, R.J., et al., *Control of cellular iron homeostasis by iron-responsive elements in vivo*. The FEBS Journal, 1994. **220**(3): p. 927-931.
402. Zhang, Z., et al., *Iron-induced oxidative damage and apoptosis in cerebellar granule cells: attenuation by tetramethylpyrazine and ferulic acid*. European journal of pharmacology, 2003. **467**(1): p. 41-47.
403. Willmore, L.J. and J.J. Rubin, *Formation of malonaldehyde and focal brain edema induced by subpial injection of FeCl₂ into rat isocortex*. Brain research, 1982. **246**(1): p. 113-119.
404. Zhang, Y., et al., *Basic FGF, NGF, and IGFs protect hippocampal and cortical neurons against iron-induced degeneration*. Journal of Cerebral Blood Flow & Metabolism, 1993. **13**(3): p. 378-388.
405. Bian, S., et al., *The self-crosslinking smart hyaluronic acid hydrogels as injectable three-dimensional scaffolds for cells culture*. Colloids and Surfaces B: Biointerfaces, 2016. **140**: p. 392-402.
406. Gautam Rajpal and P. Arvan, *Disulfide Bond Formation*, in *Handbook of biologically active peptides*, K. Abba, Editor. 2013, Academic press.
407. Riddles, P.W., R.L. Blakeley, and B. Zerner, *Ellman's reagent: 5, 5'-dithiobis (2-nitrobenzoic acid)—a reexamination*. Analytical biochemistry, 1979. **94**(1): p. 75-81.
408. Shu, X.Z., et al., *Disulfide cross-linked hyaluronan hydrogels*. Biomacromolecules, 2002. **3**(6): p. 1304-1311.
409. Khunmanee, S., Y. Jeong, and H. Park, *Crosslinking method of hyaluronic-based hydrogel for biomedical applications*. Journal of tissue engineering, 2017. **8**: p. 2041731417726464.

410. Chen, Y.-N., et al., *Ameliorative effect of curcumin-encapsulated hyaluronic acid-PLA nanoparticles on thioacetamide-induced murine hepatic fibrosis*. International journal of environmental research and public health, 2017. **14**(1): p. 11.
411. Xu, J., et al., *PEGylation of deferoxamine for improving the stability, cytotoxicity, and iron-overload in an experimental stroke model in rats*. Frontiers in bioengineering and biotechnology, 2020: p. 1150.
412. Greco, V., et al., *Hyaluronan-carnosine conjugates inhibit A β aggregation and toxicity*. Scientific reports, 2020. **10**(1): p. 1-14.
413. Gevaert, M., *Engineering 3D tissue systems to better mimic human biology*. Bridge, 2012. **42**(4): p. 48-55.
414. Białkowska, K., et al., *Spheroids as a type of three-dimensional cell cultures—Examples of methods of preparation and the most important application*. International journal of molecular sciences, 2020. **21**(17): p. 6225.
415. Edmondson, R., et al., *Three-dimensional cell culture systems and their applications in drug discovery and cell-based biosensors*. Assay and drug development technologies, 2014. **12**(4): p. 207-218.
416. Sant, S. and P.A. Johnston, *The production of 3D tumor spheroids for cancer drug discovery*. Drug Discovery Today: Technologies, 2017. **23**: p. 27-36.
417. Li, X., *Bioengineering strategies for central nervous system regeneration*. 2012, Clemson University.
418. Thau, L., V. Reddy, and P. Singh, *Anatomy, Central Nervous System*. 2019.
419. Herculano-Houzel, S., *The remarkable, yet not extraordinary, human brain as a scaled-up primate brain and its associated cost*. Proceedings of the National Academy of Sciences, 2012. **109**(Supplement 1): p. 10661-10668.

420. Stiles, J. and T.L. Jernigan, *The basics of brain development*. Neuropsychology review, 2010. **20**(4): p. 327-348.
421. Jawabri, K.H. and S. Sharma, *Physiology, cerebral cortex functions*. 2019.
422. Ludwig, P.E., V. Reddy, and M. Varacallo, *Neuroanatomy, central nervous system (CNS)*. 2017.
423. Herculano-Houzel, S., *The human brain in numbers: a linearly scaled-up primate brain*. Frontiers in human neuroscience, 2009. **3**: p. 31.
424. Basinger, H. and J.P. Hogg, *Neuroanatomy, brainstem*. 2019.
425. Nógrádi, A. and G. Vrbová, *Anatomy and physiology of the spinal cord*, in *Transplantation of neural tissue into the spinal cord*. 2006, Springer. p. 1-23.
426. Neulinger, K., et al., *Prospective memory and frontal lobe function*. Aging, Neuropsychology, and Cognition, 2016. **23**(2): p. 171-183.
427. Berlucchi, G. and G. Vallar, *The history of the neurophysiology and neurology of the parietal lobe*. Handbook of clinical neurology, 2018. **151**: p. 3-30.
428. Klingner, C.M. and O.W. Witte, *Somatosensory deficits*. Handbook of clinical neurology, 2018. **151**: p. 185-206.
429. Huff, T., N. Mahabadi, and P. Tadi, *Neuroanatomy, visual cortex*. StatPearls [Internet], 2020.
430. Nourski, K.V., *Auditory processing in the human cortex: An intracranial electrophysiology perspective*. Laryngoscope investigative otolaryngology, 2017. **2**(4): p. 147-156.
431. Binder, J.R., *Current controversies on Wernicke's area and its role in language*. Current neurology and neuroscience reports, 2017. **17**(8): p. 1-10.

432. Reeber, S.L., T.S. Otis, and R.V. Sillitoe, *New roles for the cerebellum in health and disease*. *Frontiers in systems neuroscience*, 2013. **7**: p. 83.
433. Deistung, A., et al., *High-resolution MR imaging of the human brainstem in vivo at 7 Tesla*. *Frontiers in human neuroscience*, 2013. **7**: p. 710.
434. Ng, S. and A. Lee, *Traumatic brain injuries: pathophysiology and potential therapeutic targets*. *Front. Cell. Neurosci.* **13**: 528. 2019.
435. Black, K.L., et al., *Blunt versus penetrating violent traumatic brain injury: frequency and factors associated with secondary conditions and complications*. *The Journal of head trauma rehabilitation*, 2002. **17**(6): p. 489-496.
436. Warden, D., *Military TBI during the Iraq and Afghanistan wars*. *The Journal of head trauma rehabilitation*, 2006. **21**(5): p. 398-402.
437. Ling, G.S. and J.M. Ecklund, *Traumatic brain injury in modern war*. *Current Opinion in Anesthesiology*, 2011. **24**(2): p. 124-130.
438. Cernak, I. and L.J. Noble-Haeusslein, *Traumatic brain injury: an overview of pathobiology with emphasis on military populations*. *Journal of Cerebral Blood Flow & Metabolism*, 2010. **30**(2): p. 255-266.
439. Risdall, J.E. and D.K. Menon, *Traumatic brain injury*. *Philosophical Transactions of the Royal Society B: Biological Sciences*, 2011. **366**(1562): p. 241-250.
440. Bruns Jr, J. and W.A. Hauser, *The epidemiology of traumatic brain injury: a review*. *Epilepsia*, 2003. **44**: p. 2-10.
441. Andriessen, T.M., B. Jacobs, and P.E. Vos, *Clinical characteristics and pathophysiological mechanisms of focal and diffuse traumatic brain injury*. *Journal of cellular and molecular medicine*, 2010. **14**(10): p. 2381-2392.

442. National Academies of Sciences, E. and Medicine, *Diagnosis and Assessment of Traumatic Brain Injury*, in *Evaluation of the Disability Determination Process for Traumatic Brain Injury in Veterans*. 2019, National Academies Press (US).
443. Dewan, M.C., et al., *Estimating the global incidence of traumatic brain injury*. *Journal of neurosurgery*, 2019. **130**(4): p. 1080-1097.
444. Tagliaferri, F., et al., *A systematic review of brain injury epidemiology in Europe*. *Acta neurochirurgica*, 2006. **148**(3): p. 255-268.
445. Rutland-Brown, W., et al., *Incidence of traumatic brain injury in the United States, 2003*. *The Journal of head trauma rehabilitation*, 2006. **21**(6): p. 544-548.
446. Hemphill, J. and N. Phan, *Traumatic brain injury: Epidemiology, classification, and pathophysiology*. UpToDate. UpToDate, 2012. **21**.
447. Faul, M. and V. Coronado, *Epidemiology of traumatic brain injury*. In *Handbook of clinical neurology 2015 Jan 1 (Vol. 127, pp. 3-13)*, in *Handbook of clinical neurology J. Grafman and A.M. Salazar, Editors*. 2015, Elsevier. p. 3-13.
448. Langlois, J.A., W. Rutland-Brown, and M.M. Wald, *The epidemiology and impact of traumatic brain injury: a brief overview*. *The Journal of head trauma rehabilitation*, 2006. **21**(5): p. 375-378.
449. Peterson, A.B., et al., *Surveillance report of traumatic brain injury-related emergency department visits, hospitalizations, and deaths, United States, 2014*. 2019.
450. !!! INVALID CITATION !!! {}.
451. Peterson, A.B., et al., *Surveillance Report of Traumatic Brain Injury-related Hospitalizations and Deaths by Age Group, Sex, and Mechanism of Injury - United States, 2016 and 2017*. 2021, Centers for Disease Control and Prevention. p. 1-36.

452. Taylor, C.A., et al., *Traumatic brain injury–related emergency department visits, hospitalizations, and deaths—United States, 2007 and 2013*. MMWR Surveillance Summaries, 2017. **66**(9): p. 1.
453. Brazinova, A., et al., *Epidemiology of traumatic brain injury in Europe: a living systematic review*. Journal of neurotrauma, 2021. **38**(10): p. 1411-1440.
454. Peeters, W., et al., *Epidemiology of traumatic brain injury in Europe*. Acta neurochirurgica, 2015. **157**(10): p. 1683-1696.
455. Roozenbeek, B., A.I. Maas, and D.K. Menon, *Changing patterns in the epidemiology of traumatic brain injury*. Nature Reviews Neurology, 2013. **9**(4): p. 231-236.
456. Prevention, C.f.D.C.a. *Traumatic Brain Injury and Concussion*. 2021 [2012]; Available from: <https://www.cdc.gov/traumaticbraininjury/data/index.html>.
457. Peterson, A.B., et al., *Surveillance report of traumatic brain injury-related emergency department visits, hospitalizations, and deaths, United States, 2014*. 2019.
458. Skandsen, T., et al., *Prevalence and impact of diffuse axonal injury in patients with moderate and severe head injury: a cohort study of early magnetic resonance imaging findings and 1-year outcome*. Journal of neurosurgery, 2010. **113**(3): p. 556-563.
459. Smith, D.H., D.F. Meaney, and W.H. Shull, *Diffuse axonal injury in head trauma*. The Journal of head trauma rehabilitation, 2003. **18**(4): p. 307-316.
460. Saatman, K.E., et al., *Classification of traumatic brain injury for targeted therapies*. Journal of neurotrauma, 2008. **25**(7): p. 719-738.
461. Ray, S., C. Dixon, and N. Banik, *Molecular mechanisms in the pathogenesis of traumatic brain injury*. Histology and histopathology, 2002.
462. Chamoun, R., et al., *Role of extracellular glutamate measured by cerebral microdialysis in severe traumatic brain injury*. Journal of neurosurgery, 2010. **113**(3): p. 564-570.

463. Girouard, H., et al., *NMDA receptor activation increases free radical production through nitric oxide and NOX2*. Journal of Neuroscience, 2009. **29**(8): p. 2545-2552.
464. Sattler, R., et al., *Specific coupling of NMDA receptor activation to nitric oxide neurotoxicity by PSD-95 protein*. Science, 1999. **284**(5421): p. 1845-1848.
465. Hiebert, J.B., et al., *Traumatic brain injury and mitochondrial dysfunction*. The American journal of the medical sciences, 2015. **350**(2): p. 132-138.
466. Lifshitz, J., et al., *Mitochondrial damage and dysfunction in traumatic brain injury*. Mitochondrion, 2004. **4**(5-6): p. 705-713.
467. Singh, I.N., et al., *Time course of post-traumatic mitochondrial oxidative damage and dysfunction in a mouse model of focal traumatic brain injury: implications for neuroprotective therapy*. Journal of Cerebral Blood Flow & Metabolism, 2006. **26**(11): p. 1407-1418.
468. Naga, K.K., P.G. Sullivan, and J.W. Geddes, *High cyclophilin D content of synaptic mitochondria results in increased vulnerability to permeability transition*. Journal of Neuroscience, 2007. **27**(28): p. 7469-7475.
469. Tsujimoto, Y. and S. Shimizu, *Role of the mitochondrial membrane permeability transition in cell death*. Apoptosis, 2007. **12**(5): p. 835-840.
470. Sullivan, P.G., et al., *Cytochrome c release and caspase activation after traumatic brain injury*. Brain research, 2002. **949**(1-2): p. 88-96.
471. Lewen, A., P. Matz, and P.H. Chan, *Free radical pathways in CNS injury*. Journal of neurotrauma, 2000. **17**(10): p. 871-890.
472. Xiong, Y., et al., *Mitochondrial dysfunction and calcium perturbation induced by traumatic brain injury*. Journal of neurotrauma, 1997. **14**(1): p. 23-34.
473. Shohami, E. and R. Kohen, *The role of reactive oxygen species in the pathogenesis of traumatic brain injury*, in *Oxidative Stress and Free Radical Damage in Neurology*. 2011, Springer. p. 99-118.

474. Hall, E.D., et al., *Peroxynitrite-mediated protein nitration and lipid peroxidation in a mouse model of traumatic brain injury*. Journal of neurotrauma, 2004. **21**(1): p. 9-20.
475. Deng, Y., et al., *Temporal relationship of peroxynitrite-induced oxidative damage, calpain-mediated cytoskeletal degradation and neurodegeneration after traumatic brain injury*. Experimental neurology, 2007. **205**(1): p. 154-165.
476. Ansari, M.A., K.N. Roberts, and S.W. Scheff, *Oxidative stress and modification of synaptic proteins in hippocampus after traumatic brain injury*. Free Radical Biology and Medicine, 2008. **45**(4): p. 443-452.
477. Lozano, D., et al., *Neuroinflammatory responses to traumatic brain injury: etiology, clinical consequences, and therapeutic opportunities*. Neuropsychiatric disease and treatment, 2015. **11**: p. 97.
478. Xiong, Y., A. Mahmood, and M. Chopp, *Current understanding of neuroinflammation after traumatic brain injury and cell-based therapeutic opportunities*. Chinese Journal of Traumatology, 2018. **21**(3): p. 137-151.
479. Lotocki, G., et al., *Alterations in blood-brain barrier permeability to large and small molecules and leukocyte accumulation after traumatic brain injury: effects of post-traumatic hypothermia*. Journal of neurotrauma, 2009. **26**(7): p. 1123-1134.
480. Loane, D.J. and A. Kumar, *Microglia in the TBI brain: the good, the bad, and the dysregulated*. Experimental neurology, 2016. **275**: p. 316-327.
481. Zhang, R., et al., *Anti-inflammatory and immunomodulatory mechanisms of mesenchymal stem cell transplantation in experimental traumatic brain injury*. Journal of neuroinflammation, 2013. **10**(1): p. 1-12.
482. Hellewell, S., B.D. Semple, and M.C. Morganti-Kossmann, *Therapies negating neuroinflammation after brain trauma*. Brain research, 2016. **1640**: p. 36-56.

483. Kumar, A. and D.J. Loane, *Neuroinflammation after traumatic brain injury: opportunities for therapeutic intervention*. Brain, behavior, and immunity, 2012. **26**(8): p. 1191-1201.
484. Guido, S., J. Sebastian, and M. Schroeter, *Detrimental and beneficial effects of injury-induced inflammation and cytokine expression in the nervous system*. Molecular and Cellular Biology of Neuroprotection in the CNS, 2003: p. 87-113.
485. Tang-Schomer, M.D., et al., *Mechanical breaking of microtubules in axons during dynamic stretch injury underlies delayed elasticity, microtubule disassembly, and axon degeneration*. The FASEB Journal, 2010. **24**(5): p. 1401-1410.
486. Saatman, K.E., et al., *Traumatic axonal injury results in biphasic calpain activation and retrograde transport impairment in mice*. Journal of Cerebral Blood Flow & Metabolism, 2003. **23**(1): p. 34-42.
487. Büki, A. and J. Povlishock, *All roads lead to disconnection?—Traumatic axonal injury revisited*. Acta neurochirurgica, 2006. **148**(2): p. 181-194.
488. Hellewell, S.C., et al., *Post-traumatic hypoxia exacerbates brain tissue damage: analysis of axonal injury and glial responses*. Journal of neurotrauma, 2010. **27**(11): p. 1997-2010.
489. Pierce, J., et al., *Immunohistochemical characterization of alterations in the distribution of amyloid precursor proteins and beta-amyloid peptide after experimental brain injury in the rat*. Journal of Neuroscience, 1996. **16**(3): p. 1083-1090.
490. Ma, J., et al., *Progress of research on diffuse axonal injury after traumatic brain injury*. Neural plasticity, 2016. **2016**.
491. Huang, L., et al., *Glial scar formation occurs in the human brain after ischemic stroke*. International journal of medical sciences, 2014. **11**(4): p. 344.
492. Fawcett, J.W. and R.A. Asher, *The glial scar and central nervous system repair*. Brain research bulletin, 1999. **49**(6): p. 377-391.

493. Asher, R.A., et al., *Chondroitin sulphate proteoglycans: inhibitory components of the glial scar*. Progress in brain research, 2001. **132**: p. 611-619.
494. Asher, R.A., et al., *Neurocan is upregulated in injured brain and in cytokine-treated astrocytes*. Journal of Neuroscience, 2000. **20**(7): p. 2427-2438.
495. Asher, R.A., et al., *Versican is upregulated in CNS injury and is a product of oligodendrocyte lineage cells*. Journal of Neuroscience, 2002. **22**(6): p. 2225-2236.
496. Zhang, Y., et al., *Tenascin-C expression and axonal sprouting following injury to the spinal dorsal columns in the adult rat*. Journal of neuroscience research, 1997. **49**(4): p. 433-450.
497. Pasterkamp, R.J., P.N. Anderson, and J. Verhaagen, *Peripheral nerve injury fails to induce growth of lesioned ascending dorsal column axons into spinal cord scar tissue expressing the axon repellent Semaphorin3A*. European Journal of Neuroscience, 2001. **13**(3): p. 457-471.
498. De Winter, F., et al., *Injury-induced class 3 semaphorin expression in the rat spinal cord*. Experimental neurology, 2002. **175**(1): p. 61-75.
499. Glezer, I., A. Simard, and S. Rivest, *Neuroprotective role of the innate immune system by microglia*. Neuroscience, 2007. **147**(4): p. 867-883.
500. Rolls, A., R. Shechter, and M. Schwartz, *The bright side of the glial scar in CNS repair*. Nature Reviews Neuroscience, 2009. **10**(3): p. 235-241.
501. Reier, P.J. and J.D. Houle, *The glial scar: its bearing on axonal elongation and transplantation approaches to CNS repair*. Advances in neurology, 1988. **47**: p. 87-138.
502. Roitbak, T. and E. Syková, *Diffusion barriers evoked in the rat cortex by reactive astrogliosis*. Glia, 1999. **28**(1): p. 40-48.
503. Yiu, G. and Z. He, *Glial inhibition of CNS axon regeneration*. Nature Reviews Neuroscience, 2006. **7**(8): p. 617-627.

504. Ughrin, Y.M., Z.J. Chen, and J.M. Levine, *Multiple regions of the NG2 proteoglycan inhibit neurite growth and induce growth cone collapse*. Journal of neuroscience, 2003. **23**(1): p. 175-186.
505. Fehlings, M.G., *Critical care in spinal cord injury*. 2013, Future Medicine.
506. WHO. *Spinal Cord Injury Fact Sheet*. 2013; Available from: <https://www.who.int/news-room/fact-sheets/detail/spinal-cord-injury>.
507. Alizadeh, A., S.M. Dyck, and S. Karimi-Abdolrezaee, *Traumatic spinal cord injury: an overview of pathophysiology, models and acute injury mechanisms*. Frontiers in neurology, 2019. **10**: p. 282.
508. Chen, Y., et al., *Causes of spinal cord injury*. Topics in spinal cord injury rehabilitation, 2013. **19**(1): p. 1-8.
509. Bickenbach, J., et al., *International perspectives on spinal cord injury*. 2013: World Health Organization.
510. New, P.W., R.A. Cripps, and B.B. Lee, *Global maps of non-traumatic spinal cord injury epidemiology: towards a living data repository*. Spinal cord, 2014. **52**(2): p. 97-109.
511. Guilcher, S., et al., *Health care utilization in non-traumatic and traumatic spinal cord injury: a population-based study*. Spinal Cord, 2010. **48**(1): p. 45-50.
512. Ahuja, C.S., et al., *Traumatic spinal cord injury*. Nature reviews Disease primers, 2017. **3**(1): p. 1-21.
513. Ziu, E. and F.B. Mesfin, *Spinal Shock*. 2017.
514. Ayas, T.N., et al., *Breathlessness in spinal cord injury depends on injury level*. The journal of spinal cord medicine, 1999. **22**(2): p. 97-101.
515. Spungen, A., et al., *Self-reported prevalence of pulmonary symptoms in subjects with spinal cord injury*. Spinal Cord, 1997. **35**(10): p. 652-657.

516. Hagen, E.M., *Acute complications of spinal cord injuries*. World journal of orthopedics, 2015. **6**(1): p. 17.
517. Acheson, M., et al., *High-resolution CT scanning in the evaluation of cervical spine fractures: comparison with plain film examinations*. American journal of roentgenology, 1987. **148**(6): p. 1179-1185.
518. Woodring, J.H. and C. Lee, *Limitations of cervical radiography in the evaluation of acute cervical trauma*. The Journal of trauma, 1993. **34**(1): p. 32-39.
519. Kirshblum, S.C., et al., *Reference for the 2011 revision of the international standards for neurological classification of spinal cord injury*. The journal of spinal cord medicine, 2011. **34**(6): p. 547-554.
520. Schuld, C., et al., *International standards for neurological classification of spinal cord injury: impact of the revised worksheet (revision 02/13) on classification performance*. The journal of spinal cord medicine, 2016. **39**(5): p. 504-512.
521. Spinalcord.com. *Complete vs Incomplete Spinal Cord Injury: What You Need to Know*. 2020; Available from: <https://www.spinalcord.com/blog/complete-vs.-incomplete-spinal-cord-injuries>.
522. SpinalCord.com. *Spinal Cord Injury Types*. 2020; Available from: <https://www.spinalcord.com/types-of-spinal-cord-injuries>.
523. Cedars-Sinai. *Acute Spinal Cord Injury*. 2021; Available from: <https://www.cedars-sinai.org/health-library/diseases-and-conditions/a/acute-spinal-cord-injury-1.html>.
524. Athanasou, J.A., *Spinal cord injury*, in *Encountering Personal Injury*. 2016, Springer. p. 157-164.
525. Shimizu, S., et al., *Weaning from long-term mechanical ventilation utilizing closed-loop ventilation mode (IntelliVent®-ASV®) in a patient with spinal cord injury*. Spinal cord series and cases, 2018. **4**(1): p. 1-4.

526. Tansey, K.E., *Profiling motor control in spinal cord injury: moving towards individualized therapy and evidence-based care progression*. The journal of spinal cord medicine, 2012. **35**(5): p. 305-309.
527. Nas, K., et al., *Rehabilitation of spinal cord injuries*. World journal of orthopedics, 2015. **6**(1): p. 8.
528. Spinalcord.com. *Living with Paraplegia: Cures, Therapies, Exercises, and More*. 2021; Available from: <https://www.spinalcord.com/paraplegia>.
529. SpinalCord.com. *Thoracic Spinal Cord Injuries*. 2020; Available from: <https://www.spinalcord.com/thoracic-spinal-cord-injury>.
530. SpinalCord.com. *Lumbar (L1-L5) Spinal Cord Injuries*. 2021; Available from: <https://www.spinalcord.com/lumbar-l1-l5-vertebrae-spinal-cord-injury>.
531. SpinalCord.com. *Sacral (S1-S5) Spinal Cord Injuries*. 2020; Available from: <https://www.spinalcord.com/sacral-spine-s1-s5-vertebrae-injuries-sacral-sparing>.
532. Malekzadeh, H., et al., *Direct cost of illness for spinal cord injury: a systematic review*. Global spine journal, 2021: p. 21925682211031190.
533. James, S.L., et al., *Global, regional, and national burden of traumatic brain injury and spinal cord injury, 1990–2016: a systematic analysis for the Global Burden of Disease Study 2016*. The Lancet Neurology, 2019. **18**(1): p. 56-87.
534. Chiu, W.-T., et al., *Epidemiology of traumatic spinal cord injury: comparisons between developed and developing countries*. Asia Pacific Journal of Public Health, 2010. **22**(1): p. 9-18.
535. Center, N.S.C.I.S. *Spinal cord injury facts and figures at a glance: 2020 SCI data sheet [Internet]*. 2020. Available from: <https://www.nscisc.uab.edu/Public/Facts%20and%20Figures%20-%202021.pdf>.
536. Jain, N.B., et al., *Traumatic spinal cord injury in the United States, 1993-2012*. Jama, 2015. **313**(22): p. 2236-2243.

537. Miyakoshi, N., et al., *A nationwide survey on the incidence and characteristics of traumatic spinal cord injury in Japan in 2018*. Spinal Cord, 2021. **59**(6): p. 626-634.
538. Noonan, V.K., et al., *Incidence and prevalence of spinal cord injury in Canada: a national perspective*. Neuroepidemiology, 2012. **38**(4): p. 219-226.
539. McDaid, D., et al., *Understanding and modelling the economic impact of spinal cord injuries in the United Kingdom*. Spinal Cord, 2019. **57**(9): p. 778-788.
540. Mitchell, J., et al., *Epidemiology of traumatic spinal cord injury in New Zealand (2007–2016)*. Epidemiology, 2020. **133**(1509).
541. Furlan, J.C., et al., *Global incidence and prevalence of traumatic spinal cord injury*. Canadian journal of neurological sciences, 2013. **40**(4): p. 456-464.
542. Botelho, R.V., et al., *Epidemiology of traumatic spinal injuries in Brazil: systematic review*. Arquivos Brasileiros de Neurocirurgia: Brazilian Neurosurgery, 2014. **33**(02): p. 100-106.
543. Mirzaeva, L., et al., *Incidence of adult traumatic spinal cord injury in Saint Petersburg, Russia*. spinal cord, 2019. **57**(8): p. 692-699.
544. Rahimi-Movaghar, V., et al., *Prevalence of spinal cord injury in Tehran, Iran*. The journal of spinal cord medicine, 2009. **32**(4): p. 428-431.
545. Robert, A.A. and M.M. Zamzami, *Traumatic spinal cord injury in Saudi Arabia: a review of the literature*. The Pan African medical journal, 2013. **16**.
546. Santos, E.A.S., et al., *Epidemiology of severe cervical spinal trauma in the North area of São Paulo City: a 10-year prospective study*. Journal of Neurosurgery: Spine, 2009. **11**(1): p. 34-41.
547. Chen, Y., Y. He, and M.J. DeVivo, *Changing demographics and injury profile of new traumatic spinal cord injuries in the United States, 1972–2014*. Archives of physical medicine and rehabilitation, 2016. **97**(10): p. 1610-1619.

548. Van den Berg, M., et al., *Incidence of spinal cord injury worldwide: a systematic review*. Neuroepidemiology, 2010. **34**(3): p. 184-192.
549. Lenehan, B., et al., *The epidemiology of traumatic spinal cord injury in British Columbia, Canada*. Spine, 2012. **37**(4): p. 321-329.
550. DeVivo, M.J., *Epidemiology of traumatic spinal cord injury: trends and future implications*. Spinal cord, 2012. **50**(5): p. 365-372.
551. DeVivo, M.J. and Y. Chen, *Trends in new injuries, prevalent cases, and aging with spinal cord injury*. Archives of physical medicine and rehabilitation, 2011. **92**(3): p. 332-338.
552. Facts, S.C.I., *Figures at a Glance 2020 SCI Data Sheet*.(2020). 2020.
553. Cao, Y., A.W. Selassie, and J.S. Krause, *Risk of death after hospital discharge with traumatic spinal cord injury: a population-based analysis, 1998–2009*. Archives of physical medicine and rehabilitation, 2013. **94**(6): p. 1054-1061.
554. Krassioukov, A.V., J.C. Furlan, and M.G. Fehlings, *Medical co-morbidities, secondary complications, and mortality in elderly with acute spinal cord injury*. Journal of neurotrauma, 2003. **20**(4): p. 391-399.
555. Rubenstein, L.Z., *Falls in older people: epidemiology, risk factors and strategies for prevention*. Age and ageing, 2006. **35**(suppl_2): p. ii37-ii41.
556. Dumont, R.J., et al., *Acute spinal cord injury, part I: pathophysiologic mechanisms*. Clinical neuropharmacology, 2001. **24**(5): p. 254-264.
557. Zhang, Y., et al., *Acute spinal cord injury: Pathophysiology and pharmacological intervention*. Molecular Medicine Reports, 2021. **23**(6): p. 1-18.
558. Rowland, J.W., et al., *Current status of acute spinal cord injury pathophysiology and emerging therapies: promise on the horizon*. Neurosurgical focus, 2008. **25**(5): p. E2.

559. Wasner, G., D. Naleschinski, and R. Baron, *A role for peripheral afferents in the pathophysiology and treatment of at-level neuropathic pain in spinal cord injury? A case report.* Pain, 2007. **131**(1-2): p. 219-225.
560. Min-Te Choo, A., et al., *Modeling spinal cord contusion, dislocation, and distraction: characterization of vertebral clamps, injury severities, and node of Ranvier deformations.* Journal of neuroscience methods, 2009. **181**(1): p. 6-17.
561. Fehlings, M.G., et al., *Perioperative and delayed complications associated with the surgical treatment of cervical spondylotic myelopathy based on 302 patients from the AOSpine North America Cervical Spondylotic Myelopathy Study: Presented at the 2011 Spine Section Meeting.* Journal of Neurosurgery: Spine, 2012. **16**(5): p. 425-432.
562. Figley, S.A., et al., *Characterization of vascular disruption and blood–spinal cord barrier permeability following traumatic spinal cord injury.* Journal of neurotrauma, 2014. **31**(6): p. 541-552.
563. Fehlings, M.G. and L.H. Sekhon, *Restoration of spinal cord function*, in *Orthopaedic Knowledge Update: Spine 2*, D.F. Fardon, Editor. 2002, Amer Academy of Orthopaedic. p. 483-488.
564. Fehlings, M.G., et al., *Early versus delayed decompression for traumatic cervical spinal cord injury: results of the Surgical Timing in Acute Spinal Cord Injury Study (STASCIS).* PLoS ONE, 2012. **7**.
565. O’Shea, T.M., J.E. Burda, and M.V. Sofroniew, *Cell biology of spinal cord injury and repair.* The Journal of clinical investigation, 2017. **127**(9): p. 3259-3270.
566. Káradóttir, R. and D. Attwell, *Neurotransmitter receptors in the life and death of oligodendrocytes.* Neuroscience, 2007. **145**(4): p. 1426-1438.
567. Verkhratsky, A. and C. Steinhäuser, *Ion channels in glial cells.* Brain research reviews, 2000. **32**(2-3): p. 380-412.

568. Gottlieb, M. and C. Matute, *Expression of ionotropic glutamate receptor subunits in glial cells of the hippocampal CA1 area following transient forebrain ischemia*. Journal of Cerebral Blood Flow & Metabolism, 1997. **17**(3): p. 290-300.
569. Fernyhough, P. and N.A. Calcutt, *Abnormal calcium homeostasis in peripheral neuropathies*. Cell calcium, 2010. **47**(2): p. 130-139.
570. Leist, M. and P. Nicotera, *Calcium and neuronal death*. Reviews of Physiology Biochemistry and Pharmacology, Volume 132, 1998: p. 79-125.
571. Verkhratsky, A. and O.H. Petersen, *The endoplasmic reticulum as an integrating signalling organelle: from neuronal signalling to neuronal death*. European journal of pharmacology, 2002. **447**(2-3): p. 141-154.
572. Verkhratsky, A. and E. Toescu, *Endoplasmic reticulum Ca²⁺ homeostasis and neuronal death*. Journal of cellular and molecular medicine, 2003. **7**(4): p. 351-361.
573. Pivovarova, N.B. and S.B. Andrews, *Calcium-dependent mitochondrial function and dysfunction in neurons*. The FEBS journal, 2010. **277**(18): p. 3622-3636.
574. Duchen, M.R., *Mitochondria, calcium-dependent neuronal death and neurodegenerative disease*. Pflügers Archiv-European Journal of Physiology, 2012. **464**(1): p. 111-121.
575. Li, S. and P. Stys, *Na⁺-K⁺-ATPase inhibition and depolarization induce glutamate release via reverse Na⁺-dependent transport in spinal cord white matter*. Neuroscience, 2001. **107**(4): p. 675-683.
576. Duchen, M.R., *Mitochondria in health and disease: perspectives on a new mitochondrial biology*. Molecular aspects of medicine, 2004. **25**(4): p. 365-451.
577. Gooch, C.L., E. Pracht, and A.R. Borenstein, *The burden of neurological disease in the United States: A summary report and call to action*. Annals of neurology, 2017. **81**(4): p. 479-484.

578. Maas, A.I., et al., *Traumatic brain injury: integrated approaches to improve prevention, clinical care, and research*. The Lancet Neurology, 2017. **16**(12): p. 987-1048.
579. van Dijck, J.T., et al., *In-hospital costs after severe traumatic brain injury: a systematic review and quality assessment*. PLoS One, 2019. **14**(5): p. e0216743.
580. Alkadamani, R. *Spinal Cord Injuries in Australia – The case for investing in new treatments*. 2020; Available from: <https://www.spinalcure.org.au/media-releases/spinal-cord-injuries-in-australia-the-case-for-investing-in-new-treatments/>.
581. Krueger, H., et al., *The economic burden of traumatic spinal cord injury in Canada. Chronic diseases and injuries in Canada*, 2013. **33**(3).
582. Singh, A., et al., *Global prevalence and incidence of traumatic spinal cord injury*. Clinical epidemiology, 2014. **6**: p. 309.
583. Ma, V.Y., L. Chan, and K.J. Carruthers, *Incidence, prevalence, costs, and impact on disability of common conditions requiring rehabilitation in the United States: stroke, spinal cord injury, traumatic brain injury, multiple sclerosis, osteoarthritis, rheumatoid arthritis, limb loss, and back pain*. Archives of physical medicine and rehabilitation, 2014. **95**(5): p. 986-995. e1.
584. Tuominen, R., P. Joelsson, and O. Tenovuo, *Treatment costs and productivity losses caused by traumatic brain injuries*. Brain injury, 2012. **26**(13-14): p. 1697-1701.
585. DeVivo, M., et al., *Costs of care following spinal cord injury*. Topics in spinal cord injury rehabilitation, 2011. **16**(4): p. 1-9.
586. Deutsch, A., et al., *Characteristics and outcomes of aged Medicare beneficiaries with a traumatic spinal cord injury: 2002-2005*. Topics in Spinal Cord Injury Rehabilitation, 2011. **16**(4): p. 17-26.
587. Cao, Y. and J. Krause, *Economic Costs of Traumatic Spinal Cord Injury—A Population Based Study*. Archives of Physical Medicine and Rehabilitation, 2021. **102**(10): p. e58-e59.

588. Dryden, D.M., et al., *Direct health care costs after traumatic spinal cord injury*. Journal of Trauma and Acute Care Surgery, 2005. **59**(2): p. 441-447.
589. Radhakrishna, M., et al., *Effects of injury level and severity on direct costs of care for acute spinal cord injury*. International Journal of Rehabilitation Research, 2014. **37**(4): p. 349-353.
590. Bradbury, C.L., et al., *Traumatic brain injury in patients with traumatic spinal cord injury: clinical and economic consequences*. Archives of Physical Medicine and Rehabilitation, 2008. **89**(12): p. S77-S84.
591. Munce, S.E., et al., *Direct costs of adult traumatic spinal cord injury in Ontario*. Spinal Cord, 2013. **51**(1): p. 64-69.
592. Marin, J.R., M.D. Weaver, and R.C. Mannix, *Burden of USA hospital charges for traumatic brain injury*. Brain injury, 2017. **31**(1): p. 24-31.
593. Edmonds, C. *The Steep Cost of Brain Injury Recovery*. 2015; Available from: <https://www.nextavenue.org/the-steep-cost-of-brain-injury-recovery/>.
594. Lo, J., L. Chan, and S. Flynn, *A systematic review of the incidence, prevalence, costs, and activity and work limitations of amputation, osteoarthritis, rheumatoid arthritis, back pain, multiple sclerosis, spinal cord injury, stroke, and traumatic brain injury in the United States: A 2019 update*. Archives of physical medicine and rehabilitation, 2021. **102**(1): p. 115-131.
595. Salim, A., et al., *The presence of the adult respiratory distress syndrome does not worsen mortality or discharge disability in blunt trauma patients with severe traumatic brain injury*. Injury, 2008. **39**(1): p. 30-35.
596. Ahmed, N. and Y.-H. Kuo, *Early versus late tracheostomy in patients with severe traumatic head injury*. Surgical infections, 2007. **8**(3): p. 343-348.

597. Palmer, S., et al., *The impact on outcomes in a community hospital setting of using the AANS traumatic brain injury guidelines*. Journal of Trauma and Acute Care Surgery, 2001. **50**(4): p. 657-664.
598. Mayer, N.H., et al., *Characterization and correlates of medical and rehabilitation charges for traumatic brain injury during acute rehabilitation hospitalization*. Archives of physical medicine and rehabilitation, 2003. **84**(2): p. 242-248.
599. NBIA. *Brain Injury Statistics*. 2021; Available from: <https://www.nbia.ca/brain-injury-statistics/>.
600. Chen, A., et al., *Direct cost associated with acquired brain injury in Ontario*. BMC neurology, 2012. **12**(1): p. 1-12.
601. McGarry, L.J., et al., *Outcomes and costs of acute treatment of traumatic brain injury*. Journal of Trauma and Acute Care Surgery, 2002. **53**(6): p. 1152-1159.
602. Cao, Y. and J.S. Krause, *Estimation of indirect costs based on employment and earnings changes after spinal cord injury: an observational study*. Spinal cord, 2020. **58**(8): p. 908-913.
603. Wright, D.W., et al., *CDC grand rounds: reducing severe traumatic brain injury in the United States*. MMWR. Morbidity and mortality weekly report, 2013. **62**(27): p. 549.
604. Fu, T.S., et al., *Health & economic burden of traumatic brain injury in the emergency department*. Canadian Journal of Neurological Sciences, 2016. **43**(2): p. 238-247.
605. Greenberg, M.S. and N. Arredondo, *Handbook of neurosurgery*. 6th ed. 2006, New York: Thieme Medical Publishers.
606. Feldman, Z., et al., *Effect of head elevation on intracranial pressure, cerebral perfusion pressure, and cerebral blood flow in head-injured patients*. Journal of neurosurgery, 1992. **76**(2): p. 207-211.
607. Kinoshita, K., *Traumatic brain injury: pathophysiology for neurocritical care*. Journal of intensive care, 2016. **4**(1): p. 1-10.

608. Carney, N., et al., *Guidelines for the management of severe traumatic brain injury*. Neurosurgery, 2017. **80**(1): p. 6-15.
609. Torbic, H., et al., *Use of antiepileptics for seizure prophylaxis after traumatic brain injury*. American journal of health-system pharmacy, 2013. **70**(9): p. 759-766.
610. Sandestig, A., B. Romner, and P.-O. Grände, *Therapeutic hypothermia in children and adults with severe traumatic brain injury*. Therapeutic hypothermia and temperature management, 2014. **4**(1): p. 10-20.
611. Burke, A.M., et al., *The effects of mannitol on blood viscosity*. Journal of neurosurgery, 1981. **55**(4): p. 550-553.
612. Grubb Jr, R.L., et al., *The effects of changes in PaCO₂ cerebral blood volume, blood flow, and vascular mean transit time*. Stroke, 1974. **5**(5): p. 630-639.
613. Bullock, M.R., et al., *Surgical management of acute subdural hematomas*. Neurosurgery, 2006. **58**(suppl_3): p. S2-16-S2-24.

Appendix A

Central Nervous System Injuries and Treatments

A.1 Structure, Organization and Function of the Central Nervous System

The human central nervous system (CNS) is intricate and sophisticated. Anatomically, the CNS is composed of the brain and spinal cord. The brain is contained within the cranial cavity of the skull and the spinal cord lies within the vertebral cavity of the vertebral column or spinal canal.[418] Although the bones of the skull and spine provide the bulk of protection and

structural support for the CNS, they are insufficient to safeguard the brain and spinal cord. The meninges helps to anchor the CNS in place, for example, preventing the brain from moving about in the skull. Additionally, the meninges contain cerebrospinal fluid (CSF) which acts as a cushion for the brain and provides a suspension solution in which the brain can maintain its shape.

The human brain weighs approximately three pounds but this small organ is the most complex part of the human body.[419] The adult brain consists of three basic units: the forebrain (prosencephalon), the midbrain (mesencephalon) and the hindbrain (rhombencephalon).[420] The forebrain is the most evolved and largest component of the human brain: it consists primarily of the cerebrum and the structures of the inner brain. The cerebrum consists of the right and left cerebral hemispheres separated by the falx cerebri of the dura mater. The cerebrum has four lobes named according to the corresponding cranial bone that covers each part: frontal, parietal, temporal, and occipital lobes.[421, 422] The midbrain is the smallest division of the human brain and it consists of three regions: the cerebral aqueduct, the tectum, and the tegmentum. The hindbrain consists of the medulla oblongata, the pons, and the cerebellum. The human brain is comprised of ~100 billion neurons (nerve cells) and 1000 billion glial (support) cells.[423]

The brainstem, consisting of the midbrain and hindbrain, is the posterior stalk-like part of the brain that connects the brain to the spinal cord.[424] The spinal cord is a long, delicate tube-like structure that runs from the end of the brainstem down the center of the back to almost the bottom of the spine. The spinal cord lies in the spinal canal and is covered and protected by the meninges (three layers of thin membranes). The vertebrae (backbones) surround the spinal cord and meninges, offering further protection from injury. The spinal cord is comprised of nerve tissues called spinal nerves; these nerves divide into five sections from the top to the bottom of the spinal cord as follows: cervical (neck), thoracic, lumbar, sacral, and coccygeal. The regions of the spinal

cord contain varying numbers of spinal nerves: the cervical, thoracic, lumbar, sacral, and coccygeal contain 8 pairs, 12 pairs, 5 pairs, 5 pairs, and 1 pair of spinal nerves, respectively. The spinal cord and nerves are very fragile.[422, 425]

The CNS, the central processing unit or control panel of the human body, controls our mental and bodily functions. It controls our thoughts (cognition), senses, emotions, desires, movements, and our physiological processes such as our heart rate, breathing, release of certain hormones, body temperature, and much more.[422] The CNS defines who we are. The brain, the central control module of the body, receives information through our five senses and coordinates activities throughout the body. It controls our thought, memory and speech as well as exerting control over bodily motions and the interpretation of sensory information. Different parts of the brain carry out specific functions while multiple parts of the brain may work synchronously to perform more complex higher-order functions. The cerebrum is responsible for complex functions such as interpreting touch, vision and hearing, as well as speech, reasoning, emotions, learning, and fine control of movement.[421] The lobes of the cerebral hemispheres have functions that are specific as well as functions that they perform together. The frontal lobe is responsible for personality, behavior, emotion, speech, judgement, problem solving, planning, intelligence, concentration, awareness, and body movement.[426] The parietal lobe controls sensations and interprets them; additionally it interprets language, words, and interprets signals from vision, hearing, motor, sensory and memory as well as the control of spatial and visual perceptions.[427, 428] The occipital lobe interprets vision particularly color, light and movement.[429] The temporal lobe is responsible for understanding language, memory retention, hearing, and sequencing and organization of information.[430, 431] The cerebellum coordinates muscle movement, maintains posture and balance while the brainstem acts as a relay center connecting the cerebrum and

cerebellum to the spinal cord.[432] Additionally, the brainstem performs a number of involuntary functions such as maintaining body temperature, heart rate, breathing, wake and sleep cycle, digestion, vomiting, sneezing, coughing and swallowing.[433]

The spinal cord plays a vital role in many areas of the body's functioning. It is the pathway for messages sent by the brain to the body and vice versa. The spinal cord carries signals from the brain that control movement and autonomic functions. The spinal cord nerves also transmits messages from other parts of the body to the brain such as sensation of touch, pressure, and pain. The spinal cord also acts independently of the brain in conducting spinal reflexes that are associated with many of the protective functions necessary for survival. Common examples of spinal reflexes include stretch reflex (muscle contraction in response to stretching within the muscle) and withdrawal reflex (protects the body from damaging stimuli such as touching a hot object).

A.2 Central Nervous System Injuries

Injuries to the CNS can cause tissue damage in the brain or spinal cord and can occur from neurological disorders or physical trauma. This leads to a disruption of the CNS framework and subsequent loss of neuronal cell bodies, axons, and related glial support. The result of physical injury to the CNS include traumatic brain injury (TBI) and spinal cord injury (SCI). If an injury is mild, a person may experience a full recovery. However, if an injury is severe, the outcome could be a permanent disability or death.

CNS injuries are a leading cause of death and disability worldwide. These injuries are well-known public health priorities because they are preventable and their management require significant healthcare resources and can leave the afflicted and society with an enormous economic

burden. The economic impacts of living with a CNS injury depends on the severity of injury and the age at which the injury occurred. Currently, global CNS injury statistics are difficult to estimate due to the absence of research activities specific to SCI and TBI in many countries and the cost for starting and maintaining a trauma registry and population-based health data system. Consequently, estimates of the incidence and prevalence of TBI and SCI vary significantly depending on the source.

A.2.1 Traumatic Brain Injury

Consistent with the unique mode of physical injury, TBI has three distinct categories: (1) closed head, (2) penetrating, and (3) explosive blast TBI. Closed head TBI results from a blunt impact to the head mainly from falls, domestic abuse, motor vehicle accidents, and sports activities. This form of TBI is most common among civilians. Contact with the powerful blunt and compressive force disrupts brain function directly underneath the place of impact, causing immediate damage to brain vasculature and neurons. Consequently, the vibrations and shock generated during the impact may cause the brain to compress, reducing cerebral blood flow. Closed head TBI may result in focal localized contusions or diffuse axonal injury to other regions of the brain.[434]

Penetrating TBI occurs when a foreign object such as a gunshot or knife penetrates the skull and propagates through the dura into the brain parenchyma. As with closed head TBI, laceration of brain tissues generally results in focal damage, intracranial hemorrhage, cerebral edema and ischemia. Penetration of the brain by a rapidly moving projectile can cause tissue cavitation, further exacerbating the injury. The type and extent of neurological damage depends on the size, speed, route, and strength of the external body entering the brain. This form of TBI

has a relatively high chance of infection due to the exposure of brain tissue to the hostile environment. Due to the invasiveness of this type of injury, penetrating TBI is associated with acute medical complications such as respiratory failure, non-infectious pneumonia, hypotonia, and cerebrospinal fluid leakage compared to closed head TBI.[434, 435]

Explosive blast TBI is a relative new class of TBI that emerged over the last two decades. The incidence and prevalence of war-related explosive blast TBI is high among military personnel who served in wars in Afghanistan and Iraq.[436] In an explosive blast TBI, the rapid pressure shock waves generated from the explosion impacts the brain by transmitting a tremendous amount of energy from the skull into the enclosed brain parenchyma.[437] Explosive blast TBI presents different injury patterns: (1) primary where the shock waves cause internal damage, (2) secondary in which materials from the explosion penetrates the brain, and (3) tertiary resulting from physical injury by blast waves.[438, 439] The kinetic energy generated by the explosion causes deformation of the brain, resulting in extensive damage to both gray and white matter, nerve cell death, axonal damage, blood brain barrier (BBB) damage, vasospasm, pseudoaneurysm, hyperemia, contusion and cerebral edema.[438] In addition to the clinical characteristics mentioned above, post-traumatic stress disorder (PTSD) is often associated with explosive TBI.[439]

The symptoms of TBI vary according to the type and severity of the injury. The signs of severe TBI include prolonged unconsciousness, headache, repeated vomiting or nausea, slurred speech, seizure, amnesia, loss of coordination and increased agitation and confusion. These symptoms are noticeable within minutes of TBI; however, some of these symptoms may persist for months or years.[440, 441] A health care provider determines a TBI diagnosis after taking a survey regarding the symptoms and details of the injury, performing a neurologic exam, doing an imaging test (CT scan or MRI), a psychological test and the Glasgow Coma Scale (GCS) to determine the severity

of the TBI. The GCS scores patients based on their symptoms and classifies TBI as mild (score: 13-15), moderate (score: 9-12) or severe (score <9). These subdivisions are predictive of a patient's long-term outcome.[442]

A.2.1.1 Epidemiology of Traumatic Brain Injury

TBI is a major public health concern because it is the greatest contributor of disability and death worldwide among all trauma-related injuries. Even though the global statistics are uncertain, recent estimates show that the annual global incidence and prevalence of TBI ranged from 64 – 74 million and 53 - 58 million, respectively.[443] A comparison of the epidemiology of TBI in developed countries and developing countries showed that the incidence and prevalence of TBI is greater in developed countries than in developing countries.[444] The incidence and prevalence of TBI in developed countries are 1507 per 100, 000 and 708 per 100, 000 persons, respectively compared to 811 per 100,000 and 629 per 100, 000 cases in developing countries, respectively.[154]

A TBI could happen to anyone; but the rates of TBI are highest in the very young (0 – 4 years old), in adolescents and young adults (15 – 24 years old), and older adults (age > 65 years).[445] Additionally, men and older adults are at the greatest risk for hospitalization and death from a TBI. The occurrence of TBI is significantly higher in males compared to females with ratios ranging from 2.0 to 1 and 2.8 to 1. The gender ratios are higher in cases of severe TBI, 3.5 to 1.[446] For example, the incidence rate of TBI hospitalization in Ontario Canada is 22 per 100,000 persons for females and 52 per 100,000 persons for males.[447, 448] Even though, TBI affects the lives of people of all ages, data suggests that some groups are at higher risk of dying from a TBI or experiencing long-term health problems after the injury. Examples of groups more likely to suffer from TBI include service members and veterans, racial and ethnic minorities, incarcerated people, survivors of domestic abuse and people who experienced homelessness. Falls and motor vehicle

accidents are the leading causes of TBI, globally.[449, 450] Falls cause significantly higher incidences of TBI in the older population (age > 65 years) while motor vehicle accidents cause significantly higher incidence of TBI in the adolescent to young adult population.[449, 451, 452]

Recent reviews of TBI epidemiology in Europe indicate that there is a wide range of incidence rates among countries included in the report. In 2021, the incidence rate ranged from 47.3 per 100,000 population per year to 849 per 100,000 population per year.[453] In 2006 and 2015, Tagliaferri et al. and Peeters et al. reported a similar variation of incidence rates among reporting countries.[444, 454] Additionally, in the 2021 review of TBI epidemiology in Europe, Brazinova et al. concluded that the incidence rates for TBI across Europe are not increasing but remained broadly the same as those reported in the 2006 report. Another important finding of this recent review is that there seemed to be a shifting pattern in the mechanism of injury overtime. The trend shows that, as the number of TBIs from motor vehicle accidents decrease, the contribution of falls have increased.[453, 455] This change in pattern relates to improved road infrastructure and traffic safety rules resulting in a decline in road traffic-related TBIs incidence. Conversely, there is a change in the demographics of many countries, the ageing population is increasing and as a result older individuals are more prone to falls, hence the change in pattern.

In 2014, the Centers for Disease Control and Prevention (CDC) reported ~ 2.87 million TBI-related emergency room visits, hospitalization and death (TBI-ERHDs) in the US, a 53% increase from 2006, a year in which there were about 1.88 million TBI-ERHDs. In that year, TBI-related hospitalization accounted for 10% (288,000) of TBI-ERHDs and ~2% (56,800) of those visits resulted in TBI-related deaths.[449] In 2016-2018, the CDC reported a decrease in TBI-related hospitalization: 227,000, 224,000, and 223,050 in 2016, 2017, and 2018, respectively. Additionally the number of TBI-related deaths increased remained at ~61000 from 2016-

2019.[456] In the US, TBI is a major cause of death, accounting for ~30% of all injury-related deaths.[452, 457] The leading causes of TBI in the US include falls (47.9%), struck by or against an object (17.1%), and motor vehicle crashes (13.2%). Rates of TBI-related ER visits attributable to being unintentionally struck by or against an object were highest among children and adolescents (5-14 years), infants and toddlers (0-4 years), and adolescent and young adults (15-24). While TBI-related injuries in adolescents and young adults (15-24 years) were attributable to motor vehicle crashes. Motor vehicle injury is the leading cause of TBI-related deaths and adults 20-24 years have the highest mortality rate. Adults ages 75 years and older have the highest rates of TBI-related hospitalizations and death. However, in every age groups, TBI rates are higher for males than for females and males 0-4 years have the highest rates of TBI-related ERHDs.[451, 452, 456]

A.2.1.2 The Pathophysiology of Traumatic Brain Injury

Pathophysiology of TBI is a complex process resulting from damages to neuronal tissues in the brain. These damages fall into two categories: (1) primary injury, the damages arising from the mechanical forces during the physical impact to the head and (2) secondary injury, which pertains to further cellular and tissue damages following the primary injury.[1] The direct physical impact of different mechanical insults to the brain can lead to localize or diffuse injury patterns. Localize injury results from concussion/compression forces while diffuse axonal shearing injuries arise from indirect trauma mechanisms, such as sudden deceleration or rotational acceleration. Even though ~70% of all TBI are diffuse axonal injuries, clinical studies show that localize and diffuse injuries can coexist in patients who suffer from moderate and severe TBI.[2, 458] The primary injury causes damage to neuronal cell bodies, axons and glial cells and may ultimately lead to necrosis due to the compromise of the blood supply at the injury site. This cause the occurrence

of hematomas and epidural, subdural and intracerebral hemorrhages at the confined layers of the brain.[2] Primary TBI damaged can lead to cognitive impairments, behavioral changes, and muscle weakness. Diffuse axonal injuries (DAI) can cause stretching and shearing injuries in cerebral brain tissues and these strong tensile forces lead to damage of the axons, glial support and the blood vasculature. This leads to the occurrence of brain edema and ischemia.[459] The main indicator of diffuse TBI is widespread axonal damage predominantly in subcortical and deep white matter tissue such as the brain stem and corpus callosum. This damage involves impairment of the axonal transport and degradation of axonal cytoskeleton. DAIs can persist for months following TBI, denoting its association with delayed secondary pathology of hemorrhages and brain edema.[460] The extent of the DAI and neuronal degeneration are main factors that help to determine the severity of TBI.

Secondary injuries are associated with the cascade of inflammatory, biochemical, cellular and physiological events occurring after the primary injury and can persist for a few hours to years. The secondary injury processes are complex and numerous molecular mechanisms are involved such as excitotoxicity, mitochondrial dysfunction, oxidative stress, lipid peroxidation, neuro-inflammation, axon degeneration and apoptotic cell death.[461] Excitotoxicity is rapid influx and overload of calcium ions (Ca^{2+}) into the neuronal cytoplasm due to excessive release of excitatory amino acids such as glutamate and aspartate from the synaptic nerve terminals. Glutamate, the principal excitatory neurotransmitter in the CNS, is toxic to neurons when present in large amounts. The excessive activation of glutamate receptors (N-methyl-d-aspartate (NMDA) and α -amino-3-hydroxy-5-methyl-4-isoxazole propionate (AMPA) receptors) also induce an influx of sodium ions (Na^+), mitochondrial dysfunction, changes in dendrite morphology ultimately leading to cell death via rapid necrosis or delayed apoptosis.[462] Further, the hyperactivation of NMDA

receptors by excessive glutamate promotes the production of reactive oxygen species (ROS) and nitric oxide (NO) which worsen the secondary injuries.[463, 464]

Mitochondrial dysfunction is another hallmark event of secondary damages that result in the release of ROS and a reduction of ATP production when excessive intracellular Ca^{2+} flows into the mitochondria.[465-467] This leads to interruption or collapse of the electron transport chain, which impedes the oxidative phosphorylation processes causing cell death and disruption of the regulation of the calcium cycle. These conditions activate the mitochondrial permeability transition pores (mPTP) to open. For example, the mPTP opens and the permeability of the inner membrane of the mitochondria increased due to conformational changes of adenine nucleotide translocator (ANT) when it binds with cyclophilin D.[468, 469] Other mitochondrial proteins such as cytochrome c and apoptosis inducing factor (AIF) plays a critical role in cell death when released into the cytoplasmic matrix.[467, 470]

Research evidence suggest that oxidative stress plays a substantial role in the pathogenesis of TBI. Oxidative stress in TBI denotes a state of imbalance in which ROS overwhelms the scavenging antioxidants system in the brain.[434, 471] Endogenous ROS and oxygen-derived free radicals include agents such as hydrogen peroxide (H_2O_2), superoxide anions ($\cdot\text{O}_2^-$), hydroxyl ($\text{OH}\cdot$) and peroxy ($\text{ROO}\cdot$) radicals.[471, 472] Several sources including enzymatic processes, activated neutrophils, excitotoxic pathways and dysfunctional mitochondria continuously generate these species following TBI.[472, 473]

The production of excess NO following TBI also contributes to the build-up of free radicals at the injury site. Injury-induced excitotoxicity cause the accumulation of Ca^{2+} after TBI, which promotes the production NO via the increased activity of nitric oxide synthase (NOS). The excess NO reacts with the superoxide anion radical to form peroxynitrite (PN), which induces oxidative

stress and the amount of oxidative markers, 3-nitrotyrosine (3-NT) and 4-hydroxynonenal (4-HNE) present determines extent of the oxidative damage.[474] A number of researcher demonstrated an increased level of these oxidative markers after inducing TBI in animal models.[467, 474-476]

Neuro-inflammation is a secondary injury response to TBI, which involves the activation of immune cells and the release of inflammatory mediators within the brain as well as the marshalling of peripheral immune cells.[477-479] Even though all cell types within the brain are capable of producing pro-inflammatory cytokines, microglia derived from macrophages are the principal immune cells of the brain. Following TBI, peripheral macrophages infiltrate the brain and transform into microglia in response to TBI. In the injured brain, microglia produce anti-inflammatory mediators, scavenge cellular debris and promotes neuro-restorative process to facilitate healing post TBI. On the other hand, microglia can produce excessive pro-inflammatory mediators that are cytotoxic to neurons, thus it exacerbates brain damage, and retards brain repair and functional recovery.[480] For example, several research groups use TBI animal models and post mortem human brain tissues to show that when levels of pro-inflammatory cytokines and chemokines increase, the levels of the anti-inflammatory cytokines decrease in the brain. An increase was observed in the levels of pro-inflammatory cytokines such as interleukin-1beta, (IL-1 β), IL-6 β , IL-7 β , tumor necrosis factor- α (TNF- α) and interferon- γ (IFN- γ) and chemokines such as macrophage chemotactic protein-1 (MCP-1) and macrophage inflammatory proten-2 (MIP-2) and chemokine (C-C motif) ligand (CCL5). While simultaneously, they observed a decrease in the levels of the anti-inflammatory cytokines such as IL-4, IL-10, IL-13, and transforming growth factor- β 1 (TGF- β 1).[480-484]

TBI injury disrupts the glial support and in a DAI, Wallerian degeneration is noticeable within minutes and can go on for days to months after the injury. Characteristics of Wallerian degeneration include myelin degradation, diminished axonal transport, and accumulation of axonal transport protein.[485-487] Formation of retraction bulbs is the main attribute of a DAI and is due to dissociation of axonal connections. The formation of retraction bulbs and the accrual of axonal transport protein in the node result in prolonged swelling of injured axons and the programmed cell death of neurons and oligodendrocytes.[487] Even though different parts of the brain has retraction tubes, it is predominantly located in the corpus callosum and pyramidal tract of the brain stem.[488, 489] Retraction bulbs are detected by axonal markers such as β -amyloid precursor protein (β -APP) and neuro-filament (NF) as early as 24 hours and up to 14 days in diffuse TBI experimental models.[488, 490] Hellewell et al show the correlation between axonal damage in corpus callosum and the infiltration of microglia and macrophages, which result in vascular disruption, axonal degeneration, oligodendrocyte damage, and white matter deformation.[488]

Following TBI, the brain triggers a widespread glial reaction called gliosis. This reactive cellular process involves activation and proliferation of astrocytes and the subsequent infiltration of reactive astrocytes in the lesion site causing reactive astrogliosis, accompanied by hypertrophy and increased complexity of their processes.[491, 492] TBI animal model and post mortem tissues from TBI patients indicate that there is an increased expression of specific markers during the process of gliosis, such as glial fibrillary acid proteins (GFAP) for astrocytes, various extracellular matrix (ECM) molecules like chondroitin sulfate proteoglycans (neurocan and versican), and other inhibitory molecules in the lesion such as tenascins and semaphorin 3A. The presence of these molecules inhibit axonal growth and in severe cases, reactive gliosis ultimately results in the formation of a glial scar surrounding the injury site. [491, 493-498]

Research shows that the glial scar can be both detrimental and beneficial to TBI recovery. Within the first 24 hours of TBI, glial scar formation is critical and beneficial for sealing the injury site to facilitate remodeling of the tissues and spatiotemporally control the local immune response.[499, 500] The glial scar acts as a barrier protecting the area from additional microbial infections, containing the spread of cellular damage, regulating extracellular ion and fluid balance, mitigating excessive inflammatory and growth factor responses and counteracting free radical production.[500-502] Further, the glial scar promotes revascularization of blood capillaries to enhance the nutritional, trophic, and metabolic support of the nervous tissues. However, the formation of the glial scar is detrimental to TBI recovery in the chronic phase because the reactive astrocytes secrete several growth inhibitors that chemically hinders axonal extensions and imposes a major barrier to regeneration.[503, 504]

A.2.2 Traumatic Spinal Cord Injuries

Spinal cord injury (SCI) is damage to the vertebrae, ligaments or disc of the spinal column, to any part of the spinal cord or nerves at the end of the spinal cord canal that temporarily or permanently causes changes in its normal motor, sensory, or autonomic function.[505] Etiologically, over 90% of SCI cases are traumatic and the remainder non-traumatic.[506] Traumatic spinal cord injury (TSCI) is due to a sudden blow to the spine that fractures, dislocates, crushes or compresses one or more vertebrae.[507] Additionally, a TSCI can also result from a gunshot or knife wound that penetrates and cuts the spinal cord. Common causes of TSCI in the US are motor vehicle accidents, falls, sports and recreational-related injuries, and acts of violence.[508, 509] A non-traumatic spinal cord injury could results from arthritis, tumor, inflammation, infections, and degenerative disc disease of the spine.[510-512] The symptoms of

SCI vary depending on the severity and location of the injury. Initially, the injured may experience spinal shock that causes loss of sensation, muscle movement and reflexes below the level of the injury.[513] Typically, spinal shock last from several hours to several weeks and as the shock attenuates, other symptom surfaces. Generally, the higher up the level of the injury on the spinal cord, the more severe the symptoms. For example, an injury to the first and second vertebrae in the spinal column (C1, C2), or the mid-cervical vertebrae (C3, C4, and C5) affects the respiratory muscles and the ability to breathe.[514, 515] A lower injury, in the lumbar vertebrae, may affect nerve and muscle control to the bladder, bowel, and legs, and sexual function.[516]

TSCI is a medical emergency; to diagnose a suspected injury to the spinal cord requires a full medical evaluation and testing. Initially, the injured undergoes a physical exam and diagnostic tests during which the healthcare provider attains the medical history of the injured and learns how the SCI occurred. Diagnostic test may include blood tests, x-rays, computer tomography scan (CT or CAT scan) and magnetic resonance imaging (MRI).[512, 517, 518] The classification of a TSCI depends on the location of injury on the spinal cord and the extent of damage to it.

Most clinicians use the International Standards for Neurological Classification of Spinal Cord Injury (ISNCSCI) to classify TSCI.[519, 520] This classification system considers three different neurological summary scores that is the American Spinal Injury Association (ASIA) score, the ASIA sensory score, and the ASIA Impairment Scale score. The ASIA) score grades muscle power from the muscles served by a spinal nerve root (myotome), the ASIA sensory score measures light touch and pin prick sensations in 28 areas of the skin innervated by one spinal nerve root (dermatomes), and the ASIA Impairment Scale score determines the grade of SCI and the extent of remaining sensorimotor function.[519] The ASIA Impairment Scale is used to determine the grade of spinal cord injury (SCI), which ranges from ASIA Impairment Scale grade A

(the most severe injury with complete sensorimotor loss) to ASIA Impairment Scale grade E (the least severe injury with no neurological deficit). Based on the definition of these scale grades, neurological outcomes are determined and the SCI placed under two distinct categories: (1) complete SCI or (2) incomplete SCI.[507] These classes of SCI depends on the extent of damage to the spinal cord. A complete SCI can happen at any level of the spinal cord and it occurs when the spinal cord is completely constricted or transected, preventing communication between the brain and below the point of injury.[521] For example, a complete SCI in the lumbar region of the spinal cord may lead to paralysis below the waist, while movement in the upper body may be preserved.[522] By contrast, an incomplete SCI is one in which the injured person retains some sensation and/or function below the injury site. For example, there could be movement in one limb more than the other, feelings in parts of the body, or more function on one side of the body. Incomplete injuries can happen at any level of the spinal cord.[523]

An alternate classification scheme for SCI stems from the type of motor and sensory function loss experienced by the injured. There are three main classes: (1) tetraplegia, (2) paraplegia, and (3) triplegia.[524] Tetraplegia is paralysis affecting the arms and legs due to SCI in the cervical region (C1 - C7). The tetraplegic will experience varying sensations and mobility post injury contingent upon which cervical vertebrae was injured.[525] For example, if an individual has a C1 injury, the injured will require the use of a ventilator and will experience paralysis from the neck down; by contrast, if the individual has a C7 injury, the individual will have upper limb movement including the ability to control the triceps and biceps.[525, 526] Paraplegia is damage to the thoracic, lumbar or sacral region of the spinal cord causing paralysis of all or part of the trunk, legs and pelvic organs. These injuries affect the lower body because signals cannot travel to the lower region of the body from the brain down the spinal cord and vice versa.[524, 527] As a

result, paraplegics experience loss of movement and sensation below the level of the injury. Sensation loss may vary based the extent of the injury; some paraplegics may experience a tingling feeling or reduced sensation below the level of the injury to a complete inability to feel anything below the injury site.[528] While thoracic level injuries to the spinal cord are less common because of the protection provided by the rib cage, paraplegics with T1 – T12 may most likely use a manual wheel chair, drive an adapted vehicle, and can stand in a standing frame or may walk with braces.[529] Additionally, they will experience significant weakness in the legs or loss of sensation, loss of sensation in the genital or rectal regions, and minimal or no voluntary control of bowel or bladder. Paraplegics who suffer lumbar and sacral SCI generally lose some function in the hips and legs; have minimal or no voluntary control of bowel and bladder but can manage on their own with special equipment. Paraplegics with lumbar SCI, depending on the strength in their legs may need a wheel chair or may walk with braces while those with sacral SCI may most likely be able to walk.[530, 531]

A.2.2.1 Epidemiology of Traumatic Spinal Cord Injury

The 2016 study of the Global Burden of Diseases, Injuries, and Risk Factors (GBD) reported that the global annual incidence and prevalence of TSCI ranged from 0.78 to 1.16 million and 24.98 to 30.15 million individuals, respectively.[532, 533] The incidence and prevalence of TSCI varies worldwide by regions and countries; the incidence and prevalence of TSCI are higher in developed countries than in developing countries because there is a greater expansion of activities, higher rates of self-harm, violent crimes, and road traffic accidents.[512, 534] The incidence of TSCI in the US, Japan, Canada, New Zealand, and the United Kingdom are 54, 49, 41, 22, and 16

cases per million per year, respectively.[535-540] While the estimated prevalence of TSCI in these countries are 906, 787, 1298, 534, and 478 per million per year, respectively.[85, 533, 535, 538] By contrast, the incidence of TSCI for developing countries like India, Brazil, Russia, Iran, and Saudi Arabia are 20, 21, 17.6, 44, and 38 cases per million, respectively.[541-545] While the estimated prevalence is 236, 112, 514, 440 and 627 per million cases, respectively.[533, 541, 544-546]

Comparatively, there is a higher risk of males sustaining a TSCI than females; the gender ratio is ~4 to 1.[547] Even though it is likely for TSCI to occur in any age group, data shows that the highest distribution occurs in the age range 15-29 and there is a growing trend in those >50 years old.[548, 549] In the US since 2015, 24% of new TSCI cases occur in the African American/Black population, a large disparity when compared with their population distribution (13%) in the US. A comparative study of the incidence of TSCI in the geriatric population (≥ 60 years old) shows that the incidence rate has increased from 4.6% in 1970 to 13.2 % in 2014 and the pattern is expected to continue into the future as the number of elderly in the US population increase.[547, 550, 551]

According to National Spinal Cord Injury Statistical Center (NSCISC), the annual incidence of SCI is 54 cases per one million people in the US, or ~17810 new SCI cases each year and the prevalence of SCI is ~939 cases per million people, or range of 250,000 to 368,000 persons. They also reported the most common cause of TSCI in the US as automobile crashes (leading cause of injury), falls (leading cause in the geriatric population), acts of violence (primarily gunshot wounds) and sports/recreation activities. In 2020, traffic accidents, falls, violence, sports, and other causes accounted for 38.6%, 32.2%, 14.0%, 7.8%, and 7.4 % of TSCI, respectively. [552] TSCI in younger individuals were from high-energy impact activities such as traffic accidents and sport-related injuries whereas TSCI in older age groups (>60 years of age) were

from low-energy impact activities such as falls. Falls are the primary cause of TSCI in the elderly because they may have existing co-morbidities such as degenerative cervical myelopathy, osteoarthritis, poor vision, and illnesses that impair balance.[541, 549, 551, 553-555] The incidence of TSCI is greatest at the level of the cervical spine (~54%), with C5 being the most common level affected. Injuries at the level of the thoracic and lumbosacral spine accounts for ~35% and 11% of all TSCI, respectively as the spinal cord in those region of the spine is afforded the extra-protection that the ribcage offers.[507, 547]

A.2.2.2 The Pathophysiology of SCI

The pathophysiology of SCI is complex and consists of the initial primary injury and ensuing secondary injury. Primary injury results from the initial mechanical force that contacts the spinal cord at the time of injury, causing compression, dislocation, or fracture of the spinal cord.[181, 556, 557] Primary injury occurs via four mechanisms: (1) compression forces, (2) distraction forces, (3) flexion or extension forces, or (4) transection/laceration.[556, 558, 559] The spinal cord injuries occur via compression, which usually result from burst fractures with bone fragments constricting the spinal cord or via fracture-dislocation injuries.[556, 560, 561] TSCI due to distraction forces arise when adjacent vertebrae separates because of shearing forces, which causes the spinal column to stretch and tear in the axial plane.[556, 560] TSCI injuries due to flexion or extension forces arise from the rotation of the penetrating object as it traverse the spinal cord or strain to the neural tissues or vascular structures.[559] Finally, transection/laceration injuries arise when projectiles from a blast or sharp objects contacts the spine and may vary from minor injuries to completely severing the spinal cord.[556] Irrespective of the mechanism of primary injury, these forces directly damage the ascending and descending tracts of the spinal cord and disrupt the

macro- /micro-vasculature and cell membranes. The result being spinal shock, systemic hypotension, vasospasm, ischemia, ionic imbalance and up-regulation of neurotransmitter.[558, 562, 563] Currently, early surgical decompression is most effective clinical treatment to mitigate tissue damage following primary injury of the spinal cord.[564]

The primary injury initiates a plethora of secondary injuries having diverse mechanisms, which can come into play within minutes and may even ensue for weeks or even months following TSCI.[3] Secondary damages refers to a sequence of cellular, molecular biochemical phenomena that cause destruction of the spinal cord tissues via apoptosis and the expansion of necrotic tissues beyond the injury site.[4]

Secondary injury is transitory, consisting of the acute, sub-acute, and chronic phases. The acute phase starts directly after the physical insult to the spinal cord and involves vascular damage, increased cell permeability, ionic imbalance, neurotransmitter accumulation, excitotoxicity, free radical formation, lipid peroxidation, inflammation, edema and necrotic cell death.[3-5] The sub-acute injury phase evolves within 48 hours to 14 days following TSCI. It involves programmed cell death (apoptosis), axon demyelination, Wallerian degeneration, retraction of axon from the lesion site (axonal dieback), ECM remodeling and glial scar formation at the injury site. The chronic phase begins three (3) months following TSCI, with progressive axonal dieback as a cystic cavity forms at the injury site and maturation of the glial scar.[3, 6-9]

Components of the acute phase of secondary injury are key contributors to the pathophysiology of TSCI. Hypo-perfusion due to disruption of the spinal cord vasculature is an initial consequence of primary injury.[10] Following TCSI, larger vessels such as the anterior spinal artery usually remain intact, while the microvasculature (smaller vessels such as capillaries), which are more predisposed to traumatic damage ruptures leading to the extravasation of leucocytes and red blood

cells.[10-12] Increased pressure due to spinal cord edema and hemorrhage-induced vasospasm in the intact vessels promotes further disruption in blood flow to the injury site. Spinal cord ischemia is rare but its consequences are substantial in causing additional damage at the injury site. The damaged vascular system, along with hemorrhage and ischemia eventually lead to cell death and tissue destruction via multiple mechanisms such as excitotoxicity, free radical formation, hypoxia, ionic imbalance and necrotic cell death.[13] Glutamate is an excitatory neurotransmitter that is released in the CNS; during TSCI necrotic neurons and glial cells release excessive glutamate.[10] Interaction between glutamate and glutamate receptors such as AMPA and NMDA during TSCI greatly increase glutamate concentration, which leads to glutamate excitotoxicity and cell death. Other events related to the excessive glutamate levels include mechanical stress, failure of Na^+/K^+ ATPase in axonal membrane, and lipid peroxidation.[565]

A high concentration of Ca^{2+} influx into neuronal and glial cells when glutamate binds to NMDA and AMPA.[566-568] Under normal physiological conditions, the free Ca^{2+} concentration in different parts of the cell range from 50-100 nM but in the lumen of the endoplasmic reticulum the range is 0.5 -1.0 mM. A sustained accumulation of Ca^{2+} in the cytoplasmic matrix, endoplasmic reticulum or mitochondria has dire consequences for the cell.[569-573] Mitochondria play an important role in Ca^{2+} -dependent neuronal cell death. In the acute phase of TSCI, during neuron-related glutamate-induced excitotoxicity, hyperactivation of NMDA leads to mitochondrial Ca^{2+} overload which produces apoptotic or necrotic cell death.[573] Additionally, Ca^{2+} overload activates a plethora of protein kinases and phospholipases that yield calpain-mediated protein degradation and oxidative stress because of mitochondrial failure.[10] Soon after TSCI, the mitochondrial calcium uniporter (MCU) transports Ca^{2+} to the mitochondria and upregulation of

MCU signaling promotes mitochondrial calcium overload, which hinders mitochondrial respiration, depletes ATP and disables Na^+/K^+ ATPase and increase intracellular Na^+ . [574-576] Free radicals and nitric oxide production occur at the injury site during TSCI. [574] Mitochondrial Ca^{2+} overload activates NADPH oxidase (Nox) and promotes generation of superoxide via electron transport chain.

After SCI, hemorrhage and cell death creates a milieu in which iron accumulates at the injury site. Most of this intracellular iron released from ferritin and transferrin co-localizes with activated microglia/macrophages. [21] The released iron redox cycle between Fe^{2+} and Fe^{3+} while producing more superoxide anion radicals. Subsequently, the Fenton reaction between Fe^{3+} and hydrogen peroxide produces highly reactive hydroxyl radicals. [22] ROS are able to cause oxidative damage to macromolecules such as lipids, proteins, and DNA leading to lipid peroxidation, formation of protein-protein crosslinks, and oxidation of polypeptide backbones resulting in protein fragmentation, DNA damage and DNA strand breakage. High doses of ROS, generated during acute or chronic TSCI are cytotoxic. [23]

Cell death is a major event in the secondary injury mechanisms that affects neurons and glia after SCI (142–145). Cell death can happen through various mechanisms in response to various injury-induced mediators. Necrosis, apoptosis, necroptosis and autophagy are major cell death mechanisms following SCI (146–148). Following SCI, neurons and glial cells die through necrosis as the result of mechanical damage at the time of primary injury that also continues to the acute and subacute stages of injury (7, 150). Necrosis occurs due to a multitude of factors including accumulation of toxic blood components (151), glutamate excitotoxicity and ionic imbalance (152), ATP depletion (153), pro-inflammatory cytokine release by neutrophils and lymphocytes (154, 155), and free radical formation (142, 156–158). Programmed necrosis or “necroptosis” are

highly regulated, caspase-independent cell death with similar morphological characteristics as necrosis (160). Necroptosis is a receptor-mediated process. It is induced downstream of the TNF receptor 1 (TNFR1) and is dependent on the activity of the receptor interacting protein kinase 1 (RIPK1 and RIPK3).

Apoptosis is the most studied mechanism of cell death after SCI. Apoptosis represents a programmed, energy dependent mode of cell death that begins within hours of primary injury (7). This process takes place in cells that survive the primary injury but endure enough insult to activate their apoptotic pathways (142). In apoptosis, the cell shrinks and is eventually phagocytosed without induction of an inflammatory response (156). Apoptosis typically occurs in a delayed manner in areas more distant to the injury site and most abundantly affects oligodendrocytes.

SCI also results in a dysregulated autophagy (174). Normally, autophagy plays an important role in maintaining the homeostasis of cells by aiding in the turnover of proteins and organelles. In autophagy, cells degrade harmful, defective or unnecessary cytoplasmic proteins and organelles through a lysosomal dependent mechanism (175, 176). The process of autophagy starts with the formation of an autophagosome around the proteins and organelles tagged for autophagy (176). Next, fusion of the phagosome with a lysosome form an autolysosome that begins a recycling process (176). In response to cell injury and endoplasmic reticulum (ER) stress, autophagy activates and limits cellular loss (177, 178). Current evidence suggests a neuroprotective role for autophagy after SCI (175, 179). Dysregulation of autophagy contributes to neuronal loss (174, 180).

A.3 Economic Burden of CNS Injuries

In 2017, Gooch et al provided a summary overview of neurological diseases having the most sizable current and future economic impact; TBI and SCI are among those listed.[577] The annual global economic impact of TBI is approximately \$400 billion while existing data do not allow for a global estimate of the cost of SCI.[506, 578, 579] However, the existing cost estimates for SCI from a number of developed countries suggest that its global annual cost could sum to billions of dollars. The annual estimated cost associated with SCI in Australia, Canada, the United Kingdom and the United States are USD \$2.68 billion, \$2.10 billion, \$1.43 billion and \$21.5 billion, respectively.[539, 580-583]

The cost of CNS injuries fall into two categories: direct and indirect cost. Direct costs are associated with expenditures arising from the injuries and the responsible parties are the patient and health care facilities. Typically, direct cost include but are not limited to doctor's fee, hospital's stay charges, cost for laboratory tests, and imaging (x-rays, MRI, and CT scans).[584] In the US, for instance, the costs associated with SCI-related acute hospital care, post TSCI in-patient rehabilitation, and average first-year cost ranged from \$92,220 to \$337,400, \$32,220 to \$190,620, and \$300,880 to \$634,500, respectively.[532, 585-587] By comparison, in Canada, the costs attributable to SCI-related acute hospital care, post TSCI inpatient rehabilitation and average first-year cost ranged from \$39,330 to \$138,620, \$106,890 to \$180,460, and \$32,240 to \$167,640, respectively.[588-591]

In the US, average lifetime cost of medical treatment for severe TBI range from \$600,000 to \$3 million. Additionally, survivors of TBI face long-term neuropsychiatric issues and their treatment requires a significant health care expenditure.[592, 593] In 2010, the estimated economic burden of TBI in the US was \$76.5 billion, with ~30% of the cost attributable to direct cost (~\$23 billion) and 70% to indirect cost (\$54 billion).[594] The economic burden associated with TBI-related

acute hospital care is substantial, especially for patients with severe TBI. In 2010, the total annual cost for TBI-related in-hospital stay was 21.4 billion.[579, 592] In 2019, van Dijk et al conducted a systematic review on the cost of in-hospital stay and treatment in the US of patients with TBI.[579] The in-hospital cost after severe TBI ranged from \$258,790 to \$401,808.[595-597] Inpatient rehabilitation is an important component of TBI recovery and the associated cost contributes significantly to the total cost of TBI. Mayer et al. evaluated the charge for TBI inpatient rehabilitation in the US and determined that the total average charge per day per person was ~\$1600 and that the overall cost per person was ~\$46000. They associated most of these charges with room and board, hospital services and rehabilitation therapy.[598] By comparison, the total economic burden of TBI in Canada is over \$12.7 billion per year.[599] In Canada, the costs attributable to TBI-related acute hospital care, post TSCI inpatient rehabilitation and average first-year cost ranged from \$16,436 (CAD) to \$43,123 (CAD), \$15,646 (CAD) to \$43,062 (CAD), and \$32132 (CAD) to \$38013 (CAD), respectively.[600]

Indirect cost also arise from the injuries, but third parties such as employers, insurance companies and society as a whole covers this cost. Indirect cost are associated with expenditures arising from sick leave, early retirement or pre-mature death.[581] Indirect cost can account for most of the overall cost of CNS injuries. For example, productivity losses due to premature death is approximately 10 times those of direct cost. The overall treatment cost for severe injuries are significantly higher than less severe cases. [584, 601] The lifetime indirect cost of TSCI per person depends on a number of factors including age at the time of injury, the overall health of the individual pre-injury and the severity of the injury. Cao et al. reported that the lifetime indirect cost for an individual injured at 25 years old differ by the severity of the injury, ranging from 0.5 to 2.3 million US dollars. By comparison, the life time indirect cost for an individual injured at 50

years old varied by severity of injury as well as health condition prior to injury, ranging from 0.3 to 0.6 million US dollars.[602] Krueger et al. estimated the lifetime indirect cost of TSCI per person in Canada as ranging from \$0.7 million to \$1.3 million in 2011 for a person injured at 35 years old.[581] Ma et al. and Wright et al. reported that indirect cost of TBI in 2010 ranged from 51.2 billion to 65.0 billion. An estimate of the lifetime indirect cost of TBI estimated from these values for an individual injured at 25 years old ranged \$1.0 million to \$1.3 million.[583, 603] By comparison, between 2009 and 2010 Fu et al. estimated the total lifetime indirect cost of TBI in Canada as ranging from \$653 million to \$793 million. The estimated lifetime indirect cost per person for TBI from these values ranged from \$0.17 million to \$0.21 million.[604]

A.4 Treatment of CNS Injuries

Currently, no clinical treatment exists that will regenerate and restore the damaged CNS. The existing treatment strategy involves medical management of the primary injuries and neuroprotection with pharmacological agents to mitigate the deleterious effects of the secondary damages. Further, rehabilitation plays a central role in the treatment of CNS injuries: Cognitive Rehabilitation for individuals with TBI and Physical Therapy for individuals with SCI.

A.4.1 Medical Intervention

Medical intervention typically start at the scene of injury; the emergency medical technician (EMT) will assess the circumstances of the injury to help guide appropriate emergency care. First, the EMT will secure and preserve the airway to maintain breathing and maintain effective circulation. Additionally, they will immobilize the patient because movement has the potential to exacerbate the already sustained injury. Depending on the extent of observed injury, the EMT may use different immobilization devices such as hard collar and tape for cervical immobilization or

spinal boards to immobilize the entire body. Besides, spinal boards are an effective means of transferring trauma patients from the scene to the ambulance and then to the emergency room.

To optimize emergency care for CNS injuries, therapeutic goals should integrate CNS and systemic care, especially in cases where there are multiple system dysfunction. After the initial assessment by emergency room staff, the goal is to lower intracranial pressure (ICP)/intraspinal pressure (ISP) and maintain cerebral blood flow (CBF). In the case of TBI, elevating the head of the patient rapidly reduce ICP by displacing cerebrospinal fluid (CSF) from the intracranial compartment as well as promoting venous out flow, and maintaining CBF.[605, 606] In terms of SCI,

Hyperventilation is a commonly used medical intervention for the reduction of ICP and ISP by lowering the intra-arterial carbon dioxide partial pressure (PaCO_2), which subsequently results in vasoconstriction.[607] In Europe, emergency room doctors administers prophylactic hyperventilation (targeting a PaCO_2 of 35 mm Hg) to more than 50 % of TBI patients. In the guideline for the management of severe TBI, Carney et al. do not recommends the protracted use of prophylactic hyperventilation targeting a PaCO_2 of 25 mm Hg. This guideline also recommends avoiding the use of hyperventilation targeting a PaCO_2 of 35 mmHg during the first 24 h after injury.[608]

Other medical interventions used in the treatment of CNS injuries include prophylactic antiepileptic, hypothermia, hyperosmolar therapy, and medically inducing a comatose state. Prophylactic antiepileptic is effective against seizures in the early stages of TBI; however, TBI guidelines recommend that patients discontinue use after the first week due its ineffectiveness in preventing late-stage seizures.[609] Therapeutic cooling partially relief oxidative stress, which could happen within several minutes after the TBI. Lowering the body temperature reduces the

brain's metabolic demand and so there is downregulation of metabolites that create ROS and RNS. On the other hand, lowering the temperature may alter the platelet count, coagulation factors and blood glucose level, which lead to unpredictable results.[610] Hyperosmolar therapy decreases the viscosity of blood, increase CSF then induce the body to auto-regulate CBF by temporally constrict the blood vessel.[611] A medically induced coma is the last resort to manage the primary injury caused by TBI; to achieve this state the anesthesiologist prescribes a benzodiazepine or a barbiturate. A medically induced comatose greatly decrease the metabolic demand in the brain and are commonly used after invasive ICP monitoring device has been applied.[612]

A.4.2 Surgical Intervention

In many cases, especially if epidural hematoma, subdural hematoma or severe internal bleeding occurs, craniotomy surgical intervention is necessary. Decompressive craniectomy is a common countermeasure against epidural hematomas, which may rapidly progress in size then increase ICP to a critical level.[613] After the acute phase of TBI, neurosurgeons may perform surgery to evacuate subdural hematomas to release the blood.[24] In some cerebral edemas, where obliteration of the basal cisterns occurs, hemicraniectomy and/or bilateral decompressive craniectomy saves the patient from life threatening danger.[25]

A.4.3 Pharmacological Treatment

Anatomical and functional damages to the brain caused by structural, cellular, and vascular injury after the initial impact are hallmarks of TBI. After the initial mechanical impact, complex molecular and cellular cascade reactions ensue. By studying the fundamentals of these reactions and using animal models of TBI, researchers have proposed promising pharmacological treatments to remediate the secondary injury. Currently, studies on pharmacological treatments are focusing

on excitatory amino acids (EAA) modulation, calcium channel blocker, reactive oxygen species (ROS) scavenging, inflammation control, caspases inhibitors, calpain inhibitors, endocrinological treatment, etc.

EAA modulation treatments on ionotropic and metabotropic receptors. TBI induced excessive These receptors activity causes influx of Na^+ and Ca^{2+} while efflux of K^+ and Mg^{2+} , which triggers numerous neurotoxic properties.[26] Many compounds were studied to modulate receptors under these two types of N-methyl-D-aspartate (NMDA) receptor antagonists and AMPA/KA receptor inhibitors are still unclear for their effectiveness [27-29], while research about metabotropic receptor inhibitors and glutamate release inhibitors illustrate their potential to prevent the secondary damages.[30-33]

Immediately after TBI, a rapidly increase in intracellular and decrease of extracellular calcium (Ca^{2+}) due to an increase in membrane permeability cause an increased influx of Ca^{2+} . High Ca^{2+} levels may induce reactive oxygen species and activate calpains (vide infra) and endonucleases, which link to cell death and damage.[34] Calcium blockers, such as (S)-emopamil, omega-conopeptide SNX 111, nimodipine, etc. can restrict the influx of Ca^{2+} , potentially protecting the cells from secondary damage.[35-37]

Due to the high concentration of oxidizable fatty acids in the brain but low levels of antioxidants, oxidative damage results from lipid peroxidation (LPO).[38] additionally, the pathophysiology of TBI indicate that iron accumulates at the TBI injury site and iron initiates the formation of ROS.[39] The inhibition of ROS and ROS-mediated damage has been the topic of many studies. Medicines in the Tirilazad mesylate family show limited protective capability but has very limited BBB penetration. It mainly lowers ROS level indirectly through maintaining normal blood-brain barrier (BBB) permeability.[40, 41] Metal chelators, such as deferoxamine,

mediate ROS by removing the catalyst metal ions in the ROS formation process.[42, 43] Compounds in Choline family protect brain tissue from ROS damage by attenuate the activation of phospholipase A2.[44, 45] Nitron compounds exhibit neuroprotective capability by adducting with ROS.[46, 47] Antioxidant enzyme superoxide dismutase and endothelial Nitric oxide also exhibit neuron protective ability.[48, 49] Compounds targeting brain inflammation, caspases, and neuroendocrine abnormalities are also extensively studied.[50-58]

The most common clinical interventions for SCI is the administration of high doses of methylprednisolone to reduce secondary injury processes. This treatment is controversial due to the adverse side effects, which include gastric bleeding, sepsis, pneumonia, acute corticosteroid myopathy, and wound infection.[59] Baclofen and opioid painkillers are other pharmacological agents used to treat spasticity and severe to moderate pain in SCI, respectively.[60, 61] Morphine is a popular opioid analgesic used in SCI management because morphine has a strong affinity for the mu-receptor located in the CNS.[61]

A.4.5 Cell treatment

Stem Cells (SCs) treatment of TBI is promising and several therapies recently entered the clinic trail.[62, 63] In regenerative medicine, SCs differentiate to brain cells, then restore the functionality of the injured area.[64] There are many studies in the preclinical stage on TBI animal models where SCs transplantation show the potential to improve neurological activities.[65] In most of the cases, neural stem cells (NSCs) and mesenchymal stem cells (MSCs) show the capability to regenerate brain tissue in several vivo studies.[64, 65]

Websites hosting information on Clinical trial for SC treatments are www.clinicaltrial and www.clinicaltrials.org. Limited data are available from the clinical trials posted since many of

them are in the patient recruitment phase. Two trials that completed phase 2 are NCT02416492 and NCT01575470. NCT02416492 used allogeneic modified bone marrow-derived mesenchymal (BM-MSCs) stem cells (SB623) through stereotactic intracranial injection to treat TBI. Current results show that the transplant is safe and the motor function is partially restored or improved based on Fugl–Meyer Motor Scale (FMMS).[64] The NCT01575470 clinical trial studied the safety and efficacy of bone marrow mononuclear cells (BMMNCs) transplanted in TBI patients (GCS score 5–8). Although the treatment was safe, the therapy mainly preserved the brain function against secondary damage but did not show clear regenerative results.[372] Clinical trial (NCT02525432) focused on MM-MNCs is ongoing and will terminate in October 2022. The above-mentioned clinical trials treated patients with acute TBI, normally 24-48 hours after the initial injury. Clinical Trials NCT02795052 and NCT04063215 provided MSCs therapy to patients 6 months post injury and unfortunately, there is no available data to report.

SC therapy holds much potential for the treatment of SCI because there are multiple features in SCI pathology that stem cell transplantation can target. Experimental cell culture models, animal and clinical trials tested numerous types of SCs including bone marrow mesenchymal stem cells (BM-MSCs), umbilical mesenchymal stem cells (U-MSCs), adipose-derived mesenchymal stem cells (AD-MSCs), neural stem cells (NSCs), neural progenitor cells (NPCs), embryonic stem cells (ESCs), and induced pluripotent stem cells (i-PSCs). Researchers and clinicians have come to realize that mono-modal cell therapy offers limited benefits to regeneration in SCI.[66]

A.5 Our Approach

Spontaneous regeneration in the CNS is deficient following injury and the main reason is the hostile microenvironment at the injury site, which is comprised of many inhibitory factors. Extensive research efforts are in progress to shed light on the mechanisms that drives these inhibitory factors, which is the core strategic principle in promoting regeneration in the CNS. Stem cell are promising for repair in the CNS but low viability of the transplanted cells becomes a major hurdle to neuroregeneration. This work addresses this issue by creating an artificial niche for stem cells via the synthesis of a series of in situ crosslinkable hydrogels based on PEGTA and iron-chelator polymer-conjugates. The iron-chelator polymer-conjugate is comprised of small a molecule chelator (5-amino-8-hydroxyquinoline, curcumin or quercetin), PEG, and hyaluronic acid. The in situ crosslinkable hydrogels demonstrated its ability to grow and proliferate hNSCs both in two and three dimensional cell culture. Additionally, this crosslinkable hydrogel mitigates oxidative stress and lipid peroxidation in *in vitro* experiments.

Vita

Debbie S. Campbell-Rance was born on the 16th day of September 1975 in Kingston, Jamaica. She grew up in Hanover, Jamaica and graduated from Montego Bay High School in St. James and

Holy Childhood High School in Kingston in 1993 and 1995, respectively. She earned a Bachelor of Science degree in Chemistry from the University of the West Indies in 1999 and worked in industry for five years. In 2011, she earned a Master of Science degree in Chemistry at Virginia Commonwealth University and currently teaches at Virginia State University as an Instructor in Engineering (2016-present) and Chemistry (2011- 2016). Dr. Xuejun Wen, Alice T. and William H. Goodwin Jr. Endowed Chair Professor in Regenerative Medicine Institute for Engineering and Medicine in the Department of Chemical and Life Science Engineering at Virginia Commonwealth University supervised her doctoral studies.